Ulm University
Medical Faculty
Institute of Biochemistry and Molecular Biology
Head of the Institute: Prof. Dr. Michael Kühl

# Functions of the ribosomal factors block of proliferation 1 and ribosomal protein L5 during embryogenesis of *Xenopus laevis*

Dissertation submitted in partial fulfilment of the requirements for the degree of „Doctor rerum naturalium“ (Dr. rer. nat.)
of the International Graduate School in Molecular Medicine Ulm

**Corinna Nicoline Gärtner**
née Schreiner

born in Ulm

2022

**Current dean of the Medical Faculty:**

Prof. Dr. Thomas Wirth

**Current chairman of the Graduate School:**

Prof. Dr. Bernd Knöll

**Thesis Advisory Committee:**

First supervisor: Prof. Dr. Michael Kühl, Ulm University, Germany

Second supervisor: Prof. Dr. Karin Danzer, Ulm University, Germany

Third supervisor: PD Dr. Kerstin Feistel, University of Hohenheim, Germany

**External reviewer:**

Prof. Dr. Annette Borchers, University of Marburg, Germany

**Day doctorate awarded:**

5th of December, 2022

Results gained in my thesis have previously been published in the following publications:

**Gärtner, C.***, Meßmer, A.*, Dietmann, P., Kühl, M., & Kühl, S. J. (2022). Functions of block of proliferation 1 during anterior development in Xenopus laevis. *PLoS One*, 17(8): e0273507. * contributed equally

**Schreiner, C.***, Kernl, B.*, Dietmann, P., Riegger, R. J., Kühl, M., & Kühl, S. J. (2022). The Ribosomal Protein L5 Functions During Xenopus Anterior Development Through Apoptotic Pathways. *Front. Cell Dev. Biol.*, 10, 777121. * contributed equally

Graphics and figures were reused only with the permission of the publishers. The respective figures were published under Creative Commons License (CC BY 4.0) as indicated beneath the respective figures.

A complete list of all publications that were published with my participation during my time as a PhD student can be found in the Appendix.

# Content

**List of abbreviations ..... VI**

**1 Introduction ..... 1**

1.1 Ribosomal biogenesis in vertebrates ..... 1

1.2 Ribosomopathies ..... 2

1.3 Block of proliferation 1 ..... 6

1.4 Ribosomal protein L5 ..... 9

1.5 *Xenopus laevis* as model organism for embryonic development and established methods for gene editing ..... 10

1.6 *Xenopus laevis* as model organism for the study of ribosomal proteins ..... 13

1.7 *Xenopus laevis* neural development ..... 14

1.8 Aim of the study ..... 15

**2 Material and Methods ..... 16**

2.1 Material ..... 16

2.1.1 Organisms ..... 16

2.1.2 DNA and oligonucleotides ..... 16

2.1.3 Antibodies, recombined proteins, and enzymes ..... 21

2.1.4 Antibiotics ..... 22

2.1.5 Chemicals and reagents ..... 22

2.1.6 Commercial kits ..... 25

2.1.7 Solutions, buffers, gels, and media ..... 26

2.1.8 Equipment ..... 30

2.1.9 Consumables ..... 32

2.1.10 Software ..... 33

2.2 Methods ..... 34

2.2.1 Bioinformatics ..... 34

2.2.2 Molecular biological methods ..... 35

2.2.3 Handling mature *Xenopus laevis* ..... 47

2.2.4 *Xenopus laevis* embryos: microinjection, manipulation, cultivation and staining methods ..... 48

2.2.5 Imaging ..... 53

2.2.6 Evaluation and statistics ..... 54

**3 Results ..... 55**

3.1 Bop1 functions during *Xenopus laevis* embryonic development ..... 55

3.1.1 The rRNA precursor is available during embryonic development ..... 55

3.1.2 *bop1* is conserved across species ..... 56

3.1.3 *bop1* is specifically expressed in *Xenopus laevis* wild-type embryos ..... 57

3.1.4 Bop1 morpholino oligonucleotides bind specifically and efficiently ..... 60

3.1.5 Bop1 knockdown using morpholino oligonucleotides induces head and brain phenotypes ..... 62

3.1.6 Bop1 depletion results in eye phenotypes ..... 64

3.1.7 Gain of Bop1 function does not affect embryonic development ..... 66
3.1.8 Proliferative pathways are not affected upon Bop1 knockdown ..... 67
3.1.9 Apoptotic pathways are not affected upon Bop1 depletion ..... 69
3.1.10 Loss of Bop1 function does not generally affect translation ..... 70
3.1.11 Expression of pan-neural marker *sox3* is disturbed upon Bop1 knockdown ..... 73
3.1.12 Expression of NCC marker gene *foxd3* is reduced upon Bop1 depletion ..... 76
3.1.13 *foxd3* overexpression does not rescue the microcephalic phenotype ..... 77
3.1.14 Bop1 knockdown reduces expression of brain-specific marker gene *pax6* ..... 78
3.1.15 Expression of eye-specific marker genes is reduced upon Bop1 knockdown ..... 79
3.1.16 Bop1 and Pax6 act in a common signaling pathway ..... 82
3.1.17 *bop1* knockout via CRISPR/Cas9 induces phenotypes in anterior tissue ..... 84
3.1.18 *bop1* knockout using the CRISPR/Cas9 system does not affect early marker gene expression ..... 88
3.2 Rpl5 functions during *Xenopus laevis* embryonic development ..... 90
3.2.1 *rpl5* is conserved across different species ..... 90
3.2.2 *rpl5* is specifically expressed in *Xenopus laevis* wild-type embryos ..... 91
3.2.3 Loss of Rpl5 function leads to phenotypes of anterior tissue ..... 96
3.2.4 Loss of Rpl5 function leads to disturbed erythropoiesis and heart edema ..... 98
3.2.5 Rpl5 depletion does not generally affect translation ..... 100
3.2.6 Rpl5 depletion affects proliferative and apoptotic pathways ..... 103
3.2.7 c-Myc is affected upon Rpl5 knockdown ..... 105
3.2.8 Apoptosis contributes to phenotype upon loss of Rpl5 function ..... 109
**4 Discussion ..... 116**
4.1 Ribosomal factor Bop1 during *Xenopus laevis* development ..... 116
4.1.1 *bop1* expression in disease-relevant tissue ..... 116
4.1.2 Bop1 is required for early anterior neural development in *Xenopus laevis* ..... 117
4.1.3 Ribosomal biogenesis-dependent pathways are not disturbed in Bop1 morphants ..... 119
4.1.4 Molecular basis of the Bop1 MO-induced phenotype ..... 121
4.1.5 Potential extra-ribosomal function of Bop1 during *Xenopus laevis* embryogenesis ..... 123
4.2 Ribosomal protein Rpl5 during *Xenopus laevis* development ..... 125
4.2.1 *rpl5* expression in *Xenopus laevis* is located in disease-relevant tissues ..... 125
4.2.2 Rpl5 is required for early development of *Xenopus laevis* ..... 126
4.2.3 Molecular mechanisms underlying the Rpl5 MO-induced phenotype ..... 127
4.3 Conclusion ..... 131
**5 Summary ..... 132**
**6 List of References ..... 134**
**7 Appendix ..... 150**
**Statutory Declaration ..... 166**
**Acknowledgements ..... 167**

# List of abbreviations

| | | |
|---|---|---|
| **A** | aa | amino acid |
| | Actc1 | cardiac actin |
| **B** | b | brain |
| | ba | branchial arch |
| | BAG | Bcl2-associated athanogene |
| | BCIP | 5-bromo-4-chloro-3-indolyl phosphate |
| | Bcl2 | B-cell lymphoma 2 |
| | Bop1 | block of proliferation 1 |
| | bp | base pairs |
| | BrdU | 5- bromo-2'-deoxy-uridine |
| | BSA | bovine serum albumin |
| **C** | c-MYC | MYC protooncogene |
| | Cas | CRISPR associated |
| | cDNA | complementary DNA |
| | Celf1 | CUGBP elav-like family member 1 |
| | chr.L | chromosome L |
| | CHX | cycloheximide |
| | cmz | ciliary marginal zone |
| | CoMO | control morpholino oligonucleotide |
| | CRISPR | clustered regularly-interspaced short palindromic repeats |
| | crRNA | CRISPR RNA |
| | cryba1 | crystallin beta a1 |
| **D** | DBA | Diamond Blackfan anemia |
| | dd$H_2O$ | deionized water |
| | DEPC | diethylpyrocarbonate |
| | DMSO | dimethyl sulfoxide |
| | DNA | deoxynucleic acid |
| | dNTP | deoxynucleoside triphosphate |
| **E** | *E. coli* | *Escherichia coli* |
| | EDTA | ethylene diamine tetraacetic acid |
| | EGTA | ethylene glycol tetraacetic acid |

| | | |
|---|---|---|
| | EMT | epithelial-mesenchymal transition |
| | ETS | external transcribed spacer |
| **F** | FBS | fetal bovine serum |
| | FCS | fetal calve serum |
| | Foxc1 | forkhead box c1 |
| | Foxd3 | forkhead box d3 |
| **G** | Gapdh | glyceraldehyde 3-phosphate dehydrogenase |
| | Gata2 | GATA-binding factor 2 |
| | GFP | green fluorescent protein |
| | gRNA | guide RNA |
| **H** | ha | hyoid arch |
| | Hba3 | hemoglobin alpha 3 subunit |
| | hBCL2 | human BCL2 |
| | hCG | human chorionic gonadotropin |
| | HEPES | 4-(2-hydroxyethyl)-1-piperazineethansulforic acid |
| **I** | inj. | injected |
| | ITS | internal transcribed spacer |
| **L** | le | lens |
| | lin. | linearization |
| **M** | m | mesencephalon |
| | MAPK | mitogen-activated protein kinase |
| | ma | mandibular arch |
| | mc | Meckel’s cartilage |
| | MDM2 | mouse double minute 2 |
| | MO | morpholino oligonucleotide |
| | mRNA | messenger RNA |
| | MS222 | tricaine methane sulfonate |
| | mv | mesencephalic ventricle |
| **N** | n.s. | non-significant |
| | NBT | 4-nitro blue tetrazolium chloride |
| | nc | notochord |
| | NCC | neural crest cell |
| | NF-kB | nuclear factor kappa B |

| | | |
|---|---|---|
| | Nol11 | nucleolar protein 11 |
| | np | neural plate |
| | npb | neural plate border |
| | nt | neural tube |
| | NT | N-terminal |
| **O** | OD | optical density |
| | odc | ornithine decarboxylase 1 |
| | of | optical field |
| | Otx2 | orthodenticle homeobox 2 |
| **P** | PAM | protospacer adjacent motif |
| | Pax6 | paired box protein 6 |
| | PCR | polymerase chain reaction |
| | PeBoW | pescadillo-bop1-WDR12 |
| | Pes1 | pescadillo ribosomal biogenesis factor 1 |
| | PFA | paraformaldehyde |
| | pH3 | phospho histone H3 |
| | pm | periocular mesenchyme |
| | PMSF | phenylmethylsulfonyl fluoride |
| | Pol | polymerase |
| | Ppan | peter pan homolog |
| | Prox1 | prospero homeobox 1 |
| **Q** | qPCR | quantitative PCR |
| **R** | r | retina |
| | Rax | retina and anterior neural fold homeobox |
| | rDNA | ribosomal DNA |
| | RISC | RNA-induced silencing complex |
| | RNA | ribonucleic acid |
| | RNP | ribonucleoprotein |
| | RP | ribosomal protein |
| | Rpl5 | ribosomal protein L5 |
| | Rpl11 | ribosomal protein L11 |
| | rpm | rounds per minute |
| | rRNA | ribosomal RNA |

| | | |
|---|---|---|
| | RT | reverse transcriptase |
| **S** | s | somite |
| | S.O.C. | super optimal broth |
| | SBDS | SBDS ribosome maturation factor |
| | SDS | Shwachman Diamond syndrome |
| | sec | second |
| | SEM | standard error of the means |
| | Shh | sonic hedgehog |
| | Slc35b1 | solute carrier family 35 member b1 |
| | Snai2 | snail family zinc finger 2 |
| | snoRNA | small nucleolar RNA |
| | Sox2 | SRY-box transcription factor 2 |
| | Sox3 | SRY-box transcription factor 3 |
| **T** | ta | tectum anterius |
| | TCOF1 | treacle ribosome biogenesis factor 1 |
| | TCS | Treacher Collins syndrome |
| | TdT | terminal deoxynucleotidyl transferase |
| | TIDE | tracking of indels by decompensation |
| | Tp53 | tumor protein p53 |
| | trcrRNA | trans-activating CRISPR RNA |
| | TUNEL | TdT-mediated dUTP Nick-End Labeling |
| | Twist1 | twist family bHLH transcription factor 1 |
| **U** | uninj. | uninjected |
| | UTR | untranslated region |
| **W** | WDR12 | WD repeat domain 12 |
| | WMISH | whole mount *in situ* hybridization |
| | WT | wild-type |

# 1 Introduction

## 1.1 Ribosomal biogenesis in vertebrates

Ribosomes are the molecular machine that translate the genetic information from the intermediate messenger RNA (mRNA) into a protein; a crucial step for cellular function and proliferation (Melnikov et al., 2012). The biogenesis of cytosolic 80S ribosomes is a complex process that requires ribosomal RNAs (rRNA), small nucleolar RNAs (snoRNAs), ribosomal proteins (RP), RNA polymerases, further regulatory, processing, assembling, and maturation factors, as well as a tremendous amount of energy (Jenner et al., 2012; Kressler et al., 2017).

The ribosomal synthesis starts in the nucleolus, a cell compartment located in the nucleus, which is not segregated by a membrane (Fig. 1). Herein, RNA polymerase I (Pol I) transcribes ribosomal DNA (rDNA). In eucaryotic cells, around 35-60% of total transcription comprises of transcription of rDNA (Moss and Stefanovsky, 2002). The resulting 47S pre-rRNA (45S pre-rRNA in *Xenopus*) consists of a 5' and a 3' external transcribed spacer (ETS), two internal transcribed spacers (ITS1 and ITS2), and the 18S, 5.8S, and 28S rRNA (Fig. 1) (Baßler and Hurt, 2019).

After initial pre-rRNA transcription, ETSs and ITSs are cleaved and further processing as well as cleavage steps give rise to mature 18S rRNA - for which the final maturation takes place in the cytoplasm - 5.8S rRNA and 28S rRNA - final maturation takes place in the nucleus (Aubert et al., 2018; Henras et al., 2015).

RNA Pol III transcribes 5S rRNA in the nucleus that is later transported into the nucleolus, this contrasts with the other rRNAs that are directly transcribed in the latter (Aubert et al., 2018).

RPs, other ribosomal factors as well as snoRNAs are transcribed in the cytoplasm by RNA Pol II. In the nucleolus, RPs assemble with pre-rRNA and form pre-ribosomal particles, namely pre-60S and pre-40S (Pecoraro et al., 2021). Further processing steps are necessary to produce the mature 40S and 60S subunits, which eventually assemble into the functional ribosome particle (Fig. 1) (Baßler and Hurt, 2019).

In the mature ribosome, the 40S subunit consists of the 18S rRNA and 33 RPs and decodes mRNAs by aminoacyl-transfer RNA. The 60S subunit consists of the

5S rRNA, 5.8S rRNA, 28S rRNA, and 47 RP and is necessary for catalyzing peptide bond formation by a peptidyl-transferase reaction.

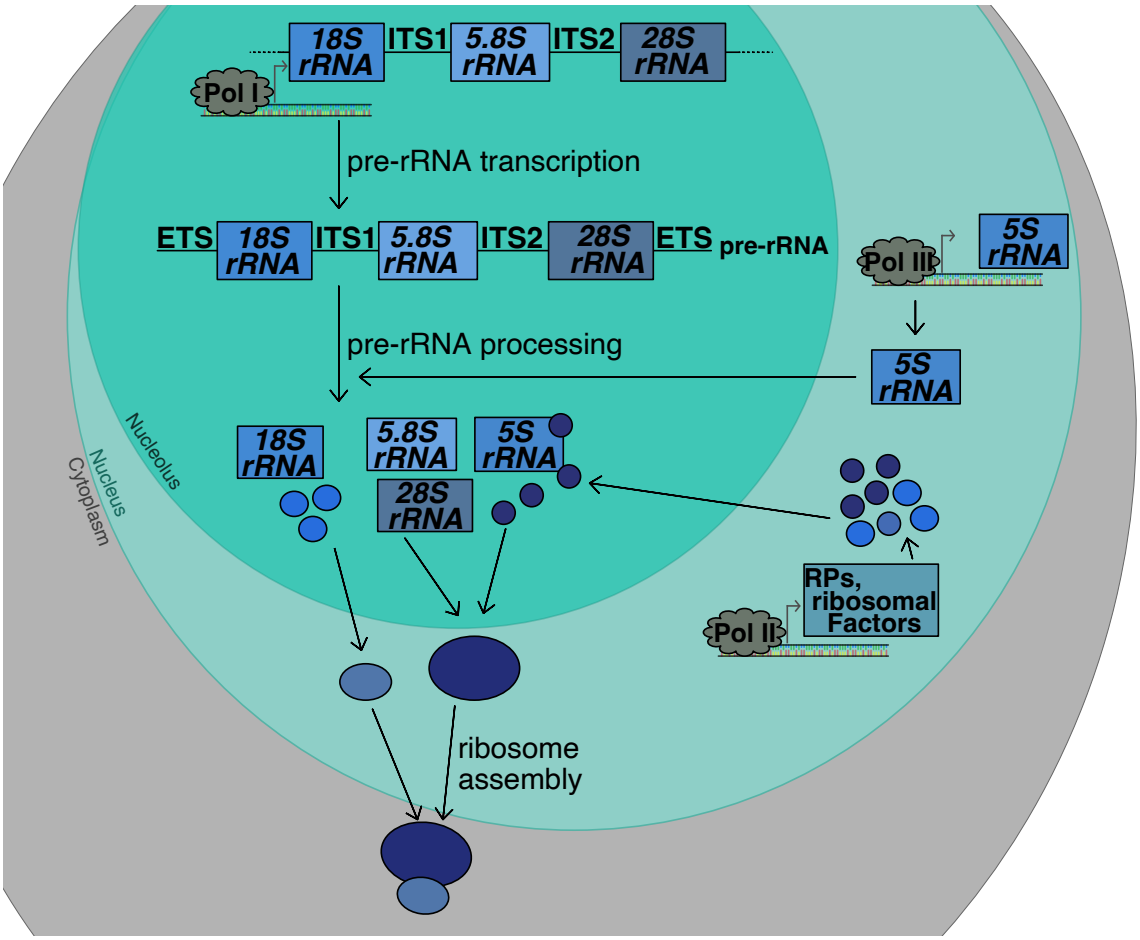


**Figure 1: Ribosomal biogenesis in vertebrates.**
In the nucleolus, ribosomal RNA (rRNA) genes are transcribed by RNA polymerase I (Pol I) giving rise to the pre-rRNA. The rRNA precursor consists of a 5' and a 3' external transcribed spacer (ETS), two internal transcribed spacers (ITS1 and ITS2) and the 18S, 5.8S, and 28S rRNA. 5S rRNA is transcribed by RNA polymerase III (Pol III) in the nucleus and imported into the nucleolus. Pre-rRNA processing drives modification and maturation of rRNAs. mRNAs encoding for ribosomal proteins (RP) and ribosomal factors are transcribed by RNA Polymerase II (Pol II). Pre-ribosomal particles are generated which are exported into the nucleus and cytoplasm and eventually assembled to a functional ribosome.

## 1.2 Ribosomopathies

Congenital diseases called ribosomopathies arise when ribosomal biogenesis, e.g., the function of an RP or a ribosomal biogenesis factor, is perturbed and the number of functional ribosomes decreases. The first described ribosomopathy was the Diamond Blackfan anemia (DBA) in 2005 (Léger-Silvestre et al., 2005). Today, several ribosomopathies are known besides DBA, e.g., Dyskeratosis congenita,

Shwachman Diamond syndrome (SDS), or Treacher Collins syndrome (TCS) (Farley-Barnes et al., 2019; Kang et al., 2021; Narla and Ebert, 2010).

Ribosomopathies manifest a variety of different symptoms and although ribosomes are ubiquitously required in every cell of every organism, these symptoms are often tissue-specific. Clinical manifestations include skin pigmentation defects, bone marrow failure, cardiac defects, neurological impairments, anemia, or defects in craniofacial morphology (Brooks et al., 2014; Farley-Barnes et al., 2019; Jenkinson et al., 2016; Kostjukovits et al., 2017; Myers et al., 2014; Narla and Ebert, 2010; Ross and Zarbalis, 2014; Shwachman et al., 1964; Vlachos et al., 2018). Furthermore, the likelihood of developing tumors and eventually cancer is increased in nearly all ribosomopathies (De Keersmaecker et al., 2015).

How this hypo-proliferative state (e.g., bone marrow failure, anemia) shifts towards a hyper-proliferative state (increased tumor incidence), also known as the Dameshek's Riddle (Dameshek, 1967), remains unclear but several mechanisms - which are non-mutually exclusive - have been proposed to contribute to the pathophysiology of ribosomopathies and ultimately to the development of cancer. These mechanisms include nucleolar stress, altered translation, and extra-ribosomal functions.

Nucleolar stress results from impaired ribosome biogenesis, leaving free RPs - not incorporated into the ribosome - behind, which can activate tumor protein p53 (Tp53).

During non-pathological conditions, E3 ubiquitin ligase mouse double minute 2 (MDM2) regulates Tp53 by ubiquitinating the molecule whereby Tp53 is degraded (Fig. 2A).

During nucleolar stress, the activation of Tp53 is accomplished by binding of free ribosomal protein L5 (Rpl5), free ribosomal protein L11 (Rpl11), or the 5S-ribonucleoprotein (RNP) complex to MDM2 (Dai and Lu, 2004). By this, MDM2 is inactivated and cannot degrade the Tp53 molecule (Fig. 2B). Downstream, Tp53 stabilization results in apoptosis and cell cycle arrest - a hypo-proliferative state (Dai and Lu, 2004; Fumagalli et al., 2012; Schreiner et al., 2022; Sulima et al., 2019; Zhang and Lu, 2009).

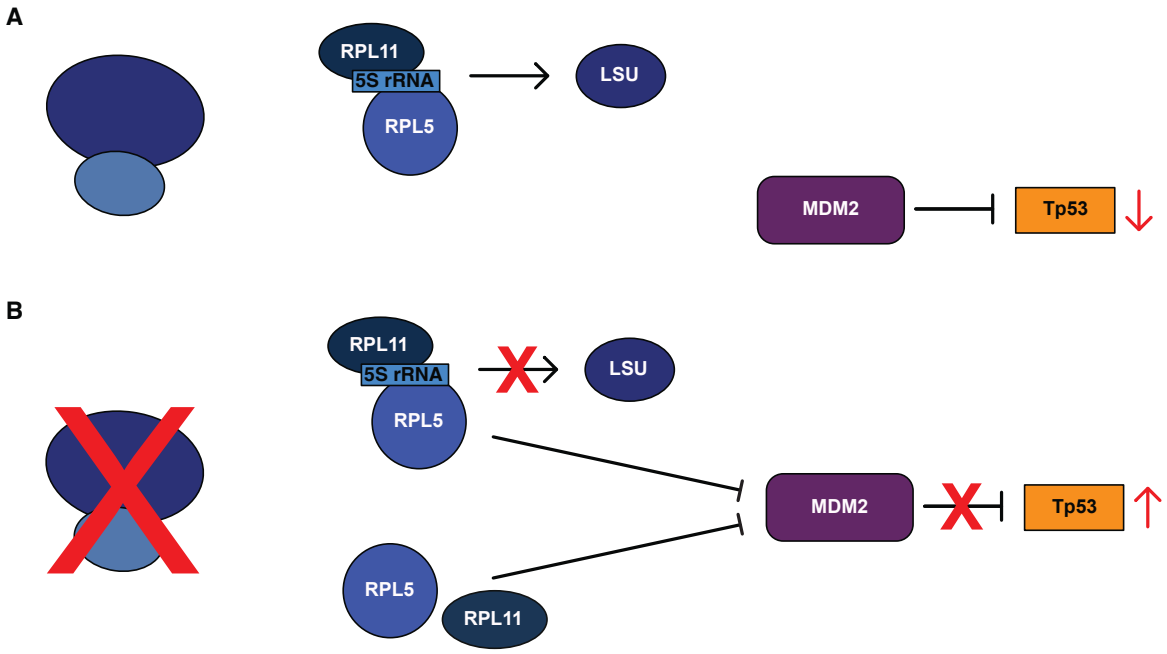


**Figure 2: 5S RNP complex and MDM2/Tp53 pathway during normal conditions and nucleolar stress.** **A** During functional ribosomal biogenesis, Rpl5, Rpl11, and 5S rRNA assemble to the 5S RNP complex, which is incorporated into the large ribosomal subunit. **B** During nucleolar stress, ribosomal biogenesis is perturbed. Therefore, an increased number of free RPs (Rpl11 and Rpl5) and 5S RNP complexes not incorporated into the ribosome occur. Free Rpl5, free Rpl11, or free 5S RNP complex bind to MDM2 leading to its inhibition. MDM2 cannot ubiquitinylate Tp53 whereby Tp53 accumulates initiating the pro-apoptotic pathway. Abbreviations: LSU, large ribosomal subunit; MDM2, mouse double minute 2; RP, ribosomal protein; rRNA, ribosomal RNA; Tp53, tumor protein p53.

Studies in frogs, zebrafish, and mice have shown that some clinical manifestations, e.g., craniofacial malformations, can be rescued upon co-depletion of Tp53 (Calo et al., 2018; Griffin et al., 2015; Jones et al., 2008). Eventually, by a selective pressure towards loss-of-function mutations in Tp53 by the process of cellular compensation, the cells may enter a state of hyper-proliferation (Ajore et al., 2017).

Nucleolar stress and the successive increased number of free RPs also affect MYC proto-oncogene (c-Myc) and its pathways. c-Myc drives transcriptional activity of the three RNA polymerases (Pol I-III) necessary for ribosomal synthesis (Fig. 3A) (Arabi et al., 2005; Gomez-Roman et al., 2003; van Riggelen et al., 2010). Hence, c-Myc is a crucial molecule in this process and majorly contributes to the synthesis of new ribosomes.

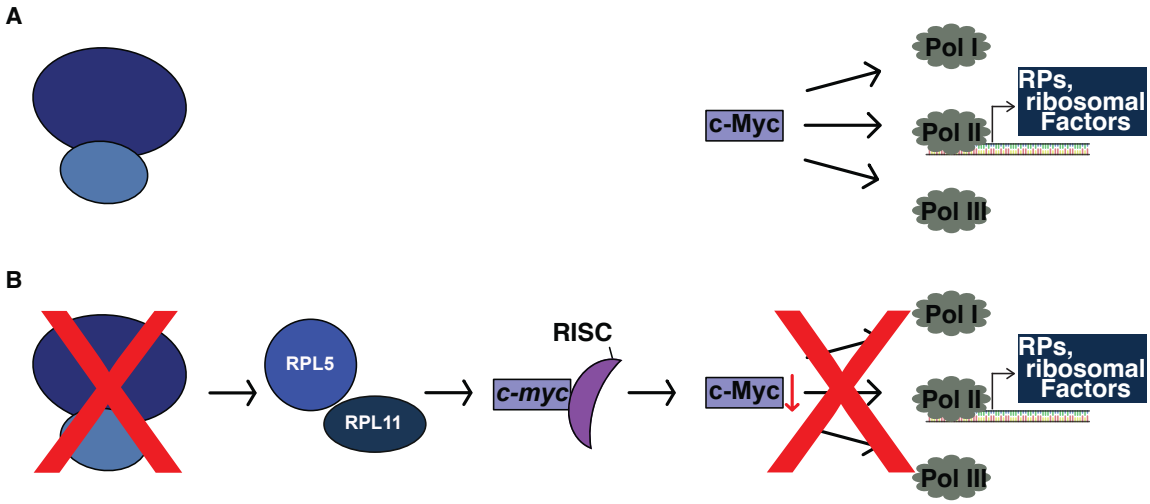


**Figure 3: c-Myc pathway during normal conditions and during disturbed ribosomal biogenesis.**
**A** During functional ribosmal biogenesis, c-Myc enhances the transcriptional activity of the three RNA polymerases I-III. **B** When ribosomal biogenesis is disturbed, the increased number of free RPs, Rpl5 and Rpl11, recruits *c-myc* RNA to RISC. Consequently, c-Myc cannot enhance polymerase activity. Abbreviations: c-MYC, MYC protooncogene; Pol, polymerase; RISC, RNA-induced silencing complex; RP, ribosomal protein.

Liao and colleagues showed in human cells that free Rpl5 or Rpl11 - resulting from impaired ribosomal biogenesis - accumulate and bind to *c-myc* RNA. Next, *c-myc* is transported to the RNA-induced silencing complex (RISC) where it is degraded (Fig. 3B). Furthermore, they showed that consequently the overexpression of *rpl5* leads to a reduction of *c-myc* RNA, whereas Rpl5 knockdown increases c-Myc levels (Liao et al., 2014).

Impaired ribosome biogenesis is further accompanied by dysfunctional ribosomes and a reduced number of functional ribosomes. Dysfunctional ribosomes might result in altered translation and so-called specialized ribosomes, which furthermore contribute to the pathophysiology of ribosomopathies. Specialized ribosomes are one theory by which changes in ribosome structure and composition lead to further abilities in naturally occurring diverse ribosomes in distinct tissues (Genuth and Barna, 2018). These specialized ribosomes might eventually alter the translation from a tumor-suppressive to oncogene-favoring translation (Aspesi and Ellis, 2019; Farley-Barnes et al., 2019; Sulima et al., 2019).
Another hypothesis by which altered or reduced ribosome biogenesis can contribute to manifestations of ribosomopathies is the ribosome concentration hypothesis. It is based on the theory that the translation of specific mRNAs may be sensitive to

decreased ribosome concentration, which might lead to differences in the translational landscape (Mills and Green, 2017).

A lot of effort has been made to elucidate the exact underlying mechanisms of the pathophysiology of ribosomopathies. Besides nucleolar stress and altered translation, it is possible that RPs and ribosomal biogenesis factors further contribute to this pathology by implementing extra-ribosomal functions.
Proteins that implement multiple functions are termed “moonlighting proteins”. Several moonlighting proteins have been found that indeed exert extra-ribosomal functions. Many extra-ribosomal functions include the contribution of RPs to the pathology of cancer (Molavi et al., 2019). Furthermore, RPs have been shown to be part of immune signaling, e.g., activation of nuclear factor kappa B (NF-kB) by RPS3 (Wan et al., 2007) or viral production reduction (Green et al., 2012).
Activation of the Tp53 apoptotic pathway by binding the Tp53 regulator MDM2 is one function of RPs independent of the ribosome (Dai and Lu, 2004). Additionally, the proto-oncogene c-Myc has been found to be regulated by RPs (Liao et al., 2014).

The molecular basis of ribosomopathies comprises a wide variety of different defects during ribosome synthesis. Many genes have been found, whose mutations are associated with impaired pre-rRNA transcription, pre-rRNA processing, or ribosome assembly and therefore resulting in the pathological condition of ribosomopathies. For instance, mutations in *TCOF1* (*treacle ribosome biogenesis factor 1*) result in TCS, mutations in *SBDS* (*SBDS ribosome maturation factor*) result in SDS, and mutations in *RPL5* result in DBA (Jenkinson et al., 2016; Kostjukovits et al., 2017; Valdez et al., 2004; Warren, 2018; Weaver et al., 2015).

## 1.3 Block of proliferation 1

A factor necessary for ribosomal synthesis - and hence a possible contributor to ribosomopathies - is Block of proliferation 1 (Bop1; ribosomal biogenesis factor Bop1) which is encoded in humans by the gene *BOP1*. In humans, *BOP1* is localized on chromosome 8. In the South-African clawed frog, *Xenopus laevis*, which is an important model organism to study human diseases (see chapter 1.6),

*bop1* is located on chromosomes 6S and 6L and is expressed maternally and zygotically (zygotic expression starts around stage 9) (Session et al., 2016). The protein consists of 748 amino acids in humans and 728 amino acids in *Xenopus laevis* including an N-terminal (NT) domain and a WD40 domain (Fig. 4). WD40 repeats consist of approximately 40 amino acids, often terminated with tryptophan and aspartic acid, and are repeated successively (Klein et al., 2002).

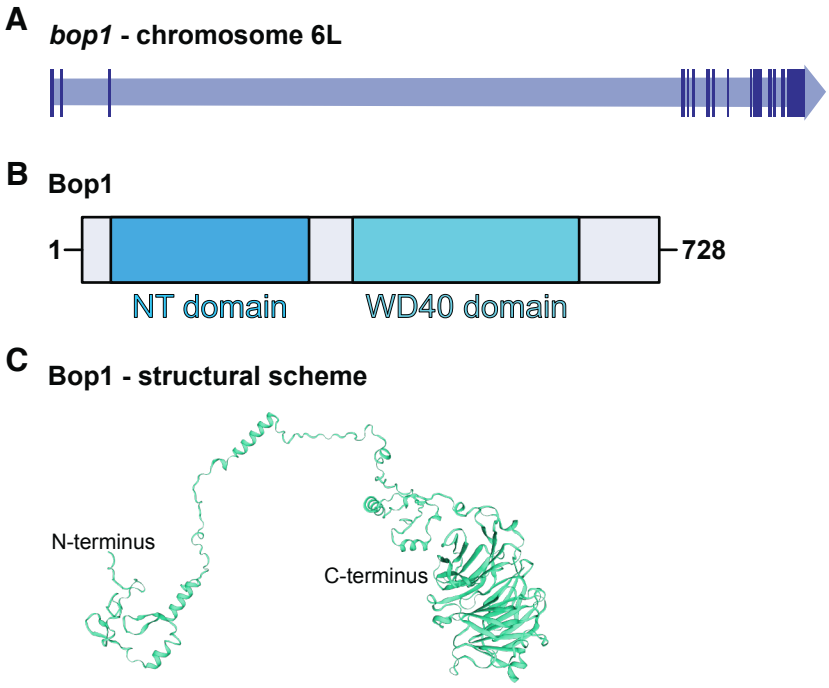


**Figure 4: Block of proliferation 1 in *Xenopus laevis*.**
**A** The gene *bop1* is located on chromosome 6L and 6S, respectively. Here, *bop1* on chromosome 6L is depicted. Dark blue stripes describe exons on the gene. **B** The protein Bop1 consists of 728 amino acids and the two domains, NT domain and WD40 domain. **C** A structural scheme of Bop1 generated using the online tool SWISS-MODEL is depicted (Bienert et al., 2017; Waterhouse et al., 2018). Abbreviation: Bop1, Block of proliferation 1.

During ribosomal biogenesis, Bop1 forms a trimeric complex together with two other proteins, WD repeat domain 12 (WDR12) and Pescadillo homolog 1 (Pes1) (Hölzel et al., 2005; Strezoska et al., 2000). This complex is called Pescadillo-Bop1-WDR12 (PeBoW) complex and is located in the nucleolus. For translocation into the nucleolus, Bop1 requires Pes1 (Rohrmoser et al., 2007). The protein stability of Pes1, WDR12, and Bop1 is interdependent and requires incorporation into the trimeric complex (Kellner et al., 2015).

The integrity of the PeBoW complex is required for rRNA processing; hence, for ribosomal synthesis and cell proliferation (Hölzel et al., 2005; Rohrmoser et al., 2007). In detail, bound into the trimeric complex, Bop1 contributes to the maturation

of the 5.8S rRNA and the 28S rRNA by processing 32S rRNA, which is an intermediate product of the 47S rRNA precursor. Additionally, Strezoska and colleagues have shown that the trimeric complex including Bop1 is also required for processing ITS1, ITS2, and 3'ETS (Strezoska et al., 2002). Consequently, Bop1 is an assembly factor for the 60S ribosomal subunit of the 80S ribosome (Strezoska et al., 2000).

In line with the above-described features of Bop1, previous studies have shown that in mouse-derived cell lines, dominant-negative mutants of Bop1 suffer a cell cycle arrest in the G1 phase, therefore resulting in impaired proliferation (Pestov et al., 2001; Strezoska et al., 2002). Furthermore, Bop1 knockdown leads to drastically decreased protein synthesis in human cell lines (Liu et al., 2014).

Even though the functions of Bop1 lead to the assumption that mutations in the *bop1* gene may lead to a ribosomopathy, Bop1 has not been associated with the disease until today. Nevertheless, Bop1 has been connected to several cancers.

In humans, deregulation of *BOP1* has been associated with colorectal tumorigenesis (Killian et al., 2006; Qi et al., 2016), hepatocellular carcinomas (Chung et al., 2011), and prostate cancer (Vellky et al., 2020). Here, BOP1 intensifies cellular invasiveness and cell migration.

Patients suffering from aortic dissection show lower BOP1 levels in the aortic tissue. Lower BOP1 levels lead to a decreased ribosome biogenesis, which resulted in Tp53-dependent proliferative inhibition, oxidative stress, and apoptosis. Furthermore, this study revealed that overexpression of *BOP1* inhibited apoptosis in human aortic smooth muscle cells (Wu et al., 2019).

Temporal inactivation of Bop1 might also confer cytoprotection against chemotherapeutics in a Tp53-dependent manner and hence could be a possible drug target (Sapio et al., 2017). Furthermore, the loss of BOP1, which occurs during several melanomas, is associated with drug resistance to BRAF kinase inhibitors due to an activation of the mitogen-activated protein kinase (MAPK) pathway (Gupta et al., 2019).

## 1.4 Ribosomal protein L5

Rpl5 is encoded by the gene *RPL5*, transcribed by RNA Pol II and has been shown to lead to the ribosomopathy DBA when mutated (Cmejla et al., 2009; Gazda et al., 2008; Quarello et al., 2010). The gene is localized on chromosome 1 in humans and in *Xenopus laevis*, on chromosomes 4S and 4L, respectively, and is maternally and zygotically expressed throughout the embryonic development. *Xenopus laevis* Rpl5 consists of 296 amino acids (Fig. 5); the human RPL5 consists of 297 amino acids (Wormington, 1989).

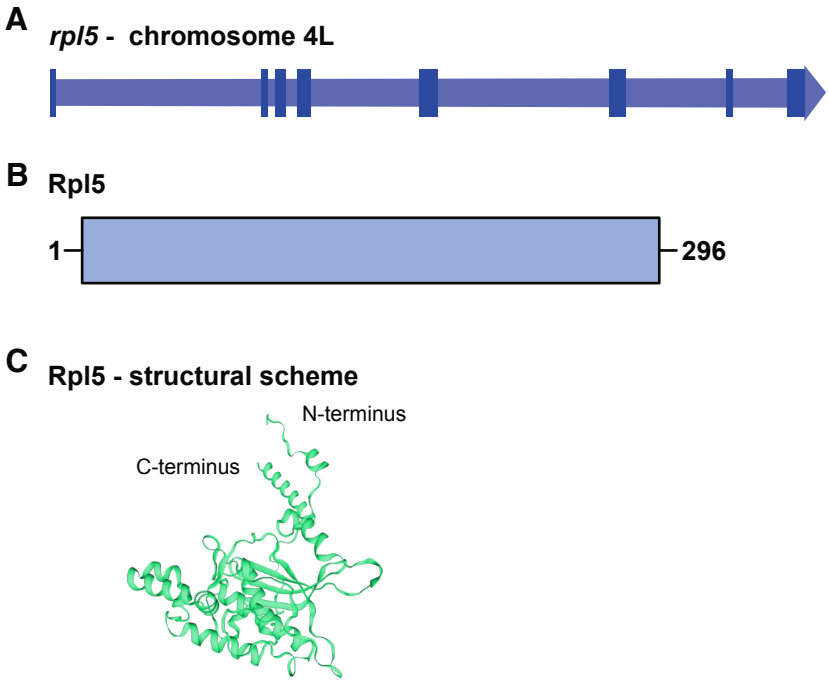


**Figure 5: Ribosomal protein L5 in *Xenopus laevis*.**
**A** The gene *rpl5* is located on chromosome 4L and 4S, respectively. Here, *rpl5* on chromosome 4L is depicted. Dark blue stripes describe exons on the gene. **B** The protein Rpl5 consists of 296 amino acids. **C** A structural scheme of Rpl5 generated using the online tool SWISS-MODEL is depicted (Bienert et al., 2017; Waterhouse et al., 2018). Abbreviation: Rpl5, Ribosomal protein L5.

Upon translation of Rpl5 in the cytoplasm, it is transported to the nucleolus. This transport is facilitated by the transport adaptor Symportin 1, which simultaneously translocates Rpl11 (Kressler et al., 2017). In the nucleolus, Rpl5 assembles to the 5S-RNP complex together with Rpl11 and 5S rRNA. This intermediate RNP complex is later incorporated into the large ribosomal subunit (Bange et al., 2013; Kressler et al., 2017; Zhang et al., 2007).

Mutations in the *RPL5* gene are associated with DBA. Epidemiologically, this ribosomopathy occurs in 7 out of 1 000 000 live births and is usually diagnosed before an age of 1 (Vlachos et al., 2008). In general, the genotype of DBA is very heterogenous, thus 20 genes have been identified whose mutation results in the pathological condition of DBA (Da Costa et al., 2020). Around 25% of DBA cases show heterozygous mutations in *RPS19*. In second place of gene mutation frequency is *RPL5* with 7%. All found mutations are heterozygous - homozygous mutations are most likely lethal - leading to haploinsufficiency (Cmejla et al., 2009; Gazda et al., 2008; Quarello et al., 2010; Ulirsch et al., 2018).

As mentioned above, Tp53 is a major contributor to the pathology of ribosomopathies, such as DBA. Previous studies showed that mutations in *RPS19*, *RPL5*, or *RPL11* lead to Tp53 pathway activation in mice, fish, and human cell lines (Chakraborty et al., 2009; Danilova et al., 2008; Devlin et al., 2010; Dutt et al., 2011; McGowan et al., 2008)

## 1.5 *Xenopus laevis* as model organism for embryonic development and established methods for gene editing

The South-African clawed frog, *Xenopus laevis*, is one of the oldest model organisms to study embryogenesis and congenital diseases. It is an allotetraploid species that emerged around 17-18 million years ago from a hybridization event between two diploid progenitors (Session et al., 2016). First mentioned in 1802 by Daudin (Daudin, 1802), *Xenopus laevis* has evolved into a suitable model organism to study human diseases.

At the basal level, genes between different vertebrates (e.g., humans and frogs) are highly conserved (Blum and Ott, 2018). Hence, the many advantages of *Xenopus laevis* can be used to gain a deeper understanding of human diseases.

The husbandry of adult *Xenopus laevis* is easy and unelaborate. The frogs are robust and ovulation of female frogs can be initiated by injection of human chorionic gonadotropin (hCG) enabling independence of natural and seasonal reproduction and facilitating studies at any given time point. The clutch size of *Xenopus laevis* reaches up to 2000 eggs per day, which are 1-1.2 mm in size. This allows easy manipulation of a large number of embryos (Sive et al., 2000). Additionally, well-defined cell fate maps exist for *Xenopus laevis* embryos, which makes sole

manipulation of target tissue possible (Fig. 6). As early as 1954, Nieuwkoop and Faber described in detail the developmental stages of *Xenopus laevis*, which are still used by developmental biologists today (Nieuwkoop and Faber, 1954).

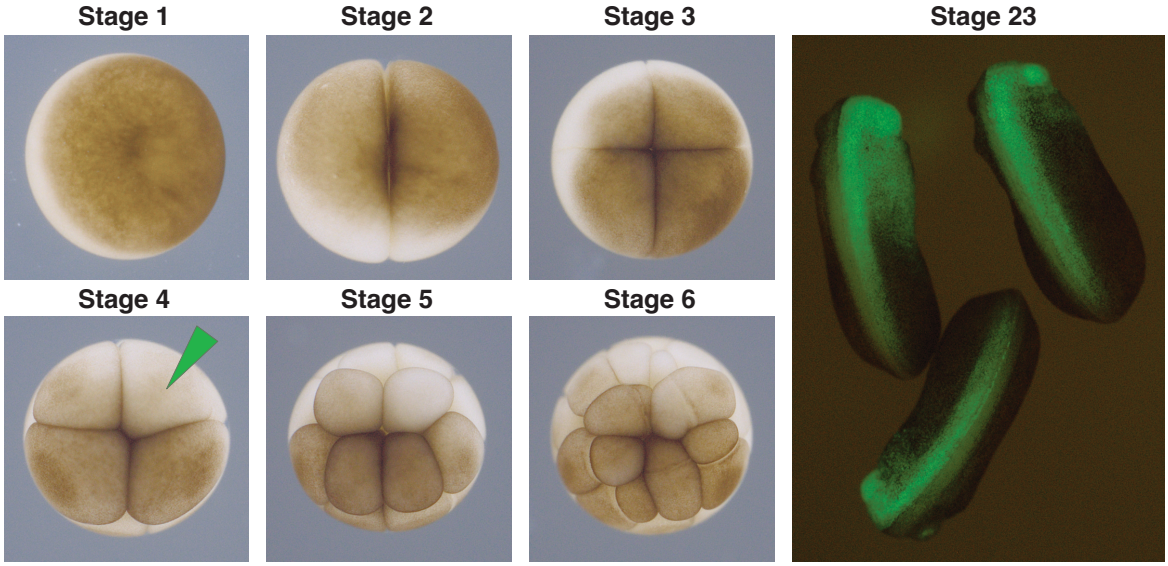


**Figure 6: *Xenopus laevis* developmental stages 1-6 and stage 23 embryos expressing GFP.**
Embryos are staged according to Nieuwkoop and Faber (Nieuwkoop and Faber, 1954). First five cleavage stages are shown (animal views are given). Stage 23 embryos (dorsal view) were injected using *GFP* RNA into one animal-dorsal blastomere at eight-cell stage. This blastomere is indicated by a green arrow at stage 4. By injection into an animal-dorsal blastomere only anterior neural tissue is targeted (indicated by fluorescence). Abbreviation: GFP, green fluorescent protein; RNA, ribonucleic acid.

Furthermore, embryonic development takes place *ex utero* facilitating easy manipulation and observation throughout the entire developmental process.

A variety of methods exist by which gene expression can be altered in *Xenopus laevis*. Gain-of-function experiments of genes can be achieved by microinjection of *in vitro* generated mRNA. For loss-of-function experiments, morpholino oligonucleotides (MO) are a suitable *antisense*-based approach in which short oligonucleotides containing about 25 nucleotides induce a knockdown of the targeted gene. Upon microinjection, MOs hybridize to the complementary mRNA with high affinity - regardless of whether mRNA is maternally supplied or zygotically transcribed - and thus prevents translation into the protein by steric inhibition (Summerton and Weller, 1997). The mode of action of MOs is depicted in figure 7.

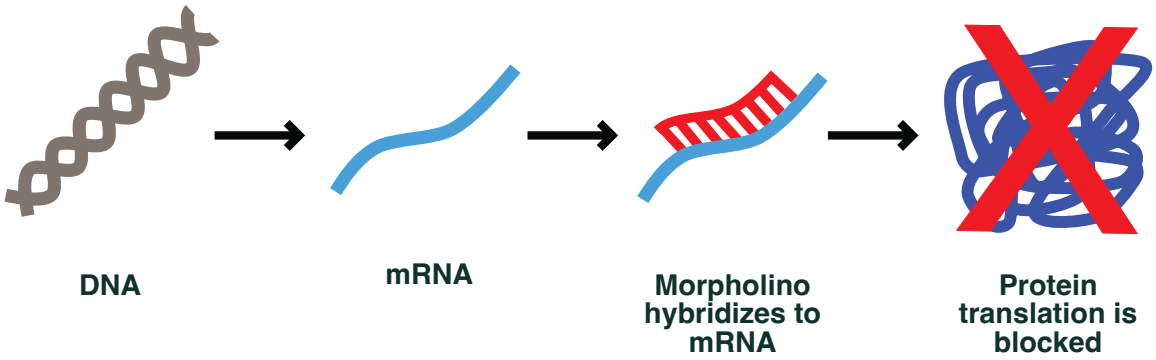


**Figure 7: Morpholino oligonucleotide mode of action.**
In a first step, DNA is transcribed into mRNA. Synthetic MOs hybridizes to its complementary mRNA and thereby inhibit protein translation via steric blockage. Abbreviations: DNA, desoxyribonucleic acid; MO, morpholino oligonucleotide; mRNA, messenger ribonucleic acid.

The clustered regularly-interspaced short palindromic repeats (CRISPR) / CRISPR-associated proteins (Cas) system is another method by which gene expression can be altered. Here, alteration is implemented on the genomic level. The CRISPR/Cas system is adapted from the bacterial immune system for scientific approaches. Here, it is part of the adaptive defense mechanism against bacteriophages (Hryhorowicz et al., 2017). In science, it is used for directed knock-ins as well as knock-outs.

The best-studied system is the CRISPR/Cas9 system. Here, the RNA-guided DNA endonuclease Cas9 originates from *Streptococcus pyogenes*. CRISPR RNA (crRNA), which is the complementary sequence of the target DNA (~20 nucleotides), and trans-activating CRISPR RNA (trcrRNA) are fused to one guide RNA (gRNA). The gRNA and Cas9 form an RNP complex. For the gRNA to recruit Cas9 to the target site, the genomic target sequence must be followed by a protospacer adjacent motif (PAM) sequence (nucleotides: nGG; n can be any nucleotide). Cas9 induces a cleavage around 4 base pairs (bp) upstream of the PAM sequence. This DNA cleavage is then repaired by non-homologous end joining, which is a repair mechanism by which nucleotides are inserted and/or deleted randomly and by which mutations are induced into the target gene (Hryhorowicz et al., 2017; Nakayama et al., 2014). The mode of action of the CRISPR/Cas9 system is shown in figure 8.

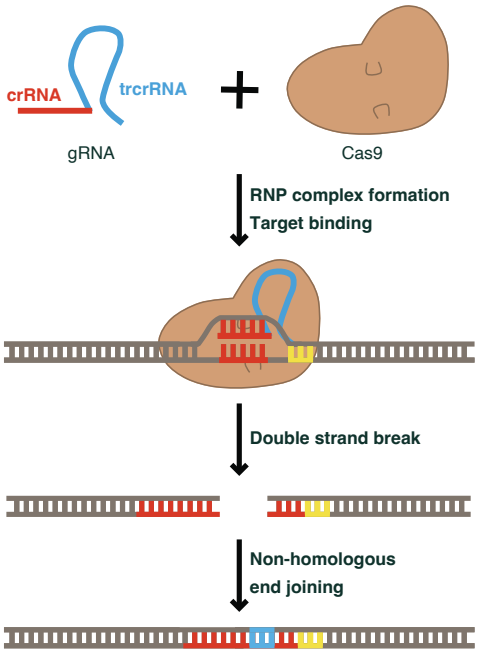


**Figure 8: CRISPR/Cas9 system mode of action.**
In the beginning, gRNA, which contains the complementary sequence of the genomic target site (red part), forms a ribonucleoprotein complex together with Cas9. Further, the gRNA recruits the Cas9 to the target site which is recognized by the help of the PAM sequence (yellow bases). The Cas9 endonuclease induces a double strand break, which is repaired in a final step via non-homologous end joining (repaired bases in blue). Abbreviations: Cas, CRISPR associated protein; CRISPR, clustered regularly-interspaced short palindromic repeat; crRNA, CRISPR RNA; gRNA, guide RNA; RNA, ribonucleic acid; PAM, protospacer adjacent motif; trcrRNA, trans-activating CRISPR RNA.

## 1.6 *Xenopus laevis* as model organism for the study of ribosomal proteins

Mature *Xenopus laevis* oocytes have a maternal supply of mRNAs, proteins, and around $10^{12}$ ribosomes (Brown and Gurdon, 1964; Wallace, 1960). Hence, the early embryonic development of *Xenopus laevis* is independent of zygotic synthesis and does not require *de novo* ribosomal biogenesis. This was shown in the anucleolate mutant, which is a homozygous mutant that lacks rDNA clusters and therefore cannot synthesize the rRNA precursor and eventually ribosomes. Nevertheless, these mutant embryos survive until swimming tadpole stage (~stage 26) (Brown, 1964; Pierandrei-Amaldi and Amaldi, 1994).

Even though *Xenopus laevis* is presumably independent of ribosomal biogenesis, mRNAs of RPs and ribosomal factors, such as *bop1* mRNA or *rpl5* mRNA, exist throughout the early embryonic development at low levels (Briggs et al., 2018;

Pierandrei-Amaldi and Amaldi, 1994; Session et al., 2016). This gives rise to the question of whether these RPs and ribosomal factors might implement additional functions - hence, are moonlighting proteins -, which are independent of ribosomal biogenesis.
Previous studies conducted in the working group of PD Dr. Susanne Kühl identified the complex partner of Bop1, Pes1, to carry out extra-ribosomal functions during *Xenopus laevis* pronephric and neural development (Gessert et al., 2007; Tecza et al., 2011). Furthermore, Peter pan homolog (Ppan), which is an interaction partner of Pes1, carries out extra-ribosomal functions during early embryonic development in *Xenopus laevis* (Bugner et al., 2011). These studies showed that the knockdown of respective mRNAs resulted in early phenotypes, which were not found upon inhibiting pre-rRNA processing by microinjection of an ITS2 MO (IT2 MO inhibits cleavage of 5.8S rRNA from ITS2) (Bugner et al., 2011). Hence, these proteins implement functions independent of ribosomal biogenesis.

These findings give rise to the question whether Bop1 or Rpl5 also exert extra-ribosomal functions which may further contribute to the pathology of ribosomopathies or other diseases like cancer.

## 1.7 *Xenopus laevis* neural development

In *Xenopus laevis,* the development of the anterior neural tissue starts with the induction of the anterior neural plate immediately after gastrulation. In this area, the eye field is induced that later splits into the two eye anlagen during neurulation. Optic vesicles which induce lens placodes in the overlying ectoderm are formed by the diencephalon. By invagination of the optic vesicles and lens placodes the optic cups including the retinal pigmented epithelium and the neural retina are formed (Chow and Lang, 2001). At the end of neurulation, anterior neural crest cells (NCCs) undergo an epithelial-mesenchymal transition (EMT), migrate ventrally and further differentiate into diverse structures such as the cranial cartilage. Simultaneously, the primary brain vesicles are developed by the anterior neural tube (Chow and Lang, 2001): the prosencephalon, which is further divided into the telencephalon and the diencephalon, the mesencephalon, and the rhombencephalon, that divides into the metencephalon and the myelencephalon.

For *Xenopus laevis*, several marker genes exist which can be utilized for analyzing the induction and differentiation of specific tissues. For instance, *sox3* (*SRY-box transcription factor 3*) is a pan-neural marker gene (Maurus et al., 2005), *rax* (*retina and anterior neural fold homeobox*) and *pax6* (*paired box protein 6*) can be used as marker genes for eye- and brain development (Furukawa et al., 1997; Hollemann et al., 1998), and *foxd3* (*forkhead box d3*) is a marker gene for the NCCs (Pohl and Knöchel, 2001).

## 1.8 Aim of the study

Ribosomal biogenesis is a major biological process involving hundreds of different proteins and factors. Defects in ribosomal biogenesis can lead to life-threatening diseases and even though extensive studies have been conducted remaining questions still exist. Therefore, following objectives were addressed in the here presented study.

1) Does Bop1 depletion via morpholino oligonucleotides or the CRISPR/Cas9 system affect embryonic development of *Xenopus laevis*? Does Bop1 implement functions which are independent of the ribosome?
2) Does the knockdown of Rpl5 affect embryonic development in *Xenopus laevis*? Are the arising phenotypes comparable between *Xenopus laevis* and humans? Which mechanisms contribute to the phenotype?

To approach these open questions, the two proteins Bop1 and Rpl5 were investigated during the early development of the model organism *Xenopus laevis*.
The first aim was to deepen previous analyses of the spatio-temporal expression of the ribosomal biogenesis factor Bop1 and analyses of loss-of-function experiments. Furthermore, the molecular mechanism underlying the Bop1 phenotype as well as a possible extra-ribosomal function were investigated.
The second aim was to investigate the RP Rpl5 during the early embryonic development of *Xenopus laevis* and to extend previous work on this protein accomplished in the working group of PD Dr. Susanne Kühl. Therefore, *rpl5* expression was analyzed, loss-of-function studies were carried out, and downstream pathways were investigated to elucidate the molecular background of the Rpl5 MO-induced phenotype.

# 2 Material and Methods

## 2.1 Material

### 2.1.1 Organisms

#### 2.1.1.1 *Xenopus laevis*

Mature female and male *Xenopus laevis* were purchased from Nasco (Wisconson, USA). The Tierforschungszentrum of Ulm University took care of the frogs. All here performed experiments were reviewed and approved by German state administration Baden-Württemberg (Regierungspräsidium Tübingen; License No.: I.89 and I.92).

#### 2.1.1.2 Bacterial strain

*Escherichia coli* (*E. coli*) One Shot TOP10 from Invitrogen (Carlsbad, USA) were used for DNA recombination experiments in this study.

### 2.1.2 DNA and oligonucleotides

#### 2.1.2.1 Primers

Primers for polymerase chain reactions (PCR), real-time quantitative PCR (qPCR), and sequencing are listed in table 1.

**Table 1: List of primers used for polymerase chain reactions (PCR), real-time quantitative PCRs (qPCR), sequencing, and respective sequences.**

| Primer | Sequence |
|---|---|
| bop1 gRNA #1 6L-for. | 5'-GTA TGT TCC ATC TCA CTT CCT GC-3' |
| bop1 gRNA #1 6L-rev. | 5'-GTA CCA GTG CAG GGA AAC AAT-3' |
| bop1 gRNA #1 6S-for. | 5'-TCT CTT CCC CTG TTG GCT CCT-3' |
| bop1 gRNA #1 6S-rev. | 5'-AAG ACA TGT AGC GGC AGT GTA A-3' |
| bop1 gRNA #2+#3 6L+6S-for. | 5'-GGA GCT CCT CCC TTG CAC ATA TC-3' |
| bop1 gRNA #2+#3 6L+6S-rev. | 5'-GGC ACA GAC CTT CTG GTG TTT-3' |
| c-myc-for. | 5'-GCA GCC CTG CTT CTT CTT TC-3' |
| c-myc-rev. | 5'-AGC CAC TCC ACA TAC AGT CCT-3' |
| Gapdh-for. | 5'-GCC GTG TAT GTG GAA TCT-3' |
| Gapdh-rev. | 5'-AAG TTG TCG TTG ATG ACC TTT GC-3' |

| Primer | Sequence |
|---|---|
| odc qPCR-for. | 5'-TGC ACA TGT CAA GCC AGT TC-3' (Kietzmann et al., 2012) |
| odc qPCR-rev. | 5'-GCC CAT CAC ACG TTG GTC-3' (Kietzmann et al., 2012) |
| rRNA Precursor-for. | 5'-TCA TCG ACA CTT CGA ACG CA-3' |
| rRNA Precursor-rev. | 5'-GCT TAA ATT CAG CGG GTC GC-3' |
| slc35b1 qPCR-for. | 5'-CGC ATT TCC AAA CAG GCT CC-3' (Mughal et al., 2018) |
| slc35b1 qPCR-rev. | 5'-CAA GAA GTC CCA GAG CTC GC-3' (Mughal et al., 2018) |
| sox2 qPCR-for. | 5'-AAC TCT GCG TCC AAC AAC CA-3' |
| sox2 qPCR-rev. | 5'-TGT GCA TCT TGG GGT TCT CC-3' |
| sox3 qPCR-for. | 5'-GGA TCA GGA TCG GGT GAA GC-3' |
| sox3 qPCR-rev. | 5'-GCT GAT CTC CGA GTT GTG CA-3' |
| tp53-for. | 5'-GCA CCG CAA AGT CTG TTA CC-3' |
| tp53-rev. | 5'-GCG GTT CAT CCC TCC CAT AC-3' |

Primers designed for the MO binding specificity constructs are listed in table 2.

**Table 2: List of primers used for morpholino oligonucleotide binding specificity constructs.**

| Primer | Sequence |
|---|---|
| Bop1 MO2 bs-GFP-for. | 5'-GAT CCG AGA CAG GGA AAA ACG TGT TTC TAC G-3' |
| Bop1 MO2 bs-GFP-rev. | 5'-AAT TCG TAG AAA CAC GTT TTT CCC TGT CTC G-3' |
| Bop1 MO bs Chr.L-GFP-for. | 5'-GAT CCC CCG AGT CCT GAG TGA AAC ATG AAG-3' |
| Bop1 MO bs Chr.L-GFP-rev. | 5'-AAT TCT TCA TGT TTC ACT CAG GAC TCG GGG-3' |
| Bop1 MO2 bs Chr.L-GFP-for. | 5'-GAT CCG AGA CAG GGA GAA ACG TGT TTG TGC G-3' |
| Bop1 MO2 bs Chr.L-GFP-rev. | 5'-AAT TCG CAC AAA CAC GTT TCT CCC TGT CTC G-3' |

All primers were obtained from Biomers (Ulm, Germany).

### 2.1.2.2 Vectors

For generation of injection RNAs the pSC2+ vector (4.1 kb) (Rupp et al., 1994) was used.

### 2.1.2.3 gRNAs and respective oligonucleotides

gRNAs were designed using the online tool CRISPRscan (crisprscan.org) and are depicted in table 3 and 4.

**Table 3: List of designed gRNAs.**
Sequences, exon location, and DNA strand location of gRNAs are given.

| gRNA | Sequence | Exon | DNA strand |
|---|---|---|---|
| bop1 #1 | 5´-GGT ACC TGT GCC CGC GCC AG-3´ | 8 | + |
| bop1 #2 | 5´-GGG ACC AAC CAC TGC CCC GA-3´ | 10 | - |
| bop1 #3 | 5´-GGG CTA CCA GCC CCC CGA GG-3´ | 12 | + |

**Table 4: List of oligonucleotides utilized to generate gRNAs for injection.**

| Oligonucleotide | Sequence |
|---|---|
| forward bop1 #1 | 5´-GCA GCT AAT ACG ACT CAC TAT AgG TAC CTG TGC CCG CGC CAG GTT TTA GAG CTA GAA ATA GCA AG-3´ |
| forward bop1 #2 | 5´-GCA GCT AAT ACG ACT CAC TAT AGg GAC CAA CCA CTG CCC CGA GTT TTA GAG CTA GAA ATA GCA AG-3´ |
| forward bop1 #3 | 5´-GCA GCT AAT ACG ACT CAC TAT AgG GCT ACC AGC CCC CCG AGG GTT TTA GAG CTA GAA ATA GCA AG-3´ |
| reverse oligonucleotide | 5´-AAA AGC ACC GAC TCG GTG CCA CTT TTT CAA GTT GAT AAC GGA CTA GCC TTA TTT TAA CTT GCT ATT TCT AGC TCT AA AAC-3´ (Nakayama et al., 2014) |

Additional bases to increase transcription; T7 Promotor (requires 2 Gs for efficient transcription – lower case = mismatch); Target site without PAM; Backbone (Nakayama et al., 2014)

All oligonucleotides used for gRNAs were ordered from Biomers (Ulm, Germany).

### 2.1.2.4 Whole mount *in situ* hybridization (WMISH) probes

*Antisense* RNA probes were generated from plasmids obtained from the institute's internal plasmid library. *Antisense* RNA probes are listed in table 5.

**Table 5: List of generated *antisense* RNA probes for whole mount *in situ* hybridization (WMISH).**
*Antisense* RNA probes used for WMISH and additional information regarding generation, i.e., restriction enzymes, polymerases (Pol) for transcription, and references.

| Probe | Restriction enzyme | Pol | Reference |
|---|---|---|---|
| *actc1* | *Pvu*II | Sp6 | cDNA clone MGC:52636 IMAGE:4681379 |
| *bop1* | *Not*I | T3 | (Gärtner et al., 2022) |
| *c-myc* | *Hind*III | T7 | (Bugner et al., 2011) |
| *celf1* | *Not*I | Sp6 | (Day and Beck, 2011) |
| *cryba1* | *Not*I | Sp6 | (Day and Beck, 2011) |
| *foxc1* | *Eco*RI | T7 | (Köster et al., 1998) |
| *foxd3* | *Eco*RI | T7 | (Pohl and Knöchel, 2001) |
| *gata2* | *Xba*I | Sp6 | cDNA clone MGC:131004 IMAGE:7978680 |
| *hba3* | *Pst*I | T7 | cDNA clone MGC:64476 IMAGE:6881400 |
| *otx2* | *Not*I | T7 | (Lamb et al., 1993) |
| *pax6* | *Not*I | T7 | (Hitchcock et al., 1996) |
| *prox1* | *Bam*HI | T7 | (Dyer et al., 2003) |
| *rax* | *Xho*I | Sp6 | (Furukawa et al., 1997) |
| *rpl5* | *Not*I | T3 | (Schreiner et al., 2022) |
| *shh* | *Not*I | T3 | provided by Thomas Hollemann |
| *snai2* | *Cla*I | Sp6 | provided by Michael G. Sargent (clone ID: pMX363) |
| *sox2* | *Eco*RI | T7 | sequence ID: LC164013.1 |
| *sox3* | *Hind*III | T3 | (Maurus et al., 2005) |
| *twist1* | *Xba*I | T7 | (Gessert et al., 2007) |
| *tp53* | *Bam*HI | T7 | (Schreiner et al., 2022) |

#### 2.1.2.5 *Sense* RNAs for injection

*Sense* RNAs for injection (listed in table 6) were generated from plasmids obtained from the institute's internal plasmid library.

**Table 6: List of generated *sense* RNAs for injection.**
*Sense* RNAs and additional information for generation, i.e., linearization (Lin.) enzymes, polymerases (Pol) for transcription, and references.

| RNA | Lin. enzyme | Pol | Reference |
|---|---|---|---|
| *Δ5'UTR bop1MO bs-GFP* | *Not*I | Sp6 | (Gärtner et al., 2022) |
| *bop1* | *Not*I | Sp6 | (Gärtner et al., 2022) |
| *bop1 MO bs-GFP* | *Not*I | Sp6 | (Gärtner et al., 2022) |
| *bop1 MO bs chr.L-GFP* | *Not*I | Sp6 | (Gärtner et al., 2022) |
| *bop1 MO2 bs-GFP* | *Not*I | Sp6 | (Gärtner et al., 2022) |
| *bop1 MO2 bs chr.L-GFP* | *Not*I | Sp6 | (Gärtner et al., 2022) |
| *c-myc* | *Not*I | Sp6 | (Bugner et al., 2011) |
| *foxd3* | *Not*I | Sp6 | (Pohl and Knöchel, 2001) |
| *GFP* | *Not*I | Sp6 | Prof. Dr. Dr. W. Knöchel (Ulm, Germany) |
| *hBCL2* | *Sfi*I | T3 | (Bugner et al., 2011) |
| *pax6* | *Not*I | Sp6 | Provided by Thomas Hollemann (Acc. No. U76386.1) |
| *tp53* | *Not*I | Sp6 | (Hampp et al., 2016) |

#### 2.1.2.6 Morpholino oligonucleotides

*Antisense* MOs (listed in table 7) were purchased from Gene Tools LLC (Philomath, USA) and diluted in DEPC-$H_2O$.

**Table 7: List of *antisense* morpholino oligonucleotides (MOs) that were used in this study and MO-specific references.**

| MO | Sequence | Reference |
|---|---|---|
| Bop1 MO | 5´-TTC ATG TCT CAC TCA GGG CTC GGG-3´ | (Gärtner et al., 2022) |
| Bop1 MO2 | 5´-GTA GAA ACA CGT TTT TCC CTG TCT C-3´ | (Gärtner et al., 2022) |

| MO | Sequence | Reference |
|---|---|---|
| c-Myc MO | 5´-TGG GAA AAT TGG CGT TAA GAG GCA T-3´ | (Bellmeyer et al., 2003) |
| Control MO | 5´-CCT CTT ACC TCA GTT ACA TTT ATA-3´ | (Summerton, 1999) |
| Pax6 MO | 5´-GCT GTG ACT GTT CTG CAT GTC GAG-3´ | (Rungger-Brändle et al., 2010) |
| Rpl5 MO | 5´-CAT TTT GCT CTA TTT TGT CCC GTC G-3´ | (Schreiner et al., 2022) |
| Tp53 MO | 5´-CCA TGC CGG TCT TCA GAG GAA GGT TC-3´ | (Cordenonsi et al., 2003) |

### 2.1.3 Antibodies, recombined proteins, and enzymes

**Table 8: List of antibodies and used working dilutions.**

| Antibody | Working dilution | Manufacturer |
|---|---|---|
| Anti-Digoxygenin-AP-Fab Fragments | 1:10 000 | Roche, Basel, Switzerland |
| Anti-phospho Histone H3 (Ser10) | 1:100 | Merck Millipore, Billerica, USA |
| Anti-Rabbit-IgG-AP | 1:1000 | Sigma-Aldrich, St. Louis, USA |

**Table 9: List of recombined proteins and enzymes used in the present study.**

| Recombined protein / Enzyme | Manufacturer |
|---|---|
| Cas9 protein (CP01) | PNA Bio, Newbury Park, USA |
| human Chorionic Gonadotropin | NOVITEC, Freiburg, Germany |
| DNase I (RNase free) | Roche, Basel, Switzerland |
| Lysozyme | Roth, Karlsruhe, Germany |
| Pfu DNA Polymerase (500U) | Promega; Fitchburg, USA |
| Phire Hot Start II DNA Polymerase | Thermo Fisher Scientific, Waltham, USA |
| Proteinase K | Roche, Basel, Switzerland |
| RNase A | Roche, Basel, Switzerland |

| Recombined protein / Enzyme | Manufacturer |
|---|---|
| RNase T1 | Roche, Basel, Switzerland |
| RNaseOut, recombinant ribonuclease inhibitor | Invitrogen, Carlsbad, USA |
| shrimp alkaline phosphatase | USB, Cleveland, USA |
| Sp6 RNA Polymerase | Roche, Basel, Switzerland |
| Superscript II | Invitrogen, Carlsbad, USA |
| T3 RNA Polymerase | Roche, Basel, Switzerland |
| T7 RNA Polymerase | Roche, Basel, Switzerland |

All restriction enzymes were obtained from New England Biolabs (Ipswich, USA).

### 2.1.4 Antibiotics

**Table 10: Antibiotics and utilized working concentrations.**

| Antibiotic | Working concentration | Manufacturer |
|---|---|---|
| Ampicillin | 50 µg/ml | Roth, Karlsruhe, Germany |
| Gentamycin | 50 µg/ml | Sigma-Aldrich, St. Louis, USA |
| Nystatin | 50 U/ml | Sigma-Aldrich, St. Louis, USA |

### 2.1.5 Chemicals and reagents

**Table 11: List of chemicals used in the present study.**

| | Chemical | Manufacturer |
|---|---|---|
| A | acetic acid | Merck Millipore, Billerica, USA |
| | acetic anhydride | Sigma-Aldrich, St. Louis, USA |
| | agarose | Lonza, Basel, Switzerland |
| B | ß-mercaptoethanol | Sigma-Aldrich, St. Louis, USA |
| | blocking reagent | Roche, Basel, Switzerland |
| | BM-purple AP substrate precipitating | Roche, Basel, Switzerland |
| | boric acid ($H_3BO_3$) | Sigma-Aldrich; St. Louis; USA |
| | bovine serum albumin (BSA) | Biofroxx, Einhausen, Germany |
| | bromphenol blue | Merck Millipore, Billerica, USA |

| | Chemical | Manufacturer |
|---|---|---|
| | 5-bromo-4-chloro-3-indolyl phosphate (BCIP) | Roche, Basel, Switzerland |
| C | calcium chloride ($CaCl_2$) | Sigma-Aldrich, St. Louis, USA |
| | Chaps | Roth, Karlsruhe, Germany |
| | chloroform | Merck Millipore, Billerica, USA |
| | cycloheximide | ENZO Life Sciences, Farmingdale, USA |
| | L-Cysteine monohydrate hydrochloride | Sigma-Aldrich, St. Louis, USA |
| D | deoxynucleotide triphosphate (dNTPs) | Invitrogen, Carlsbad, USA |
| | diethylpyrocarbonate (DEPC) | Sigma-Aldrich, St. Louis, USA |
| | DIG RNA Labeling Mix | Roche, Basel, Switzerland |
| | digoxigenin-11-dUTP | Roche, Basel, Switzerland |
| | dimethyl sulfoxide (DMSO) | Roth, Karlsruhe, Germany |
| E | ethylenediaminetetraacetic acid (EDTA) | Applichem, Darmstadt, Germany |
| | ethylene glycol tetraacetic acid (EGTA) | Sigma-Aldrich, St. Louis, USA |
| | ethanol, absolute | Sigma-Aldrich, St. Louis, USA |
| F | fetal bovine serum (FBS) | Gibco, Waltham, USA |
| | fetal calve serum (FCS) | Invitrogen, Carlsbad, USA |
| | Ficoll™ PM 400 | GE-Healthcare, Little Chalfont, UK |
| | formaldehyde, 37% | AppliChem, Darmstadt, Germany |
| | formamide, deionized | AppliChem, Darmstadt, Germany |
| G | gelatin from bovine skin | Sigma-Aldrich, St. Louis, USA |
| | GeneRuler™DNA Ladder Mix | Fermentas, Waltham, USA |
| | L-glutamine | Sigma-Aldrich, St. Louis, USA |
| | glutaraldehyde, grade I, 25% | Sigma-Aldrich, St. Louis, USA |
| | glycerin | Roth, Karlsruhe, Germany |
| | glycerol | Sigma-Aldrich, St. Louis, USA |
| | glycin | AppliChem, Darmstadt, Germany |

| | Chemical | Manufacturer |
|---|---|---|
| H | 4-(2-hydroxyethyl)-1-piperazineethansulforic acid (HEPES) | AppliChem, Darmstadt, Germany |
| | $H_2O_{ultrapure}$ (DNAse/RNAse free) | Thermo Fisher Scientific, Waltham, USA |
| | horse serum, heat inactivated | Gibco, Waltham, USA |
| | hydrochloric acid | Sigma-Aldrich, St. Louis, USA |
| | hydrogen chloride (HCl) | Roth, Karlsruhe, Germany |
| | hydrogen peroxide, 30% ($H_2O_2$) | Otto Fischar, Saarbrücken, Germany |
| I | isopropanol | Avantor Chemicals |
| L | LB Agar | Invitrogen, Carlsbad, USA |
| | LB Broth base | Invitrogen, Carlsbad, USA |
| | Leibovitz's L-15 Media | GIBCO |
| M | magnesium chloride ($MgCl_2$) | Merck Millipore, Billerica, USA |
| | maleic acid | Merck Millipore, Billerica, USA |
| | methanol | Sigma-Aldrich, St. Louis, USA |
| | methyl cellulose | Sigma-Aldrich, St. Louis, USA |
| | Midori Green Advance DNA stain | Biozym, Oldendorf, Germany |
| | MOPS | Sigma-Aldrich, St. Louis, USA |
| N | 4-Nitro blue tetrazolium chloride (NBT) | Roche, Basel, Switzerland |
| P | paraformaldehyde (PFA) | Merck Millipore, Billerica, USA |
| | phenylmethylsulfonyl fluoride (PMSF) | Sigma-Aldrich, St. Louis, USA |
| | potassium chloride (KCl) | Merck Millipore, Billerica, USA |
| R | RNA, torula yeast type VI | Sigma-Aldrich, St. Louis, USA |
| | random primer | Invitrogen, Carlsbad, USA |
| S | saccharose | Fluka, St. Louis, USA |
| | selective agar | Invitrogen, Carlsbad, USA |
| | sodium chloride (NaCl) | Sigma-Aldrich, St. Louis, USA |
| | sodium dodecyl sulfate (SDS) | Roth, Karlsruhe, Germany |
| | sodium hydroxide (NaOH) | Merck Millipore, Billerica, USA |
| | sucrose | Merck Millipore, Billerica, USA |

| | Chemical | Manufacturer |
|---|---|---|
| | super optimal broth (S.O.C) media | Inresa Arzneimittel GmbH, Freiburg, Germany |
| T | Titriplex III | Merck Millipore, Billerica, USA |
| | transcription buffer | Roche, Basel, Switzerland |
| | tricaine methanesulfonate (MS222) | Sigma-Aldrich, St. Louis, USA |
| | triethanolamine 98% | Sigma-Aldrich, St. Louis, USA |
| | tris base | AppliChem, Darmstadt, Germany |
| | 2,4,6-tris(dimethylaminomethyl)phenol | Fluka, St. Louis, USA |
| | Triton X-100 | Merck Millipore, Billerica, USA |
| | Tween®20 | Merck Millipore, Billerica, USA |
| X | XGal 5 | Peqlab, Erlangen, Germany |
| Y | 2x YT media | Roth, Karlsruhe, Germany |

### 2.1.6 Commercial kits

**Table 12: Commercial kits that were utilized in this study.**

| Commercial kit | Manufacturer |
|---|---|
| 5-Bromo-2´-deoxy-uridine (BrdU) Labeling Mix and Detection kit | Roche, Basel, Switzerland |
| IllustraTM MicroSpinTM G-50 columns | GE-Healthcare, Little Chalfont, UK |
| Ligate-IT-Rapid Ligation kit | USB, Cleveland, USA |
| MEGAshortscript T7 Transcription kit | Thermo Fisher Scientific, Waltham, USA |
| mMESSAGE mMACHINE Sp6 kit | Thermo Fisher Scientific, Waltham, USA |
| mMESSAGE mMACHINE T3 kit | Thermo Fisher Scientific, Waltham, USA |
| mMESSAGE mMACHINE T7 kit | Thermo Fisher Scientific, Waltham, USA |
| peqGOLD RNApure™ | Peqlab, Erlangen, Germany |
| Plasmid Midi kit | Qiagen, Hilden, Germany |
| Plasmid Maxi kit | Qiagen, Hilden, Germany |
| QIAquick Gel Extraction kit | Qiagen, Hilden, Germany |
| QIAquick PCR Purification kit | Qiagen, Hilden, Germany |
| QuantiTect® SYBR® Green PCR Kit | Qiagen, Hilden, Germany |

| Commercial kit | Manufacturer |
|---|---|
| RNeasy Micro kit | Qiagen, Hilden, Germany |
| RNeasy Mini kit | Qiagen, Hilden, Germany |
| RNeasy Midi kit | Qiagen, Hilden, Germany |
| TdT, recombinant | Invitrogen, Carlsbad, USA |

### 2.1.7 Solutions, buffers, gels, and media

If not indicated differently, all solutions, buffers, and media were prepared with deionized water (dd$H_2$o) and autoclaved if necessary. Solutions, buffers, media, and gels are listed in table 13.

**Table 13: Prepared solutions, buffers, media, and gels and respective compositions.**

| Solution/Buffer/Gel | Composition |
|---|---|
| agarose gel | 1-2% agarose in TBE buffer |
| | + 0.05 µl/ml Midori green advanced DNA stain |
| Alcian blue staining | 1% Alcian blue |
| solution | 0.5% glacial acetic acid |
| alkaline phosphatase | 100 mM Tris/HCl, pH9.5 |
| buffer | 100 mM $MgCl_2$ |
| | 50 mM NaCl |
| | 0.1% Tween®20 |
| blocking solution | 1xMAB/2% blocking reagent (BMP) |
| (WMISH, TUNEL) | 8.3% horse serum |
| | 0.05% Tween®20 |
| L-Cysteine hydrochloride | 2% L-Cysteine hydrochloride in 0.1x MBSH |
| solution | adjust pH 8.2-8.4 |
| 10% Chaps | 10% in DEPC-$H_2O$ |
| Denhardt's | 0.5% BSA |
| | 0.5% Ficoll™ PM 400 |
| | 0.5% polyvinylpyrrolidone |
| DEPC-$H_2O$ | 0.1% DEPC in dd$H_2O$ |

| Solution/Buffer/Gel | Composition |
|---|---|
| DNA loading dye | 40 mM Tris/HCl, pH 8.3 |
| | 0.5% SDS |
| | 1 mM EDTA, pH 8.0 |
| | 0.25% bromphenol blue |
| | 50% glycerol |
| euthanasian solution | 5% MS222 |
| | adjust to pH 7 with $NaHCO_3$ |
| | Storage at 4 °C; protected from light |
| 3% Ficoll | 3% Ficoll™ PM 400 in 1x MBSH |
| gelatin (for sections) | 2.2 g gelatin |
| | 135 g BSA |
| | 90 g sucrose |
| | *ad* 500 ml with PBS |
| hybridization buffer | 50% formamide |
| | 5x SSC |
| | 1x Denhardt's |
| | 0.1% Tween® 20 |
| | 0.1% Chaps |
| | 10 mM EDTA, pH 8 |
| lysis buffer | 50 mM Tris, pH 8.8 |
| | 1 mM EDTA |
| | 0.5% Tween®20 |
| | freshly add proteinase K to final conc.: 200 µg/ml |
| 5x MAB | 0.5 M maleic acid |
| | 0.75 M NaCl |
| MBSH | 10 mM HEPES |
| | 88 mM NaCl |
| | 1 mM KCl |
| | 0.33 mM $Ca(NO_3)_2$ x $(H_2O)_4$ |
| | 0.41 mM $CaCl_2$ x $(H_2O)_2$ |
| | 0.82 mM $MgSO_4$ x $(H_2O)_7$ |
| | 2.4 mM $NaHCO_3$ |

| Solution/Buffer/Gel | Composition |
|---|---|
| 1 % methylcellulose | 1% methylcellulose in dd$H_2O$ |
| MEMFA | 0.1 M MOPS |
| | 2 mM EGTA |
| | 1 mM $MgSO_4$ x $(H_2O)_7$ |
| | 4% formaldehyde |
| MEMFAT | 0.1 M MOPS |
| | 2 mM EGTA |
| | 1 mM $MgSO_4$ x $(H_2O)_7$ |
| | 4% formaldehyde |
| | 0.1% Tween®20 |
| NBT/BCIP | 4.5 µl NBT |
| | 3.5 µl BCIP |
| | *ad* 1 ml Alkaline phosphatase buffer |
| OCM media | 15 mM HEPES, pH 7.8 |
| | 1 mM L-glutamine |
| | 50 µg/ml gentamycin |
| | 50 U/ml nystatin |
| | 0.4 µg/ml BSA |
| | 50% Leibovitz's L-15 |
| | 10% FCS |
| Orange G 10x loading | 20 g Sucrose |
| dye | in 40 ml dd$H_2O$ |
| | + 100 mg Orange G |
| PBS | 137 mM NaCl |
| | 2.7 mM KCl |
| | 4.3 mM $Na_2HPO_4$ |
| PBST | 137 mM NaCl |
| | 2.7 mM KCl |
| | 4.3 mM $Na_2HPO_4$ |
| | 0.1% Tween®20 |
| RNase A solution | 20 mg RNase A |
| | *ad* 1 ml $H_2O$ and boil 20 min at 100 °C |

| Solution/Buffer/Gel | Composition |
|---|---|
| 20x SSC | 3 M NaCl |
| | 0.3 M $Na_3$citrate x $(H_2O)_2$ |
| TBE | 8.9 mM Tris/HCl |
| | 8.9 mM $H_3BO_3$ |
| | 2 mM EDTA |
| TBS | 50 mM Tris/HCl, pH 7.4 |
| | 150 mM NaCl |
| TBST | 50 mM Tris/HCl, pH 7.4 |
| | 150 mM NaCl |
| | 0.1% Tween®20 |
| TE buffer | 3 M Tris/HCl, pH 8 |
| | 0.5 M EDTA |
| TE/RNase buffer | 999 µl TE buffer |
| | 1 µl RNase A solution |
| TELT buffer | 50 mM Tris/HCl, pH 7.5 |
| | 62.5 mM EDTA |
| | 2.5 mM LiCl |
| | 0.4% Triton X-100 |
| triethanolamine 0.1 M | 750 µl triethanolamine |
| | 100 µl HCl (32%) |
| | *ad* 50 ml DEPC-$H_2O$ |
| 2x YT-agar plates | 31 g 2x YT-medium |
| | 15 g Select agar |
| | 50 µg/ml ampicillin |
| | *ad* 1 l dd$H_2O$ |
| 2x YT-medium | 31 g 2x YT-medium |
| | 50 µg/ml ampicillin |
| | *ad* 1 l dd$H_2O$ |

### 2.1.8 Equipment

**Table 14: List of devices utilized in the present study.**

| | Device | Model | Manufacturer / Source |
|---|---|---|---|
| A | autoclave | SteriV | MuenchnerMedizinMechanik (MMM), Planegg, Germany |
| B | balance | EW4200-2NM | Kern & Sohn GmbH, Balingen, Germany |
| | | TE64-OCE | Satorius, Göttingen, Germany |
| | binocular microscope | SWF 10x | H. Saur, Reutlingen, Germany |
| C | centrifuge | Megafuge 11R | Heraeus, Hanau, Germany |
| | | Biofuge 15 | Heraeus, Hanau, Germany |
| | | Biofuge pico | Heraeus, Hanau, Germany |
| | | Biogfuge pico 17 | Thermo Fisher Scientific, Waltham, USA |
| | | Fresco 21 | Thermo Fisher Scientific, Waltham, USA |
| | | MyFuge mini centrifuge C600 | Bio-Rad Laboratories, Hercules, USA |
| | | Rotanta 460R | Hettich, Tuttlingen, Germany |
| | cold-light source | KL 750 | Schott, Augsburg, Germany |
| D | dry block heater | HBT 130 | HLC, Bovenden, Germany |
| E | electrophoresis chamber | | Workshop University Göttingen |
| F | freeze dryer | Christ Alpha 1-4 | B. Braun, Tuttlingen, Germany |
| | freezer -20 °C | MediLine | Liebherr, Bulle, Switzerland |
| | freezer -80 °C | TDE-40086FV | Thermo Fisher Scientific, Waltham, USA |
| | forceps | Dumont No 5 | Roth, Karlsruhe, Germany |
| G | glassware | flasks, beaker, bottles | Brandt/Schott/Avantor |
| H | heating oven 37 °C | Modell 200 | Memmert, Büchenbach, Germany |

| | Device | Model | Manufacturer / Source |
|---|---|---|---|
| I | ice machine | AF-10 | S. Scotsman, Vernon Hills, US |
| | incubator | WB 22K | Mytron, Heilbad Heiligen- stadt, Germany |
| | | 3201 | RUMED, Laatzen, Germany |
| | | KB400 | Binder, Tuttlingen, Germany |
| M | magnet stirrer | MR 300 | Heidolph, Schwabach, Germany |
| | micromanipulator | M1 | H. Saur, Reutlingen, Germany |
| | micropipette puller | P-97 Flaming/Brown | Sutter Instrument Company, Freiburg, Germany |
| | micropipettes (2 µl, 10 µl, 20 µl, 200 µl, 1000 µl) | Discovery Comfort | Kinesis, Portland, USA |
| | microscope | BX60 + camera DP72/DP28 | Olympus, Shinjuku, Japan |
| | | MVX10/U-RFL-T + camera UC50 | Olympus, Shinjuku, Japan |
| | | CH2 | Olympus, Shinjuku, Japan |
| | microwave | HerdGT 8004 | GerneralTechnic, Hespringen, Luxembourg |
| | multipipette | M4 | Eppendorf, Hamburg, Germany |
| N | NanoPhotometer | V 2.2.3 | Implen, München, Germany |
| P | PCR thermocycler | T3000 | Biometra, Göttingen, Germany |
| | pH meter | pH211 | HANNA Instruments, Woonsocket, USA |
| | pipettor | Pipetus | Hirschmann Laborgeraete, Eberstadt, Germany |
| | plastic ware | bakers, cylinders | Avantor, Radnortownship, USA |
| | pneumatic PicoPump | PV 820 | World Precision Instruments, Sarasota, FL, USA |
| | Power Supply | P25 Powerpack | Biometra, Göttingen, Germany |

| | Device | Model | Manufacturer / Source |
|---|---|---|---|
| Q | qRT PCR machine | CFX Connect™ | Bio-Rad Laboratories, Hercules, USA |
| R | refrigerator 4 °C | ProfiLine | Liebherr, Bulle, Switzerland |
| | | Premium | Liebherr, Bulle, Switzerland |
| | roller mixer | RM5-V30 | CAT, Staufen, Germany |
| S | shaker | KS250 | Janke&Kunkel Ika Labortechnik, Staufen, Germany |
| | | KS15 | E. Bühler, Bodelshausen, Germany |
| | | REAX 2000 | Heidolph, Schwabach, Germany |
| | | Vortex genie 2 | Scientific Insdustries, Bohe- mia, USA |
| U | UV detection system | GenoView | Avantor, Radnortownship, USA |
| | | Chroma 43B | Vetter, Ravensburg, Germany |
| V | vibratome | Vibratome 1500 | Leica, Wetzlar, Germanx |
| W | water bath | WMB 10 | Memmert, Büchenbach, Germany |

### 2.1.9 Consumables

**Table 15: List of utilized consumables.**

| | Consumable | Model | Manufacturer |
|---|---|---|---|
| C | capillaries | ∅ 1 mm | World Precision Instruments, Sarasota, USA |
| | cover slip | 50 mm x 24 mm | Avantor, Radnortownship, USA |
| F | falcon tubes | 15 ml, 50 ml | Sarstedt, Nümbrecht, Germany |
| | frog food | V7106-030 | ssniffs Spezialdiäten, Soest, Germany |
| G | glass vial + lid | 4 ml | Roth, Karslruhe, Germany |
| | gloves | Latex, “Happy Skin” | Ulma, Dornstadt, Germany |
| | | Nitril | Hartman, Heidenheim, Germany |
| | | Latex | Sempercare, Dallas, USA |

| | Consumable | Model | Manufacturer |
|---|---|---|---|
| M | microscope slides | | Avantor, Radnortownship, USA |
| P | parafilm | 100 mm x 38 m | Roth, Karlsruhe, Germany |
| | Pasteur pipettes | | Avantor, Radnortownship, USA |
| | petri dishes | 3.5 cm, 6 cm, 10 cm, 14.5 cm | Greiner, Frickenhausen, Germany |
| | pipette tips | Safe Seal Tips: 10 µl, 20 µl, 200 µl, 1 ml | Biozym, Oldendorf, Germany |
| | | 10 µl, 20 µl, 200 µl, 1 ml | Sarstedt, Nümbrecht, Germany |
| | | 20 µl (Microloader$^{TM}$) | Eppendorf, Hamburg, Germany |
| R | razor blades | single edge | Agar Scientific, Essex, UK |
| | reaction tubes | 1.5 ml, 2 ml (Save-Lock) | Eppendorf, Hamburg, Germany |
| | | 1.5 ml | Sarstedt, Nümbrecht, Germany |
| | | PCR tubes | Biozym, Oldendorf, Germany |
| S | scalpel | sterile | B. Braun, Tuttlingen, Germany |
| | stripette | 5 ml, 10 ml, 25 ml | Corning, Corning, USA |
| | syringe | 5-20 ml | BD, Flanklin Lakes, USA |
| T | transfer pipette | 1.5 ml, 3.5 ml | Sarstedt, Nümbrecht, Germany |
| Q | qPCR plate | 96 well TW-MT-plate, white | Biozym, Oldendorf, Germany |
| | qPCR plate seal | adhesive Clear qPCR Seal | Biozym, Oldendorf, Germany |
| W | well plate | 24 | Sarstedt, Nümbrecht, Germany |

### 2.1.10 Software

**Table 16: Software and respective version that was used in the present study.**

| Software | Version | Company |
|---|---|---|
| Affinity Designer | 1.10.4 | Serif Europe Ltd., Nottingham, UK |
| analySIS | 5.1 | Olympus, Shinjuku, Japan |

| Software | Version | Company |
|---|---|---|
| Bio-Rad CFX Maestro | | Bio-Rad Laboratories, Hercules, USA |
| BLAST | | The National Center for Biotechnology Information (NCBI) |
| Clustal Omega | 1.2.2 | EMBL-EBI, Hinxton, UK |
| GraphPad Prism | 9.3.0 | GraphPad, Irvine, USA |
| ImageJ | 2.0.0 | W. Rasband, National Institutes of Health, USA |
| Microsoft Word | 16.60 | Microsoft, Redmond, USA |
| Microsoft Excel | 16.60 | Microsoft, Redmond, USA |
| SnapGene Viewer | 5.3.2 | GSL Biotech LLC, Chicago, USA |
| TIDE | 3.3.0 | Data Curators VOF, Zwaag, Netherlands |
| Zotero | 5.0.03 | Project of Corporation of Digital Scholarship – global community (nonprofit) |

## 2.2 Methods

### 2.2.1 Bioinformatics

#### 2.2.1.1 Synteny Analysis

Synteny analyses were performed for the genes *bop1* and *rpl5*. For analyzing *bop1*, the NCBI Gene Bank for *Homo sapiens* (NP_056016; Gene ID: 23246), *Danio rerio* (NP_001071203; Gene ID: 777627), and *Mus musculus* (AAB19223; Gene ID: 12181) and the Xenbase platform (xenbase.org) for *Xenopus laevis* (NP_001080358; Gene ID: XB-GENE-6254226 (bop1. L); NP_001079852; Gene ID: XB-GENE-6255479 (bop1. S)) were used. For analyzing *rpl5*, the NCBI Gene Bank for *Homo sapiens* (NP_000960; Gene ID: 6125), *Mus musculus* (NP_058676; Gene ID: 100503670), *Gallus gallus* (NP_989912; Gene ID: 395269), *Danio rerio* (NP_956050; Gene ID: 326961), and the Xenbase platform (xenbase.org) for *Xenopus laevis* (NP_001079377; Gene ID: XB-GENE-6251827 [rpl5.S]; NP_001079437; Gene ID: XB-GENE-983917 [rpl5.L]) and for *Xenopus tropicalis* (NP_988881; Gene ID: XB-GENE-983912) were used.

#### 2.2.1.2 CRISPR-knockout evaluation

Evaluation of gene editing using the CRISPR/Cas9 system was performed using the online tool TIDE (tracking of indels by decompensation) (http://shinyapps.datacurators.nl/tide) (Brinkman et al., 2014). By this method the frequency and spectrum of targeted mutation can be estimated in a pool of cells. Here, DNA pools of 10 wild-type (WT) or 10 Bop1 MO-injected embryos were sequenced using Sanger sequencing. Sequencing results and the CRISPR target site on the gene were inserted into the TIDE tool. The sequence upstream of the CRISPR target site was used for alignment; the sequence downstream of the target site was used for decompensation. TIDE compared the sequence of Bop1 MO-injected embryos to the sequence of WT embryos and by this quantified the gRNA efficacy and estimated types of deletions and insertions.

### 2.2.2 Molecular biological methods

#### 2.2.2.1 RNA isolation from *Xenopus laevis* embryos

For RNA isolation, *Xenopus laevis* embryos were transferred into reaction tubes at the different developmental stages and fixed by shock freezing at -80 °C. Next, 500 µl peqGold RNApure$^{TM}$ solution was added and homogenized by a micro pestle followed by 5 min of incubation at room temperature. The supernatant was pipetted into a new reaction tube and 100 µl chloroform was added and mixed on a shaker for 60 sec. After 10 min of incubation on ice and 5 min of centrifugation at 13 000 rpm at 4 °C, the upper aqueous layer was transferred into a new reaction tube. The same amount of isopropanol was added and mixed on a shaker. RNA was precipitated by 15 min on ice followed by 10 min of centrifugation at 13 000 rpm and 4 °C. Supernatant isopropanol was removed, and the remaining RNA pellet was washed twice with 1 ml 75% ethanol and 10 min of centrifugation at 13 000 rpm and 4 °C. Ethanol was removed and the RNA pellet was dried at room temperature for 5 min. Isolated RNA was dissolved in 20 µl DEPC-$H_2O$ and stored at -20 °C. The concentration of RNA was assessed by measuring the optical density (OD) via a spectrophotometer at a wavelength of 260 nm.

#### 2.2.2.2 Agarose gel electrophoresis

To separate nucleic acids according to their size, agarose gel electrophoresis was performed. Therefore, 1-2% agarose (w/v) was dissolved in 1x TBE buffer using a microwave. 0.05% Midori green advanced DNA stain was added, and the solution was poured into the gel chamber including spacer and a comb. After the gel hardened and TBE buffer was added to the gel chamber, samples premixed with 10x DNA loading dye were loaded onto the gel. GeneRuler$^{TM}$ DNA Ladder Mix served as molecular weight standard. Gel electrophoresis was performed at 80-100 V for 15-30 min. To visualize nucleic acids, UV detection systems were used.

#### 2.2.2.3 Complementary DNA (cDNA) synthesis, reverse transcriptase (RT) PCR, and real-time qPCR

<u>cDNA synthesis</u>

To synthesis complementary DNA (cDNA), 1 µg of RNA was mixed with 1 µl random primers and DEPC-$H_2O$ was added to a final volume of 12 µl. Upon 10 min of incubation at 72 °C the reaction was placed on ice and 4 µl 5x First strand buffer, 2 µl DTT, and 1 µl 10 mM dNTPs were added. For negative reverse transcriptase (-RT) reactions 1 µl DEPC-$H_2O$ was added to the tube; for positive (+) RT reactions 1 µl Superscript II reverse transcriptase was added to the tube. Reaction tubes were incubated for 50 min at 42 °C before a final incubation for 15 min at 72 °C. cDNA was stored at -20 °C.

<u>RT PCR</u>

Composition of RT PCR:

| | |
|---|---|
| 13.2 µl | $H_2O$ |
| 4 µl | 5 x Phire reaction buffer |
| 0.4 µl | 10 mM dNTPs |
| 0.5 µl | forward primer (10 µM) |
| 0.5 µl | reverse primer (10 µM) |
| 1 µl | cDNA |
| 0.4 µl | Phire Hot Start II DNA Polymerase |

PCR thermoprofile of RT PCR:

| | | |
|---|---|---|
| lid temperature | 99 °C | |
| 1. | 98 °C | 30 sec |
| 2. | 98 °C | 5 sec |
| 3. | x °C | 5 sec (x: Tm, specific for primer pair) |
| 4. | 72 °C | 30 sec → 2.: 25 – 35 cycles |
| 5. | 72 °C | 1 min |
| 6. | 14 °C | ∞ |

To evaluate RT PCR experiments, agarose gel (1.2%) electrophoresis was performed. *gapdh* +RT served as loading control, *gapdh* -RT as negative control.

Real-time qPCR

For quantitative analysis of relative gene expression, a SYBR Green-based qPCR approach was performed.

First, primer efficiency was determined using four-step cDNA dilutions (undiluted, 10-fold, 100-fold, and 1000-fold dilution) of WT cDNA and calculated as previously described (Pfaffl, 2001). Only primers with an efficiency of 100 % ± 3 % were used for further experiments.

All samples were measured in technical triplicates. *gapdh* (*glyceraldehyde 3-phosphate dehydrogenase*), *odc* (*ornithine decarboxylase 1*), and *slc35b1* (*solute carrier family 35 member b1*) served as reference genes (Kietzmann et al., 2012; Mughal et al., 2018), and were combined for normalization as previously described (Riedel et al., 2014). Experiments were carried out in 96-well plates on a CFX connect system (Bio-Rad). A $H_2O$ control in which cDNA was substituted with $H_2O_{ultrapure}$ served as negative control for each primer pair.

Composition of qPCR:

| | |
|---|---|
| 4 µl | $H_2O_{ultrapure}$ |
| 0.5 µl | forward primer (10 µM) |
| 0.5 µl | reverse primer (10 µM) |
| 1 µl | cDNA (1:10 dilution) |
| 6 µl | QuantiTect® SYBR® Green PCR kit |

Before thermocycling, the 96-well plate was sealed with an adhesive foil.

PCR thermoprofile of qPCR:

| | | | |
|---|---|---|---|
| 1. | 95 °C | 15 sec | |
| 2. | 94 °C | 15 sec | |
| 3. | 60 °C | 30 sec | |
| 4. | 72 °C | 30 sec | → 2.: 41 cycles |
| 5. | 95 °C | 5 sec | |
| 6. | 65 °C | 60 sec | |
| 7. | 65-97 °C | 5 sec, then increase of 0.5 °C | |
| 8. | 40 °C | 30 sec | |

For calculating the relative gene expression, the following formula was used:

$$R = \frac{2^{\Delta Ct_{GOI\ (control-treated)}}}{2^{\Delta Ct_{reference\ gene\ (control-treated)}}}$$

R = relative expression; ∆Ct = difference of threshold cycle; GOI = gene of interest; Control = Control MO-injected embryos; Treated = Bop1 MO-injected embryos.

2.2.2.4 DNA recombination experiments

Annealing PCR

First, previously designed primers were annealed via an annealing PCR. 10 µl forward primer and 10 µl reverse primer were mixed.

PCR thermoprofile to anneal primer:

| | | |
|---|---|---|
| 1. | 95 °C | 10 min |
| 2. | 90 °C | 10 min |
| 3. | 85 °C | 10 min |
| 4. | 80 °C | 10 min |
| 5. | 75 °C | 10 min |
| 6. | 70 °C | 10 min |
| 7. | 65 °C | 10 min |
| 8. | 60 °C | ∞ |

Restriction digest of plasmid DNA

Before insertion of the DNA fragment into the plasmid, the plasmid DNA was digested.

Composition of restriction digest of plasmid DNA for cloning the MO binding specificity construct:

| | |
|---|---|
| 5 µg | plasmid DNA |
| 2 µl | 10x buffer 3 |
| 2 µl | *Eco*RI |
| 2 µl | *Bam*HI |
| *ad* 20 µl | $H_2O$ |

The restriction digest was incubated for 4 hours at 37 °C.

For dephosphorylation of the 5'-end, 2 µl of shrimp alkaline phosphatase was added and incubated for 2 hours at 37 °C followed by 15 min of incubation at 65 °C.

Agarose gel electrophoresis was performed, and restriction digest was purified via the QIAquick Gel Extraction kit (Qiagen; protocol: QIAquick Gel Extraction Kit). Successful restriction digest was checked via agarose gel electrophoresis and concentration was determined via OD measurement (wavelength: 260 nm).

Ligation

To introduce the insert into plasmid DNA the following ligation was performed.

Composition of ligation:

| | |
|---|---|
| 300-800 ng | insert DNA |
| 80-100 ng | plasmid DNA |
| 2 µl | 5x Ligate-IT reaction buffer |
| 1 µl | Ligate-IT T4 DNA Ligase |
| *ad* 10 µl | $H_2O$ |

The ligation mix was incubated for 30 min at room temperature. 10 µl of the ligation was used to transform chemically competent cells.

Transforming chemically competent cells

*E. coli* One Shot® TOP10 were used for transformation according to manufacturer's protocols (Invitrogen; protocol: Routine Cloning Using Top10 Competent Cells). 50 µl (1 vial) of chemically competent cells were thawed on ice before gently mixed with 10 µl of ligation mix. The mix was incubated for 30 min on ice and then incubated for exactly 30 sec at 42 °C. Vials were placed on ice before adding prewarmed (37 °C) 250 µl S.O.C medium followed by an incubation for 1 hour at 100 rpm and 37 °C. Cells were plated on two 2x YT-agar plates (+ 50 µg/ml ampicillin) and incubated overnight at 37 °C. The next day, single colonies were picked and cultured in 3 ml 2x YT-medium overnight at 260 rpm and 37 °C. Plasmid DNA was prepared in TELT preparation (small scale) or Midi preparation (large scale).

Plasmid DNA preparation

For small scales of plasmid DNA preparation TELT plasmid preparation was performed. Therefore, 1.5 ml of the *E. coli* overnight culture was centrifuged for 1 min at 10 000 rpm. The supernatant was removed, and the pellet was resuspended in 150 µl TELT buffer and 15 µl lysozyme. After 5 min of incubation at room temperature the mixture was boiled at 100 °C for 2 min and afterwards placed on ice for at least 5 min. Next, the reaction tube was centrifuged for 20 min at 13 000 rpm and 4 °C and the supernatant was transferred to a new reaction tube. The plasmid DNA was precipitated by resuspending the pellet in 150 µl isopropanol. After 5 min of incubation at room temperature, the reaction tube was centrifuged for 15 min at 13 000 rpm at room temperature. The supernatant was discarded, and the remaining DNA pellet was washed with 300 µl 70% ethanol before another 10 min of centrifugation at 13 000 rpm at room temperature. The supernatant was removed, and the pellet was dried in a freeze dryer for 3 min. Plasmid DNA was resuspended in 50 µl TE/RNase buffer on a shaker for 10 min. Successful introduction of the insert into the plasmid DNA was checked with a control digest followed by agarose gel electrophoresis and sequencing, which was performed by the company Eurofins.

Composition of control digest:

| | |
|---|---|
| 4 µl | TELT-preparation |
| 1 µl | 10x buffer |
| 0.5 µl | restriction enzyme |
| *ad* 10 µl | $H_2O$ |

The control digest was incubated for 1 hour at 37 °C. Upon successful introduction, concentration was measured by OD measurement (wavelength: 260 nm).

For large scale plasmid DNA preparation Qiagen Plasmid Midi kit (Qiagen) was used. Here, 50 ml of 2x YT-medium (+ 50 µg/ml ampicillin) was inoculated with a single colony and incubated overnight at 260 rpm and 37 °C. The next day, the culture was centrifuged for 20 min at 4000 rpm at room temperature before the supernatant was removed. Plasmid DNA preparation was continued by following the manufacturer's protocol (Qiagen; protocol: Plasmid Midi Kits). The resulting pellet was freeze dried for 3 min and resuspended in 150 µl $ddH_2O$. The plasmid DNA was checked by sequencing, which was performed by the company Eurofins, and concentration was determined by OD measurement (wavelength: 260 nm).

#### 2.2.2.5 Generation of *sense* RNA for injections

In order to generate *sense* RNA for injection, the required plasmid was obtained from the internal institute's plasmid library and a restriction digest was performed to linearize the plasmid.

Composition of restriction digest of plasmid DNA for generation of *sense* RNA for injections:

| | |
|---|---|
| 5 µg | plasmid DNA |
| 2 µl | 10x buffer |
| 2 µl | restriction enzyme |
| *ad* 20 µl | $H_2O$ |

The restriction digest was incubated overnight at 37 °C. The next day, agarose gel electrophoresis was performed to confirm successful digest and the linearized

plasmid was purified using the QIAquick PCR Purification kit or the QIAquick Gel Extraction kit (Qiagen; protocol: QIAquick PCR Purification Kit; QIAquick Gel Extraction Kit). The purified plasmid was eluted twice with 15 µl DEPC-$H_2O$. Agarose gel electrophoresis was utilized to determine the amount of DNA used for *in vitro* transcription. *In vitro* transcription was performed using mMESSAGE mMACHINE Sp6, T3, or T7 kit (Thermo Fisher Scientific).

Composition of *in vitro* transcription experiments to generate *sense* RNA:

| | |
|---|---|
| ~600 ng | linearized template DNA |
| 2 µl | 10x reaction buffer |
| 10 µl | 2x NTP/Cap |
| 2 µl | Sp6 / T3 / T7 enzyme mix |
| *ad* 20 µl | $H_2O$ |

The mixture was incubated for 2 hours at 37 °C. Afterwards, 1 µl DNase I was added, and the mixture was incubated for 15 min at 37 °C. To check successful *in vitro* transcription, agarose gel electrophoresis was performed followed by purification via RNeasy Midi kit (Qiagen; protocol: RNeasy® Midi/Maxi Handbook) according to the manufacturer's protocol. Agarose gel electrophoresis was performed and OD measurement (wavelength: 260 nm) was used to determine RNA concentration. Injection mRNA was stored at -80 °C.

#### 2.2.2.6 *Antisense* RNA probes for WMISH

Plasmid DNA to generate *antisense* RNA probes for WMISH was obtained from the internal institute's library. In general, WMISH probes were generated as previously published (Hemmati-Brivanlou et al., 1990; Lufkin, 2007). First, plasmid DNA was digested.

Composition of restriction digest of plasmid DNA for generation of WMISH *antisense* probes:

| | |
|---|---|
| 5 µg | plasmid DNA |
| 2 µl | 10x buffer 3 |
| 2 µl | restriction enzyme |
| *ad* 20 µl | $H_2O$ |

Restriction digest was incubated overnight at 37 °C. Successful linearization was checked with agarose gel electrophoresis followed by purification of the linearized plasmid DNA by PCR Purification kit or Gel Extraction kit according to the manufacturer's protocols (Qiagen; protocol: QIAquick® PCR Purification Kit, QIAquick® PCR & Gel Cleanup Kit). Purified product was eluted twice in 15 µl DEPC-$H_2O$. To estimate the required amount of DNA during transcription, agarose gel electrophoresis was performed. Sp6, T3, or T7 polymerase (Roche) was used in combination with an RNA Labeling Mix (Digoxigenin) (Roche) for *in vitro* transcription.

Composition of *in vitro* transcription experiments to generate *antisense* RNA probes:

| | |
|---|---|
| ~1 µg | linearized template DNA |
| 2 µl | 10x DIG RNA Labeling Mix |
| 2 µl | 10x transcription buffer |
| 1 µl | Sp6 / T3 / T7 RNA polymerase |
| 1 µl | RNase Out |
| *ad* 20 µl | $H_2O$ |

*In vitro* transcription was incubated for 2 hours at 37 °C followed by 15 min of incubation at 37 °C with 2 µl DNase. Next, the RNA was purified using a G-50 column (GE Healthcare; protocol: illustra MicroSpin G-50 Columns) following the manufacturer's protocol. The success of the RNA transcription was checked by agarose gel electrophoresis. 2 ml hybridization buffer was added to the *antisense* RNA, which was further stored at -20 °C.

2.2.2.7 gRNA design and synthesis

gRNA design

For gRNA design the online tool CRISPRscan (crisprscan.org) was used (Moreno-Mateos et al., 2015). Here, sequences of different exons were inserted to only target exon sequences. PAM sequence was preset to NGG, which is necessary for Cas9 from *Streptococcus pyogenes*. Off-targets were minimized or excluded by blasting gRNAs using NCBI Blast. By this it was ensured that especially the core seed which is 10-12 nucleotides proximal to the PAM sequence was unique. Only gRNAs with a CRISPRscan score above 70 were used. Furthermore, the online tool inDelphi (indelphi.giffordlab.mit.edu) was used to further analyze gRNA to have a high frameshift possibility to reduce in-frame mutations. An alignment of the respective part of the *bop1* gene on the S and L homeologue including the CRISPR target sites is included in the appendix section (suppl. Fig. 1).

gRNA template synthesis

In general, gRNA synthesis was carried out based on previously published protocols (Nakayama et al., 2014). The first step in order to synthesize gRNA templates was to perform a PCR.

Composition of PCR for generation of gRNA templates:

| | |
|---|---|
| 37 µl | $H_2O$ |
| 10 µl | 5x Phire reaction buffer |
| 1 µl | 10 mM dNTPs |
| 0.5 µl | forward oligo for gRNA (100 µM) |
| 0.5 µl | reverse oligo (100 µM) |
| 1 µl | Phire Hot Start II DNA Polymerase |

Composition of annealing control:

| | |
|---|---|
| 49 µl | $H_2O$ |
| 0.5 µl | forward oligo for gRNA (100 µM) |
| 0.5 µl | reverse oligo (100 µM) |

PCR thermoprofile of PCR for generation of gRNA templates and annealing control:

| | | | |
|---|---|---|---|
| lid temperature | | 99 °C | |
| 1. | 98 °C | 30 sec | |
| 2. | 98 °C | 10 sec | |
| 3. | 62 °C | 20 sec | |
| 4. | 72 °C | 20 sec | → 2.: 10 cycles |
| 5. | 98 °C | 10 sec | |
| 6. | 72 °C | 30 sec | → 5: 25 cycles |
| 7. | 72 °C | 5 min | |

Successful template synthesis was checked via agarose gel electrophoresis and gRNA templates were purified using the PCR Purification kit or the Gel Extraction kit (Qiagen; protocol: QIAquick® PCR Purification Kit, QIAquick® PCR & Gel Cleanup Kit). Elution was achieved with two times 15 µl DEPC-$H_2O$ and concentration was measured using OD measurements (wavelength: 260 nm). Templates were stored at -20 °C.

gRNA transcription

For transcription, the MEGAshortscript T7 transcription kit (Thermo Fisher Scientific) was used.

Composition of transcription of gRNAs:

| | |
|---|---|
| 2 µl | 10x buffer |
| 2 µl | ATP |
| 2 µl | CTP |
| 2 µl | GTP |
| 2 µl | UTP |
| 2 µl | T7 RNA polymerase |
| 300 ng | gRNA template |
| *ad* 20 µl | $H_2O$ |

The reaction mix was incubated for 4 hours at 37 °C before 1 µl DNase was added and incubated for another 15 min. gRNAs were purified using the RNeasy Micro kit according to the manufacturers' protocol (Qiagen; protocol: RNeasy® Micro

Handbook). Successful gRNA transcription was checked via agarose gel electrophoresis and concentration was measured using OD measurements (wavelength: 260 nm). Finally, the gRNAs were diluted to a concentration of 150 ng/µl, aliquoted in 1 µl aliquots, and stored at -80 °C.

2.2.2.8 genomic DNA isolation from *Xenopus laevis* embryos

For DNA isolation, *Xenopus laevis* embryos were transferred into reaction tubes at different developmental stages and 100 µl lysis buffer was added. Embryos were lysed for 2-3 hours at 56 °C, followed by 10 min at 95 °C to inactivate proteinase K. Lysates were centrifuged for 10 min at 13 000 rpm and 4 °C. Supernatant (without the fatty layer) was transferred into a new reaction tube. The last two steps (centrifugation and transferring supernatant) were repeated two times. Isolated genomic DNA was stored at -20 °C.

2.2.2.9 Knockout evaluation via direct sequencing of PCR amplicons

Knockout evaluation was performed according to Nakayama et al. (Nakayama et al., 2014). To determine the knockout efficiency of the CRISPR/Cas9 system using specific gRNAs, the genomic DNA of 10 embryos per condition was pooled. Next, a PCR was performed to amplify the CRISPR site.

Composition of PCR for knockout evaluation:

| | |
|---|---|
| 13.2 µl | $H_2O$ |
| 4 µl | 5x Phire reaction buffer |
| 0.4 µl | 10 mM dNTPs |
| 0.5 µl | forward primer (10 µM) |
| 0.5 µl | reverse primer (10 µM) |
| 1 µl | genomic DNA (Pool) |
| 0.4 µl | Phire Hot Start II DNA Polymerase |

PCR thermoprofile of PCR for knockout evaluation:

| | | | |
|---|---|---|---|
| lid temperature | | 99 °C | |
| 1. | 98 °C | 30 sec | |
| 2. | 98 °C | 5 sec | |
| 3. | x °C | 5 sec | (x: Tm, specific for primer pair) |
| 4. | 72 °C | 30 sec | → 2.: 40 cycles |
| 5. | 72 °C | 1 min | |
| 6. | 14 °C | ∞ | |

To evaluate the PCR, agarose gel electrophoresis was performed followed by a purification step using the PCR purification kit (Qiagen). PCR products were eluted in 20 µl DEPC-$H_2O$ and concentration was measured using OD measurements (wavelength: 260 nm). Finally, PCR products were sequenced, which was carried out by the company Eurofins. Further knockout evaluation was performed using TIDE software.

### 2.2.3 Handling mature *Xenopus laevis*

#### 2.2.3.1 Preparation of testes

Male *Xenopus laevis* were euthanized in a euthanasian solution (5% MS222) bath for 30 min and subsequent decapitation. The abdomen was opened using sharp scissors and testes were dissected and washed in 1x MBSH. Dissociated testes were stored in OCM media at 4 °C, until it was minced in 1x MBSH and used for *in vitro* fertilization.

#### 2.2.3.2 Stimulation of oocyte production

To induce ovulation, separated female *Xenopus laevis* were subcutaneously injected with 800 U of hCG into the posterior back between backbone and the lateral line organ to target the lymph sack (Sive et al., 2000). The next morning, eggs were collected in petri dishes by gentle squeezing of the frogs. Female frogs had a regeneration period of at least 3 months between two hCG injections.

2.2.3.3 *In vitro* fertilization of oocytes and de-jellying of embryos

Upon collection, oocytes were immediately fertilized *in vitro* (Sive et al., 2000). Therefore, supernatant liquid was removed from eggs and minced testis was added. In petri dishes, minced testis was diluted 1:10 with $ddH_2O$ to facilitate proper salt concentration for sperms. After gentle mixing of oocytes and testis, 15 min of incubation at room temperature followed. Subsequent to fertilization, embryos were incubated in 0.1x MBSH at 12.5 °C.

One hour after fertilization, embryos were de-jellied using L-Cysteine hydrochloride solution to facilitate manipulation. 0.1x MBSH was removed from, and L-Cysteine hydrochloride solution was added to the embryos. Upon visible reduction of the jelly, L-Cysteine hydrochloride was removed, and embryos were washed with 0.1x MBSH at least five times. Before manipulation, embryos were incubated in 12.5 °C.

## 2.2.4 *Xenopus laevis* embryos: microinjection, manipulation, cultivation and staining methods

2.2.4.1 Microinjection and manipulation of embryos

Microinjections were carried out in 3% Ficoll using a pneumatic PicoPump and a micromanipulator. Depending on the assay, embryos were injected at different developmental stages, which is shown in the following table 17. To target specific tissue, the publication by Moody and Kline was used (Moody and Kline, 1990).

**Table 17: Assay-dependent injection mode and respective stage of injection.**

| Assay | Stage of injection | Injection mode |
|---|---|---|
| MO binding specificity assay | 2 cell | bilateral |
| expression analysis using real-time qPCR | 2 cell | bilateral |
| expression analysis using RT PCR | 2 cell | bilateral |
| investigation of anterior tissue | 8 cell | unilateral, animal-dorsal |
| investigation of ventral blood islands | 8 cell | unilateral, vegetal-ventral/dorsal |
| *shh* expression analysis | 8 cell | bilateral, animal-dorsal |
| CRISPR/Cas9 knockout evaluation | 1 cell | - |
| investigation of anterior tissue via CRISPR/Cas9 | 2 cell | unilateral |

0.5 ng *GFP* RNA was co-injected and served as lineage tracer; Control MO injection served as injection control and the uninjected side – if applicable – served as internal control. Even though in some graphs and statistics Control MO does not appear, it was injected into embryos, control morphants were analyzed and data was considered for analysis. In those cases, Control MO was not included in graphs and statistics for simplifying the figures. *GFP* RNA was used to adjust RNA levels for all experiments in which RNA was injected and Control MO was used to adjust MO levels for all experiments in which MOs were injected. If not indicated differently, 15 ng of Bop1 MO or Rpl5 MO were injected.

For CRISPR/Cas9 experiments, the gRNA was incubated at 70 °C for 2 min before directly placed on ice. In order to assemble the RNP complex, the gRNA was mixed with 1 µl Cas9 protein and 5 min of incubation at 37 °C followed (Nakayama et al., 2014). Per injection, 300 pg gRNA was injected with 1 ng Cas9 protein. Furthermore, *GFP* RNA was injected into the second blastomere to prevent secondary structures between *GFP* RNA and gRNAs but to facilitate lineage tracing. Furthermore, injections at one cell stage (knockout evaluation) were performed 20 min post fertilization. Hence, in those experiments, de-jellying was carried out right after *in vitro* fertilization.

Embryos were incubated in 3% Ficoll either 3 hours at room temperature or overnight at 12.5 °C, before they were transferred into 0.1x MBSH to prevent leakage of the injection solution.

For cycloheximide (CHX) incubation experiments, CHX dissolved in dimethyl sulfoxide (DMSO) was diluted in 0.1x MBSH. Embryos were transferred into CHX in 0.1x MBSH 3 hours after injection. In these experiments, DMSO in 0.1x MBSH was used as control.

#### 2.2.4.2 Cultivation, lineage tracing, and fixation of *Xenopus laevis* embryos

For cultivation according to Sive et al. (Sive et al., 2000), embryos were incubated in 0.1x MBSH in petri dishes at 12.5 °C to room temperature until required developmental stage was reached. Dead embryos were removed immediately and unclean 0.1x MBSH was replaced with fresh one.

To check whether the injection targeted the correct tissue, *GFP* RNA was co-injected, which was further traced using a fluorescence microscope between stage 13 and 28 depending on the tissue targeted.
When the required developmental stage was reached, embryos were fixed in glass vials using 2 ml MEMFA(T) for at least 2 hours at room temperature. For DNA isolation and RT PCR experiments, embryos were fixed in lysis buffer and at -80 °C for at least 30 min, respectively.

2.2.4.3 Whole mount *in situ* hybridization (WMISH)

WMISH using specific *antisense* RNA probes was performed to analyze the expression and localization of different genes (Hemmati-Brivanlou et al., 1990; Lufkin, 2007). Before WMISH, embryos were cultured until desired developmental stage and fixed using MEMFAT. Experiments were performed using glass vials at room temperature. While incubation steps with 1x TBST, glass vials were mixed on a roller mixer. After fixation, embryos were incubated three times in 4 ml 1x TBST for 5 min. TBST was removed, 1 ml 1 M triethanolamine was added followed by 10 min of incubation. Subsequently, two incubation steps with 2.5 µl acetic anhydride for 5 min were performed. Embryos were washed twice for 5 min in 1x TBST before 500 µl MEMFAT was added for a 30 min incubation. Embryos were washed three times for 5 min in 4 ml 1x TBST. Buffer was removed up to a small residual and 300 µl hybridization buffer was added. Buffer was removed, and 300 µl hybridization buffer was added to the embryos followed by 4 hours of incubation at 65 °C. The buffer was removed, and embryos were covered with 350-1000 µl pre-heated *antisense* RNA probe before overnight incubation at 65 °C. The next day, probes were removed and 300 µl of 65 °C warm hybridization buffer was added for a 20 min incubation at 65 °C. Embryos were incubated with 1 ml of pre-heated 2x SSC at 65 °C for 30 min followed by a 40 min incubation with 1 ml 2x SSC + 0.05% Tween®20 + 20 µg/ml RNase A + 10 U/ml RNase T1 at 37 °C. Next, embryos were incubated in 1 ml 2x SSC + 0.05% Tween®20 for 15 min and subsequently in 1 ml 0.2x SSC + 0.05% Tween®20 for 30 min at 65 °C. For washing, 4 ml 1x TBST was added twice and incubated for 10 min, respectively. 500 µl blocking solution was added and incubated for 1 hour before 500 µl diluted Anti-Dig antibody was added and embryos were incubated for 2.5 hours. Overnight, embryos were

incubated with 1x TBST at 4 °C. The next morning, embryos were washed five times for 30 min in 1x TBST before being transferred into a 24 well plate. 10 min of incubation with AP buffer followed before staining with 500 µl BM Purple took place. The staining was stopped with 1 ml MEMFAT.

#### 2.2.4.4 5-Bromo-2´-deoxy-uridine (BrdU) staining

To stain proliferative cells, BrdU Labeling Mix and Detection kit (Roche) was used according to Hardcastle and Papalopulu (Hardcastle and Papalopulu, 2000). Embryos were cultured until stage 21 before 10 nl BrdU was injected - several small injections containing 1 nl BrdU – bilaterally into anterior tissue. Embryos were cultured at room temperature until they reached stage 23, when they were fixed with MEMFA. The following steps were performed in glass vials at room temperature. Embryos were incubated in 4 ml 1x PBS and mixed on a roller mixer five times for 10 min. Embryos were incubated in 1 ml 2 N HCl for 60 min before they were washed five times 5 min in 4 ml 1x PBST while mixing on a roller mixer. Next, embryos were incubated twice in 1 ml 1x PBS + 0.3% Triton X-100 for 30 min. 60 min of incubation with 1 ml PBS + 3% horse serum were performed, followed by 15 min on incubation with 200 µl incubation buffer. Hybridization took place for 4 hours at 37 °C with 200 µl Anti-BrdU antibody solution. Antibody was removed and embryos were incubated in 4 ml 1x PBST at 4 °C. The next morning, embryos were washed with 4 ml 1x PBST five times for 30 min while mixed on a roller mixer. 1 ml PBS + 20% horse serum was added to the embryos and incubated for 60 min before 250 µl diluted Anti-mouse-IgG antibody was added for 2.5 hours. Afterwards, embryos were washed 3 times 30 min using 4 ml 1x PBST and mixing on a roller mixer. Overnight, embryos were incubated with 4 ml 1x PBST at 4 °C. On the third day, embryos were washed twice with 4 ml 1x PBST for 5 min and mixed on a roller mixer before they were transferred to a 24 well plate. 1 ml AP buffer was added twice with 5 min of incubation in between. Staining was performed with either 500 µl BM Purple or 1 ml AP buffer + 4.5 µl NBT + 3.5 µl BCIP and stopped using 1 ml MEMFAT.

#### 2.2.4.5 Phospho histone 3 (pH3) staining

pH3 staining was used as a mitosis marker and performed according to established protocols (Cizelsky et al., 2013; Gessert et al., 2007). Therefore, embryos were

cultured until desired stage and fixed using MEMFAT. pH3 staining was performed in glass vials at room temperature. First, embryos were washed five times with 4 ml PBS for 10 min and mixed on a roller mixer. The embryos were blocked with 1 ml 1x PBS + 10% horse serum for 60 min before 150 µl Anti-phospho Histone H3 antibody diluted in 1x PBS + 10% horse serum was added for an overnight incubation on a shaker. The next day, embryos were washed four times with 4 ml 1x PBS + 0.1% Tween®20 for 30 min on a roller mixer. 1 ml 1x PBST + 20% horse serum was added and incubated for 60 min before 150 µl Anti-Rabbit-IgG-AP diluted in 1x PBST + 20% horse serum was added for 5-6 hours, slowly mixed on a shaker. Overnight, embryos were incubated in 4 ml 1x PBS + 0.1% Tween®20 at 4 °C. On the next day, embryos were washed with 4 ml 1x PBS + 0.1% Tween®20 5 times for 30 min on a roller mixer. Embryos were transferred into a 24 well plate. Remaining buffer was removed and 1 ml AP buffer was added, followed by 10 min of incubation. 500 µl BM Purple was added and incubated for 60 min in the dark at room temperature. Staining was stopped using MEMFAT.

#### 2.2.4.6 TdT-mediated dUTP Nick-End Labeling (TUNEL) staining

To stain late apoptotic cells, TUNEL staining was performed using the TdT recombinant kit (Invitrogen) as described (Gessert et al., 2007). Embryos were cultured until desired stage and fixed using MEMFA. TUNEL staining was performed using glass vials at room temperature. On the first day, embryos were washed five times for 10 min with 4 ml 1x PBST and mixed on a roller mixer, followed twice with 1 ml 0.1 M triethanolamine. 2.5 µl acetic anhydride was added twice with 5 min of incubation in between. Afterwards, embryos were washed twice with 2 ml 1x PBST for 5 min. For fixation, 500 µl MEMFAT was added. Embryos were washed with 4 ml 1x PBST and mixed on a roller mixer three times for 15 min and another three times for 5 min. 150 µl of 1x TdT buffer was added, and a 60 min incubation followed. Buffer was removed and 150 µl 0.5 M digoxygenin-dUTP + 15 U/ml TdT in 1x TdT buffer was added and incubated overnight. The next day, 1 ml 1 mM EDTA/PBS was added and two times 30 min of incubation at 65 °C followed. Embryos were washed four times for 1 hour in 4 ml 1x PBST on a roller mixer. Next, embryos were incubated for 1 hour in 500 µl blocking solution before 500 µl of diluted Anti-Dig antibody was added for 2.5 hours while gently mixing on a shaker. Overnight,

embryos were incubated with 4 ml 1x PBST at 4 °C. On the third day, embryos were washed with 4 ml 1x PBST five times 30 min on a roller mixer. Embryos were transferred into a 24 well plate. 1 ml AP buffer was added and incubated for 10 min before 1 ml BM Purple was added. BM Purple was removed and 1 ml MEMFAT was added to stop staining.

#### 2.2.4.7 Alcian blue staining and cranial cartilage dissection

To stain the cranial cartilage of *Xenopus laevis* embryos, Alcian blue staining was performed according to Bellmeyer et al. (Bellmeyer et al., 2003). Whole embryos were fixed with MEMFA at stage 45. All steps were performed at room temperature using glass vials and a roller mixer. 4 ml Alcian blue staining solution was added to the embryos and incubated for 95 min. They were washed twice in 80% ethanol/20% glacial acetic acid for 1 hour, before an overnight incubation with 80% ethanol/20% glacial acetic acid. The next day, embryos were bleached using 30% $H_2O_2$ and washed with 1x PBS. Dissecting cranial cartilages was achieved using fine tweezers and a binocular.

#### 2.2.4.8 Vibratome sections

Embryos were cultured until desired developmental stage and fixed using MEMFAT. Between stage 1 and stage 37, embryos were incubated for at least 24 hours in gelatin. Embryos older than stage 37 were first equilibrated in 30% glycerin and then 70% glycerin, both for at least 12 hours. Embedding of embryos was performed in blocks of 75 µl glutaraldehyde in 1 ml gelatin and transversal, horizontal, and sagittal sections of 25 µm were prepared (Gessert et al., 2007).

### 2.2.5 Imaging

Whole mount *Xenopus laevis* embryos were imaged using an Olympus MVX10 microscope and an Olympus UC50 camera. Vibratome sections were photographed with an Olympus BX60 microscope and an Olympus DP28 or DP70 camera. Images were further processed using ImageJ64 for quantification and Affinity Designer.

### 2.2.6 Evaluation and statistics

For evaluation, experiments had to meet the requirement of a survival rate of at least 50% and a survival number of at least 20 individuals. Furthermore, the control group had to show less than 20% phenotype rate.

Quantitative measurements were performed with ImageJ using pictures of *Xenopus laevis* embryos of one representative experiment. The area of the eye, the apex angle of coloboma, the head width (distance between midline and the lateral edge of the embryo), the area of dissected brains (brains were provided by Annika Meßmer), and the width of *sox3* expression were measured. Area of *sox3*, *pax6*, *tp53*, and *c-myc* expression was determined after injection and WMISH using the respective *antisense* RNA probes. The area of expression was selected and measured. The intensity of GFP expression was analyzed by the mean of grey values which was measured at defined areas and normalized to the control group.

For statistical analysis the software GraphPad Prism 9 was used. Statistical differences were calculated with a one-tailed nonparametric Mann-Whitney rank sum test. For real-time qPCR analysis a paired t-test was performed upon checking for normal distribution using a Shapiro-Wilk test. Error bars indicate standard error of the means (SEM). In case of “box and whiskers”-representation, whiskers indicate minimum and maximum. Only p-values of ≤ 0.05 were considered to be statistically significant. *, $p \leq 0.05$; **, $p \leq 0.01$; ***, $p \leq 0.001$; and ****, $p \leq 0.0001$.

# 3 Results

## 3.1 Bop1 functions during *Xenopus laevis* embryonic development

In this study the ribosomal factor Bop1 was analyzed during the embryonic development of the model organism *Xenopus laevis*. In detail, bioinformatic analyses of the *bop1* gene, the spatio-temporal expression pattern, the loss of Bop1 function, as well as the question if Bop1 exerts a function which is independent of its known ribosomal function was investigated.

### 3.1.1 The rRNA precursor is available during embryonic development

It has been shown that Bop1 is required for processing the rRNA precursor during ribosomal synthesis, in detail for the maturation of 5.8S and 28S rRNA (Hölzel et al., 2005; Rohrmoser et al., 2007). As a first step, it was analyzed if and at which timepoint the rRNA precursor is available during *Xenopus laevis* development and primers targeting the rRNA precursor were designed (Fig. 9A). Total RNA of embryos of different stages (3, 4, 5, 8, 13, 23, and 38) was isolated and the rRNA precursor was visualized by RT PCR. The correct sequence was checked via Sanger sequencing (Fig. 9A). The rRNA precursor was found in all analyzed developmental stages (Fig. 9B).

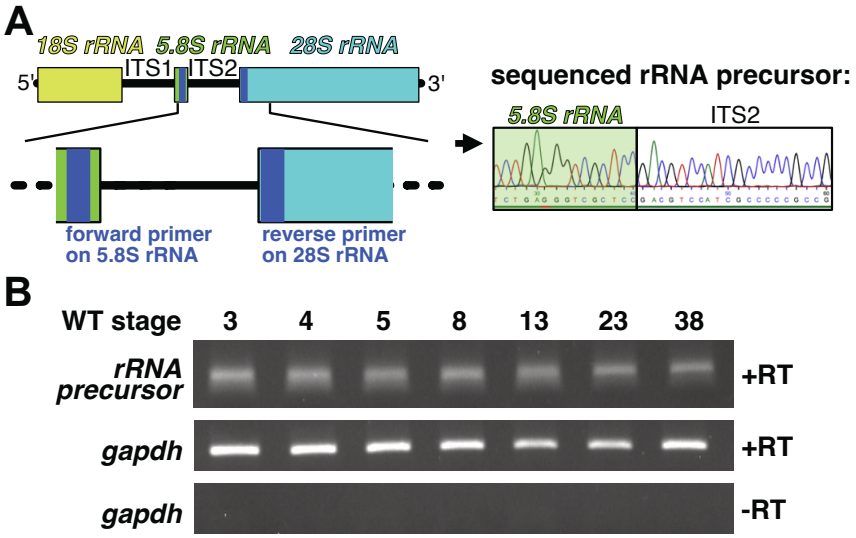


**Figure 9: rRNA precursor is available during early *Xenopus laevis* embryonic development.**
**A** rRNA precursor consisting of 18S rRNA, ITS1, 5.8S rRNA, ITS2, and 28S rRNA. Forward primer (dark blue) is located on 5.8 S rRNA and reverse primer (dark blue) is located on 28S rRNA. Sanger sequencing confirmed the correct sequence of the precursor. **B** total RNA of wild-type (WT) embryos at different stages (3, 4, 5, 8, 13, 23, and 38) was isolated and the amount of the rRNA precursor was analyzed using RT PCR. *gapdh* served as loading control. *gapdh* minus reverse transcriptase served as negative control. Abbreviations: ITS, internal transcribed spacer, *gapdh*, *glyceraldehyde 3-phosphate dehydrogenase*; rRNA, ribosomal RNA; RT, reverse transcriptase; WT, wild-type.

Conclusively, the rRNA precursor is maternally and zygotically supplied and Bop1 may process the 5.8S and 28S rRNA throughout all developmental stages.

### 3.1.2 *bop1* is conserved across species

Since Bop1 was investigated in the model organism *Xenopus laevis,* an *in silico* synteny analysis was performed to assess whether *bop1* is conserved across different species. The genomic region of *bop1* of *Homo sapiens*, *Xenopus laevis* (both homeologues), *Mus musculus*, and *Danio rerio* was investigated (Fig. 10). In general, the synteny analysis showed a higher conservation between *Xenopus laevis bop1* on chromosome 6L and the other investigated species compared to *bop1* on chromosome 6S and the other investigated species. Some genes show a conserved location; other genes are inverted. Conclusively, even though some deletions and insertions were observed, the genomic region around *bop1* is conserved across the analyzed species and it can be assumed that the same gene is considered for experiments.

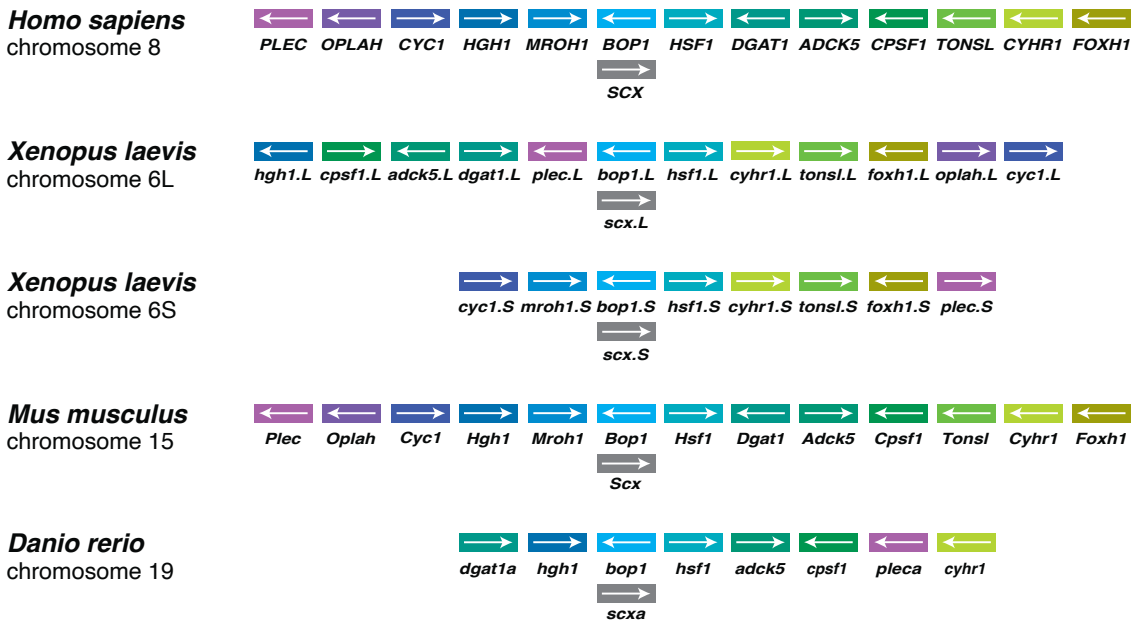


**Figure 10: Synteny analysis of *bop1*.**
*In silico* synteny analysis of *bop1* in *Homo sapiens*, *Xenopus laevis* (L and S chromosome), *Mus musculus*, and *Danio rerio*. Genes surrounding *bop1* were analyzed revealing a conservation of the genomic region across the different species. Modified from (Gärtner et al., 2022) under CC BY 4.0 (https://creativecommons.org/licenses/by/4.0/).

### 3.1.3 *bop1* is specifically expressed in *Xenopus laevis* wild-type embryos

To thoroughly analyze the expression pattern of *bop1* during embryonic development of *Xenopus laevis*, WMISH was performed at different developmental stages using a *bop1*-specific *antisense* probe (Fig. 11 A-F).

The fertilized oocyte as well as stage 6 embryos showed *bop1* expression at the animal pole (purple arrowhead) (Fig. 11A). During gastrulation, *bop1* transcripts were found in the mesoderm surrounding the blastoporus (blue arrowhead) (Fig. 11A). At stage 13 - an early neurula stage - *bop1* expression is located in the anterior neural plate and in the optic field (Fig. 11A). At stage 17, shortly after the induction of the NCCs, *bop1* transcripts were found in the NCCs (white arrow) as well as the developing eye (black arrow) (Fig. 11B). At stage 23, when eye cells differentiate, *bop1* expression was found in the migrating NCCs (white arrow) and in the eye anlage (black arrow) (Fig. 11B). During early tailbud stage 26, *bop1* was visualized in the eye anlage (black arrow), the NCCs of the hyoid arch and branchial arches (anterior and posterior branchial arch), and the brain (light green arrow) (Fig. 11B). At late tailbud stages 30 and 35/36, expression of *bop1* was located in

the developing eye (black arrow), the brain (light green arrow), the otic vesicle (teal arrow), the NCCs of the hyoid arch, and branchial arches, the tailbud, and the ventral blood islands (blue arrow) (Fig. 11C). By vibratome sections of stage 30 and stage 35/36 embryos, *bop1* expression in the brain, the eye (lens, and retina), and the arches (mandibular, hyoid, and branchial) was confirmed (Fig. 11 D-F).

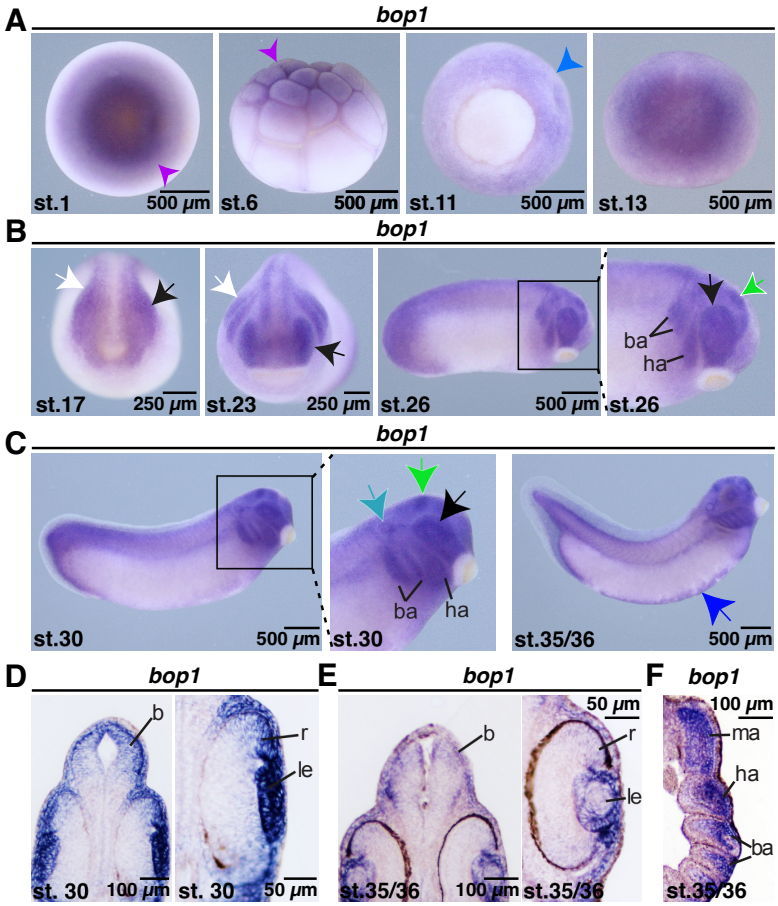


**Figure 11: Spatio-temporal expression pattern of *bop1* during *Xenopus laevis* embryonic development.** **A** Animal (st. 1), lateral (st. 6), ventral (st. 11), and anterior (st. 13) views are given. *bop1* expression was found in the animal pole (purple arrowhead) at stage 1 and stage 6. Stage 11 embryos show expression of *bop1* in the ectoderm and mesoderm surrounding the blastoporus (blue arrowhead). *bop1* transcripts were found in the anterior neural plate and optic field at stage 13. **B** Anterior (st. 17 and st. 23) and lateral (st. 26) views are shown. At stage 17 and 23, *bop1* was visualized in the eye anlage (black arrow) and the migrating neural crest cells (NCC) (white arrow). Expression of *bop1* was found in the hyoid arch (ha) and branchial arches (ba) as well as the developing eye (black arrow), and the brain (light green arrow) at stage 26. **C** Lateral views are shown. At late tailbud stages 30 and 35/36, *bop1* transcripts were located in the tailbud, the otic vesicle (teal arrow), the hyoid arch and the branchial arch, the developing eye (black arrow), the brain (light green arrow), and the ventral blood islands (blue arrow). **D, E** Transversal sections (dorsal (upper part) to ventral (lower part)) orientation) revealed *bop1* expression in the brain (b) and in lens (le) and retina (r) at stage 30 and 35/36. **F** Longitudinal sections (sections orientation is anterior (upper part) to posterior (lower part)) confirmed *bop1* expression in the mandibular, hyoid, and branchial arches at stage 35/36. Abbreviations: b, brain; ba, branchial arch; ha, hyoid arch; le, lens; ma, mandibular arch; r, retina; st., stage. Modified from (Gärtner et al., 2022) under CC BY 4.0 (https://creativecommons.org/licenses/by/4.0/).

Furthermore, *antisense* probes of marker genes of relevant tissues were used to specify expression of *bop1* (Fig. 12 A-C). By the two marker genes *rax* and *pax6* that are specifically expressed in the optic field (here shown in vibratome sections) expression of *bop1* was confirmed (Fig. 12A). *bop1* expression in the NCCs was confirmed by analyzing sections of the NCC-specific marker gene *foxd3* (Fig. 12B). Furthermore, using eye-specific marker genes *rax* (retina) and *prox1* (*prospero homeobox 1*) (mainly lens), *bop1* expression was verified at stage 30 (Fig. 12C).

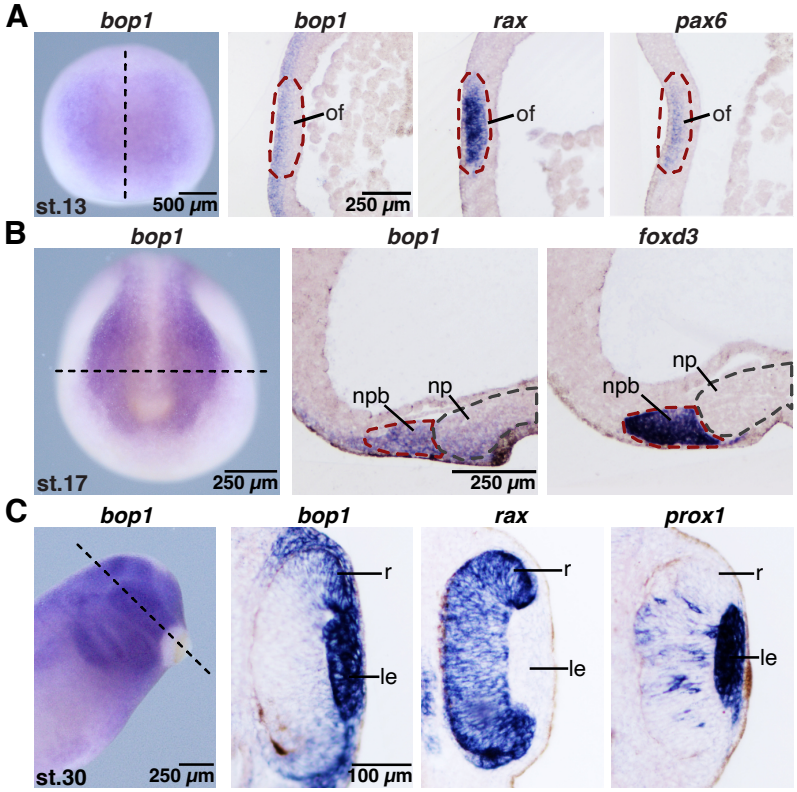


**Figure 12: Expression of *bop1* and tissue-specific marker genes during *Xenopus laevis* embryonic development.**

**A** Anterior view of whole embryo is given. At stage 13, expression of *bop1* and the two eye-specific marker genes *rax* and *pax6* are found in the optic field (red dotted line indicates optic field). Black dotted line represents level of sagittal sections (section orientation is dorsal (upper part) to ventral (lower part)). **B** Anterior view of whole embryo is shown. Expression of *bop1* and the NCC-specific marker gene *foxd3*. Black dotted line represents level of horizontal sections shown in the right-hand panels (section orientation is posterior (upper part) to anterior (lower part)). *bop1* transcripts are found in the neural plate (grey dotted line) and the neural plate border (red dotted line), where *foxd3* is expressed as well. **C** Lateral view of whole embryo is given. Expression of *bop1* and the two eye-specific marker genes *rax* and *prox1* at stage 30. Black dotted line indicates level of transversal sections shown in the right-hand panels (section orientation is dorsal (upper part) to ventral (lower part)). *bop1* expression is visualized in the retina (r), where *rax* expression is located as well, and in the lens (le), where *prox1* is expressed. Abbreviations: le, lens; np, neural plate; npb, neural plate border; of, optic field; r, retina. Modified from (Gärtner et al., 2022) under CC BY 4.0 (https://creativecommons.org/licenses/by/4.0/).

In summary, *bop1* is expressed in tissues that are highly relevant during pathological ribosomal synthesis in humans, e.g., anterior tissues like the eye, the brain, and the NCCs, or the ventral blood islands, since symptoms during ribosomopathies often occur in these tissues.

### 3.1.4 Bop1 morpholino oligonucleotides bind specifically and efficiently

To analyze if loss of Bop1 function induces phenotypes in *Xenopus laevis* embryos which are comparable to phenotypes during ribosomopathies, an *antisense*-based MO approach was used to knockdown Bop1. Therefore, two Bop1 MOs were designed specifically targeting the S homeologue. Bop1 MO targeting the 5'UTR and the start codon and Bop1 MO2 targeting further upstream in the 5'UTR of *bop1* (Fig. 13A and 13B). To demonstrate MO's binding specificity and effectiveness to both homeologues S and L, the binding site of Bop1 MO and Bop1 MO2 on L and S homeologue were cloned in frame and in front of *GFP* resulting in *bop1 MO bs-GFP*, *bop1 MO bs chr.L-GFP*, *bop1 MO2 bs-GFP*, and *bop1 MO2 bs chr.L-GFP*. These constructs were co-injected with 10 ng of the respective Bop1 MO or with 10 ng Control MO. Both Bop1 MOs, Bop1 MO and Bop1 MO2, efficiently blocked GFP expression in both respective constructs and hence, specifically bind to the MO binding sites on both homeologues (Fig. 13C and 13D).

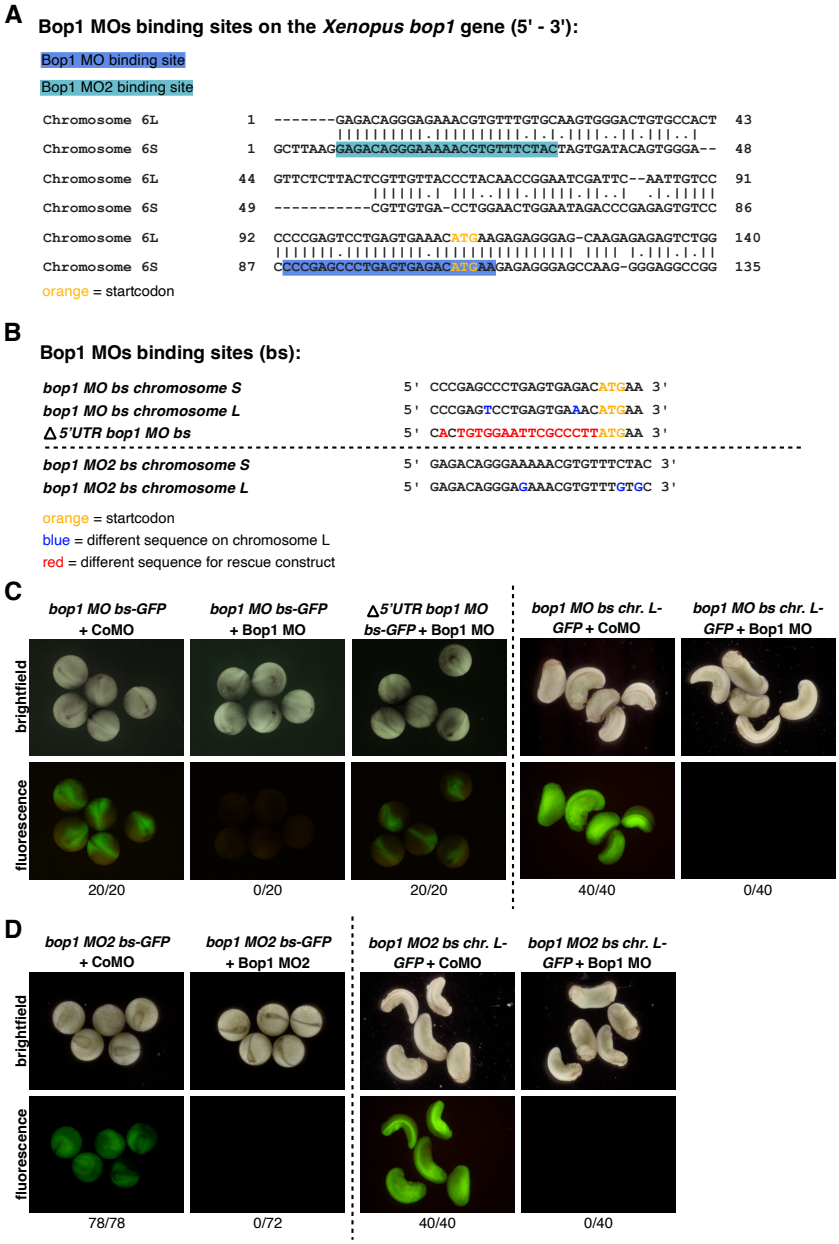


**Figure 13: Bop1 MOs binding specificity test.**

**A** Binding site of Bop1 MO (highlighted in blue) and Bop1 MO2 (highlighted in turquois) are indicated on the *Xenopus laevis bop1* gene. Chromosome 6L and 6S are shown. *bop1* start codon is highlighted in orange. **B** Bop1 MOs binding sites on chromosome L and S. Differences in sequence are highlighted in blue. Differences of *Δ5'UTR bop1 MO bs* sequence compared to *bop1 MO bs* on chromosome S are highlighted in red. *bop1* start codon is indicated in orange. **C** Binding specificity test of Bop1 MO to both homeologues. 10 ng Control MO was co-injected with 1 ng of *bop1 MO bs-GFP* or 1 ng of *bop1 MO bs chr.L-GFP*. At stage 18, GFP expression was detected in both approaches. But upon co-injecting Bop1 MO with the respective construct (*bop1 MO-bs GFP* and *bop1 MO2-bs GFP*, or 1 ng of *Δ5'UTR bop1 MO bs-GFP*) GFP expression was efficiently blocked. **D** Binding specificity test of Bop1 MO2. Co-injection of 10 ng Control MO together with 1 ng of *bop1 MO2 bs-GFP* or 1 ng of *bop1 MO2 bs chr.L-GFP* led to GFP translation. In contrast, GFP translation was efficiently blocked upon co-injection of 10 ng Bop1 MO2 together with 1 ng of *bop1 MO2 bs-GFP* or 1 ng of *bop1 MO2 bs chr.L-GFP*. Number below fluorescence photos indicate number of fluorescent embryos per total number of embryos analyzed. Abbreviations: Bop1 MO, block of proliferation 1 morpholino oligonucleotide; CoMO, control morpholino oligonucleotide; *GFP*, *green fluorescent protein*. Modified from (Gärtner et al., 2022) under CC BY 4.0 (https://creativecommons.org/licenses/by/4.0/).

The specificity and effectiveness of both Bop1 MOs, Bop1 MO and Bop1 MO2, was shown with this experiment and both MOs were used for further experiments during the present study.

### 3.1.5 Bop1 knockdown using morpholino oligonucleotides induces head and brain phenotypes

Since *bop1* expression was found to a great extent in the NCCs, the brain, and the eyes, and because ribosomopathy patients often suffer from malformations in the eye or craniofacial defects, 15 ng of Bop1 MO2 was injected into one animal-dorsal blastomere of eight-cell stage embryos to specifically target and analyze the anterior tissue upon Bop1 depletion (Moody and Kline, 1990). Control MO injection served as injection control and the uninjected side served as internal control. Morphants were fixed at stage 42 and analyzed regarding phenotypes of the anterior tissue. Bop1 MO2-injected embryos showed a reduced head size (microcephaly). Therefore, the distance between the midline and lateral edge of the embryo head of stage 42 morphants was measured and the injected side was compared to the uninjected side. The head width was significantly reduced upon Bop1 depletion. The co-injection of 0.5 ng ∆*5'UTR bop1* RNA rescued this phenotype (Fig. 14A and 14B). ∆*5'UTR bop1* RNA is a rescue construct with an altered 5'UTR sequence; therefore, ∆*5'UTR bop1* RNA cannot be targeted by Bop1 MO2 and Bop1 MO. For simplification, ∆*5'UTR bop1* RNA is depicted as *bop1* in all figures. In addition to the external measurements, cranial cartilage was dissected from stage 45 Bop1 morphants and stained using Alcian blue to assess whether the reduced head size is due to defects in this specific tissue. Bop1 morphants showed deformed and smaller cranial cartilage structures, such as the Meckel's cartilage, tectum anterius, and branchial arch (Fig. 14C)

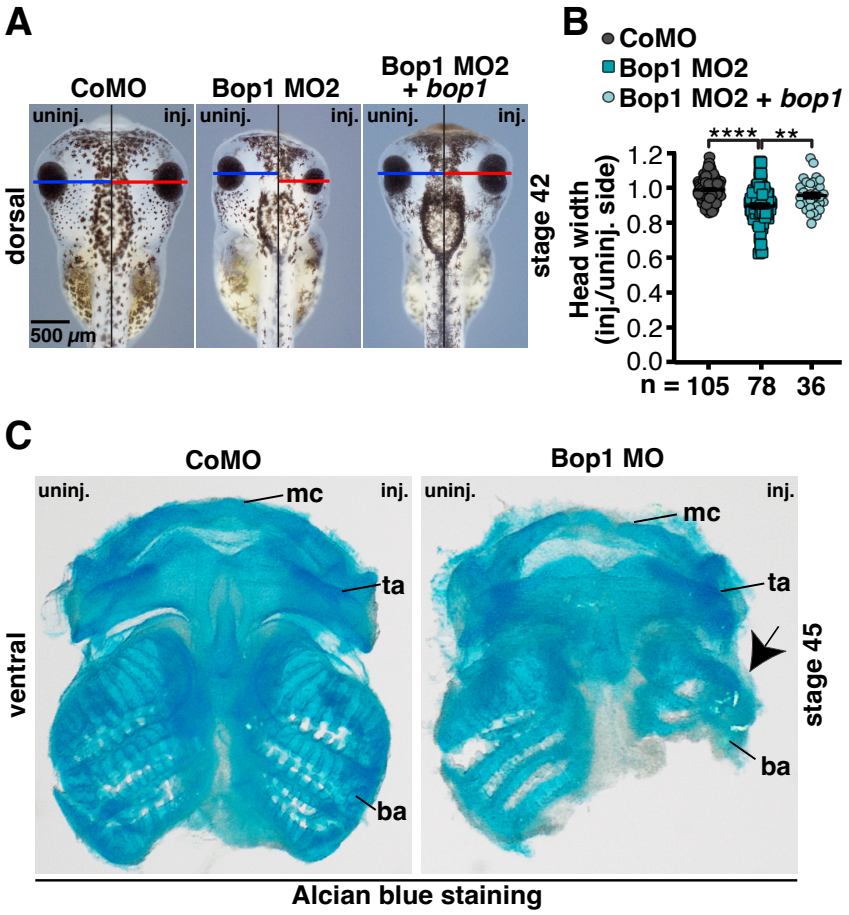


**Figure 14: Bop1 depletion results in microcephaly.**
**A** 15 ng Control MO, 15 ng Bop1 MO2, or 15 ng Bop1 MO2 + 0.5 ng Δ*5'UTR bop1* RNA was injected into one animal-dorsal blastomere. At stage 42, embryos were fixed and photographed. Head width was measured (distance between midline (black line) to lateral edge of the embryo head) using ImageJ and the injected side (red line) was compared to the uninjected side (blue line). **B** Bop1 morphants show significantly narrower heads of the injected side whereas Control MO injection did not affect head width. The phenotype was rescued upon co-injection of Δ*5'UTR bop1* RNA. **C** Cranial cartilage was dissected from stage 45 embryos and stained via Alcian blue staining. Control MO injection did not affect cartilage structures, whereas Bop1 depletion resulted in smaller and deformed structures (indicated by black arrow), e.g., the Meckel's cartilage (mc), the tectum anterius (ta), and the branchial arch (ba). Abbreviations: ba, branchial arch; Bop1 MO2, block of proliferation 1 morpholino oligonucleotide 2; CoMO, control morpholino oligonucleotide; inj., injected; mc, Meckel's cartilage; n, number of independent experiments; ta, tectum anterius; uninj., uninjected. *bop1* is the Δ*5'UTR bop1* RNA used for rescues. Error bars indicate standard error of the mean. **, $p \leq 0.01$; ****, $p \leq 0.0001$. Modified from (Gärtner et al., 2022) under CC BY 4.0 (https://creativecommons.org/licenses/by/4.0/).

The observed cranial cartilage phenotype is comparable to craniofacial malformations that occur in patients suffering from ribosomopathies.

Previous studies in the working group of PD Dr. Susanne Kühl showed that injection of the first Bop1 MO led to the same phenotypes as shown here for Bop1 MO2 (Gärtner et al., 2022).

Since Bop1 depletion resulted in a microcephaly phenotype, isolated brains of Bop1 morphants were analyzed. The area of these brains was measured using ImageJ and the injected side was compared to the uninjected side. Bop1 MO injection led to a decrease in the brain area as shown in the following figure 15.

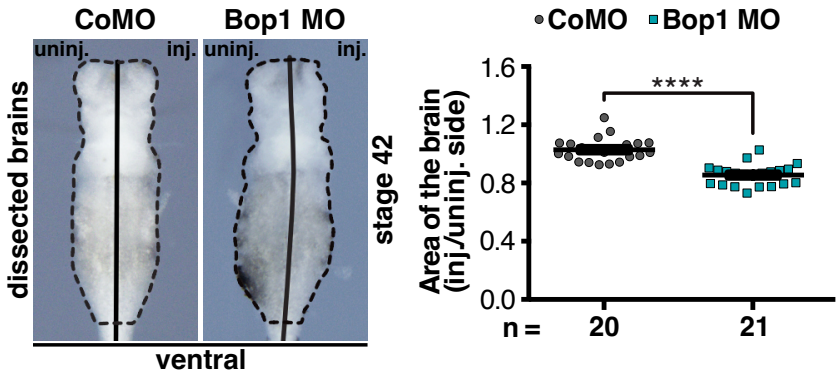


**Figure 15: Bop1 depletion leads to a reduced area of the brain.**
The brain area (black dotted line) of stage 42 embryos was measured and the area of the injected side was compared to the uninjected side (segregated by black solid line). The brain area on the Bop1 MO-injected side was significantly smaller. Control MO injection did not alter the area of the brain. Abbreviations: Bop1 MO, block of proliferation 1 morpholino oligonucleotide; CoMO, control morpholino oligonucleotide; inj., injected; n, number of independent experiments; uninj., uninjected. Error bars indicate standard error of the mean. ****, $p \leq 0.0001$. Dissected brains were provided by Annika Meßmer. Modified from (Gärtner et al., 2022) under CC BY 4.0 (https://creativecommons.org/licenses/by/4.0/).

During brain and head development, Bop1 knockdown resulted in severe phenotypes. Hence, Bop1 is crucial for proper head and brain development and arising phenotypes recapitulate phenotypes that occur during ribosomopathies (Farley-Barnes et al., 2019; Narla and Ebert, 2010).

### 3.1.6 Bop1 depletion results in eye phenotypes

In addition to the head and brain phenotype, Bop1 morphants showed malformed and smaller eyes (microphthalmia) in a significant manner. This eye phenotype was rescued upon co-injecting 0.5 ng *Δ5'UTR bop1* RNA (Fig. 16).

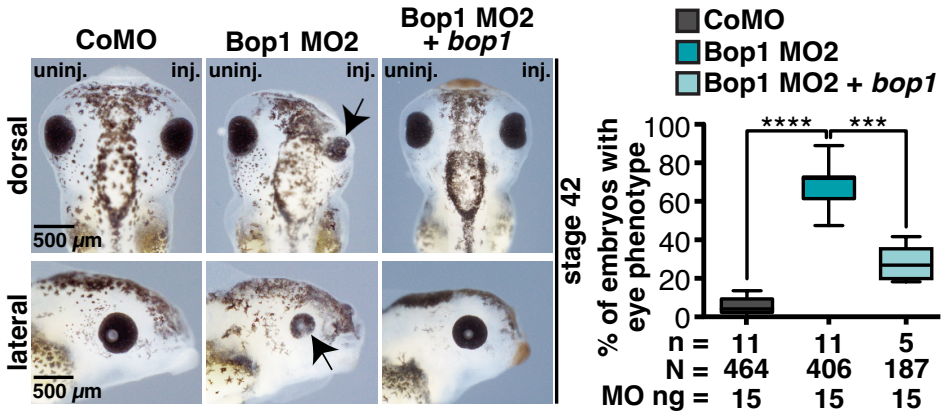


**Figure 16: Bop1 MO2 induces microphthalmia.**

15 ng of Control MO, Bop1 MO2, or Bop1 MO2 + 0.5 ng Δ*5'UTR bop1* RNA were unilaterally injected into one animal-dorsal blastomere. Embryos were analyzed at stage 42 regarding an eye phenotype. The injected side was compared to the uninjected side. Dorsal and lateral view of embryos is given. Bop1 MO2 injection led to smaller and deformed eyes (indicated by black arrow) in a high number of embryos. The co-injection of Δ*5'UTR bop1* RNA rescued the eye phenotype. Abbreviations: Bop1 MO2, block of proliferation 1 morpholino oligonucleotide 2; CoMO, control morpholino oligonucleotide; inj., injected; n, number of independent experiments; N, number of injected and analyzed embryos; uninj., uninjected. *bop1* is the Δ*5'UTR bop1* RNA used for rescues. Whiskers indicate standard minimum to maximum values; ***, $p \leq 0.001$; ****, $p \leq 0.0001$. Modified from (Gärtner et al., 2022) under CC BY 4.0 (https://creativecommons.org/licenses/by/4.0/).

To analyze the arising eye phenotype in more detail, the area of the eye was measured, and the injected side was compared to the uninjected side. Upon Bop1 depletion, the eye area of *Xenopus laevis* embryos significantly reduced (Fig. 17A and 17B). Additionally, the angle of occurring eye fissures was measured revealing a tendency of the Bop1 morphants to develop a coloboma phenotype (Fig. 17C and 17D). Upon co-injection of 0.5 ng Δ*5'UTR bop1* RNA, both eye phenotypes were rescued.

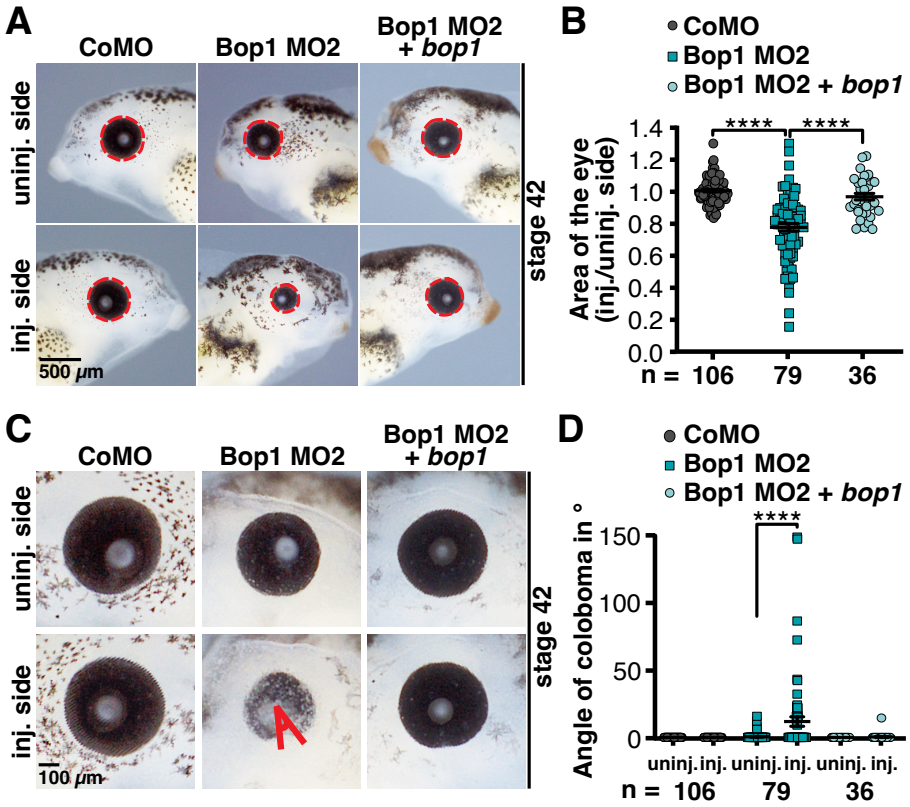


**Figure 17: Knockdown of Bop1 leads to smaller eyes and coloboma.**
**A** Lateral view of embryos is depicted. Area of the eye (red dotted line) of Control MO, Bop1 MO2, and Bop1 MO2 + 0.5 ng Δ*5'UTR bop1* RNA injected embryos was measured at stage 42 and the injected side was compared to the uninjected side. Bop1 depletion led to significantly smaller eyes. Co-injection of Δ*5'UTR bop1* RNA rescued the reduced eye area. **B** Statistical analysis of data shown in A. **C** The angle of occurring eye fissures (red angle) was measured showing an increased incidence of coloboma development in Bop1 morphants. **D** Statistical analysis of data shown in C. The co-injection of Δ*5'UTR bop1* RNA rescued the coloboma phenotype. Abbreviations: Bop1 MO2, block of proliferation 1 morpholino oligonucleotide 2; CoMO, control morpholino oligonucleotide; inj., injected; n, number of independent experiments; uninj., uninjected. *bop1* is the Δ*5'UTR bop1* RNA used for rescues. Error bars indicate standard error of the mean. ****, $p \leq 0.0001$. Modified from (Gärtner et al., 2022) under CC BY 4.0 (https://creativecommons.org/licenses/by/4.0/).

In conclusion, loss of Bop1 function resulted in microphthalmia, microcephaly, and a smaller brain in *Xenopus laevis* embryos. Phenotypes that are highly comparable to the symptoms that arise during ribosomopathies, e.g., eye malformations, craniofacial defects, and neurological impairments (Farley-Barnes et al., 2019; Narla and Ebert, 2010).

### 3.1.7 Gain of Bop1 function does not affect embryonic development

In addition to the loss of Bop1 function, gain of Bop1 function was analyzed during *Xenopus laevis* development. 0.5 ng or 1 ng *bop1* RNA was injected into one

animal-dorsal blastomere of eight-cell stage embryos. The overexpression of *bop1* did not induce a phenotype in the anterior tissue (Fig. 18).

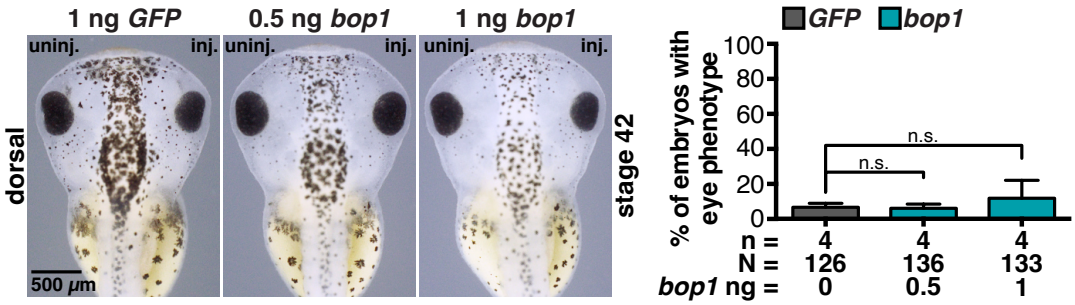


**Figure 18: Gain of Bop1 function does not lead to a phenotype.**
Embryos were injected with 1 ng *GFP* RNA or 0.5 ng or 1 ng *bop1* RNA at eight-cell stage into one animal-dorsal blastomere. Embryos were fixed at stage 42 and analyzed regarding a phenotype of the anterior tissue. Dorsal view of embryos is given. Gain of Bop1 function did not induce a phenotype. Abbreviations: *bop1*, *block of proliferation 1*; *GFP*, *green fluorescent protein*; inj., injected; n, number of independent experiments; N, number of injected and analyzed embryos; n.s., non-significant; uninj., uninjected. Error bars indicate standard error of the mean. Modified from (Gärtner et al., 2022) under CC BY 4.0 (https://creativecommons.org/licenses/by/4.0/).

In contrast to Bop1 depletion, the gain of Bop1 function did not affect the development of *Xenopus laevis* anterior tissue.

### 3.1.8 Proliferative pathways are not affected upon Bop1 knockdown

Since 1) Bop1 is a factor necessary for ribosomal synthesis and therefore downstream crucial for proliferation, and 2) Bop1 dominant negative mutants of mouse-derived cell lines suffer a cell cycle arrest (Pestov et al., 2001; Strezoska et al., 2002), proliferative processes were investigated upon Bop1 knockdown.

To stain proliferative cells, the BrdU staining method was applied to control and Bop1 morphants at stage 23. Stained proliferative cells on the injected side were compared to the uninjected side. Bop1 MO injection did not affect the number of proliferative cells (Fig. 19).

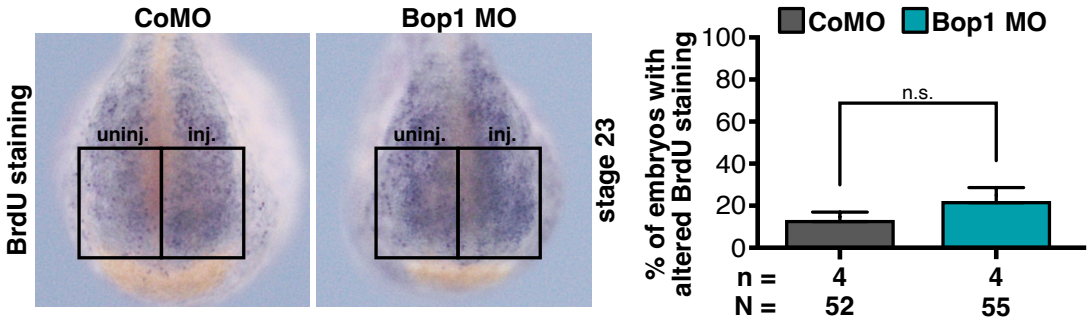


**Figure 19: Bop1 depletion does not affect the number of proliferative cells.**
Control MO and Bop1 MO was injected into one animal-dorsal blastomere at stage 8. BrdU staining was performed at stage 23. Embryos were fixed and photographed. Anterior view of embryos is shown. Injected side was compared to uninjected side (area of comparison is indicated by black boxes). Bop1 depletion did not affect proliferation. Abbreviations: Bop1 MO, block of proliferation 1 morpholino oligonucleotide; BrdU, 5-Bromo-2´-deoxy-uridine; CoMO, control morpholino oligonucleotide; inj., injected; n, number of independent experiments; N, number of injected and analyzed embryos; n.s., non-significant; uninj., uninjected. Error bars indicate standard error of the mean.

In previous studies, the molecule c-Myc – as enhancer of ribosomal synthesis and hence proliferation – has been shown to be affected and *c-myc* expression has been shown to be reduced upon depletion of other RPs and ribosomal factors (Challagundla et al., 2011; Schreiner et al., 2022). Therefore, Bop1 and c-Myc were investigated and a rescue approach with *c-myc* RNA was performed. 15 ng Bop1 MO was injected alone and co-injected with 0.5 ng *c-myc* RNA and occurring phenotypes were analyzed at stage 42. The Bop1 MO-induced phenotype was not rescued by co-injecting 0.5 ng *c-myc* RNA (Fig. 20).

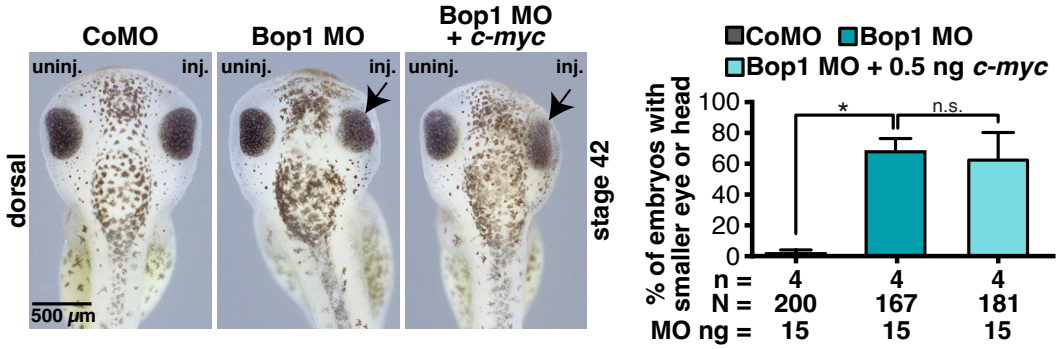


**Figure 20: *c-myc* overexpression does not rescue the Bop1 MO-induced phenotype.**
Control MO, Bop1 MO, and Bop1 MO + 0.5 ng *c-myc* RNA was injected into one animal-dorsal blastomere of eight-cell stage embryos. At stage 42, embryos were fixed and analyzed regarding a smaller eye (indicated by black arrow) and smaller head phenotype. Dorsal view of embryos is given. Bop1 MO injection resulted in smaller eyes and heads. The co-injection of Bop1 MO and *c-myc* RNA did not rescue this Bop1 MO-induced phenotype. Abbreviations: Bop1 MO, block of proliferation 1 morpholino oligonucleotide; *c-myc*, *myc protooncogene*; CoMO, control morpholino oligonucleotide; inj., injected; n, number of independent experiments; N, number of injected and analyzed embryos; n.s., non-significant; uninj., uninjected. Error bars indicate standard error of the mean. *, $p \leq 0.05$. Modified from (Gärtner et al., 2022) under CC BY 4.0 (https://creativecommons.org/licenses/by/4.0/).

Even though Bop1 is required for ribosomal biogenesis and therefore proliferative processes, Bop1 depletion did not reduce proliferation and enhancing proliferation did not rescue the Bop1 MO-induced phenotype.

### 3.1.9 Apoptotic pathways are not affected upon Bop1 depletion

Wu and colleagues have shown that lower BOP1 levels in patients suffering from aortic dissection led to oxidative stress and apoptosis (Wu et al., 2019). Therefore, apoptosis was analyzed and late-stage apoptotic cells were stained using TUNEL staining. Control and Bop1 morphants were fixed at stage 23 and TUNEL staining was performed. Neither Control MO nor Bop1 MO-injected embryos showed altered numbers of apoptotic cells on the injected side (Fig. 21).

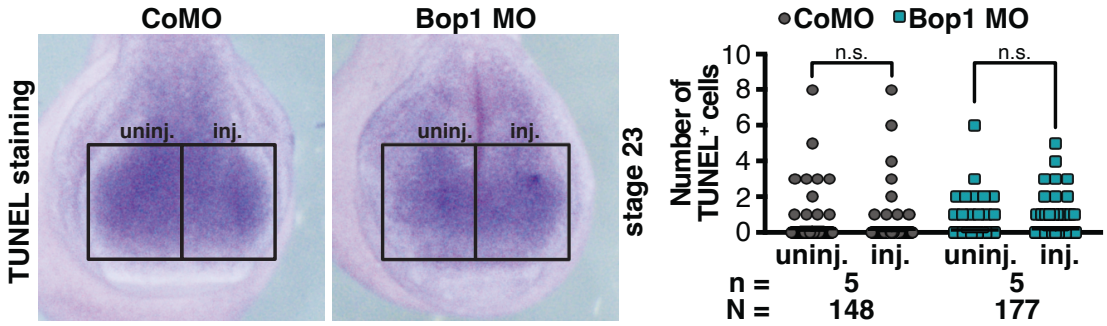


**Figure 21: Loss of Bop1 function does not affect the number of apoptotic cells.**
15 ng Control MO and 15 ng Bop1 MO were injected unilaterally into one animal-dorsal blastomere of eight-cell stage embryos. Embryos were fixed at stage 23 and TUNEL staining was performed. Anterior view of embryos is depicted. The number of apoptotic cells (counted in area indicated by black boxes) was neither affected in control morphants nor in Bop1 morphants. Abbreviations: Bop1 MO, block of proliferation 1 morpholino oligonucleotide; CoMO, control morpholino oligonucleotide; inj., injected; n, number of independent experiments; N, number of injected and analyzed embryos; n.s., non-significant; TUNEL, TdT-mediated dUTP Nick-End Labeling; uninj., uninjected. Error bars indicate standard error of the mean. Modified from (Gärtner et al., 2022) under CC BY 4.0 (https://creativecommons.org/licenses/by/4.0/).

Previous studies showed that cellular stress, which is induced by impaired ribosomal biogenesis, leads to a pro-apoptotic state via Tp53 (Dai and Lu, 2004) and that some clinical manifestations were rescued by co-depletion of Tp53 in zebrafish, mice, and frogs (Calo et al., 2018; Griffin et al., 2015; Jones et al., 2008). Hence, a rescue attempt was performed by simultaneous depletion of Bop1 and Tp53. 15 ng Bop1 MO was either injected alone or in combination with 2.5 ng or 5 ng Tp53 MO into eight-cell stage *Xenopus laevis* embryos which were phenotypically analyzed

at stage 42. Co-depletion of Tp53 did not rescue the Bop1 MO-induced anterior phenotype (Fig. 22).

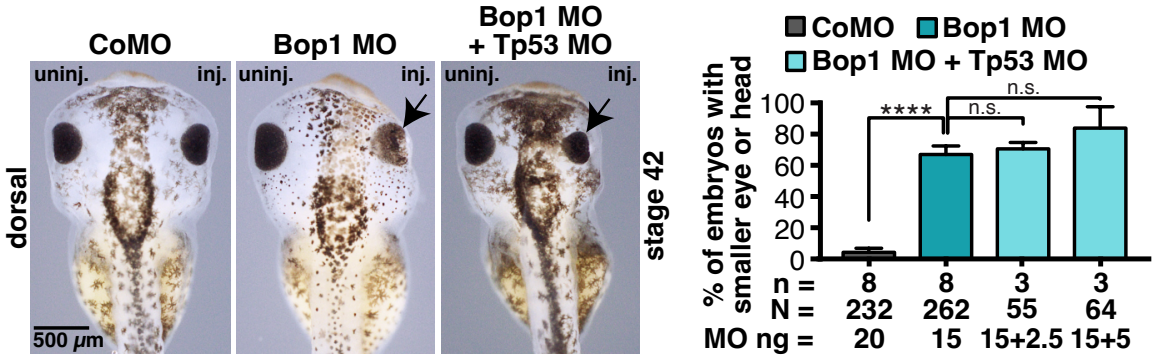


**Figure 22: Tp53 MO does not rescue Bop1 MO-induced phenotype.**
Eight-cell stage embryos were injected into one animal-dorsal blastomere with 15 ng Control MO, 15 ng Bop1 MO, or 15 ng Bop1 MO + 2.5/5 ng Tp53 MO. At stage 42, embryos were fixed and analyzed regarding an eye or head phenotype. Dorsal view of embryos is shown. Control MO injection did not affect eye or head development. Bop1 MO alone and in combination with Tp53 MO led to smaller eyes and heads (indicated by black arrow). Abbreviations: Bop1 MO, block of proliferation 1 morpholino oligonucleotide; CoMO, control morpholino oligonucleotide; inj., injected; n, number of independent experiments; N, number of injected and analyzed embryos; n.s., non-significant; Tp53 MO, tumor protein p53 morpholino oligonucleotide; uninj., uninjected. Error bars indicate standard error of the mean. ****, $p \leq 0.0001$. Modified from (Gärtner et al., 2022) under CC BY 4.0 (https://creativecommons.org/licenses/by/4.0/).

In conclusion, loss of Bop1 function did not increase the number of apoptotic cells and the co-depletion of Tp53 did not rescue the Bop1 MO-induced phenotype.

### 3.1.10 Loss of Bop1 function does not generally affect translation

Bop1 depletion did neither affect proliferative nor apoptotic pathways during *Xenopus laevis* development. Therefore, additional pathways were assessed during Bop1 knockdown in *Xenopus laevis* development to gain insight in underlying molecular mechanisms.

Since Bop1 contributes to a functional ribosome, it was investigated whether the depletion of Bop1 affects translational processes. Therefore, 1 ng *GFP* RNA was co-injected with 15 ng Bop1 MO or 15 ng Control MO. A GFP intensity analysis at stage 15 showed that Bop1 MO injection did not alter the expression of exogenous *GFP* (Fig. 23).

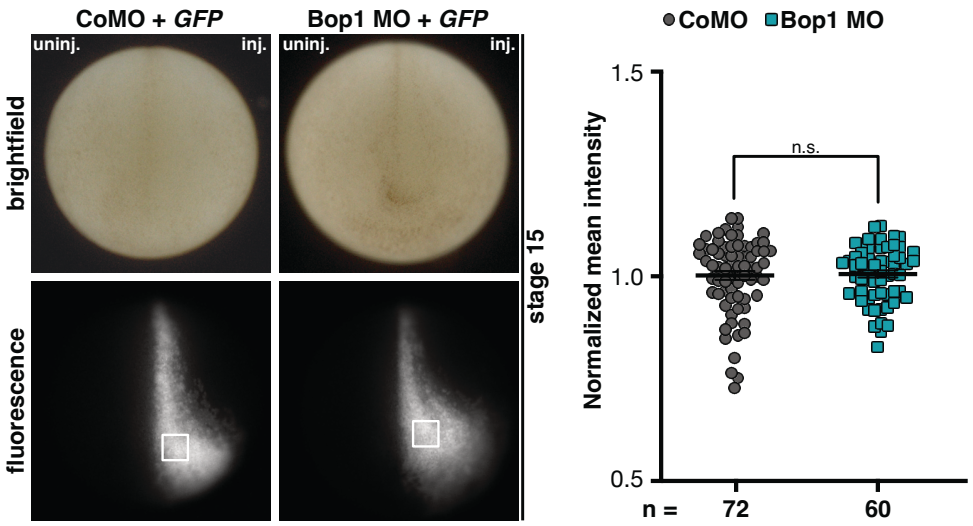


**Figure 23: Bop1 depletion does not reduce GFP expression.**
Eight-cell stage embryos were injected with 15 ng Control or Bop1 MO along with 1 ng *GFP* RNA into one animal-dorsal blastomere. At stage 15, embryos were photographed using a fluorescence microscope (8-bit greyscale). Anterior-dorsal view of embryos is given. By measuring the mean grey value (area indicated by white boxes), GFP intensity was analyzed. The mean intensities were normalized to the control group. Neither Control MO nor Bop1 MO injection altered expression of GFP. Abbreviations: Bop1 MO, block of proliferation 1 morpholino oligonucleotide; CoMO, Control morpholino oligonucleotide; *GFP*, *green fluorescent protein*; inj., injected; n, number of independent experiments; n.s., non-significant; uninj., uninjected. Error bars indicate standard error of the mean. Modified from (Gärtner et al., 2022) under CC BY 4.0 (https://creativecommons.org/licenses/by/4.0/).

Conclusively, Bop1 knockdown does not generally affect translation in *Xenopus laevis* embryos.

To further investigate translational processes, *Xenopus laevis* embryos were incubated in CHX. CHX prevents translation by inhibiting the elongation phase, in which the polypeptide chain elongates by amino acids (Schneider-Poetsch et al., 2010). First, it was investigated whether block of translation induces a phenotype in *Xenopus laevis* embryos. Therefore, WT embryos were incubated in different CHX concentration (35-350 nM CHX). Off note, starting from a concentration of 1 µM CHX, embryos died around stage 39. Embryos incubated in 350 nM CHX developed heart edema and a generally disturbed organ development such as smaller heads, deformed cranial cartilages, and a shortened body length. These phenotypes occurred in a dose dependent manner and are similar to the phenotypes upon Bop1 knockdown (Fig. 24).

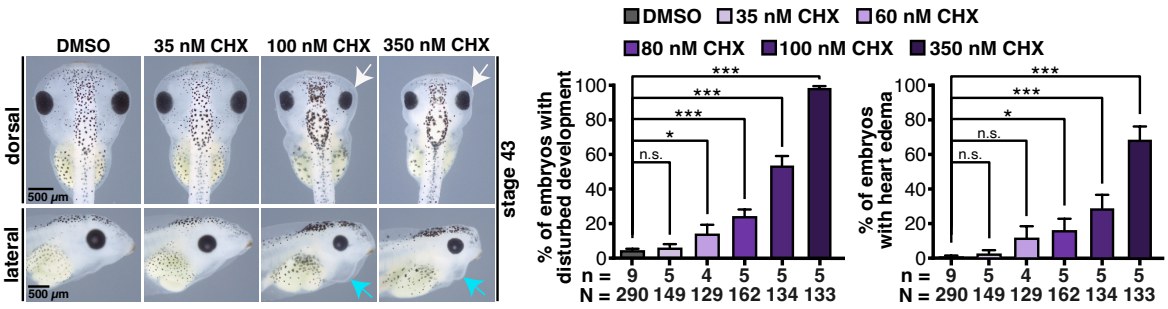


**Figure 24: Incubation in CHX disturbs *Xenopus laevis* development.**
Starting at stage 6, embryos were incubated in DMSO control and different concentrations of CHX (35 nM, 60 nM, 80 nM, 100 nM, and 350 nM). Embryos were fixed at stage 43 and occurring phenotypes were analyzed. Dorsal and lateral views are given. Embryos developed heart edema (indicated by light blue arrow), smaller heads and cranial cartilage (indicated by white arrow), and smaller eyes in a dose dependent manner. DMSO did not affect embryonic development. Abbreviations: CHX, cycloheximide; DMSO, dimethyl sulfoxide; n, number of independent experiments; N, number of injected and analyzed embryos; n.s., non-significant. Error bars indicate standard error of the mean; *, $p \leq 0.05$; ****, $p \leq 0.0001$.

In a next step, Bop1 knockdown and blockage of translation was analyzed simultaneously to assess if disturbed translation contributes to the Bop1 MO-induced phenotype. Therefore, 5 ng Bop1 MO or Control MO were injected into one animal-dorsal blastomere of eight-cell stage embryos followed by an incubation in either 80 nM DMSO or 80 nM CHX. Injection of 5 ng Bop1 MO and incubation in DMSO led to a mild phenotype on the injected side in 17% of the embryos. Injection of 5 ng Control MO and incubation in 80 nM CHX resulted in a mild phenotype in 15% of the embryos. Upon injection of 5 ng Bop1 MO and following incubation in 80 nM CHX, around 15% of the embryos showed a mild phenotype of the anterior tissue (Fig. 25).

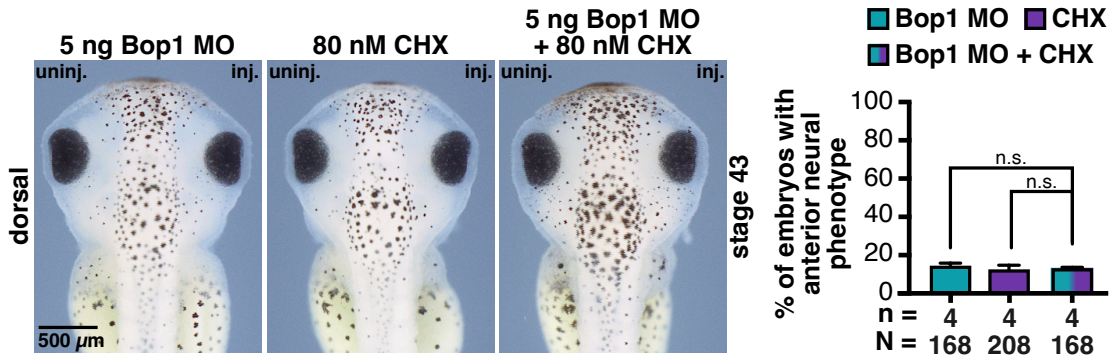


**Figure 25: Bop1 and CHX do not share a common pathway.**
5 ng Bop1 MO or 5 ng Control MO was injected unilaterally into an animal-dorsal blastomere followed by an incubation in either 80 nM DMSO or 80 nM CHX. At stage 43, embryos were fixed and analyzed regarding a phenotype of the anterior tissue. Dorsal view of embryos is depicted. Bop1 MO injection alone, incubation in CHX, and Bop1 MO injection + incubation in CHX resulted in a mild phenotype in a small number of embryos. Abbreviations: Bop1 MO, block of proliferation 1 morpholino oligonucleotide; CHX, cycloheximide; DMSO, dimethyl sulfoxide; n, number of independent experiments; N, number of injected and analyzed embryos; n.s., non-significant. Error bars indicate standard error of the mean.

Conclusively, the two phenotypes of Bop1 depletion and translation blockage by CHX treatment did not add up (regarding the number of embryos showing a phenotype and in the severity of occurring phenotypes), indicating that the Bop1 MO-induced phenotype arises through other pathways than disturbed translation. Otherwise, a synergistic effect would have been expected.

Bop1 depletion in *Xenopus laevis* embryos resulted in severe phenotypes of the anterior tissue. Yet, pathways for which Bop1 is typically required, such as proliferation, apoptosis, and translation, were not affected upon Bop1 knockdown. Based on these results, the hypothesis arose if Bop1 may exert a function independent of ribosomal synthesis. *Xenopus laevis* is an ideal model organism to study extra-ribosomal pathways, as its early embryonic development (until ~stage 26) does not require *de novo* ribosomal synthesis due to a large maternal store of ribosomes, mRNAs, and proteins (Brown, 1964; Pierandrei-Amaldi and Amaldi, 1994).

### 3.1.11 Expression of pan-neural marker *sox3* is disturbed upon Bop1 knockdown

To elucidate the molecular basis of the phenotypes upon MO injection in *Xenopus laevis* embryos and because loss of Bop1 function resulted in phenotypes of the

neural tissue, e.g., reduced brain size and smaller eyes, marker gene analysis was carried out using the pan-neural marker gene *sox3*. Stage 13 Bop1 and control morphants that were injected into one animal-dorsal blastomere were fixed and *sox3* expression was investigated using WMISH. Upon Bop1 MO injection, area of *sox3* expression was broadened, which was confirmed by measuring the width and area of *sox3* expression via the software ImageJ (Fig. 26 A-F).

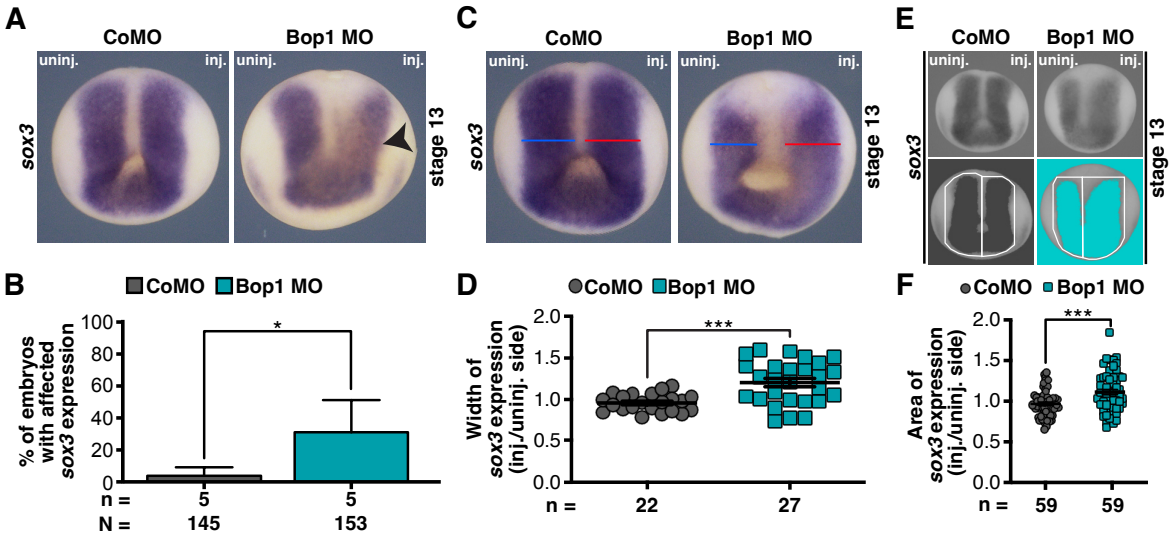


**Figure 26: Bop1 depletion alters expression of *sox3*.**

**A** Anterior view of embryos is shown. 15 ng Bop1 MO or 15 ng Control MO was injected into one animal-dorsal blastomere of eight-cell stage embryos. At stage 13, embryos were fixed and WMISH using a *sox3*-specific probe was performed. Affected *sox3* expression is indicated by black arrowhead. **B** Bop1 depletion resulted in altered *sox3* expression. **C** Anterior view of embryos is given. Embryos of one representative experiment shown in A were photographed and width of *sox3* expression was measured using the software ImageJ. Injected side (red line) and uninjected side (blue line) were compared. **D** *sox3* expression was significantly broader in Bop1 morphants compared to the control group. **E** Anterior view of embryos is shown. Area of *sox3* expression (dark grey (Control MO) and teal (Bop1 MO) area) was measured in white boxes using the software ImageJ and the injected side was compared to uninjected side. **F** Bop1 morphants show a significantly greater *sox3* expression on the injected side compared to the uninjected side and to the control group. Abbreviations: Bop1 MO, block of proliferation 1 morpholino oligonucleotide; CoMO, control morpholino oligonucleotide; inj., injected; n, number of independent experiments; N, number of injected and analyzed embryos; n.s., non-significant; *sox3*, *SRY-Box Transcription Factor 3*; uninj., uninjected; WMISH, whole mount *in situ* hybridization. Error bars indicate standard error of the mean. *, $p \leq 0.05$; ***, $p \leq 0.001$. Modified from (Gärtner et al., 2022) under CC BY 4.0 (https://creativecommons.org/licenses/by/4.0/).

As another pan-neural marker the expression of *sox2* (*SRY box transcription factor 2*) was analyzed. In stage 13 control and Bop1 morphants, WMISH was performed. *sox2* expression was unaffected upon Bop1 MO injection into one animal-dorsal blastomere (Fig. 27).

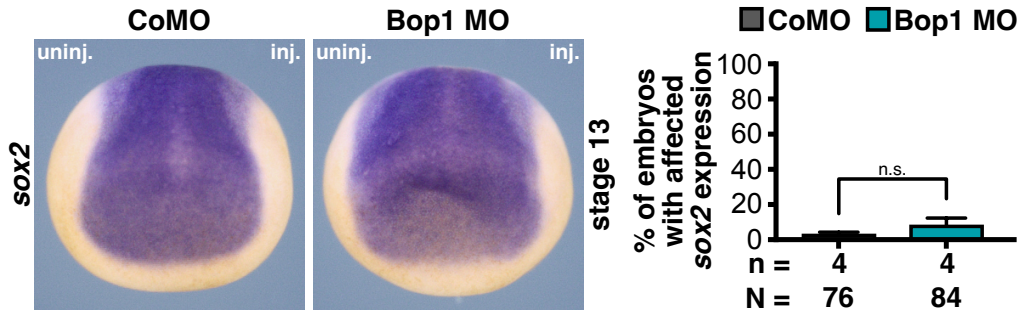


**Figure 27: Bop1 depletion does not affect expression of *sox2*.**
Anterior view of embryos is depicted. 20 ng Bop1 MO or 20 ng Control MO were injected into one animal-dorsal blastomere of eight-cell stage embryos. At stage 13, embryos were fixed and *sox2* expression was analyzed using WMISH. Expression of *sox2* was not affected in Bop1 morphants and control morphants. Abbreviations: Bop1 MO, block of proliferation 1 morpholino oligonucleotide; CoMO, control morpholino oligonucleotide; n.s., non-significant; *sox2*, *SRY-Box Transcription Factor 2*; WMISH, whole mount *in situ* hybridization. Error bars indicate standard error of the mean. Modified from (Gärtner et al., 2022) under CC BY 4.0 (https://creativecommons.org/licenses/by/4.0/).

To confirm the increase in *sox3* expression, real-time qPCR was performed. 20 ng Bop1 MO or 20 ng Control MO was injected bilaterally at two-cell stage. At stage 13, total RNA was isolated *sox3* expression was analyzed. In Bop1 MO-injected embryos, relative expression of *sox3* was increased compared to Control MO-injected embryos (Fig. 28). Additionally, the relative expression of *sox2* was analyzed. Expression of *sox2* was not affected upon Bop1 knockdown (Fig. 28).

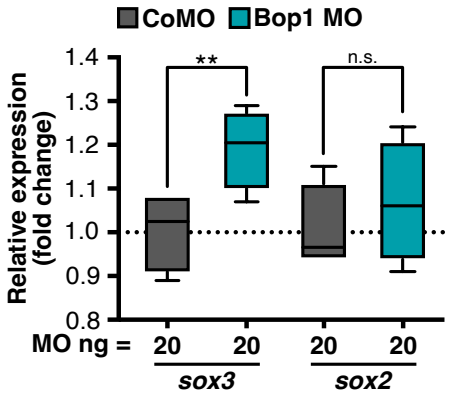


**Figure 28: Relative *sox3* and *sox2* expression upon Bop1 knockdown.**
20 ng Bop1 MO or 20 ng Control MO were bilaterally injected at two-cell stage embryos. At stage 13, relative *sox3* and *sox2* gene expression was analyzed using real-time qPCR. *sox3* and *sox2* expression was normalized to *gapdh*, *odc*, and *slc35b1*. Relative expression of *sox3* was significantly increased upon Bop1 knockdown compared to Control MO injection. Bop1 MO injection did not affect *sox2* expression. Abbreviations: Bop1 MO, block of proliferation 1 morpholino oligonucleotide; CoMO, control morpholino oligonucleotide; *gapdh*, *glyceraldehyde 3-phosphate dehydrogenase*; n.s., non-significant; *odc*, *ornithine decarboxylase 1*; *slc35b1, solute carrier family 35 member b1*; *sox2, SRY-Box Transcription Factor 2*; *sox3*, *SRY-Box Transcription Factor 3*. Whiskers indicate minimum and maximum. **, $p \leq 0.01$. Modified from (Gärtner et al., 2022) under CC BY 4.0 (https://creativecommons.org/licenses/by/4.0/).

In summary, analyzing the molecular basis of the Bop1 knockdown-associated phenotypes, a specific effect of Bop1 depletion on expression of the pan-neural marker *sox3* was detected strengthening the conclusion that Bop1 is required for early Sox3-dependent anterior neural development in *Xenopus laevis*.

### 3.1.12 Expression of NCC marker gene *foxd3* is reduced upon Bop1 depletion

Since loss of Bop1 function led to a malformed cranial cartilage (Fig. 14), which is a derivative of NCCs (Jacobson, 1991), the NCC-specific marker gene *foxd3* was investigated. Therefore, 15 ng Bop1 MO2- and 15 ng Control MO-injected embryos were fixed at stage 16, when NCCs are induced and *foxd3* expression was analyzed using WMISH. Bop1 knockdown resulted in a reduced *foxd3* expression (Fig. 29).

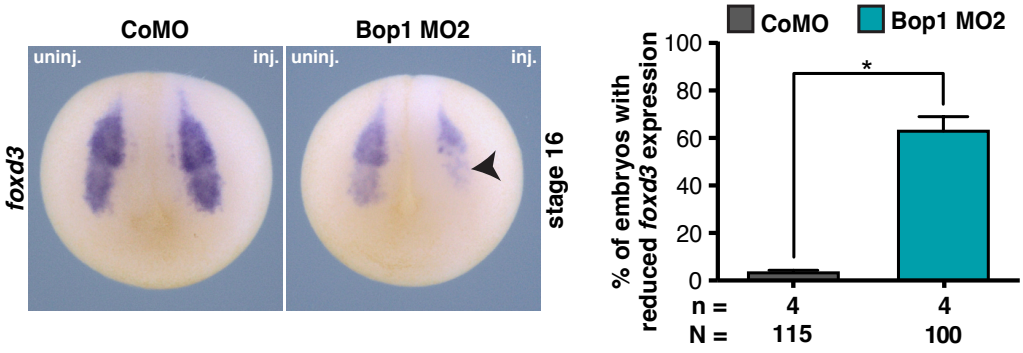


**Figure 29: Expression of NCC-specific marker gene *foxd3* is reduced upon Bop1 depletion.**
Embryos injected with Bop1 MO2 or Control MO were fixed at stage 16 and *foxd3* expression was analyzed by WMISH. Expression of *foxd3* was reduced (black arrowhead) on the Bop1 MO-injected side. Anterior view of embryos is shown. Control MO injection did not affect *foxd3* expression. Abbreviations: Bop1 MO2, block of proliferation 1 morpholino oligonucleotide 2; CoMO, control morpholino oligonucleotide; *foxd3*, *forkhead box d3*; inj., injected; n, number of independent experiments; N, number of injected and analyzed embryos; uninj., uninjected; WMISH, whole mount *in situ* hybridization. Error bars indicate standard error of the mean. *, $p \leq 0.05$.

Bop1 MO-injection led to disturbed NCC induction and malformed cranial cartilage structures implying a role of Bop1 during the development of NCC and NCC derivatives.

### 3.1.13 *foxd3* overexpression does not rescue the microcephalic phenotype

Foxd3 was further investigated regarding the question if it contributes to the Bop1 MO-induced phenotype and if Bop1 may exert an extra-ribosomal function - in addition to its ribosomal function - which is mediated through those genes.

Expression of *foxd3* was reduced upon Bop1 knockdown. Therefore, it was assessed whether the overexpression of *foxd3* can rescue the cranial cartilage phenotype of Bop1 morphants. Co-injection of Bop1 MO and *foxd3* RNA into one animal-dorsal blastomere did not rescue the phenotype (Fig. 30A and 30B). This was also confirmed upon Alcian blue staining of dissected cranial cartilages of respective embryos (Fig. 30C).

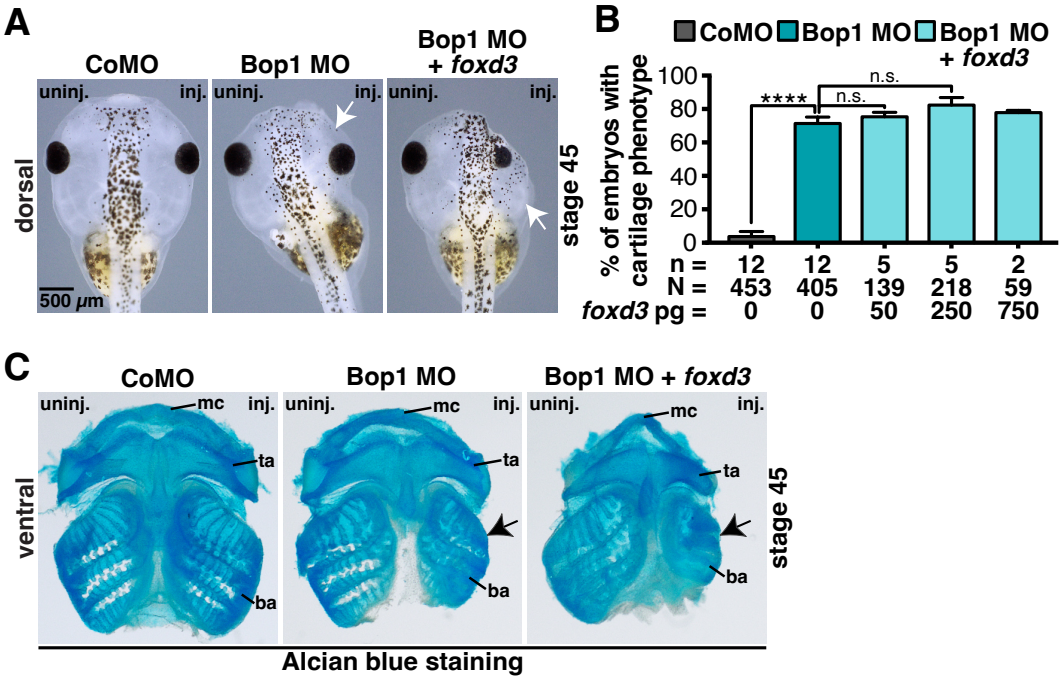


**Figure 30: *foxd3* overexpression cannot rescue the Bop1 MO-induced cranial cartilage phenotype.**
**A** Control MO, Bop1 MO, and Bop1 MO + *foxd3* RNA (50 pg, 250 pg, and 750 pg) was injected into one animal-dorsal blastomere of eight-cell stage embryos. Embryos were fixed at stage 45. First, they were analyzed regarding a head phenotype from the exterior (smaller head is indicated by white arrow). **B** Co-injection of *foxd3* RNA did not rescue the Bop1 MO-induced phenotype. **C** Second, cranial cartilage was dissected and stained using Alcian blue. Bop1 MO injection led to smaller cartilage structures (black arrows), such as the tectum anterius (ta) and the branchial arch (ba). Upon Bop1 MO + *foxd3* RNA injections, basically all cranial structures, ta, ba, and Meckel's cartilage (mc) were smaller and deformed. Abbreviations: ba, branchial arch; Bop1 MO, block of proliferation 1 morpholino oligonucleotide; CoMO, control morpholino oligonucleotide; *foxd3*, *forkhead box d3*; inj., injected; mc, Meckel's cartilage; n, number of independent experiments; N, number of injected and analyzed embryos; n.s., non-significant; ta, tectum anterius; uninj., uninjected. Error bars indicate standard error of the mean. ****, $p \leq 0.0001$. Modified from (Gärtner et al., 2022) under CC BY 4.0 (https://creativecommons.org/licenses/by/4.0/).

This result suggests that reduced *foxd3* did not or only to a small extent contribute to the Bop1 MO-induced phenotype otherwise a (partial) rescue would have been expected.

### 3.1.14 Bop1 knockdown reduces expression of brain-specific marker gene *pax6*

*bop1* transcripts were found in the brain and Bop1 depletion resulted in smaller brains in *Xenopus laevis* embryos (Fig. 15). Hence, expression of the brain marker gene *pax6* was analyzed in the neural tube (stage 13) and in the brain (stage 23) of Bop1 morphants. *pax6* expression was significantly reduced in the neural tube as well as in the developing brain upon Bop1 depletion (Fig. 31 A-F).

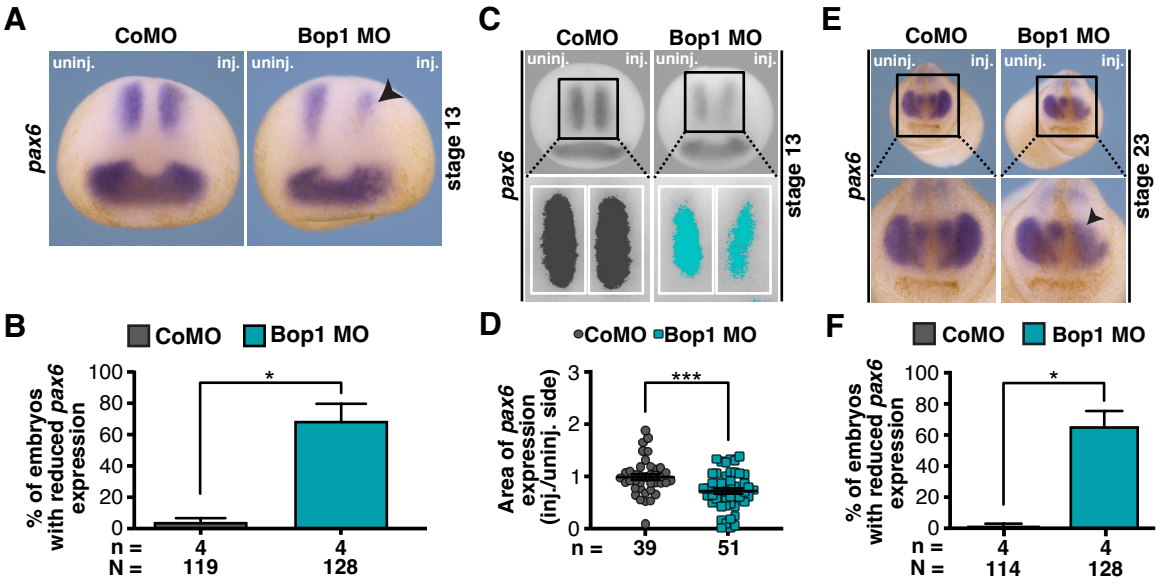


**Figure 31: Bop1 knockdown results in reduced *pax6* expression in the neural tube and developing brain.** Eight-cell stage embryos were injected with 15 ng Bop1 MO or 15 ng Control MO into one animal-dorsal blastomere and fixed at stage 13 and stage 23, respectively. Anterior view of embryos is given. **A** In the neural tube, *pax6* expression is significantly reduced (indicated by black arrowhead) on the injected side of Bop1 morphants. **B** Statistical analysis of data shown in A. **C** Area of *pax6* expression (dark grey (Control MO) and teal (Bop1 MO) area) was quantitatively measured using the software ImageJ and the injected side was compared to the uninjected side (indicated by white boxes). **D** Area of *pax6* expression was significantly smaller upon Bop1 depletion. **E** *pax6* expression in the developing brain of stage 23 embryos is reduced (indicated by black arrowhead), whereas the uninjected side and Control MO injection did not show reduced expression. **F** Statistical analysis of data shown in E. Abbreviations: Bop1 MO, block of proliferation 1 morpholino oligonucleotide; CoMO, control morpholino oligonucleotide; inj., injected; n, number of independent experiments; N, number of injected and analyzed embryos; *pax6*, *paired box 6*; uninj., uninjected; WMISH, whole mount *in situ* hybridization. Error bars indicate standard error of the mean. *, $p \leq 0.05$; *** $p \leq 0.001$. Modified from (Gärtner et al., 2022) under CC BY 4.0 (https://creativecommons.org/licenses/by/4.0/).

The above-described results that Bop1 depletion led to smaller brains and a reduced *pax6* expression in the neural tube and the developing brain indicate that Bop1 is required for proper brain development in *Xenopus laevis* embryos.

### 3.1.15 Expression of eye-specific marker genes is reduced upon Bop1 knockdown

Bop1 MO injection resulted in microphthalmia and a coloboma phenotype and *bop1* mRNA was found to be intensely expressed in the eyes. Therefore, the two eye-specific marker genes *rax* and *pax6* were analyzed during eye field induction (stage 13) and eye cell differentiation (stage 23). 15 ng Bop1 MO or 15 ng Control MO was injected, embryos were fixed and WMISH was performed using probes specific for *rax* and *pax6*. The expression of both marker genes was reduced during eye field induction as well as eye cell differentiation (Fig. 32 A-D). Reduced *pax6* expression at stage 13 was also confirmed by analyzing the area of *pax6* expression using ImageJ (Fig. 32E and 32F).

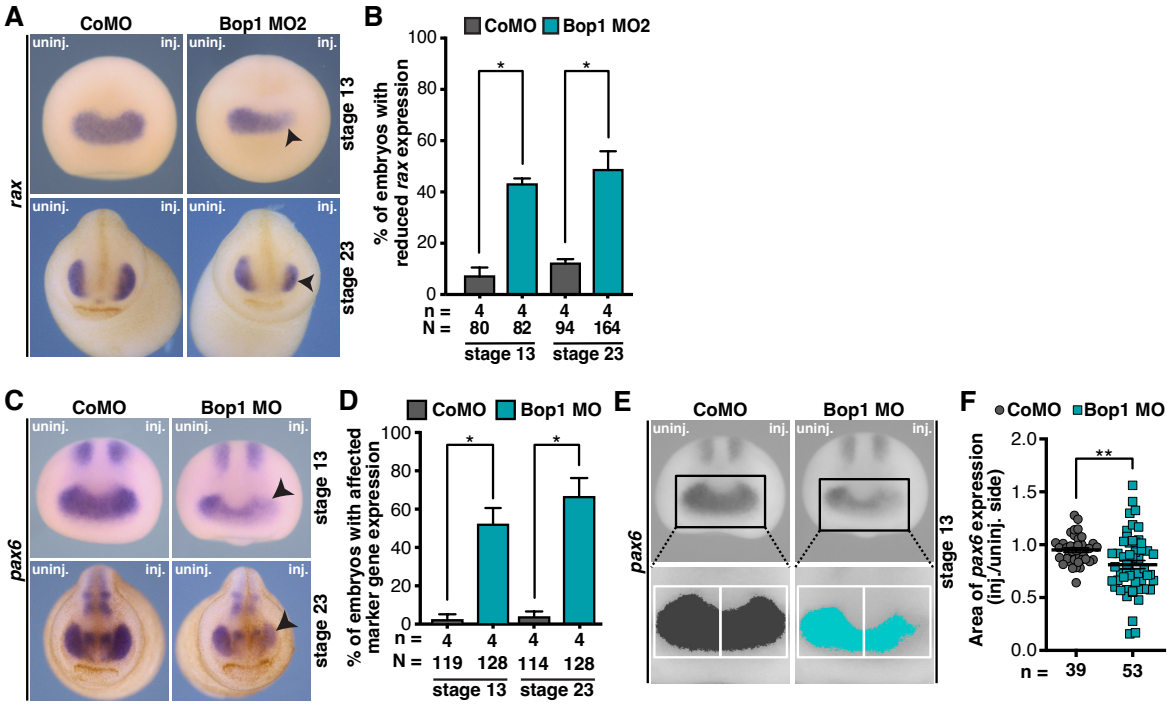


**Figure 32: Bop1 depletion leads to reduced eye marker gene expression.**
Anterior view of embryos is given. **A** 15 ng Bop1 MO2 or Control MO was injected into *Xenopus laevis* embryos at eight-cell stage. At stage 13 and 23, embryos were fixed and *rax* expression was analyzed using WMISH. Reduced expression is indicated by black arrowhead. **B** *rax* expression was significantly reduced upon Bop1 knockdown. **C** Bop1 and control morphants were fixed at stage 13 and stage 23 and *pax6* expression was analyzed via WMISH. Reduced expression is indicated by black arrowhead. **D** Expression of *pax6* was reduced during eye field induction and eye cell differentiation. **E** Area of *pax6* expression (dark grey (Control MO) and teal (Bop1 MO) area) was measured using the software ImageJ in stage 13 embryos. The injected side was compared to the uninjected side (white boxes) of Bop1 and control morphants. **F** Area of *pax6* expression was reduced upon Bop1 depletion. Abbreviations: Bop1 MO(2), block of proliferation 1 morpholino oligonucleotide (2); CoMO, control morpholino oligonucleotide; inj., injected; n, number of independent experiments; N, number of injected and analyzed embryos; n.s., non-significant; *pax6*, *paired box 6*; *rax*, *retina and anterior neural fold homeobox*; uninj., uninjected; WMISH, whole mount *in situ* hybridization. Error bars indicate standard error of the mean. *, $p \leq 0.05$; ** $p \leq 0.01$. Modified from (Gärtner et al., 2022) under CC BY 4.0 (https://creativecommons.org/licenses/by/4.0/).

During eye development, Sonic hedgehog (Shh) is necessary for midline signaling and furthermore inhibits *pax6* expression (Macdonald et al., 1995). Therefore, *shh* expression was analyzed upon Bop1 knockdown. At eight-cell stage, embryos were injected bilaterally into both animal-dorsal blastomeres with 15 ng Bop1 MO or Control MO. Embryos were fixed at stage 17 and 34/35 and expression of *shh* was analyzed using WMISH. Bop1 depletion did not affect *shh* expression (Fig. 33).

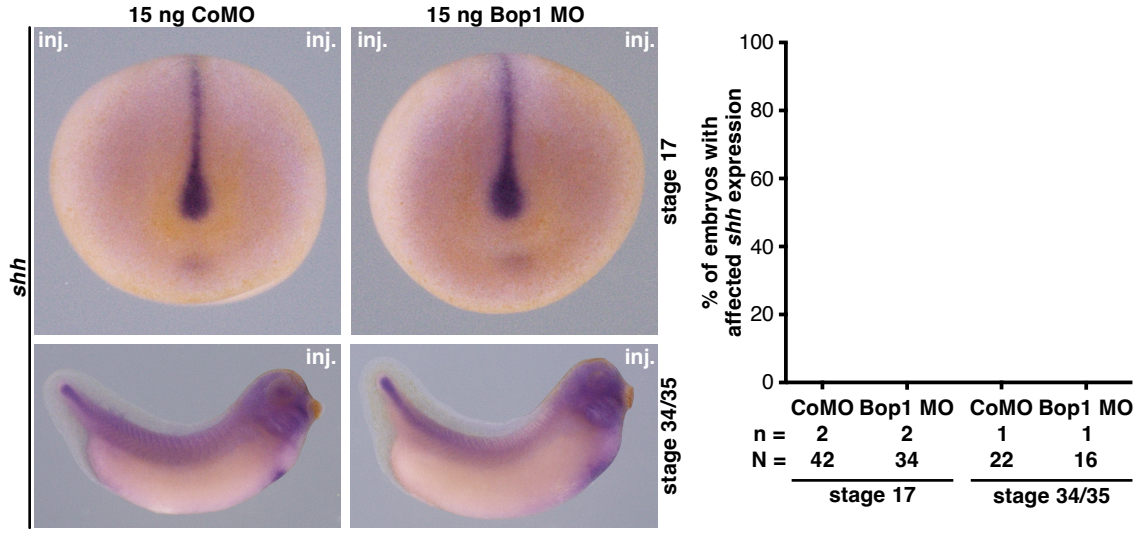


**Figure 33: Bop1 knockdown does not interfere with *shh* expression.**
15 ng Bop1 MO or Control MO were injected bilaterally into eight-cell stage embryos. At stage 17 and 34/35, embryos were fixed and *shh* expression was analyzed via WMISH. Neither stage 17 (anterior view) nor stage 34/35 (lateral view) embryos showed differences in *shh* expression upon Control MO or Bop1 MO injection. Abbreviations: Bop1 MO, block of proliferation 1 morpholino oligonucleotide; CoMO, control morpholino oligonucleotide; inj., injected; n, number of independent experiments; N, number of injected and analyzed embryos; *shh*, *sonic hedgehog*; uninj., uninjected; WMISH, whole mount *in situ* hybridization.

To sum up, Bop1 is required for proper eye development as its depletion leads to severe eye defects as well as disturbed expression of the eye-specific marker genes *rax* and *pax6*. Bop1 knockdown did not affect expression of the *pax6* counterpart *shh* indicating that midline signaling is not disturbed in general.

In conclusion, as molecular basis of the Bop1 MO-induced phenotype, marker genes of the eye, brain, and NCCs were identified. These marker genes were affected upon loss of Bop1 function during induction and differentiation of the respective tissues – tissues which are also affected during the pathological condition of ribosomopathies (Farley-Barnes et al., 2019; Narla and Ebert, 2010). However, expression of the marker genes was affected at very early embryonic stages in which *Xenopus laevis* embryos are independent of ribosomal synthesis due to a maternal supply of ribosomes, mRNAs, and proteins (Brown, 1964; Pierandrei-Amaldi and Amaldi, 1994) pointing towards an additional function of Bop1 which is independent of the ribosome.

### 3.1.16 Bop1 and Pax6 act in a common signaling pathway

Since Pax6 is a master regulator during eye development and because expression of *pax6* was drastically reduced in the developing brain and eyes (Fig. 31 and 32), Bop1 and Pax6 were further investigated regarding a common signaling pathway and if Pax6 might contribute to the Bop1 MO-induced phenotype. Therefore, Bop1 MO was injected alone and in combination with *pax6* RNA to analyze a possible rescue mechanism via *pax6* overexpression. However, a rescue of the Bop1 MO-induced phenotype was not possible with 0.2 ng, 0.5 ng, or 1 ng *pax6* RNA (Fig. 34).

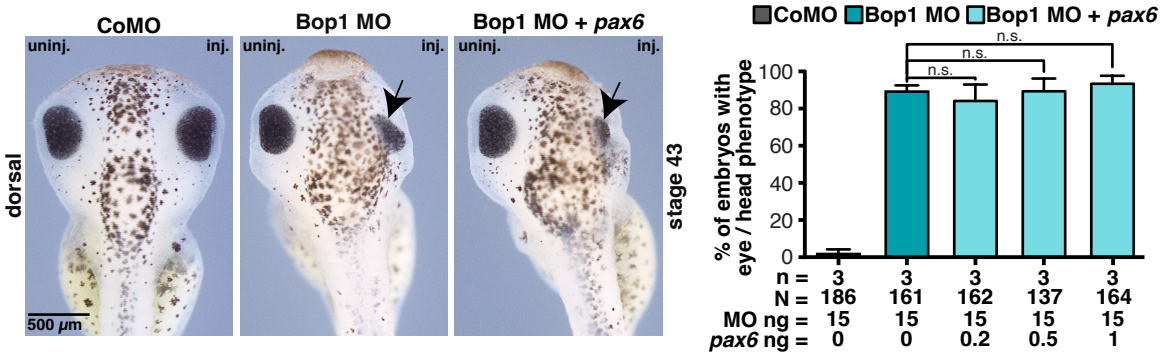


**Figure 34: Overexpression of *pax6* does not rescue the Bop1 MO-induced phenotype.**
Bop1 MO was injected alone and in combination with 0.2 ng, 0.5 ng, or 1 ng *pax6* RNA into one animal-dorsal blastomere. Embryos were fixed at stage 43 and occurring phenotypes of the eyes and heads were evaluated. Black arrows indicate smaller eyes. Dorsal view of embryos is shown. Bop1 depletion and Bop1 depletion plus simultaneous *pax6* overexpression resulted in over 80% of embryos showing a severe eye and head phenotype. Abbreviations: Bop1 MO, block of proliferation 1 morpholino oligonucleotide; CoMO, control morpholino oligonucleotide; inj., injected; n, number of independent experiments; N, number of injected and analyzed embryos; n.s., non-significant; *pax6*, *paired box 6*; uninj., uninjected. Error bars indicate standard error of the mean. Modified from (Gärtner et al., 2022) under CC BY 4.0 (https://creativecommons.org/licenses/by/4.0/).

As mentioned above, Pax6 is a master regulator of eye development and needs to be finely balanced as a slight discrepancy already leads to a severe eye phenotype. This phenotype is similar to the phenotype observed upon Bop1 depletion which was shown in earlier studies (Chow et al., 1999; Schedl et al., 1996) and confirmed here by overexpressing *pax6* - using 0.5 ng and 1 ng *pax6* RNA - in the anterior neural tissue of *Xenopus laevis* embryos (Fig. 35).

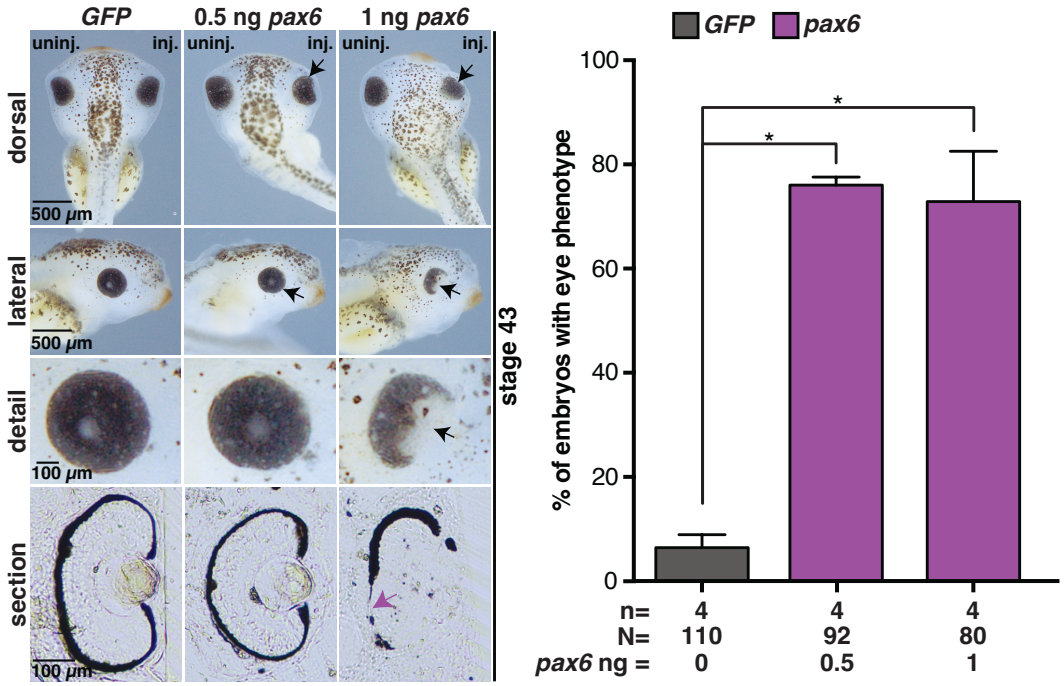


**Figure 35: Gain of Pax6 function induces severe eye phenotype in *Xenopus laevis* embryos.**
*GFP* (1 ng) or *pax6* RNA (0.5 ng and 1 ng) was injected into one animal-dorsal blastomere of eight-cell stage embryos. Embryos were fixed and analyzed at stage 43. Dorsal, lateral, and detail views, and sections are given. Gain of Pax6 led to smaller and malformed eyes (black arrows) whereas *GFP* RNA injection did not affect eye development. Sections reveal a disturbed retinal pigmented epithelium (purple arrow) upon *pax6* overexpression. Abbreviations: *GFP*, *green fluorescent protein*; inj., injected; n, number of independent experiments; N, number of injected and analyzed embryos; *pax6*, *paired box 6*; uninj., uninjected. Error bars indicate standard error of the mean. *, $p \leq 0.05$.

Not only overexpression of *pax6* resulted in an eye phenotype, also loss of Pax6 function via Pax6 MO led to smaller eyes comparable to the Bop1 MO-induced eye phenotype (Fig. 36A and 36B). Therefore, a common signaling pathway of Bop1 and Pax6 was further investigated. Low doses of Bop1 MO and Pax6 MO as well as both low doses combined were injected into one animal-dorsal blastomere of eight-cell stage embryos. At stage 42, embryos were evaluated regarding eye phenotypes. Both low doses alone did induce a mild eye phenotype in a small number of embryos. The simultaneous injection resulted in a strong eye phenotype in a more than additive manner (Fig. 36C and 36D).

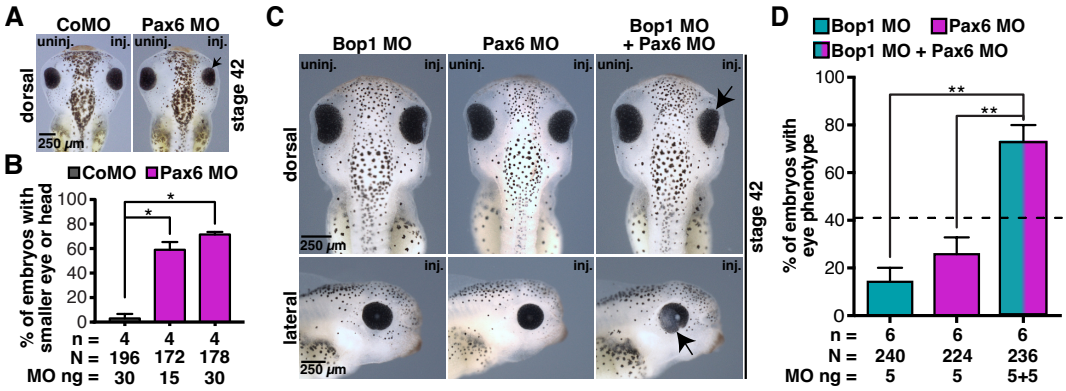


**Figure 36: Bop1 and Pax6 share a common signaling pathway.**

**A** Control MO or Pax6 MO was injected into one animal-dorsal blastomere. Embryos were fixed at stage 42 and analyzed regarding an eye or head phenotype (black arrow points towards smaller eye). Dorsal views are given. **B** Embryos injected with 15 ng or 30 ng Pax6 MO developed smaller eye and heads on the injected side. **C** 5 ng Bop1 MO and 5 ng Pax6 MO were injected alone or in combination into *Xenopus laevis* embryos. Dorsal and lateral view of embryos is shown. **D** Low doses alone resulted in a mild phenotype. The combined injection of both low doses led to a severe eye phenotype (indicated by black arrow) in a more than additive manner. Black dotted line represents sum of embryos injected with Bop1 MO or Pax6 MO showing an eye phenotype. Abbreviations: Bop1 MO, block of proliferation 1 morpholino oligonucleotide; CoMO, control morpholino oligonucleotide; inj., injected; n, number of independent experiments; N, number of injected and analyzed embryos; Pax6 MO, paired box 6 morpholino oligonucleotide; uninj., uninjected. Error bars indicate standard error of the mean. *, $p \leq 0.05$, **, $p \leq 0.01$. Modified from (Gärtner et al., 2022) under CC BY 4.0 (https://creativecommons.org/licenses/by/4.0/).

The above-described results that *pax6* expression is reduced upon Bop1 knockdown and that combined Bop1 MO and Pax6 MO injection led to a more than additive effect in *Xenopus laevis* embryos leads to the suggestion of a common signaling pathway of Bop1 and Pax6 and that the Bop1 MO-induced phenotype is at least in part mediated through Pax6.

### 3.1.17 *bop1* knockout via CRISPR/Cas9 induces phenotypes in anterior tissue

The CRISPR/Cas9 method was implemented as a second method for Bop1 depletion to proof the specificity of the loss of Bop1 function phenotype. Therefore, three gRNAs were designed targeting different exons of the *bop1* gene. To analyze a successful knockout on a genomic level, embryos were injected at one-cell stage with 1 ng Cas9 protein and 300 pg of the respective gRNA and lysed at stage 43 followed by PCR and Sanger sequencing (a pool of 10 embryos was sequenced) (Fig. 37A). Figure 37B depicts the CRISPR target sites of *bop1 gRNAs* on the *bop1* gene and location of forward primers (FP) and reverse primers (RP). Regarding the CRISPR target site of *gRNA #1*, DNA sequencing results of WT *Xenopus laevis*

embryos showed a clear and homogenous sequence around the CRISPR target site (Fig. 37C). However, the DNA sequence of *bop1* CRISPants was heterogenous starting around 4 bases upstream of the *bop1 gRNA #1* PAM sequence (Fig. 37C). Comprehensive Sanger sequencing results for chromosome 6L and chromosome 6S are depicted in the appendix (suppl. Fig. 2-5). Furthermore, sequencing results of CRISPR target sites *bop1 gRNA #2* and *bop1 gRNA #3* also showed heterogenous sequences upstream the PAM sequence. Sanger sequencing results of WT embryos and CRISPants with *bop1 gRNA #2* and *bop1 gRNA #3* targets are given in the appendix section (suppl. Fig. 6-9).

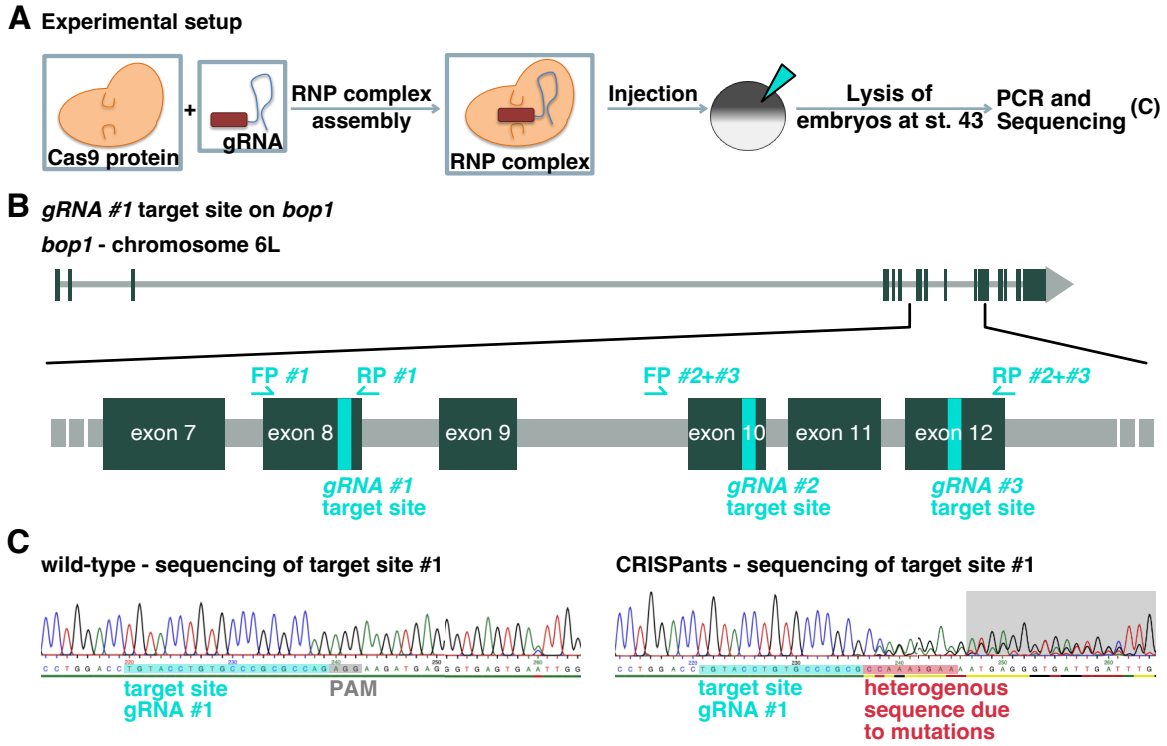


**Figure 37: Knockout evaluation of *bop1 gRNA #1*.**

**A** Experimental setup of CRISPR knockout evaluation. Cas9 protein and gRNA were incubated for 5 min at 37 °C to assemble the RNP complex, which was injected into one-cell stage embryos. Embryos were lysed at stage 43. Purified DNA of ten individual embryos was amplified and sequenced. **B** *bop1* gene on chromosome 6L. *bop1 gRNA #1, #2,* and *#3* target sites are indicated by teal stripes. Location of respective forward primers (FP) and reverse primers (RP) are also indicated. **C** DNA sequencing result of 10 WT embryos. Target site of *bop1 gRNA #1* is indicated in teal; PAM sequence is indicated in grey (AGG). DNA sequencing result of 10 CRISPants. Target site of *bop1 gRNA #1* is indicated in teal. Heterogenous sequence (different overlapping signals), which starts around 4 bases upstream of the PAM sequence, is indicated in red. Abbreviations: *bop1, block of proliferation 1*; Cas9, CRISPR-associated protein 9; FP, forward primer; gRNA, guide ribonucleic acid; PCR, polymerase chain reaction; RNP, ribonucleoprotein; RP, reverse primer; st., stage; WT, wild-type. Modified from (Gärtner et al., 2022) under CC BY 4.0 (https://creativecommons.org/licenses/by/4.0/).

This result indicates that the DNA sequence differed between the ten analyzed CRISPants, which strongly hints towards a successful *bop1* knockout.
Additionally, the online software tool TIDE was used to predict gRNA efficacy. *bop1 gRNA #1* had an efficiency of 44.8% on homeologue 6L and 59.1% on homeologue 6S (raw data from online tool can be seen in the appendix (suppl. Fig. 10-13)). A prediction was not possible for *bop1 gRNA #2* and *bop1 gRNA #3* due to software limitations.

To evaluate if the gRNAs successfully induced a phenotype, two-cell stage embryos were injected unilaterally with the pre-assembled RNP complexes. Injection of Cas9 protein alone served as negative control. At stage 43, embryos were fixed and evaluated regarding a phenotype of the anterior tissue. Injection of *bop1 gRNA #1* led to smaller eyes and heads on the injected side of the embryos. *bop1 gRNA #2* mildly induced smaller eyes and heads. Anyhow, the number of mildly affected embryos was low. *bop1 gRNA #3* and Cas9 protein alone did not affect anterior tissues of the embryos (Fig. 38).

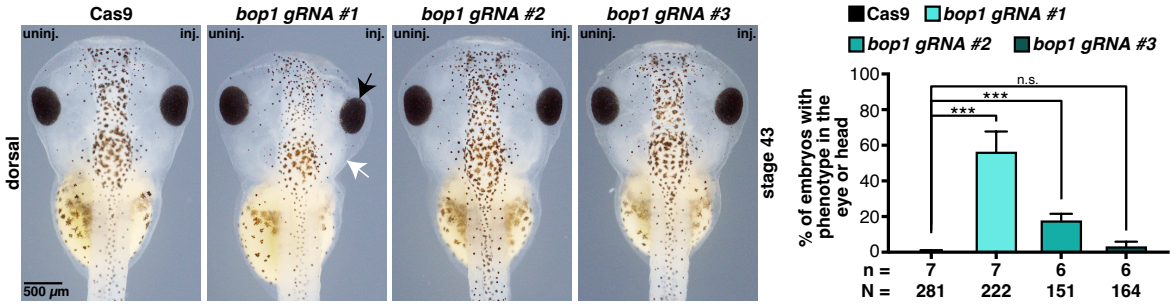


**Figure 38: *bop1* knockout using *bop1 gRNA #1* results in smaller eyes and heads.**
Dorsal view of embryos is depicted. Two-cell stage embryos were injected unilaterally with either 1 ng Cas9, 1 ng Cas9 + 300 pg *bop1 gRNA #1*, 1 ng Cas9 + 300 pg *bop1 gRNA #2*, or 1 ng Cas9 + 300 pg *bop1 gRNA #3*. At stage 43, embryos were fixed and evaluated. Injection of *bop1 gRNA #1* resulted in a high number of embryos showing smaller eyes (black arrow) and heads (white arrow). *bop1 gRNA #2* resulted in a mild phenotype in about 20% of the injected embryos. Cas9 protein alone and *bop1 gRNA #3* did not lead to any phenotype. Abbreviations: *bop1 gRNA, block of proliferation 1 guide ribonucleic acid*; Cas9, CRISPR-associated protein 9; inj., injected; n, number of independent experiments; N, number of injected and analyzed embryos; n.s., non-significant; uninj., uninjected. Error bars indicate standard error of the mean. ***, $p \leq 0.001$. Based on (Gärtner et al., 2022).

Since *bop1 gRNA #2* and *bop1 gRNA #3* only showed a mild and no phenotype, respectively, and determining gRNA efficiency was not possible for *bop1 gRNA #2* and *bop1 gRNA #3*, only *bop1 gRNA #1* was considered for further experiments.

For a more comprehensive phenotypic analysis, the area of the eyes and the head width was measured quantitively and analyzed. *bop1* CRISPants had smaller eyes and narrower heads compared to the uninjected side and compared to the control group (Fig. 39 A-D).

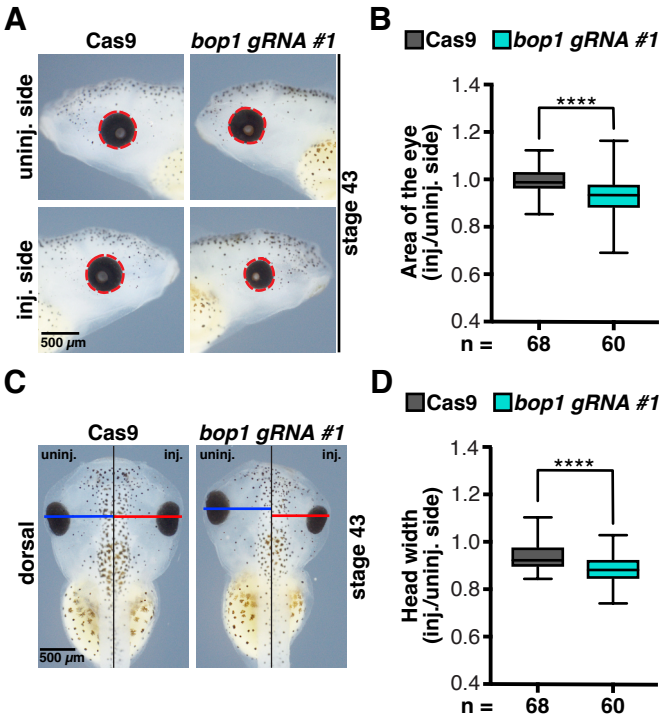


**Figure 39: *bop1 gRNA #1* injection leads to smaller eyes and narrower heads.**
**A** Upon *bop1* knockout using the CRISPR/Cas9 system, *Xenopus laevis* embryos were photographed at stage 43 and the area of the eye was measured (analyzed area is indicated by red dotted line). Lateral view of embryos is shown. **B** The area of the injected side was compared to the uninjected side. *bop1* CRISPants showed significantly smaller eyes on the injected side. **C** The head width of the injected side (red line) was compared to the uninjected side (blue line). Dorsal view is given. **D** Embryos which were injected with *bop1 gRNA #1* had significantly narrower heads on the injected side. Abbreviations: *bop1 gRNA*, *block of proliferation 1 guide ribonucleic acid*; Cas9, CRISPR-associated protein 9; inj., injected; n, number of independent experiments; N, number of injected and analyzed embryos; n.s., non-significant; uninj., uninjected. Whiskers indicate minimum and maximum. ****, $p \leq 0.0001$. Modified from (Gärtner et al., 2022) under CC BY 4.0 (https://creativecommons.org/licenses/by/4.0/).

In conclusion, the depletion of Bop1 using the CRISPR/Cas9 system led to a similar phenotype as Bop1 knockdown using the MO-based approach. Occurring phenotypes were milder using the CRISPR/Cas9 system.

### 3.1.18 *bop1* knockout using the CRISPR/Cas9 system does not affect early marker gene expression

The CRISPR/Cas9 system is distinguished from the *antisense* MO approach in that it induces mutations on a genomic level, whereas MOs target mRNAs and block translation. Hence, MOs target the maternal store of mRNAs as well as zygotically transcribed mRNAs and the CRISPR/Cas9 system only targets the genome and the maternal store of mRNA stays untouched.

To analyze whether the knockout of *bop1* via the CRISPR/Cas9 system also affects the expression of tissue-specific marker genes, WMISH was carried out in *bop1* CRISPants. Therefore, two-cell stage embryos were injected unilaterally with *bop1 gRNA #1*, fixed at stage 16, and *foxd3* expression was analyzed in the NCCs. Knockout of *bop1* did not affect expression of *foxd3* (Fig. 40).

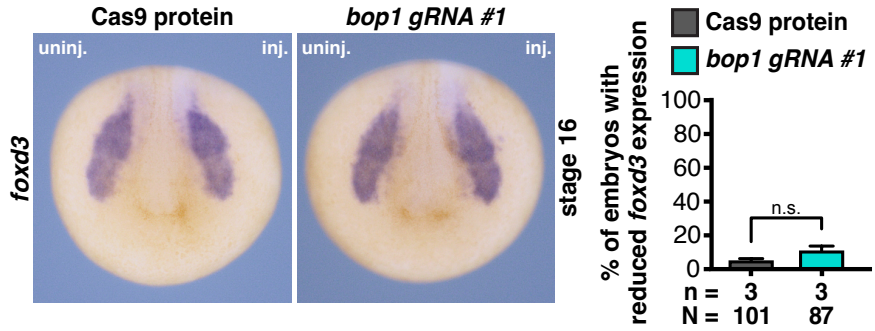


**Figure 40: Knockout of *bop1* using the CRISPR/Cas9 system does not alter *foxd3* expression.**
1 ng Cas 9 protein or 300 pg *bop1 gRNA #1* + 1 ng Cas9 protein was injected unilaterally into two-cell stage embryos. At stage 16, embryos were fixed and WMISH was performed to analyze *foxd3* expression. Anterior view of embryos is given. Embryos injected with *bop1 gRNA #1* showed normal *foxd3* expression. Abbreviations: *bop1 gRNA*, *block of proliferation 1 guide ribonucleic acid*; Cas9, CRISPR-associated protein 9; *foxd3, forkhead box d3*; inj., injected; n, number of independent experiments; N, number of injected and analyzed embryos; n.s., non-significant; uninj., uninjected; WMISH, whole mount *in situ* hybridization. Error bars indicate standard error of the mean.

Furthermore, expression of the marker gene *pax6* was analyzed at stage 13 in the eye field and the neural tube. *bop1* CRISPants normally expressed *pax6* (Fig. 41).

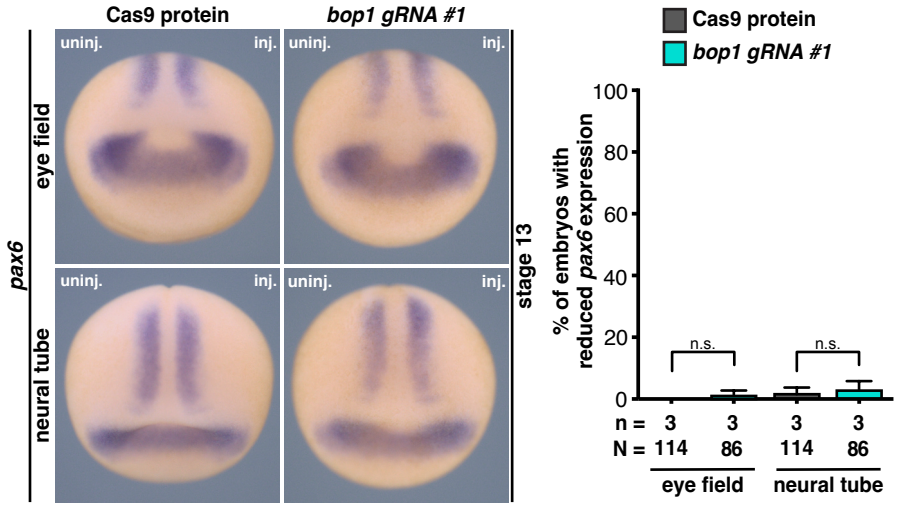


**Figure 41: Knockout of *bop1* using the CRISPR/Cas9 system does not affect *pax6* expression.**
1 ng Cas9 protein or 300 pg *bop1 gRNA #1* + 1 ng Cas9 protein was injected unilaterally into two-cell stage embryos. WMISH was performed using a *pax6*-specific probe. Anterior view is shown for the eye field; dorsal view is given for the neural tube. Expression of *pax6* was analyzed in the eye field and the posterior neural tube at stage 13. Expression of *pax6* was neither affected in Cas9 protein nor *bop1 gRNA #1*-injected embryos. Abbreviations: *bop1 gRNA*, *block of proliferation 1 guide ribonucleic acid*; Cas9, CRISPR-associated protein 9; inj., injected; n, number of independent experiments; N, number of injected and analyzed embryos; n.s., non-significant; *pax6, paired box 6*; uninj., uninjected; WMISH, whole mount *in situ* hybridization. Error bars indicate standard error of the mean.

Conclusively, Bop1 depletion using the CRISPR/Cas9 systems resulted in a head and eye phenotype. Investigating the expression of tissue-specific marker genes, *foxd3* and *pax6*, revealed that *bop1* knockout using the CRISPR/Cas9 system and hence only targeting zygotic expression did not lead in altered expression at early stage 13 and stage 16, which contrasts with the results achieved with Bop1 knockdown using the MO-based approach.

## 3.2 Rpl5 functions during *Xenopus laevis* embryonic development

The second aim of this study was to investigate the knockdown of Rpl5 during *Xenopus laevis* embryonic development, to compare Rpl5 MO-induced phenotypes to the human disease ribosomopathy, and to gain insight into possible molecular mechanisms underlying these phenotypes.

### 3.2.1 *rpl5* is conserved across different species

To test if *Xenopus laevis* Rpl5 can be compared to other species – especially *Homo sapiens* – the genomic region surrounding *rpl5* was investigated via an *in silico* synteny analysis in *Homo sapiens*, *Xenopus laevis* (both homeologues), *Mus musculus*, *Gallus gallus*, *Xenopus tropicalis*, and *Danio rerio*. The genes upstream of *rpl5* (*evi5*, *gfi1*, *rpap2*, *glmn*, *btbd8*, and *ephx4*) occur in the same order and are directed into the same direction in the different species. Only the S homeologue of *Xenopus laevis* misses the *glmn* and *rpap2* gene and *Danio rerio* misses the *ephx4* and the *btbd8* gene. Upstream of *rpl5*, the genes *dipk1a*, *mtf2*, *tmed5*, *ccdc18*, and *dr1* are located and are oriented in the same direction. Only *Danio rerio* lacks the *tmed5* and the *dr1* gene (Fig. 42).




**Figure 42: Synteny analysis of *rpl5*.**
*In silico* synteny analysis of *rpl5* in *Homo sapiens*, *Xenopus laevis* (L and S chromosome), *Mus musculus*, *Gallus gallus*, and *Danio rerio*. Analysis of the genomic region surrounding *rpl5* showed a high conservation across the different species. Modified from (Schreiner et al., 2022) under CC BY 4.0 (https://creativecommons.org/licenses/by/4.0/).

Conclusively, the genomic region surrounding *rpl5* is highly conserved across species and it can be assumed that the genes are indeed the same and further comparison between species is possible.

### 3.2.2 *rpl5* is specifically expressed in *Xenopus laevis* wild-type embryos

To enable the comparison of Rpl5 during *Xenopus laevis* development to the pathological condition in humans, the spatio-temporal expression pattern of *rpl5* in different developmental stages of *Xenopus laevis* WT embryos was investigated using WMISH and an *rpl5*-specific *antisense* probe (Fig. 43).

At stage 13, expression of *rpl5* was mainly located in the anterior neural plate. During neurulation, *rpl5* transcripts were found in the NCCs (white arrow) and the developing eyes. Stage 23 embryos showed *rpl5* expression in the developing eye (black arrow), the branchial arches (white arrow), and the somites (pink arrowhead), which was also confirmed by a transversal section (Fig. 43A). At tailbud stage, stage 30 and 35, *Xenopus laevis* embryos expressed *rpl5* in the developing eye (black arrow), the brain (light green arrow), the branchial arches (white arrow), the somites (pink arrowhead), and the ventral blood islands (blue arrow) (Fig. 43B and 43C). Vibratome sections confirmed expression in the brain, the eyes (lens (le), ciliary marginal zone (cmz)), the periocular mesenchyme, and the mandibular arch, hyoid arch, and third branchial arch (Fig. 43D).

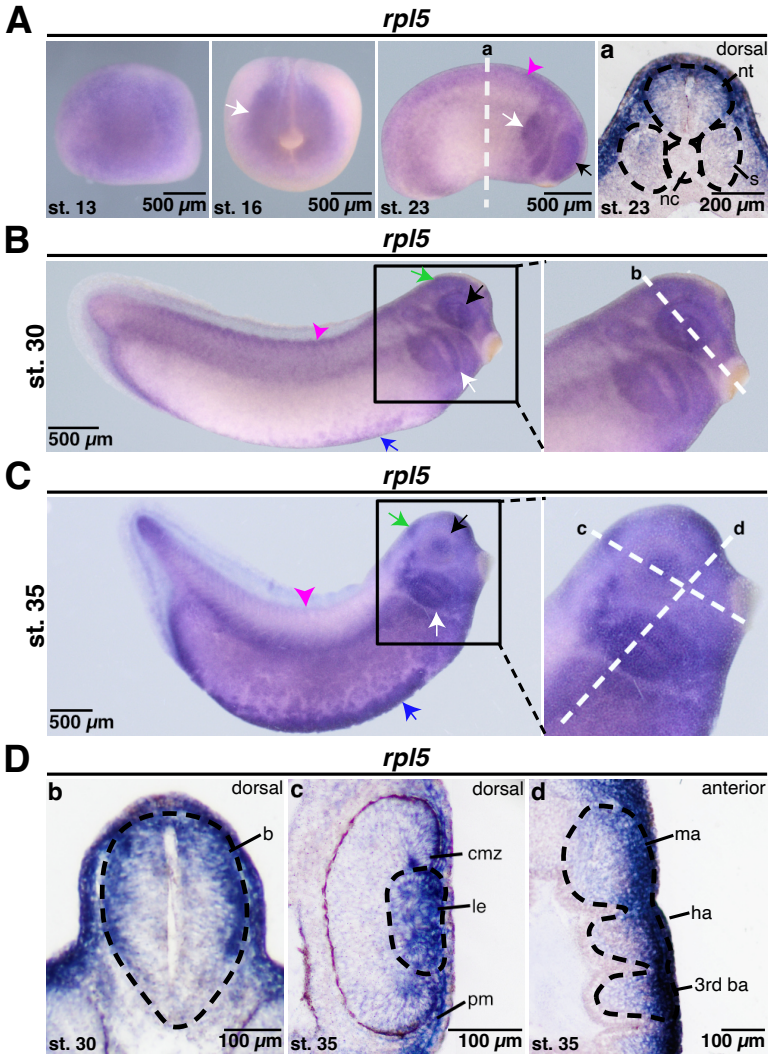


**Figure 43: Spatio-temporal expression pattern of *rpl5* in *Xenopus laevis* WT embryos.**
**A** Anterior views (st. 13 and st. 16), lateral view (st. 23), and transversal section (a, st. 23) are given. Stage 13 embryos showed *rp5* transcripts in the anterior neural plate. At stage 16, *rpl5* was mainly expressed in the neural folds (white arrow). At stage 23, *rpl5* expression was analyzed in the migrating NCCs (white arrow), the developing eye (black arrow), and somites (pink arrowhead). White dotted line indicates level of transversal section shown in a. **a** Section orientation is dorsal (upper part) to ventral (lower part). *rpl5* transcripts were found in the somites (s) as well as the neural tube (nt). **B** Lateral view is given. At stage 30, *rpl5* was expressed in the brain (light green arrow), the developing eye (black arrow), the branchial arches (white arrow), the ventral blood islands (blue arrow) and the somites (pink arrowhead). White dotted line indicates level of transversal section shown in b. **C** Lateral view is given. Stage 35 embryos show *rpl5* expression in the developing eye (black arrow), the brain (light green arrow), the branchial arches (white arrow), the somites (pink arrowhead), and the ventral blood islands (blue arrow). White dotted lines indicate level of sections shown in c and d. **D** Transversal sections (b, c) and longitudinal section (d) are shown. **b** Section orientation is dorsal (upper part) to ventral (lower part). Expression of *rpl5* is located in the brain (dorsal part of the brain shows stronger expression than the ventral part). **c** Section orientation is dorsal (upper part) to ventral (lower part). *rpl5* expression was found in the lens (le), the ciliary marginal zone (cmz), and the periocular mesenchyme (pm). **d** Section orientation is anterior (upper part) to posterior (lower part). *rpl5* transcripts were found in the mandibular arch (ma), the hyoid arch (ha), and the third branchial arch (3rd ba). Abbreviations: b, brain; ba, branchial arch; cmz, ciliary marginal zone; ha, hyoid arch; le, lens; ma, mandibular arch; nc, notochord; nt, neural tube; pm, periocular mesenchyme; s, somites. Modified from (Schreiner et al., 2022) under CC BY 4.0 (https://creativecommons.org/licenses/by/4.0/).

To deepen the spatio-temporal expression analysis, *rpl5* expression was compared to expression of tissue-specific marker genes (Fig. 44 and Fig. 45). Expression of *rpl5* in the neural plate at stage 13 was confirmed by expression of *rax* (Fig. 44A). At stage 16, *rpl5* transcripts were found in the neural plate as well as the neural plate border where *snai2* (*snail family zinc finger 2*) is expressed as well (Fig. 44B). *rpl5* expression in the somites was proven by *actc1* expression at stage 23 (Fig. 44C). Expression of *rpl5* in the ventral blood islands was confirmed by expression of the two marker genes *gata2* (*GATA-binding factor 2*) and *hba3* (*hemoglobin alpha 3 subunit*) (Fig. 44D).

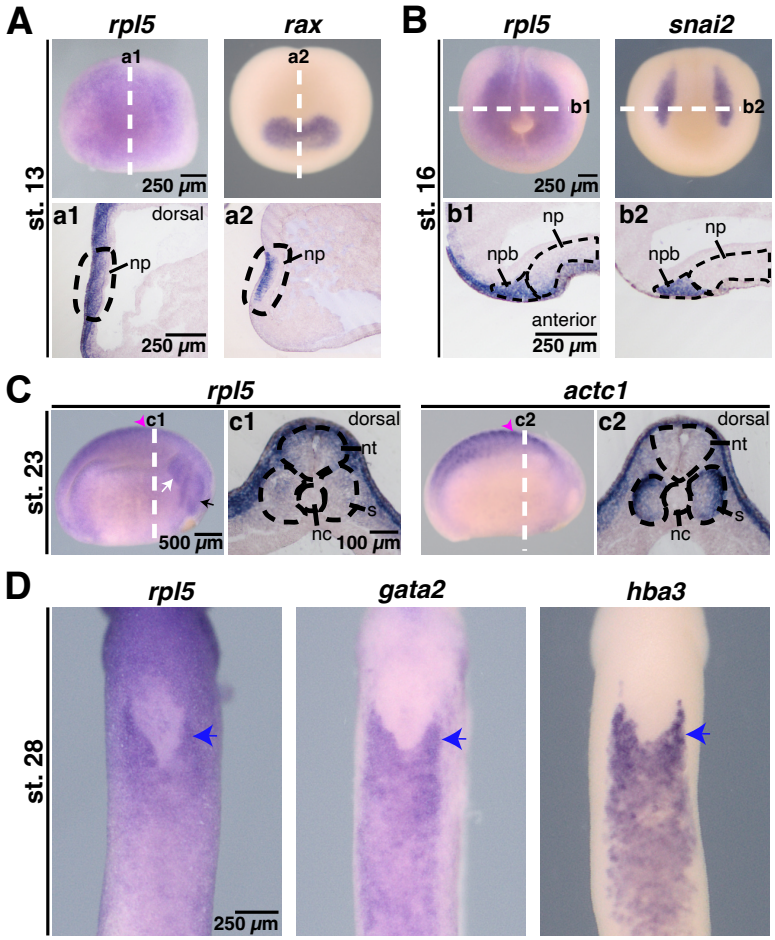


**Figure 44: Comparison of *rpl5* expression to different marker genes in stage 13-28 WT embryos.**
**A** Expression of *rpl5* and *rax* in stage 13 WT embryos. Anterior view of embryos is given. White dotted line represents level of sagittal section shown in a1 and a2 (section orientation is dorsal (upper part) to ventral (lower part)). *rpl5* expression is located in the neural plate (np) where *rax* is expressed as well. **a1, a2** This was confirmed by sections (neural plate is outlined by black dotted line). **B** At stage 16, expression of *rpl5* and *snai2* is located in the neural plate border. Anterior view of embryos is given. White dotted line represents level of longitudinal sections shown in b1 and b2 (section orientation is posterior (upper part) to anterior (lower part)). **b1, b2** Longitudinal sections are shown. Neural plate (np) and neural plate border (npb) are indicated by black dotted lines. **C** Lateral views are given. White dotted line represents level of transversal section shown in c1 and c2 (section orientation is dorsal (upper part) to ventral (lower part). Slight *rpl5* expression was found in the somites (s) (pink arrowhead), where *actc1* is expressed as well. **c1, c2** Expression in the somites (outlined by black dotted line) was confirmed by sections. For clarification, neural tube (nt) and notochord (nc) are outlined by black dotted line as well. **D** Ventral view of embryos is given. Expression of *rpl5*, and the two marker genes *gata2* and *hba3* was found in the ventral blood islands (blue arrow). Abbreviations: nc, notochord; np, neural plate; npb, neural plate border; nt, neural tube; s, somites. Modified from (Schreiner et al., 2022) under CC BY 4.0 (https://creativecommons.org/licenses/by/4.0/).

At stage 35, *rpl5* expression was found in the lens, the cmz, and the periocular mesenchyme. Here, *rax* was utilized as marker gene for the cmz, *cryba1* (*crystallin beta a1*) and *celf1* (*CUGBP elav-like family member 1*) as marker genes for the lens, and *foxc1* (*forkhead box c1*) as marker gene for the periocular mesenchyme (Fig. 45A). *rpl5* expression in the brain was compared to the expression of the two

marker genes *pax6* and *otx2* (*orthodenticle homeobox 2*). In the brain, *rpl5* expression was enriched in the dorsal part of the brain compared to the ventral area (Fig. 45B). At stage 35, expression of *rpl5* in the mandibular, hyoid, and third branchial arch was verified by expression of *twist1* (*twist family bHLH transcription factor 1*) and *foxc1* (Fig. 45C).

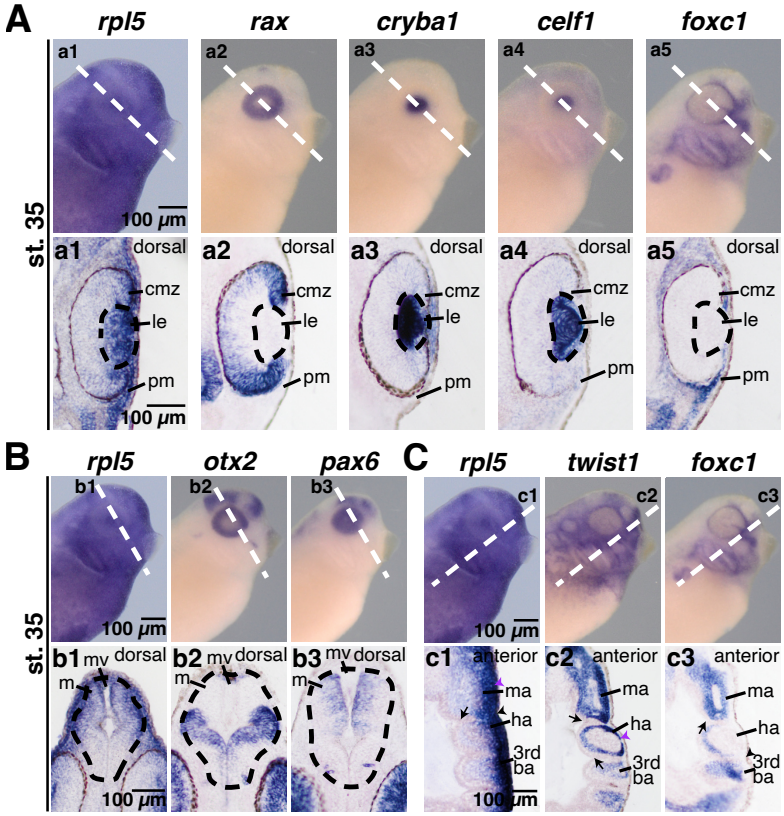


**Figure 45: Comparison of *rpl5* expression to different marker genes in stage 35 WT embryos.**
**A** Lateral view of embryos is given. White dotted line represents level of transversal section shown in a1-a5 (section orientation is dorsal (upper part) to ventral (lower part). At stage 35, expression of *rpl5* was found in the ciliary marginal zone (cmz) where *rax* is expressed as well, in the lens (le) where *cryba1* and *celf1* are expressed, and in the periocular mesenchyme (pm) in which *foxc1* is expressed as well. **a1-a5** Transversal sections are given. The lens is outlined by a black dotted line. **B** Lateral view of embryos is given. Expression of *rpl5*, *otx2*, and *pax6*. White dotted line represents level of transversal section shown in b1-b3 (section orientation is dorsal (upper part) to ventral (lower part). **b1-b3** *rpl5* transcripts are mainly found in the dorsal area of the mesencephalon (m) (outlined by black dotted line). *otx2* served as marker gene of the ventral part of the mesencephalon and *pax6* as marker gene for the dorsal part. **C** *rpl5*, *twist1*, and *foxc1* expression in stage 35 WT embryos. Lateral view of embryos is given. White dotted line represents level of longitudinal sections shown in c1-c3 (section orientation is anterior (upper part) to posterior (lower part). **c1-c3** In comparison to the two NCC marker genes *twist1* and *foxc1*, *rpl5* expression is located in the mandibular arch (ma), hyoid arch (ha), and third branchial arch (3rd ba). Black arrows indicate cranial placodes and ganglia; purple arrowheads point towards migrating NCCs and black arrows indicate the endodermal part of the pharyngeal pouches. Abbreviations: ba, branchial arch; cmz, ciliary marginal zone; ha, hyoid arch; le, lens; m, mesencephalon; ma, mandibular arch; mv, mesencephalic ventricle; pm, periocular mesenchyme. Modified from (Schreiner et al., 2022) under CC BY 4.0 (https://creativecommons.org/licenses/by/4.0/).

In summary, expression of *rpl5* in *Xenopus laevis* embryos is strongly enriched in the tissues that are affected during ribosomopathies in humans. During DBA, patients often show craniofacial malformations, which refers to *rpl5* expression in the NCCs, malformed eyes (expression in the eyes), and anemia (expression in the ventral blood islands) (Kuze et al., 2009; Narla and Ebert, 2010).

### 3.2.3 Loss of Rpl5 function leads to phenotypes of anterior tissue

During *Xenopus laevis* development, *rpl5* expression is enriched in tissues which are also affected during ribosomopathies. To further analyze if the depletion of Rpl5 induces phenotypes - as they occur in humans - in *Xenopus*, Rpl5 MO-based approaches were implemented in these tissues. An Rpl5 MO was designed targeting the 5'UTR and MO binding specificity and effectiveness was confirmed (Schreiner et al., 2022).

By animal-dorsal injection into one blastomere of eight-cell stage embryos, translation of Rpl5 was blocked in the anterior neural tissue of *Xenopus laevis* embryos. Injection of Control MO was used as injection control, the uninjected side served as internal control. Embryos were fixed at stage 43 and analyzed regarding a phenotype of the anterior tissue. Rpl5 knockdown resulted in smaller eyes and smaller heads on the injected side whereas Control MO injection did not affect eye or head size (Fig. 46).

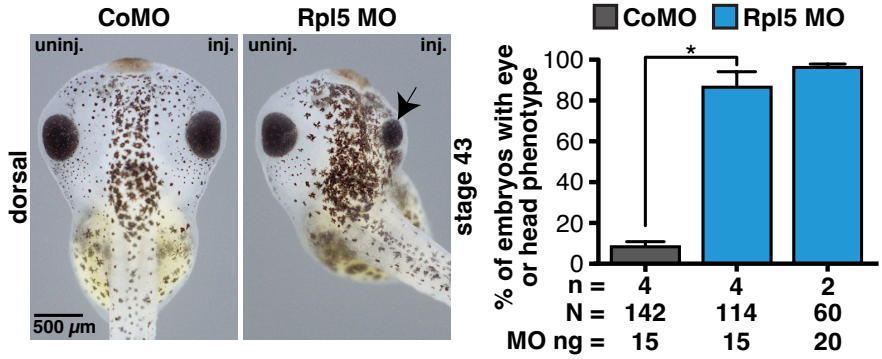


**Figure 46: Rpl5 knockdown results in smaller eyes and heads.**

15 ng Control MO or 15 ng / 20 ng of Rpl5 MO was injected into one animal-dorsal blastomere of eight-cell stage embryos. Embryos were fixed at stage 43 and occurring phenotypes of anterior tissue were analyzed. Dorsal view of embryos is given. Rpl5 knockdown resulted in smaller eyes (indicated by black arrow) and smaller heads. The uninjected side and Control MO-injected embryos did not show a phenotype of the anterior tissue. Abbreviations: CoMO, control morpholino oligonucleotide; inj., injected; n, number of independent experiments; N, number of injected and analyzed embryos; Rpl5 MO, ribosomal protein L5 morpholino oligonucleotide; uninj., uninjected. Error bars indicate standard error of the mean. *, $p \leq 0.05$.

To further analyze the starting point of eye malformation, stage 23 Rpl5 morphants were fixed and transversal sections of the anterior part of the embryos were generated. As shown in figure 47, already the evagination of the eye cup is disturbed upon Rpl5 knockdown (Fig. 47).

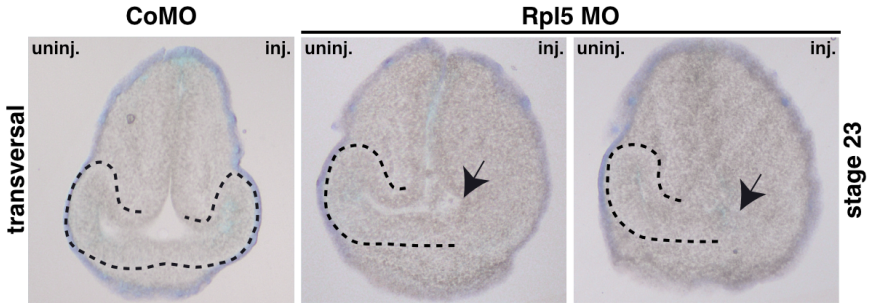


**Figure 47: Rpl5 MO injection disturbs eye cup evagination in *Xenopus laevis* embryos.**
Rpl5 MO (15 ng) and Control MO-injected embryos were fixed at stage 23 and vibratome sections were generated of the anterior part of the embryos. Transversal sections are shown; section orientation is dorsal (upper part) to ventral (lower part). Evagination of the eye cup is hindered in Rpl5 morphants (indicated by black arrow), whereas the control group showed normal eye cup evagination. Abbreviations: CoMO, control morpholino oligonucleotide; inj., injected; Rpl5 MO, ribosomal protein L5 morpholino oligonucleotide; uninj., uninjected. Modified from (Schreiner et al., 2022) under CC BY 4.0 (https://creativecommons.org/licenses/by/4.0/).

Since *rpl5* transcripts were found to a great extent in the lens and to determine whether the eye phenotype might also be a result of disturbed lens development, lens-specific marker genes were analyzed at stage 43. *celf1* served as marker for mature lens fiber cells; *cryba1* as marker gene for stem cells. Neither Control MO nor Rpl5 MO injection led to disturbed marker gene expression (Fig. 48).

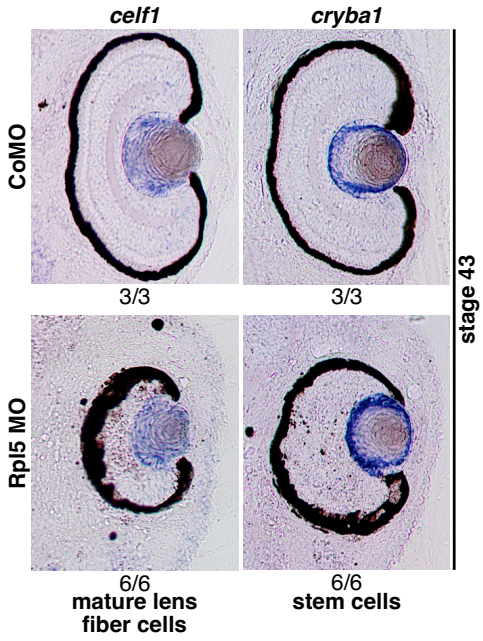


**Figure 48: Lens-specific marker genes are unaffected upon Rpl5 MO injection.**
Rpl5 MO (15 ng) and Control MO-injected embryos were fixed at stage 43 and WMISH was carried out using *celf1* and *cryba1* probes as lens-specific marker genes. Transversal sections were performed (section orientation: dorsal (upper part) to ventral (lower part)). Even though Rpl5 MO injection affected eye development, expression of *celf1* and *cryba1* were unaffected. Numbers below the columns indicate the number of embryos showing the depicted phenotypes per number of embryos analyzed. Abbreviations: *celf1*, *CUGBP elav-like family member 1*; *cryba1*, *crystallin beta a1*; CoMO, control morpholino oligonucleotide; Rpl5 MO, ribosomal protein L5 morpholino oligonucleotide; WMISH, whole mount *in situ* hybridization. Modified from (Schreiner et al., 2022) under CC BY 4.0 (https://creativecommons.org/licenses/by/4.0/).

To sum up these results, Rpl5 is required for proper head and eye development in *Xenopus laevis* embryos as its depletion leads to severe phenotypes of both tissues. These phenotypes are comparable to malformations of the anterior tissue that occur during ribosomopathies such as craniofacial malformation or eye defects (Farley-Barnes et al., 2019; Kuze et al., 2009; Narla and Ebert, 2010).

### 3.2.4 Loss of Rpl5 function leads to disturbed erythropoiesis and heart edema

Symptoms during ribosomopathies often include anemia and bone marrow failure (Farley-Barnes et al., 2019). Additionally, as shown in figure 44, *rpl5* mRNA was found in the ventral blood islands. Therefore, *gata2*, a hematopoietic transcription factor required during the early steps of erythropoiesis (Tsai et al., 1994) and *hba3*, a subunit of hemoglobin required in differentiated red blood cells, were analyzed. WMISH was performed at stage 28 in Control MO and Rpl5 MO-injected embryos (injection targeted ventral blood islands). Expression of *gata2* was unaffected upon

Rpl5 knockdown (Fig. 49A and 49B), whereas *hba3* expression was reduced on the injected side in a high number of Rpl5 morphants (Fig. 49C and 49D).

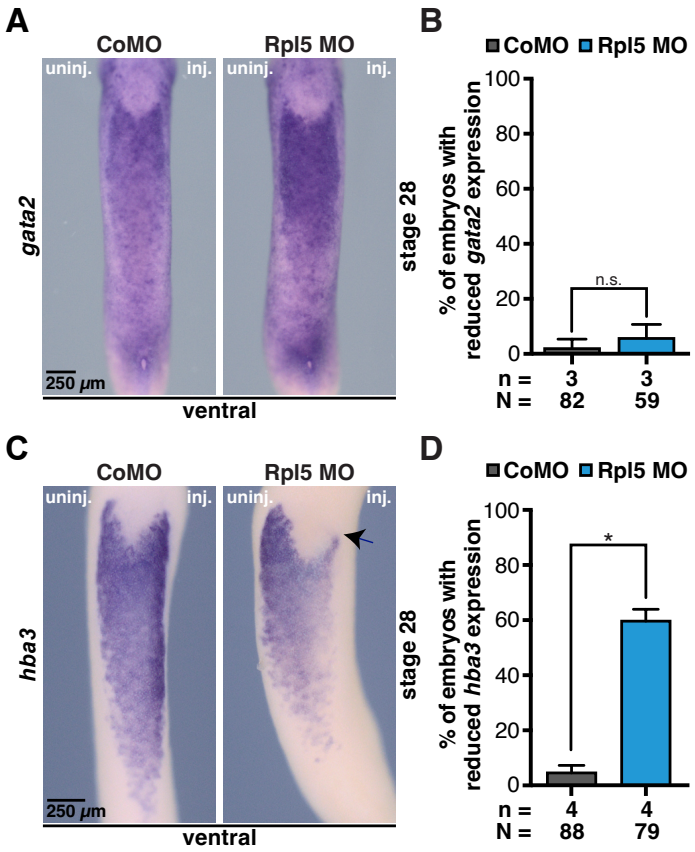


**Figure 49: Rpl5 knockdown results in reduced *hba3* expression.**
**A** At stage 28, Rpl5 MO (15 ng) and Control MO-injected embryos were fixed and *gata2* expression was analyzed using WMISH. Ventral view of embryos is given. **B** Expression of *gata2* was not affected upon Rpl5 depletion. **C** Expression of *hba3* was investigated at stage 28 control and Rpl5 morphants. Ventral view of embryos is given. Rpl5 MO injection led to reduced *hba3* expression (indicated by black arrow) on the injected side. **D** Statistical analysis of data shown in C. Abbreviations: CoMO, control morpholino oligonucleotide; *gata2*, *GATA-binding factor 2*; *hba3*, *hemoglobin alpha 3 subunit*; inj., injected; n, number of independent experiments; N, number of injected and analyzed embryos; n.s., non-significant; Rpl5 MO, ribosomal protein L5 morpholino oligonucleotide; uninj., uninjected; WMISH, whole mount *in situ* hybridization. Error bars indicate standard error of the mean. *, $p \leq 0.05$. Modified from (Schreiner et al., 2022) under CC BY 4.0 (https://creativecommons.org/licenses/by/4.0/).

Patients suffering from ribosomopathies often show cardiac defects (Farley-Barnes et al., 2019). Hence, control and Rpl5 morphants were analyzed regarding conspicuities of heart tissue. At stage 43, a high number of embryos developed heart edemas upon Rpl5 MO injection into one vegetal blastomere (Fig. 50).

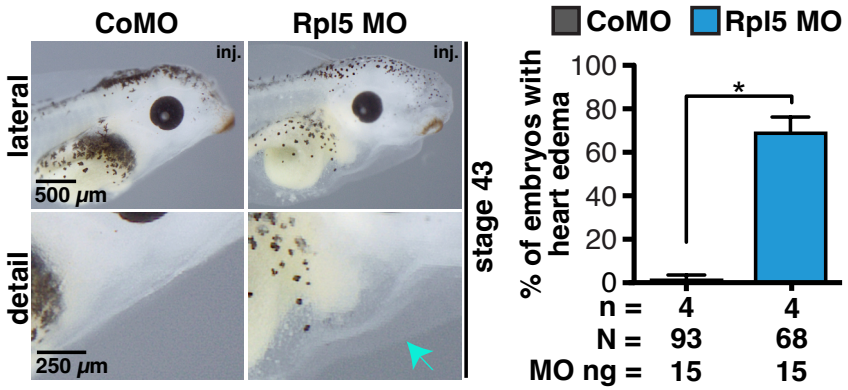


**Figure 50: Rpl5 MO injection results in heart edema**

15 ng Control MO or 15 ng Rpl5 MO were injected into one vegetal-ventral or one vegetal-dorsal blastomere of eight-cell stage embryos. At stage 43, embryos were fixed and occurring phenotypes were analyzed. Lateral and detail views of embryos are shown. Rpl5 MO injection induced heart edema in a high number of *Xenopus laevis* embryos (indicated by teal arrow). Abbreviations: CoMO, control morpholino oligonucleotide; inj., injected; n, number of independent experiments; N, number of injected and analyzed embryos; Rpl5 MO, ribosomal protein L5 morpholino oligonucleotide; uninj., uninjected. Error bars indicate standard error of the mean. *, $p \leq 0.05$.

In summary, the knockdown of Rpl5 in *Xenopus laevis* embryos resulted in microphthalmia and microcephaly, as well as disturbed blood development and heart edema. Hence, the knockdown of Rpl5 in *Xenopus laevis* recapitulates symptoms of ribosomopathies.

### 3.2.5 Rpl5 depletion does not generally affect translation

For analyzing possible molecular mechanisms underlying the Rpl5 MO-induced phenotype in *Xenopus laevis* several pathways were considered.

Since Rpl5 is part of the large ribosomal subunit of mature ribosomes and therefore is crucial for translation, it was analyzed whether the translational machinery is generally impaired. 1 ng of *GFP* RNA was injected together with Control MO, Rpl5 MO, or Pax6 MO. Pax6 MO was included as Pax6 is a molecule completely independent of ribosomal synthesis. Between stage 15 and 18, embryos were photographed using a fluorescence microscope and intensity of GFP expression was measured in the anterior neural folds. Rpl5 MO-injected embryos expressed less exogenous GFP compared to Control MO and Pax6 MO-injected embryos (Fig. 51).

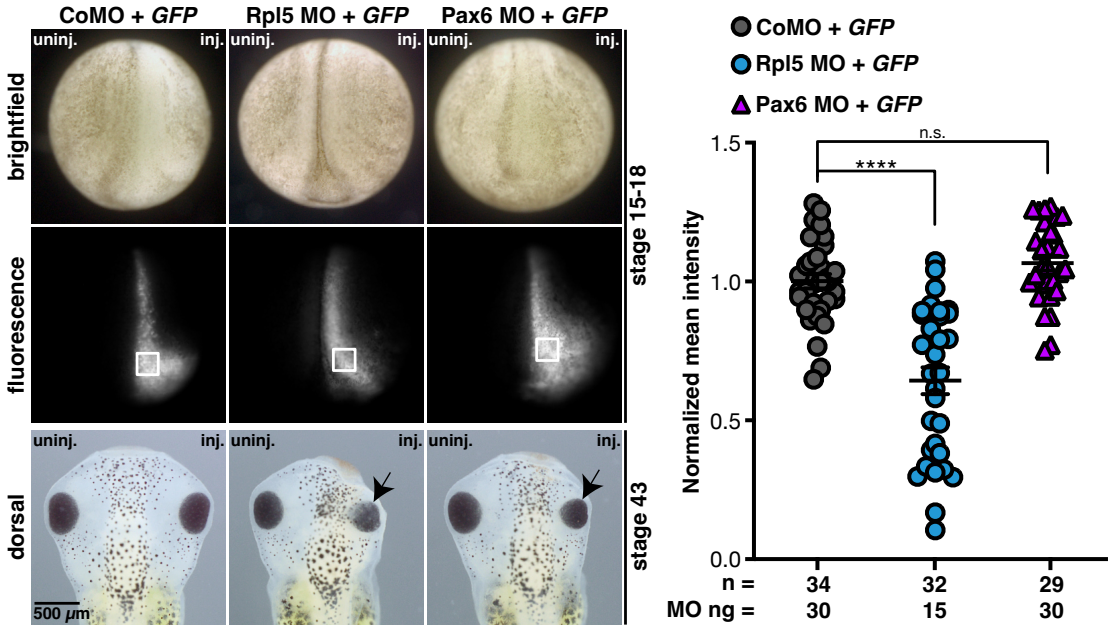


**Figure 51: Rpl5 knockdown reduces GFP expression.**
Embryos were injected with Control, Rpl5, or Pax6 MO together with 1 ng *GFP* RNA. At stage 15-18, embryos were photographed using a fluorescence microscope (8-bit greyscale). Intensity of GFP was analyzed by measuring the mean grey value in the indicated areas (white boxes). For stage 15-18 embryos, anterior-dorsal views are shown. Mean intensities were normalized to the control group. At stage 43, embryos were analyzed regarding phenotypes of the anterior neural tissue. Rpl5 MO as well as Pax6 MO led to smaller eyes and narrower heads (black arrows). Control MO did not affect embryonic development. Statistical analysis revealed a decrease in GFP expression in Rpl5 morphants, whereas control and Pax6 morphants showed a similar expression of GFP. Abbreviations: CoMO, Control morpholino oligonucleotide; GFP, green fluorescent protein; inj., injected; n, number of independent experiments; n.s., non-significant; Pax6 MO, paired box 6 morpholino oligonucleotide; Rpl5 MO, ribosomal protein L5 morpholino oligonucleotide; uninj., uninjected. Error bars indicate standard error of the means; **** $p \leq 0.0001$.

This result indicates that Rpl5 MO injection affects proper translation.

Next, it was analyzed whether the block of translation via CHX incubation also reduces the expression of exogenous GFP. Therefore, *Xenopus laevis* embryos were unilaterally injected with *GFP* RNA at two cell stage and incubated in different doses of CHX (35 nM, 100 nM, 350 nM, and 1 µM). The block of translation via CHX did not reduce the intensity of GFP expression - analyzed at stage 18 - but resulted in phenotypes of the anterior tissue at stage 43 similar to phenotypes that occurred upon Rpl5 knockdown (Fig. 52).

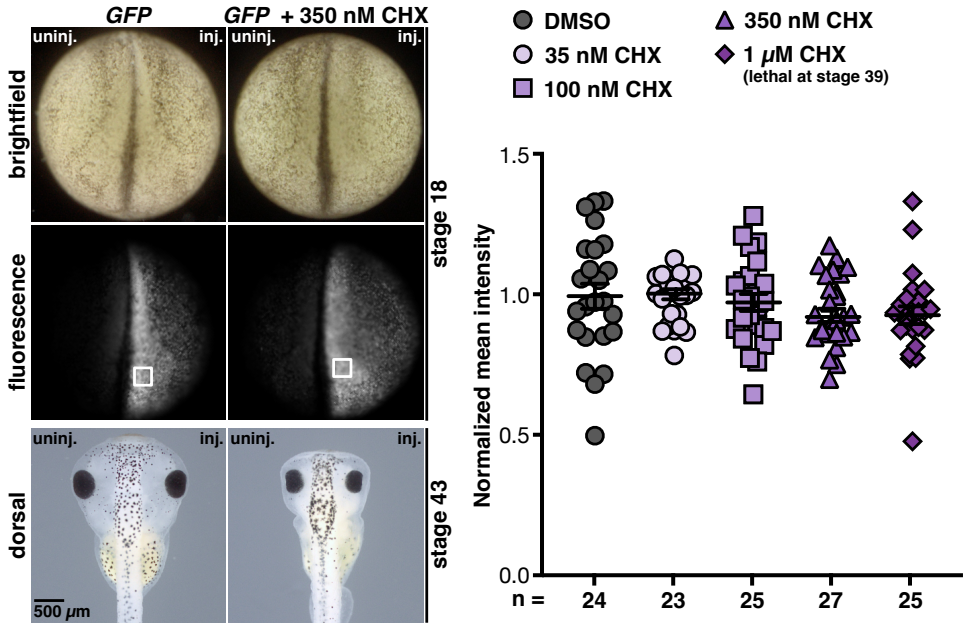


**Figure 52: Block of translation via CHX does not reduce intensity of exogenous GFP.**
Eight-cell stage embryos were injected with *GFP* RNA into one animal-dorsal blastomere. At stage 7, embryos were transferred in CHX solution or in a DMSO control. At stage 18, embryos were photographed using a fluorescence microscope (8-bit greyscale) and fluorescence intensity was measured at the indicated area (white boxes). For stage 18 embryos, anterior-dorsal views are given. At stage 43, embryos were fixed and occurring phenotypes of anterior tissue were analyzed. 1 µM CHX was lethal around stage 39, therefore embryos were only used for intensity measurements. Intensities of GFP expression was normalized to mean intensity. Intensity of GFP expression did not alter upon translation blockage. Abbreviations: CHX, cycloheximide; DMSO, dimethyl sulfoxide; GFP, green fluorescent protein; inj., injected; n, number of independent experiments; uninj., uninjected. Error bars indicate standard error of the mean.

To further investigate if the disturbed translational machinery contributes to the Rpl5 MO-induced phenotype, synergy experiments were carried out using low doses of Rpl5 MO (5 ng) and CHX (80 nM). Low doses of either Rpl5 MO or CHX resulted in a small number of embryos showing a mild phenotype. The simultaneous Rpl5 MO injection and CHX incubation also resulted in a mild phenotype in a small number of embryos (Fig. 53).

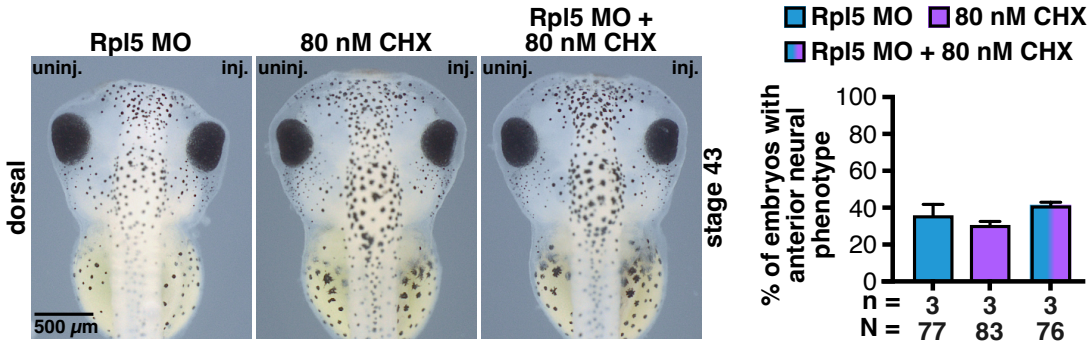


**Figure 53: Disturbed translational machinery does not contribute the Rpl5 MO-induced phenotype.**
5 ng Rpl5 MO or 5 ng Control MO was injected unilaterally into one animal-dorsal blastomere of eight-cell stage embryos. Then embryos were either incubated in 80 nM DMSO or in 80 nM CHX. Dorsal view of embryos is shown. 5 ng Rpl5 MO injection and incubation in DMSO led to the typical neural phenotype on the injected side in 35% of the embryos. 5 ng Control MO injection and incubation in 80 nM CHX led to a similar phenotype in 30% of the embryos. The combined injection of 5 ng Rpl5 MO and incubation in 80 nM CHX resulted in a phenotype of anterior tissue on the injected side in 35% of the embryos. Abbreviations: CHX, cycloheximide; inj., injected; n, number of independent experiments; N, number of injected and analyzed embryos; Rpl5 MO, ribosomal protein L5 morpholino oligonucleotide; uninj., uninjected. Error bars indicate standard error of the means.

Conclusively, although Rpl5 MO gave rise to reduced expression of exogenous GFP, the result that Rpl5 depletion and the blockage of translation by CHX treatment did not act synergistically indicates that affected translation does not contribute to the Rpl5 MO-induced phenotype.

### 3.2.6 Rpl5 depletion affects proliferative and apoptotic pathways

As possible underlying mechanisms of the Rpl5 MO-induced phenotype, proliferation and apoptosis were analyzed, since Rpl5 is part of the ribosome and hence crucial during proliferative processes.

To investigate whether the phenotypes (smaller head and smaller eyes) are the result of impaired proliferation, pH3 staining was performed at stage 13 and stage 23 upon Rpl5 MO injection. The number of proliferative cells was not affected upon Rpl5 MO injection at stage 13 (Fig. 54A and 54B). At stage 23, however, Rpl5 morphants showed a decrease in the number of pH3-positive (proliferative) cells (Fig. 54C and 54D).

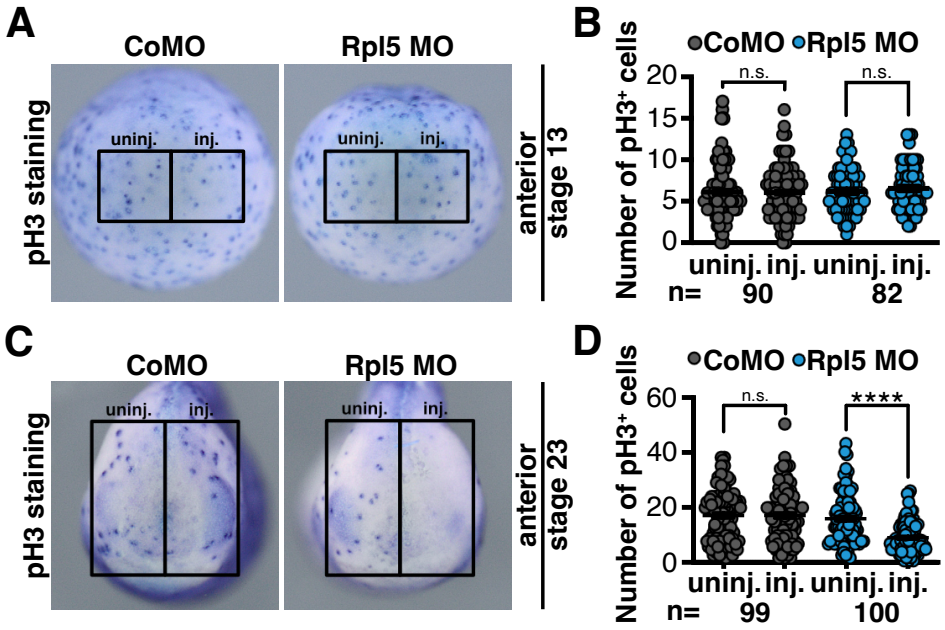


**Figure 54: Rpl5 knockdown reduces number of pH3-positive cells at stage 23.**
**A** pH3 staining was performed at stage 13 control and Rpl5 morphants. Anterior view of embryos is given. Black boxes indicate area in which proliferative cells were counted. **B** Neither Control MO nor Rpl5 MO injection affected the number of pH3-positive cells. **C** At stage 23, Rpl5 MO-injected embryos show a reduced number of proliferative cells on the injected side. Control MO injection did not affect the number of proliferative cells. Black boxes indicate area in which proliferative cells were counted. Anterior view of embryos is shown. **D** Statistical analysis of data shown in C. Abbreviations: CoMO, control morpholino oligonucleotide; inj., injected; n, number of independent experiments; n.s., non-significant; pH3, phospho histone H3; Rpl5 MO, ribosomal protein L5 morpholino oligonucleotide; uninj., uninjected. Error bars indicate standard error of the mean. ****, $p \leq 0.0001$. Modified from (Schreiner et al., 2022) under CC BY 4.0 (https://creativecommons.org/licenses/by/4.0/).

Furthermore, it was investigated whether apoptotic pathways are affected and increased in Rpl5 morphants and might contribute to the occurred phenotypes. Therefore, TUNEL staining was performed at stage 13 and stage 23 upon Rpl5 MO injection into one animal-dorsal blastomere of eight-cell stage embryos. At stage 13 as well as stage 23, Rpl5 knockdown resulted in an increase in the number of late apoptotic cells (Fig. 55 A-D). By vibratome sections at stage 23, it was shown that apoptotic cells occur in the developing eye tissue (Fig. 55C).

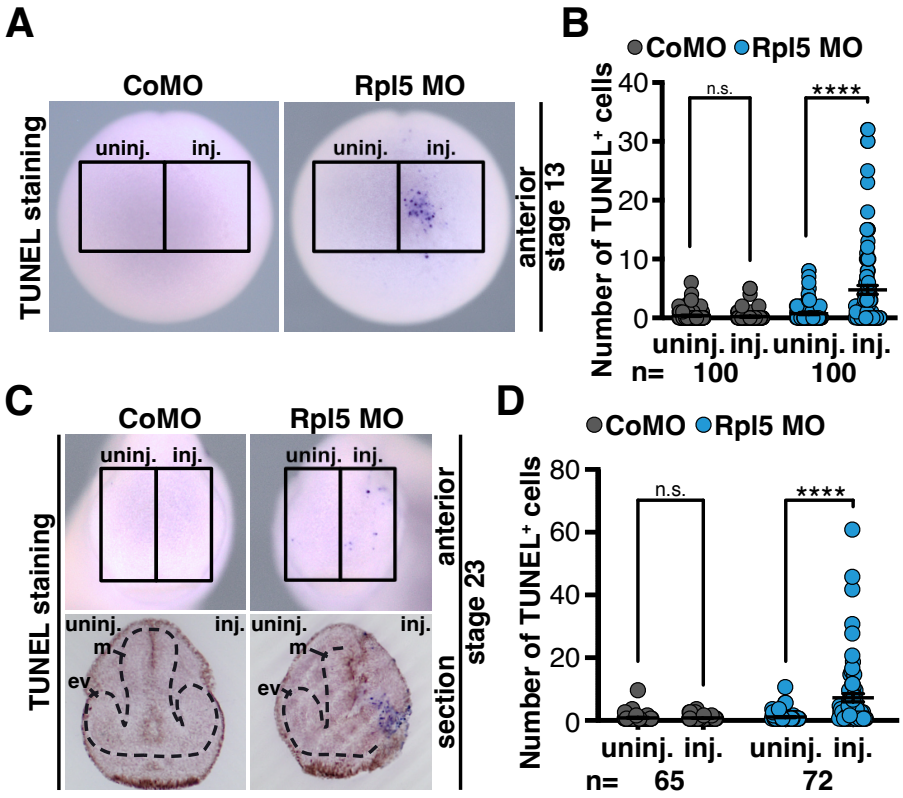


**Figure 55: Apoptotic cells increase upon Rpl5 MO injection.**
**A** The injection of 15 ng Rpl5 MO resulted in apoptotic cells (stained using TUNEL staining) in the anterior tissue of the embryo. Control MO injection did not lead to apoptotic cells. Anterior view of embryos is shown. Black boxes indicate area in which apoptotic cells were counted. **B** The injected side was compared to the uninjected side. Rpl5 MO injection resulted in a high number of apoptotic cells. **C** TUNEL staining was performed at stage 23 control and Rpl5 morphants. Anterior view of embryos and transversal section is shown (section orientation: dorsal (upper part) to ventral (lower part)). Black boxes indicate area in which TUNEL-positive cells were analyzed. Black dotted line in section outlines the eye vesicle (ev) as well as the mesencephalon (m). **D** TUNEL-positive cells were counted in indicated areas (black boxes) and injected side was compared to the uninjected side. Rpl5 MO injection resulted in an increase in the number of apoptotic cells. Abbreviations: CoMO, control morpholino oligonucleotide; ev, eye vesicle; inj., injected; m, mesencephalon; n, number of independent experiments; n.s., non-significant; Rpl5 MO, ribosomal protein L5 morpholino oligonucleotide; TUNEL, TdT-mediated dUTP Nick-End Labeling; uninj., uninjected. Error bars indicate standard error of the mean. ****, $p \leq 0.0001$. Modified from (Schreiner et al., 2022) under CC BY 4.0 (https://creativecommons.org/licenses/by/4.0/).

In summary, Rpl5 depletion affected proliferation as well as apoptosis during *Xenopus laevis* embryonic development. These pathways may contribute to the occurring phenotypes and are further investigated in the following chapters.

### 3.2.7 c-Myc is affected upon Rpl5 knockdown

As mentioned in the introduction, the molecule *c-myc* is contributing to ribosomal biogenesis by enhancing the transcriptional activity of all three RNA polymerases (Arabi et al., 2005; Gomez-Roman et al., 2003; van Riggelen et al., 2010) and

therefore plays a major role in proliferative processes. Furthermore, Liao and colleagues demonstrated that free RPs, which might occur during impaired ribosomal biogenesis and hence ribosomopathies, regulate *c-myc* levels by transporting *c-myc* to RISC, for instance (Liao et al., 2014). To analyze if c-Myc pathways are also affected during Rpl5 knockdown, expression of *c-myc* was analyzed in Rpl5 morphants using WMISH. Upon Rpl5 MO injection, *c-myc* expression drastically decreased on the injected side of stage 15 embryos (Fig. 56A and 56B). Analysis of the area of *c-myc* expression confirmed this phenotype (Fig. 56C and 56D).

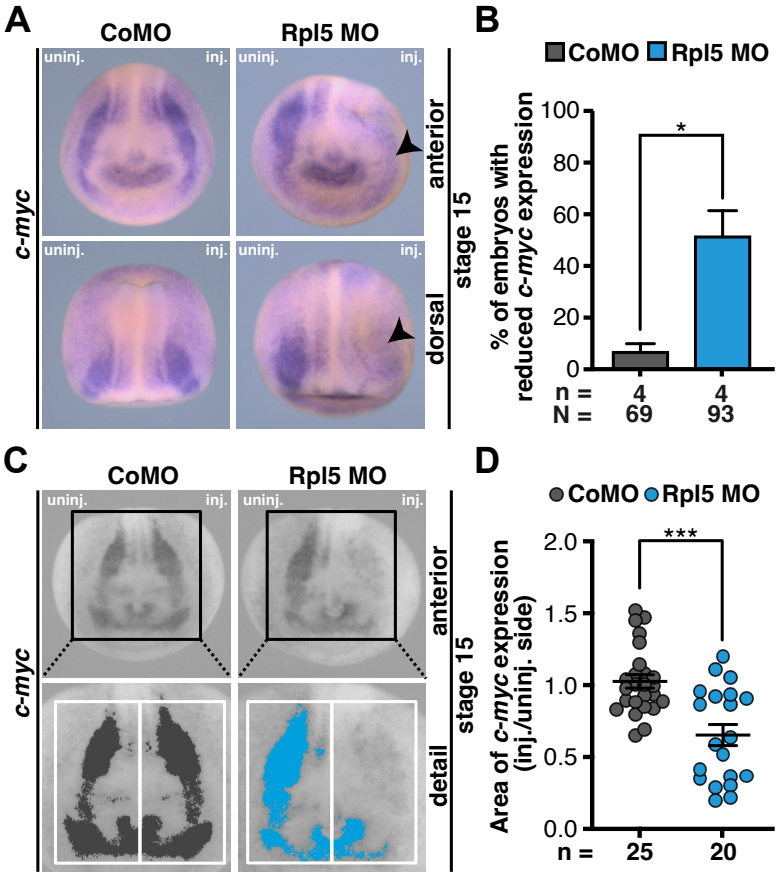


**Figure 56: Rpl5 MO injection leads to reduced *c-myc* expression.**
**A** *c-myc* expression was analyzed upon Rpl5 MO and Control MO injection at stage 15 using WMISH. Anterior and dorsal view of embryos is shown. Rpl5 knockdown led to a reduced *c-myc* expression (indicated by black arrowhead). **B** Statistical analysis of data shown in A. **C** Area of *c-myc* expression (dark grey (Control MO) and blue (Rpl5 MO) area) was measured using the software ImageJ at stage 15. The injected side was compared to the uninjected side (white boxes) of Rpl5 MO and Control MO-injected embryos. Anterior and detail view of embryos is depicted. **D** Area of *c-myc* expression was reduced upon Rpl5 knockdown. Abbreviations: *c-myc*, *MYC protooncogene*; CoMO, control morpholino oligonucleotide; inj., injected; n, number of independent experiments; N, number of injected and analyzed embryos; Rpl5 MO, ribosomal protein L5 morpholino oligonucleotide; uninj., uninjected; WMISH, whole mount *in situ* hybridization. Error bars indicate standard error of the mean. *, $p \leq 0.05$; ***, $p \leq 0.001$. Modified from (Schreiner et al., 2022) under CC BY 4.0 (https://creativecommons.org/licenses/by/4.0/).

Investigating *c-myc* levels in the whole embryo via RT PCR showed no effect of Rpl5 MO injection (gel electrophoresis upon RT PCR is shown in the appendix (suppl. Fig. 14)).

In conclusion, although *c-myc* expression was not ubiquitously affected upon Rpl5 depletion, a clear reduction in the anterior neural *c-myc* expression was detected.

For identifying possible common pathways between Rpl5 and c-Myc, synergy experiments between Rpl5 and c-Myc were carried out. Low doses of Rpl5 MO and c-Myc MO were either injected alone or simultaneously into one animal-dorsal blastomere of eight-cell stage embryos. Stage 43 embryos were analyzed regarding an occurring eye or head phenotype. Low doses of Rpl5 MO or c-Myc MO resulted in a small number of embryos showing a mild phenotype. The combined injection of both low doses led to a high number of embryos showing a severe phenotype of the eye and head on the injected side (Fig. 57).

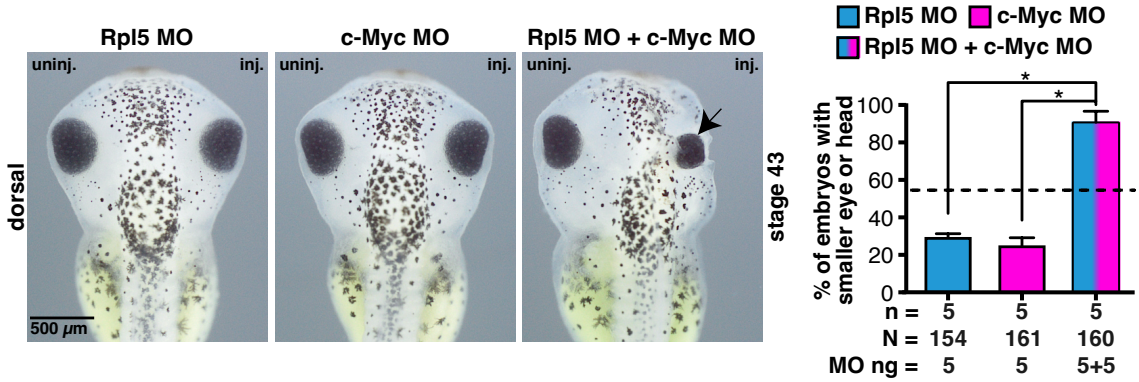


**Figure 57: Rpl5 and c-Myc share a common signaling pathway.**
Low doses of Rpl5 MO or c-Myc MO were injected alone or in combination at eight-cell stage embryos. At stage 43, *Xenopus laevis* embryos were analyzed regarding any occurring phenotypes of the eye and head. Black arrow points towards smaller eye. Dorsal view of embryos is shown. Injection of 5 ng Rpl5 MO or 5 ng c-Myc MO resulted in a small number of embryos showing a mild eye or head phenotype. The injection of 5 ng Rpl5 MO together with 5 ng c-Myc MO led to a high number of embryos with a severe eye or head phenotype. Black dotted line represents sum of embryos injected with Rpl5 MO or c-Myc MO showing an eye or head phenotype. Abbreviations: c-Myc MO, MYC protooncogene morpholino oligonucleotide; inj., injected; n, number of independent experiments; N, number of injected and analyzed embryos; Rpl5 MO, ribosomal protein L5 morpholino oligonucleotide; uninj., uninjected. Error bars indicate standard error of the mean. *, $p \leq 0.05$. Modified from (Schreiner et al., 2022) under CC BY 4.0 (https://creativecommons.org/licenses/by/4.0/).

The above-described results suggest a common pathway between Rpl5 and c-Myc. To further analyze this synergistic effect, it was investigated if the synergy between Rpl5 and c-Myc extends to proliferative processes. Again, low doses of Rpl5 MO or

c-Myc MO were injected alone and in combination into eight-cell stage *Xenopus laevis* embryos targeting anterior tissue. At stage 23, pH3 staining was performed and the number of proliferative cells was analyzed in the anterior region. The number of proliferative cells did not differ between Rpl5 MO or c-Myc MO injection alone and the combined injection of Rpl5 MO and c-Myc MO (Fig. 58).

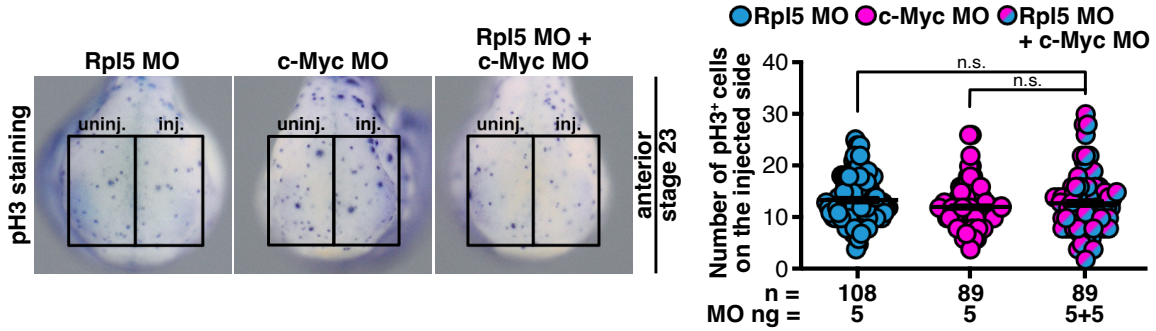


**Figure 58: Rpl5 and c-Myc synergy was not observed during proliferative processes.**
Anterior view of embryos is given. Low doses of Rpl5 MO or c-Myc MO were injected alone or in combination. pH3 staining was performed and the number of pH3-postive cells was analyzed in the anterior region at stage 23. Black boxes indicate area in which proliferative cells were counted. The number of proliferative cells did not differ between Rpl5 MO-, c-Myc MO-, or Rpl5 MO + c-Myc MO-injected embryos. Abbreviations: c-Myc MO, MYC protooncogene morpholino oligonucleotide; inj., injected; n, number of independent experiments; n.s., non-significant; pH3, phospho Histone H3; Rpl5 MO, ribosomal protein L5 morpholino oligonucleotide; uninj., uninjected. Error bars indicate standard error of the mean. Modified from (Schreiner et al., 2022) under CC BY 4.0 (https://creativecommons.org/licenses/by/4.0/).

The synergistic effect between Rpl5 and c-Myc did not extent to proliferative processes.

Since *c-myc* expression was reduced in the anterior tissue upon Rpl5 MO depletion and to comprehensively investigate the common pathway between Rpl5 and c-Myc and to clarify if c-Myc is contributing to the Rpl5 MO-induced phenotype and hence being an underlying molecular mechanism, it was analyzed if the Rpl5 MO-induced phenotype can be rescued by co-injecting *c-myc* RNA. Therefore, Rpl5 MO was injected alone and in combination with 0.25 ng *c-myc* RNA. At stage 42, the area of the eyes was measured. The injected side was compared to the uninjected side. By co-injecting *c-myc* RNA, a partial rescue of the eye phenotype was achieved (Fig. 59).

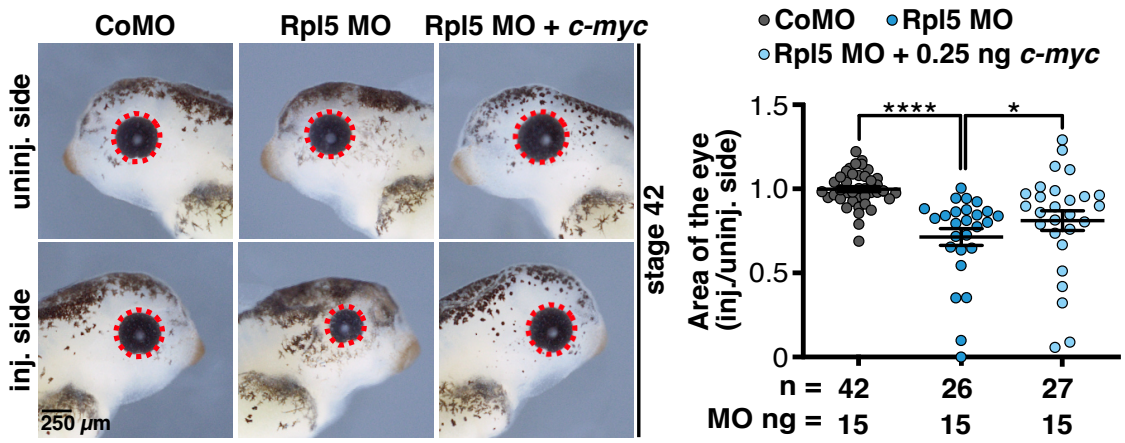


**Figure 59: Rpl5 MO-induced phenotype is partially rescued by co-injecting *c-myc* RNA.**
15 ng Control MO, 15 ng Rpl5 MO, or 15 ng Rpl5 MO + 0.25 ng *c-myc* RNA was injected into one animal-dorsal blastomere of eight-cell stage embryos. At stage 42, embryos were fixed, photographed, and the area of the eye was measured using the software ImageJ (red dotted line indicates measured area). Lateral views of embryos are depicted. Injection of Rpl5 MO alone led to smaller eyes. The co-injection of Rpl5 MO together with *c-myc* RNA resulted in a partial rescue of the eye area. Abbreviations: *c-myc*, *MYC protooncogene*; CoMO, control morpholino oligonucleotide; inj., injected; n, number of independent experiments; Rpl5 MO, ribosomal protein L5 morpholino oligonucleotide; uninj., uninjected. Error bars indicate standard error of the mean. *, $p \leq 0.05$; ****, $p \leq 0.0001$. Modified from (Schreiner et al., 2022) under CC BY 4.0 (https://creativecommons.org/licenses/by/4.0/).

Comprising these results, Rpl5 knockdown led to reduced *c-myc* expression in the anterior neural tissue of *Xenopus laevis* embryos. Rpl5 and c-Myc might share a common pathway, since simultaneous Rpl5 and c-Myc knockdown has a more than additive effect compared to Rpl5 MO or c-Myc MO injection alone. Additionally, c-Myc contributes at least partially to arising phenotypes as its overexpression rescued the eye phenotype.

### 3.2.8 Apoptosis contributes to phenotype upon loss of Rpl5 function

Previous studies have shown that upon disturbed ribosomal biogenesis free RPs, which are not incorporated into the ribosome, lead to Tp53 pathway activation. Free Rpl5, free Rpl11, or the 5S RNP complex bind and block MDM2 whereby Tp53 accumulates and the apoptotic signaling cascade is activated (Dai and Lu, 2004; Sulima et al., 2019). Since Rpl5 knockdown led to an increase in the number of apoptotic cells in *Xenopus laevis* embryos (Fig. 55) and to investigate whether Tp53 pathway activation might be an underlying molecular mechanism of the Rpl5 MO-induced phenotype, Tp53 was further investigated. By WMISH, *tp53* expression was analyzed at stage 15. Rpl5 MO-injected embryos showed an increase in *tp53* expression (Fig. 60A and 60B). This increase was also confirmed

by measuring the area of *tp53* expression using the software ImageJ (Fig. 60C and 60D).

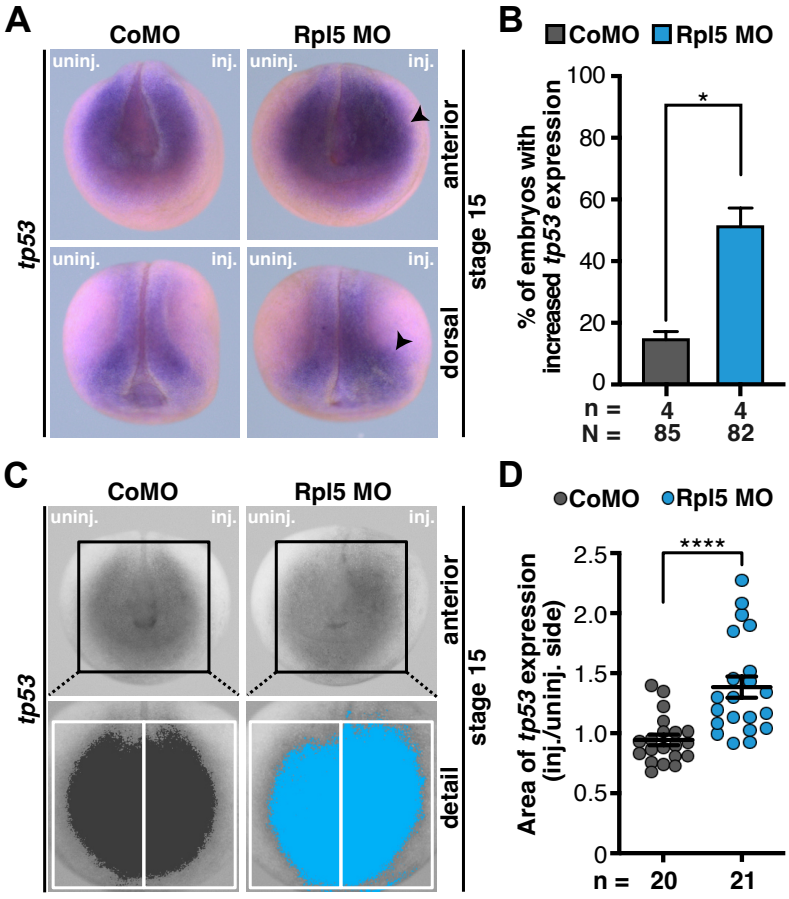


**Figure 60: *tp53* expression is increased in Rpl5 morphants.**
**A** Anterior and dorsal view of embryos is given. Expression of *tp53* was analyzed by WMISH at stage 15 control and Rpl5 morphants. Increased *tp53* expression is indicated by black arrowhead. **B** Rpl5 knockdown resulted in an increased number of embryos with elevated *tp53* expression. **C** Anterior and detail view of embryos is given. The area of *tp53* expression (dark grey (Control MO) and blue (Rpl5 MO) area) was analyzed using ImageJ. The injected side was compared to the uninjected side. Sides are defined by white boxes. **D** Rpl5 morphants showed significantly greater areas of *tp53* expression compared to the uninjected side and compared to the control group. Abbreviations: CoMO, Control morpholino oligonucleotide; inj., injected; n, number of independent experiments; N, number of injected embryos and analyzed; Rpl5 MO, ribosomal protein L5 morpholino oligonucleotide; *tp53*, *tumor protein p53*; uninj., uninjected; WMISH, whole mount *in situ* hybridization. Error bars indicate standard error of the means; *, $p \leq 0.05$; ****, $p \leq 0.0001$. Modified from (Schreiner et al., 2022) under CC BY 4.0 (https://creativecommons.org/licenses/by/4.0/).

Analyzing *tp53* expression in the whole embryo, RT PCR was performed in stage 15 Rpl5 morphants. An effect of Rpl5 MO on *tp53* expression in the whole embryos was not detected (agarose gel electrophoresis upon RT PCR is shown in the appendix (suppl. Fig. 15)).

In conclusion, Rpl5 depletion did not generally affect *tp53* expression but increased *tp53* expression in the anterior region of *Xenopus laevis* embryos; a region which has a high tendency to develop malformations during ribosomopathies in humans. Previous studies in mice, zebrafish, and *Xenopus* have shown that upon co-depletion of Tp53 a rescue of some ribosomopathy phenotypes, e.g., craniofacial malformations, is possible (Calo et al., 2018; Griffin et al., 2015; Jones et al., 2008; Zhao et al., 2014). Therefore, Rpl5 MO was co-injected with Tp53 MO in *Xenopus laevis* embryos. The simultaneous depletion of Rpl5 and Tp53 (2.5 ng or 5 ng Tp53 MO) did not rescue the Rpl5 MO-induced phenotype (Fig. 61A and 61B). To detect a subtle rescue, the area of the eyes was measured, and the injected side was compared to the uninjected side. No “hidden” rescue of the Rpl5 MO-induced phenotype by co-injecting Tp53 MO was observed (Fig. 61 C-F).

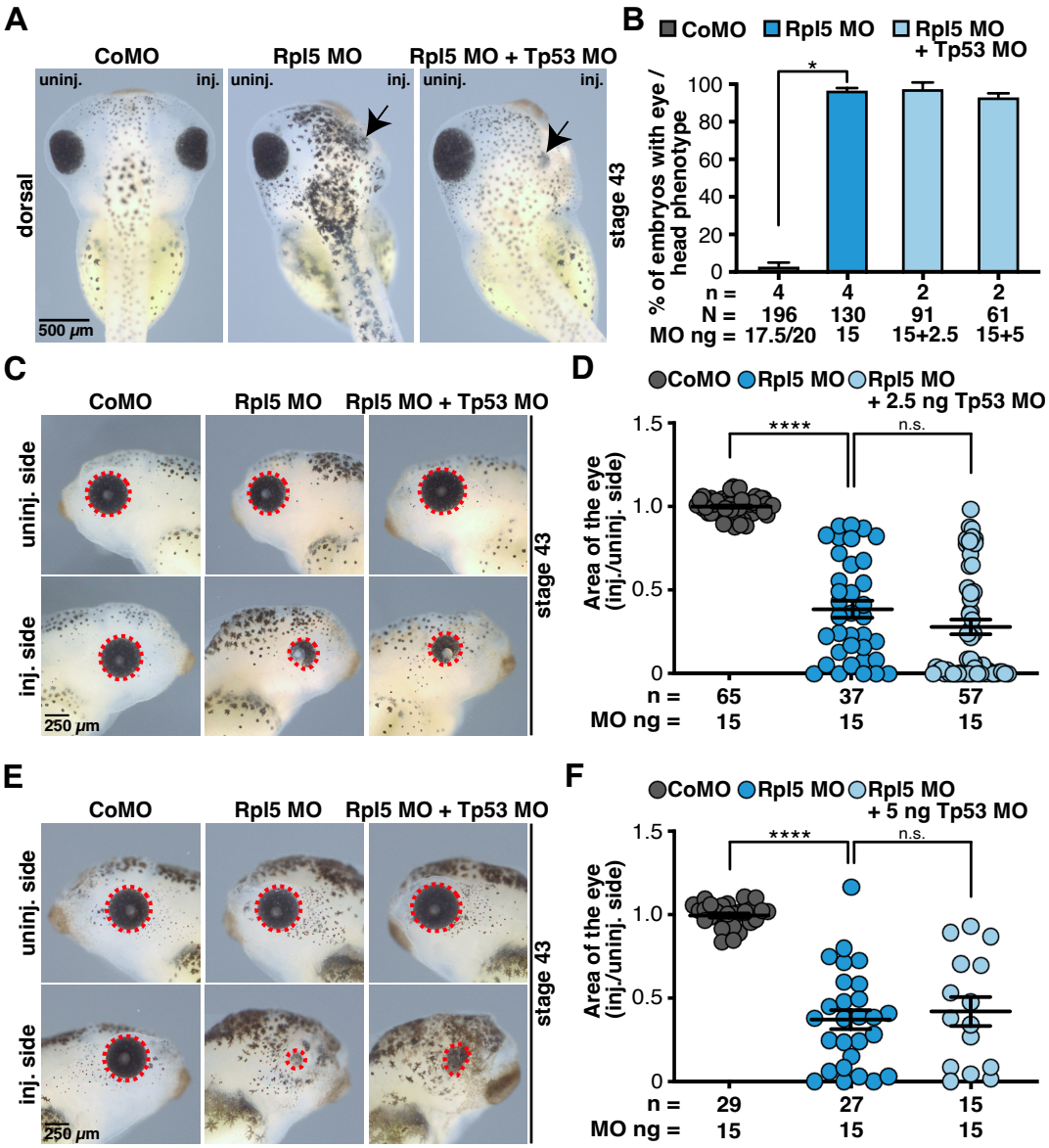


**Figure 61: Co-depletion of Rpl5 together with Tp53 did not rescue the phenotype.**

**A** Eight-cell stage embryos were injected into one animal-dorsal blastomere with Control MO, Rpl5 MO, and Rpl5 MO + Tp53 MO. At stage 43, embryos were analyzed regarding an eye or head phenotype. Dorsal view of embryos is given. Black arrows point towards smaller eyes. **B** Rpl5 MO and Rpl5 MO + Tp53 MO (2.5. ng or 5 ng) led to significantly smaller eyes or heads on the injected side. Control MO injection did not affect eye or head development. **C** The area of the eye (indicated by red dotted line) was measured and the injected side was compared to the uninjected side. Lateral view of embryos is shown. **D** Simultaneous injection of Rpl5 MO together with 2.5 ng Tp53 MO did not rescue the Rpl5 MO-induced phenotype. **E** The area of the eye (indicated by red dotted line) was measured using ImageJ and the injected side was compared to the uninjected side. Lateral view of embryos is depicted. **F** Co-depletion of Rpl5 and Tp53 (5 ng Tp53 MO) did not rescue the Rpl5 MO-induced phenotype. Abbreviations: CoMO, Control morpholino oligonucleotide; inj., injected; n, number of independent experiments; N, number of injected embryos and analyzed; n.s., non-significant; Rpl5 MO, ribosomal protein L5 morpholino oligonucleotide; Tp53 MO, tumor protein p53 morpholino oligonucleotide; uninj., uninjected. Error bars indicate standard error of the means; *, $p \leq 0.05$; ****, $p \leq 0.0001$. Modified from (Schreiner et al., 2022) under CC BY 4.0 (https://creativecommons.org/licenses/by/4.0/).

To deepen the analysis of Rpl5 and Tp53, low dose experiments were performed to investigate a possible common pathway between the two molecules. 5 ng Rpl5 MO and 0.5 ng *tp53* RNA were either injected alone or simultaneously into eight-cell stage embryos targeting anterior neural tissue. Both low doses resulted in a low percentage of embryos showing a mild phenotype of the eyes. But the co-injection of both low doses resulted in a more than additive effect, i.e., a high number of embryos showing smaller eyes (Fig. 62).

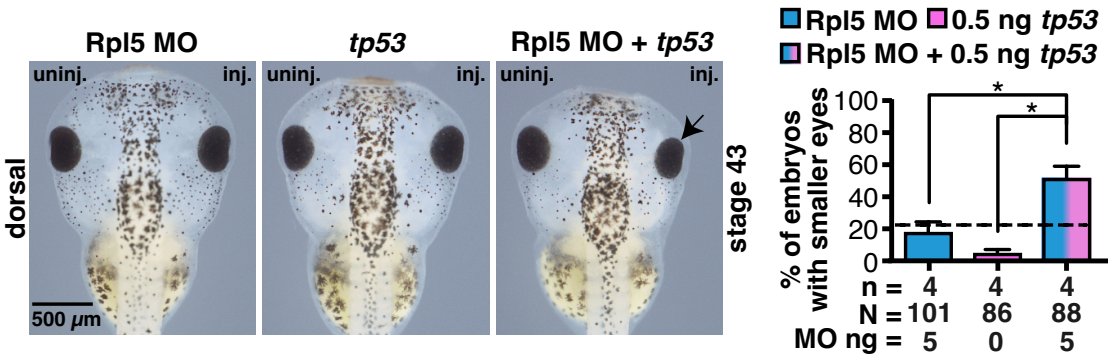


**Figure 62: More than additive effect between Rpl5 MO and *tp53* RNA**

5 ng Rpl5 MO and 0.5 ng *tp53* RNA were injected alone and in combination into one animal-dorsal blastomere of eight-cell stage embryos. Dorsal view of embryos is shown. At stage 43, embryos were analyzed regarding an eye phenotype. Black arrow indicates smaller eye. Low dose of Rpl5 MO or *tp53* RNA showed no or only a mild phenotype in a small number of embryos. Rpl5 MO together with *tp53* RNA resulted in smaller eyes in a more than additive manner. Black dotted line is the sum of embryos injected with 5 ng Rpl5 MO showing smaller eyes and embryos injected with 0.5 ng *tp53* RNA showing smaller eyes. Abbreviations: inj., injected; n, number of independent experiments; N, number of injected embryos and analyzed; Rpl5 MO, ribosomal protein L5 morpholino oligonucleotide; *tp53*, *tumor protein p53*; uninj., uninjected. Error bars indicate standard error of the means; *, $p \leq 0.05$.

Additionally, it was tested if this more than additive effect is detectable at earlier stages and apoptotic pathways. Therefore, low doses of Rpl5 MO and *tp53* RNA were injected alone as well as in combination and TUNEL staining was performed at stage 23. Indeed, Rpl5 MO and *tp53* RNA injection alone only resulted in a low number of TUNEL-positive cells, whereas the combined injection showed an increased number of apoptotic cells in a more than additive manner (Fig. 63).

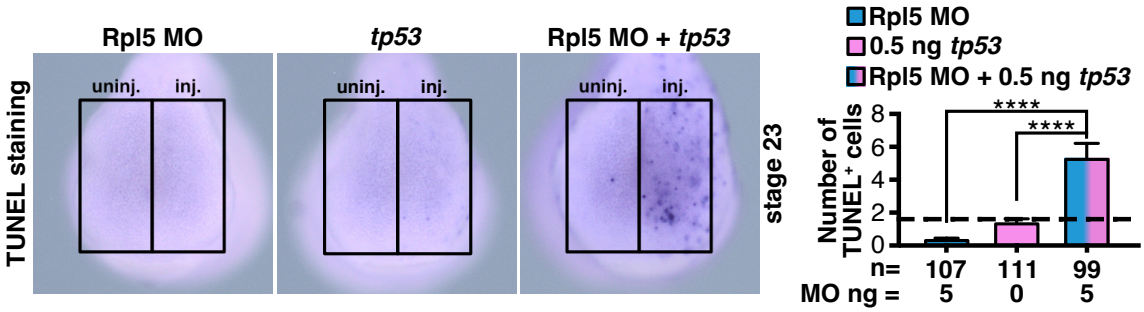


**Figure 63: More than additive effect between Rpl5 MO and *tp53* RNA is extended to the number of apoptotic cells.**

TUNEL staining was performed at stage 23 embryos that were injected with 5 ng Rpl5 MO, 0.5 ng *tp53* RNA, or 5 ng Rpl5 MO + 0.5 ng *tp53* RNA. Anterior view of embryos is given. Apoptotic cells were counted at the indicated areas (black boxes) and the injected side was compared to the uninjected side. A low number of TUNEL-positive cells was detected upon Rpl5 MO and *tp53* RNA injection alone. The simultaneous injection led to a high number of TUNEL-positive cells. Black dotted line indicates sum of TUNEL-positive cells in embryos injected with 5 ng Rpl5 MO or 0.5 ng *tp53* RNA alone. Background noise reduction was performed separately for each injection condition by subtracting the average number of TUNEL-positive cells of the uninjected side of the nominal number of TUNEL-positive cells of the injected side. In the case that this resulted in a negative value, it is displayed as zero. Abbreviations: inj., injected; n, number of independent experiments; Rpl5 MO, ribosomal protein L5 morpholino oligonucleotide; *tp53*, *tumor protein p53*; TUNEL, TdT-mediated dUTP Nick-End Labeling; uninj., uninjected. Error bars indicate standard error of the means; ****, $p \leq 0.0001$. Modified from (Schreiner et al., 2022) under CC BY 4.0 (https://creativecommons.org/licenses/by/4.0/).

To sum up, Rpl5 knockdown induced a reduction in *tp53* expression in anterior tissue and although co-depletion of Rpl5 and Tp53 did not rescue the phenotypes, the more than additive effect between Rpl5 and Tp53 suggests a common pathway between the two molecules.

To this end it was tested if apoptosis contributes to the Rpl5 MO-induced phenotype and the apoptosis blocker Bcl2 (B-cell lymphoma 2) was overexpressed in Rpl5 morphants. Bcl2 hinders apoptosis by different mechanisms (Siddiqui et al., 2015). 15 ng Rpl5 MO was injected alone and in combination with 0.25 ng *human BCL2* (*hBCL2*) into one animal-dorsal blastomere of eight-cell stage embryos. Embryos were fixed at stage 42, photographed, and the area of the eyes was measured via the software ImageJ. The eye phenotype was partially rescued upon co-injecting *hBCL2* RNA in Rpl5 morphants (Fig. 64)

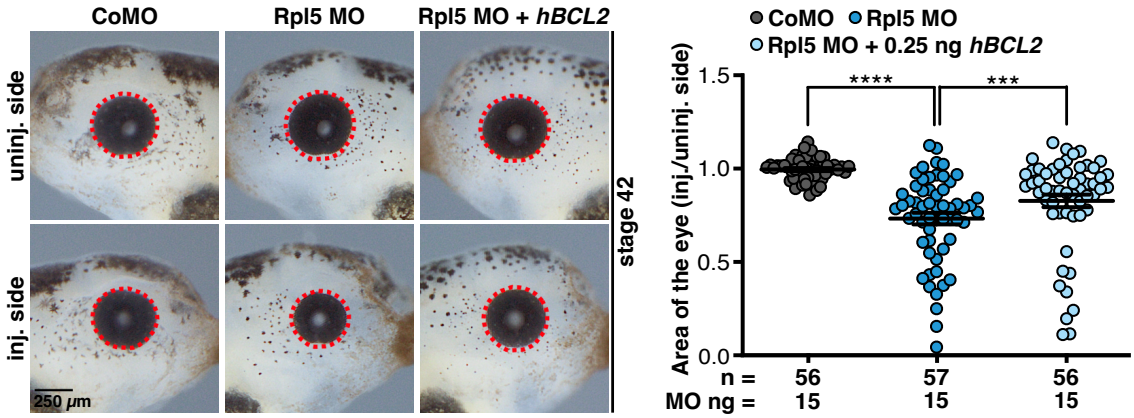


**Figure 64: Co-injecting *hBCL2* RNA rescues the Rpl5 MO-induced eye phenotype.**
15 ng Control MO, 15 ng Rpl5 MO, or 15 ng Rpl5 MO + 0.25 ng *hBCL2* RNA was injected at eight-cell stage embryos. At stage 42, embryos were photographed. The area of the eye (indicated by red dotted line) was measured and injected side was compared to the uninjected side. Lateral view of embryos is given. The co-injection of Rpl5 MO together with *hBCL2* RNA partially rescue the Rpl5 MO-induced eye phenotype. Abbreviations: CoMO, Control morpholino oligonucleotide; *hBCL2*, *human B cell lymphoma 2*; inj., injected; n, number of independent experiments; Rpl5 MO, ribosomal protein L5 morpholino oligonucleotide; uninj., uninjected. Error bars indicate standard error of the means; ***, $p \leq 0.001$; ****, $p \leq 0.0001$. Modified from (Schreiner et al., 2022) under CC BY 4.0 (https://creativecommons.org/licenses/by/4.0/).

In conclusion, the above-described experiments that 1) Rpl5 MO injection resulted in increased *tp53* levels, 2) Rpl5 and Tp53 share a common signaling pathway, and 3) the Rpl5 MO-induced phenotype is rescued by blocking apoptosis using Bcl2 indicate that apoptosis majorly contributes to the Rpl5 MO-induced phenotype.

# 4 Discussion

## 4.1 Ribosomal factor Bop1 during *Xenopus laevis* development

One aim of this study was to investigate the ribosomal factor Bop1 during the early development of the South-African clawed frog *Xenopus laevis*.

Annika Meßmer in the working group of PD Dr. Susanne Kühl started analyzing Bop1 during *Xenopus laevis* embryogenesis. The here presented study deepened these analyses and continued the elucidation of the molecular basis and possible extra-ribosomal functions of Bop1. A comprehensive expression analysis in WT embryos revealed *bop1* expression throughout the entire analyzed embryonic development. Using the potent *antisense*-based MO approach as well as the CRISPR/Cas9 system, Bop1 depletion was investigated. Upon targeting anterior tissue, late tailbud stages showed phenotypes of the eye, including microphthalmia and coloboma, the brain, and the NCC-derived cranial cartilage. Hence, even though Bop1 has not yet been associated with ribosomopathies, *Xenopus laevis* showed phenotypes that recapitulate the symptoms that occur during disturbed ribosomal biogenesis in humans. Furthermore, the molecular basis and molecular mechanisms underlying the observed phenotypes were investigated. The expression of several marker genes was reduced upon Bop1 knockdown via MO at very early developmental stages. Since *Xenopus laevis* is independent of *de novo* ribosomal synthesis during those early developmental stages, a function independent of ribosomal synthesis was considered and further investigated for Bop1.

### 4.1.1 *bop1* expression in disease-relevant tissue

The expression analysis during *Xenopus laevis* embryonic development provided a thorough and comprehensive spatio-temporal expression pattern of *bop1* that was confirmed utilizing several marker genes for study-relevant tissues. Even though Bop1 is a ribosomal factor and required ubiquitously, *bop1* transcripts were found to a great extent in the developing eye, the brain, and the NCCs. These results are in line with previous WMISH approaches in *Xenopus tropicalis* at stage 15 and stage 28 describing *bop1* expression in the neural plate (stage 15) and the brain, the retina, the otic vesicle, and branchial arches (stage 28) (Neilson et al., 2010). *bop1* is expressed in the central nervous system, the entire brain, and the liver of

developing mice (Yue et al., 2014). In human fetuses, *BOP1* expression is mainly detected in the brain (Duff et al., 2015; Fagerberg et al., 2014; *The Human Protein Atlas, BOP1 Available from V21.0.Proteinatlas.Org.*, 2022).

The above-described anterior tissues in which *bop1* expression was detected in *Xenopus laevis* are relevant during defective ribosomal biogenesis as patients suffering from ribosomopathies often show symptoms and malformations regarding those tissues (Farley-Barnes et al., 2019; Narla and Ebert, 2010). Furthermore, the here shown expression pattern is also consistent with earlier studies by Robson et al. describing the expression of several genes involved in ribosomopathies throughout different developmental stages of *Xenopus tropicalis* (Robson et al., 2016). Additionally, in *Xenopus laevis*, expression of ribosomal factors and other RPs, e.g., Ppan, Pes1, or Nol11, has been shown to be located in overlapping tissues (Bugner et al., 2011; Gessert et al., 2007; Griffin et al., 2015).

Based on previous results and here presented data, it is assumed that Bop1 inherits a function during early neural development.

### 4.1.2 Bop1 is required for early anterior neural development in *Xenopus laevis*

Knockdown using *antisense*-based MO approaches

The knockdown of Bop1 in the anterior tissue of *Xenopus laevis* embryos using MOs targeting different sequences in the 5'UTR of *bop1* led to severe malformations in the eye, a reduced brain size, and deformations in the NCC-derived cranial cartilage.

These findings are in line with earlier findings that the depletion of ribosomal factors other than Bop1 also affect proper eye, head, and brain development. Mutations in *pes1* lead to a smaller brain and smaller eyes in developing zebrafish (Allende et al., 1996; Lerch-Gaggl et al., 2002). Previous studies in the working group of PD Dr. Susanne Kühl have shown that the knockdown of Ppan as well as Pes1 (PeBoW-complex partner of Bop1) in the anterior neural tissue of *Xenopus laevis* embryos results in eye malformations, e.g., coloboma and microphthalmia, microcephaly, and affects proper development of cranial cartilage structures (Bugner et al., 2011; Gessert et al., 2007). Furthermore, Griffin and colleagues analyzed the ribosomal factor Nucleolar protein 11 (Nol11) during *Xenopus laevis*

embryonic development and detected malformed cranial cartilages in late tailbud stages (Griffin et al., 2015). Calo et al. have demonstrated that the knockdown of the TCS-associated protein Tcof1 induces craniofacial malformations in *Xenopus laevis* embryos (Calo et al., 2018).

Even though Bop1 has not been associated with ribosomopathies, the phenotypes upon knockdown resemble many symptoms that occur during these diseases. Accordingly, patients suffering from ribosomopathies exhibit a variety of symptoms affecting the eyes, brain, or head. DBA-affected people show congenital glaucoma (Young et al., 1992), exotropia (one eye deviates outward) (Kuze et al., 2009), and absent lower eyelashes (Narla and Ebert, 2010). In TCS patients, even anophthalmia and microphthalmia have been reported as well as lower lid colobomas and absent lower eyelashes (Cohen et al., 1995; Sharma et al., 2016). Furthermore, many craniofacial deformations have been described in ribosomopathies. Ocular hypertelorism (increased eye distance), deformed ears, and micrognathia (undersized lower jaw) are symptoms that have been described in DBA patients (Kuze et al., 2009; Lipton et al., 2006; Narla and Ebert, 2010). Likewise, TCS-affected people exhibit malformations of the middle ear, which may eventually result in hearing loss, microcephaly, micrognathia, a slanting forehead, and cleft lip or palate (Cohen et al., 1995; Fazen et al., 1967; Narla and Ebert, 2010; Phelps et al., 1981).

In conclusion, loss of Bop1 function in *Xenopus laevis* resulted in phenotypes at late tailbud stages which are comparable to symptoms of ribosomopathies.

Knockout using the CRISPR/Cas9 system

In addition to the Bop1 knockdown using MO-based approaches, the CRISPR/Cas9 system was utilized to reduce Bop1 levels on a genomic basis. During late tailbud stages, *Xenopus laevis* CRISPants showed microphthalmic and microcephalic phenotypes, which is in accordance with results obtained using MO-based approaches.

However, phenotypes using the CRISPR/Cas9 system were milder compared to the phenotypes upon Bop1 MO injection. This might appear due to genetic compensation. By mechanisms of genetic compensation, organisms with a

pathological mutation do not develop expected phenotypes due to compensatory mechanisms by other genes. These genes compensate for the function of mutated genes whereby the normal physiological function can be restored. Genetic compensation has been described for several zebrafish mutants, yet the underlying molecular mechanism is not fully understood (Buglo et al., 2020; Diofano et al., 2020; Moreno et al., 2018; Place and Smith, 2017; Rossi et al., 2015; Salanga and Salanga, 2021; Salanga et al., 2020). Regarding the here described *bop1* CRISPants, genetic compensation might compensate the *bop1* knockout to some extent, which led to a milder phenotype. Several theories may be conceivable in this scenario, e.g., arising mutations may only result in a partial loss of Bop1 function and by overexpressing mutated Bop1, parts of Bop1 function can be restored. Another hypothesis may be that another protein takes over the function of Bop1. This theory is more unlikely since Bop1 does not belong to a protein family in which several proteins execute similar functions as it was shown in an earlier study for Bcl2-associated athanogene 3 (BAG3) by Diofano et al. In this study, the knockout of BAG3 was genetically compensated by BAG2, which was increased on transcription and protein level in BAG3 mutants (Diofano et al., 2020). It might also be conceivable that Pes1 and WDR12 can function independently of Bop1 or at least with less Bop1 protein.

In addition to genetic compensation, a reason for milder phenotypes in *bop1* CRISPants may be that *Xenopus laevis* embryos have a maternal supply of mRNAs and proteins. This supply stays untouched during knockout using the CRISPR/Cas9 system and hence might be sufficient for the initial demand for Bop1 protein in the embryos. During the knockdown using MO-based approaches, maternally supplied mRNAs are bound and translation is blocked whereby the initial demand of Bop1 may not be met. The maternal supply of proteins stays also untouched during MO-based knockdown but alone (without mRNA transcripts) might not be sufficient.

### 4.1.3 Ribosomal biogenesis-dependent pathways are not disturbed in Bop1 morphants

In this study, several pathways were investigated which might be potential molecular mechanisms underlying the Bop1 MO-induced phenotype.

Analyzing proliferative processes using BrdU staining revealed that the knockdown of Bop1 did not affect proliferation at stage 23. This finding is intriguing since as a ribosomal factor Bop1 is crucial for cell proliferation and previous studies by others have shown that in mouse-derived cell lines, dominant-negative mutants of Bop1 suffer a cell cycle arrest (Pestov et al., 2001; Strezoska et al., 2002). Depletion of the Bop1 interaction partner Pes1 has also been associated with a decrease in proliferative cells (Gessert et al., 2007).
Furthermore, a rescue using the transcriptional enhancer *c-myc* was not possible. This is in contrast to the also here presented finding that the Rpl5 MO-induced phenotype is at least partially rescued by co-injecting *c-myc* RNA (Fig. 59) - off note Rpl5 MO injection also reduced the number of proliferative cells. In addition, depletion of the ribosomal factor Ppan has also been shown to lead to reduced *c-myc* expression in *Xenopus laevis* embryos (Bugner et al., 2011).
These results hint toward an additional and so far, unknown function of Bop1 which is independent of ribosomal biogenesis. This hypothesis would be consistent with the widely accepted idea that *Xenopus* possess a maternal store of ribosomes and do not require *de novo* ribosomal biogenesis during early development (Brown and Gurdon, 1964; Pierandrei-Amaldi and Amaldi, 1994).

The analysis of apoptotic processes using TUNEL staining showed that Bop1 knockdown did not affect apoptosis in stage 23 *Xenopus laevis* embryos. This is in contrast to earlier findings showing that the knockdown of Pes1, Ppan, and Nol11 increases apoptotic processes during *Xenopus laevis* embryogenesis (Bugner et al., 2011; Gessert et al., 2007; Griffin et al., 2015).
Earlier studies by others have shown that Tp53-dependent apoptotic pathways were activated during disturbed ribosomal biogenesis, e.g., DBA (Gazda et al., 2008; Molavi et al., 2019; Zhou et al., 2015). Furthermore, in a human cell line, lower BOP1 levels have led to decreased ribosomal synthesis resulting in Tp53-dependent proliferative inhibition, oxidative stress, and apoptosis (Wu et al., 2019). This result contrasts with the here described experiment that the Bop1 MO-induced phenotype was not rescued by the co-depletion of Tp53. However, the result that Tp53 co-depletion did not rescue the Bop1 MO-induced phenotype is in line with the result that Bop1 depletion did not increase the number of apoptotic cells.

The observation that Bop1 knockdown did not affect apoptotic processes during *Xenopus laevis* embryonic development again points towards a function independent of ribosomal synthesis and therefore Bop1-Tp53-dependent pathways might be less important here.

To investigate if the translational machinery is generally disturbed upon Bop1 MO injection, the expression of exogenous GFP was analyzed at stage 15. By measuring GFP intensity, no difference was detected between control and Bop1 morphants. For further investigation, low dose experiments with Bop1 MO and the translation blocker CHX were implemented. No additive effect regarding occurring phenotypes was detected when perturbing the two pathways simultaneously (Bop1- and translation-pathway). This result indicates that translation does not contribute to the Bop1 MO-induced phenotype. This is in contrast to earlier findings that Bop1 knockdown leads to decreased protein synthesis in human cell lines (Liu et al., 2014) and furthermore hints toward an extra-ribosomal function of Bop1 since ribosomal biogenesis is less important during early development due to the maternal ribosomal pool.

### 4.1.4 Molecular basis of the Bop1 MO-induced phenotype

Investigating the molecular basis of the Bop1 MO-induced phenotype, the expression of several marker genes was found to be affected in Bop1 morphants. Here, marker genes of tissues in which *bop1* expression was detected were analyzed.

The area of expression of the pan-neural marker gene *sox3* was found to be broadened in the anterior neural tissue at stage 13. This increase in expression was also confirmed using real-time qPCR. Earlier studies in *Xenopus laevis* embryos revealed that *sox3* overexpression induces disturbed formation and migration of NCCs and a severe phenotype of cranial cartilage structures (Rogers et al., 2009). Interestingly, a second pan-neural marker gene *sox2* was not affected upon Bop1 knockdown – neither in WMISH nor in real-time qPCR approaches. This indicates that the loss of Bop1 specifically affects *sox3* and does not generally affect neural development.

During induction of the neural plate border, the expression of NCC marker gene *foxd3* was reduced. Fairchild and colleagues have demonstrated that Foxd3 is required for the EMT of NCCs (Fairchild et al., 2014). Furthermore, previous studies have shown that BOP1 is upregulated in patients suffering from hepatocellular carcinoma and gastric cancer and that BOP1 induces EMT leading to higher invasiveness and metastasis potential (Chung et al., 2011; He et al., 2022). In conclusion, these data suggest that EMT in general requires proper BOP1 function.

Due to the severe and diverse eye phenotypes, eye marker genes *rax*, as well as *pax6*, were investigated during eye field induction (stage 13) and eye cell differentiation (stage 23). Both marker genes were reduced upon Bop1 depletion. Interestingly, the counterpart of *pax6* during eye development, *shh*, was not affected upon Bop1 depletion. In *Xenopus* and mice, mutations in the *rax* gene are associated with disturbed eye formation (Bailey et al., 2004). Also in humans, mutations in *RAX* lead to several eye defects, including coloboma, anophthalmia, and microphthalmia (Bailey et al., 2004; Lequeux et al., 2008; London et al., 2009). In line with the reduction in *pax6* expression is that previous studies in *Xenopus* show severe eye defects, e.g., disturbed retinal lamination and eye formation, upon loss of Pax6 function (Rungger-Brändle et al., 2010). In mice, homozygous *Pax6* mutants completely lack eyes (Hill et al., 1991). Mutations in human *PAX6* are associated with congenital aniridia, cataract, and corneal opacification (Cvekl and Callaerts, 2017). In addition to eye defects, *PAX6* is associated with brain defects in *Xenopus*, mice, and humans (Georgala et al., 2011; Kikkawa et al., 2019; Nakayama et al., 2015).
In line with the reduced *rax* and *pax6* expression upon Bop1 MO injection, *Xenopus laevis* embryos also express less *rax* and *pax6* upon knockdown of the ribosomal factors Ppan and Pes1 (Bugner et al., 2011; Gessert et al., 2007).

Interestingly, the knockout using the CRISPR/Cas9 system did not result in reduced expression of the marker genes *pax6* and *foxd3* at early stages 13 and 16, respectively. In chapter 4.1.2., possible explanations for a milder phenotype were given. One explanation is genetic compensation, by which other genes compensate for the pathological mutation and restore physiological function (Salanga and Salanga, 2021). In the case of *bop1* CRISPants, genetic compensation might

restore normal marker gene expression – at least to a point in which affected gene expression cannot be detected using WMISH. Furthermore, at those early developmental stages, *Xenopus laevis* embryos inherit a maternal supply of proteins and mRNAs - that stays untouched by the CRISPR/Cas9 knockout - which might be sufficient for the first demand of Bop1 and therefore results in normal early marker gene expression.

### 4.1.5 Potential extra-ribosomal function of Bop1 during *Xenopus laevis* embryogenesis

Even though many of the arising phenotypes Bop1 morphants exhibit fit to the symptoms during ribosomopathies, the fact that *Xenopus laevis* Bop1 morphants show affected marker gene expression at stage 13 is not in line with disturbed ribosomal biogenesis. *Xenopus laevis* embryos are maternally supplied with around $10^{12}$ ribosomes, mRNAs, and proteins (Brown, 1964; Pierandrei-Amaldi and Amaldi, 1994). This supply sustains *Xenopus'* embryonic development until approximately stage 26. This was shown in the anucleolate mutant, which lacks the nucleolus and hence also lacks *de novo* ribosomal biogenesis and which still survives until swimming tadpole stage (Brown and Gurdon, 1964; Wallace, 1960). Hence, in this study, marker gene expression was affected before the exhaustion of the maternal ribosome pool. Furthermore, previous studies in the working group have demonstrated that by blocking 47S rRNA precursor processing using an ITS2 MO *Xenopus laevis* embryos have reduced levels of 5.8S rRNA but do not have affected marker gene expression at very early stages – off note, at tailbud stages, marker gene expression was reduced upon ITS2 MO injection (Bugner et al., 2011).

In the same study, in *Xenopus laevis*, the ribosomal factor Ppan has been shown to lead to early phenotypes (reduced marker gene expression) which occur independently of ribosomal defects (Bugner et al., 2011). Thus, *Xenopus laevis* is an appropriate model organism to study functions of RPs and ribosomal factors that are independent of ribosome synthesis.

Interestingly, as mentioned in the introduction, loss of Bop1 confers resistance to BRAF kinase inhibitors. This function has also been found to be independent of the ribosome (Gupta et al., 2019).

Furthermore, several pathways (discussed in chapter 4.1.3) which are related to ribosomal biogenesis were not disturbed in Bop1 morphants.
Hence, functions that are independent of the ribosome were considered as underlying molecular mechanisms of the Bop1 MO-induced phenotype. Findings of altered gene expression provide a first indication of the underlying mechanism and extra-ribosomal function. Upon Bop1 knockdown, expression of *pax6* was reduced. A rescue via *pax6* RNA was not possible, which might be due to the reason that the expression of further genes (*foxd3* and *sox3*) was affected as well. However, previous studies have shown that lower Pax6 levels result in severe eye defects, e.g., microphthalmia and anophthalmia (Georgala et al., 2011; Hill et al., 1991; Rungger-Brändle et al., 2010), which are comparable to defects during Bop1 knockdown in the anterior tissue of *Xenopus laevis* shown in this study. Furthermore, simultaneous knockdown of Bop1 and Pax6 resulted in a synergistic effect of the two molecules, which strengthens the hypothesis of a common signaling pathway between Bop1 and Pax6. But not only the loss of Pax6 function leads to eye defects; in mice as well as *Xenopus*, the gain of Pax6 function also leads to severe eye defects, e.g., anophthalmia, microphthalmia, or ectopic eyes (Chow et al., 1999; Schedl et al., 1996). This indicates that the expression of Pax6 needs to be precisely balanced to facilitate proper eye development. Furthermore, these results suggest that the reduced *pax6* expression as a result of Bop1 knockdown might contribute to the Bop1 MO-induced phenotype during *Xenopus laevis* embryonic development.

In conclusion, the here presented data that Bop1 affects the early development of *Xenopus laevis* and pathways closely related to ribosomal biogenesis are not disturbed lead to the hypothesis that the Bop1 MO-induced phenotype in *Xenopus laevis* is not explainable by defects in ribosomal synthesis but instead might occur due to an extra-ribosomal function that might be at least in part mediated through Pax6.
By further investigating and understanding the molecular mechanisms underlying the Bop1 knockdown in *Xenopus laevis*, pathological processes during ribosomopathies may be further elucidated and conceived.

## 4.2 Ribosomal protein Rpl5 during *Xenopus laevis* development

The second aim of this study was to investigate the RP Rpl5 during *Xenopus laevis* embryogenesis. Previous work in the working group of PD Dr. Susanne Kühl majorly implemented by Bianka Kernl gave first insights into the role of Rpl5 during *Xenopus laevis* development. Here, analyses were deepened and studies regarding the molecular mechanisms were performed. Spatio-temporal expression analysis in WT embryos revealed *rpl5* expression in the tissues that are also affected during the pathological condition of ribosomopathy in humans. Knockdown studies via MO-based approaches were performed to analyze occurring phenotypes during *Xenopus laevis* embryonic development. By this, ribosomopathies were recapitulated in the model organism and molecular mechanisms underlying the observed phenotypes were investigated. By analyzing proliferative processes and the molecule c-Myc in greater detail, a common pathway between Rpl5 and c-Myc was elucidated during *Xenopus laevis* embryogenesis. Furthermore, apoptosis and Tp53 were investigated, which revealed a common pathway between the two molecules. By rescue experiments using the apoptosis blocker Bcl2, a major contribution of apoptosis to the Rpl5 MO-induced phenotype was found.

### 4.2.1 *rpl5* expression in *Xenopus laevis* is located in disease-relevant tissues

Analyzing the spatio-temporal expression, *rpl5* transcripts were found to be enriched in the ventral blood islands, the eye anlage, NCCs, and further tissues. These findings are consistent with previous WMISH-based analysis by Wischnewski et al. and Scholnick et al., investigating *rpl5* expression in stage 27 and stage 32 *Xenopus laevis* embryos, respectively (Scholnick et al., 1997; Wischnewski et al., 2000). Both research groups have shown expression of *rpl5* to be located in the eye, the brain, mandibular arch, hyoid arch, and branchial arch. Furthermore, *rpl5* expression patterns shown in this study are in line with previous RNA sequencing data (Session et al., 2016).

During mouse embryogenesis, *Rpl5* expression is found to a greater extent in the liver, the central nervous system, and the whole brain (Yue et al., 2014). In human fetal tissue, *RPL5* expression is enriched in the whole brain and the liver (Duff et al., 2015).

This detailed expression pattern of *rpl5* in *Xenopus laevis* confirms expression in tissues also relevant during ribosomopathies (Farley-Barnes et al., 2019; Narla and Ebert, 2010).

### 4.2.2 Rpl5 is required for early development of *Xenopus laevis*

In this study, it was shown that the knockdown of Rpl5 using *antisense*-based MO approaches leads to smaller heads and smaller and deformed eyes. In Schreiner et al. it was furthermore depicted that cranial cartilage structures are severely deformed upon Rpl5 MO injection (Schreiner et al., 2022). At stage 23, when eye cells differentiate, the evagination of the eye vesicle was perturbed. This early phenotype might already be responsible or at least contribute to a later disturbed invagination of the eye cup and malformed and smaller eyes. Expression of the lens-specific marker genes, *celf1* and *cryba1*, was not affected upon Rpl5 knockdown - even though *rpl5* expression was found to be enriched in the lens - which supposes that developmental impairments of the lens placodes do not conduce the eye phenotype and other and maybe earlier developmental processes are disturbed.

In Schreiner et al., unraveling the molecular basis of the Rpl5 MO-induced phenotype it was shown that the expression of eye-specific marker genes (*rax*, *pax6*) is reduced during eye field induction and eye cell differentiation (Schreiner et al., 2022). It was suggested that the altered expression of eye-specific marker genes in *Xenopus laevis* is the molecular basis and contributes to the eye phenotype (Schreiner et al., 2022).

As described above (chapter 4.1.2) depletion of other RPs or ribosomal factors leads to similar eye and craniofacial phenotypes as described for Rpl5 knockdown. Thus, depletion of the ribosomal factors Ppan, Nol11, and Pes1 results in microphthalmia, colobomas, microcephaly, and craniofacial defects during *Xenopus laevis* development (Bugner et al., 2011; Gessert et al., 2007; Griffin et al., 2015). Mutations in *Rps7* lead to microphthalmia, coloboma, and skeletal defects in mice (Watkins-Chow et al., 2013). In DBA patients, mutations in RPs have been identified that result in eye defects during development (Kuze et al., 2009). Additionally, several brain defects, e.g., microcephaly, seizures, aphasia, ataxia, and intellectual disability, have been shown to be caused by mutations in Rpl10 or Rps23 (Bourque et al., 2018; Brooks et al., 2014).

Furthermore, Rpl5 depletion was found to lead to heart edema in stage 43 embryos. The expression of the hematopoietic transcription factor *gata2* was unaffected, however, the expression of hemoglobin subunit *hba3* was reduced in Rpl5 morphants. These data suggest that hematopoiesis is not disturbed in general, as the transcription factor *gata2* is not affected, but further blood cell differentiation may be influenced since *hba3* expression is reduced. In humans, reduced amounts of HBA are associated with Beta-Thalassemia, a disease that is characterized by severe anemia (Origa, 1993). Furthermore, the disorder Congenital Erythrocytosis in which erythropoiesis is deregulated is linked to mutations in the *HBA* gene (Bento, 2018). Conclusively, results shown by others and in this study indicate that Rpl5 is required for proper blood development.

Rpl5-mutated mice develop anemia and bone marrow failure (Kazerounian et al., 2019). In zebrafish, mutations in *rps29* result in reduced hemoglobin levels and hence disturbed erythropoiesis (Taylor et al., 2012). Interestingly, Iskander and colleagues discovered that in DBA caused by mutations in *RPL* genes, only the differentiation of erythroid progenitors is disturbed and that DBA caused by mutations in *RPS* genes shows almost a complete lack of erythroid progenitors (Iskander et al., 2021). This is in line with the finding that *gata2* expression is not affected whereas *hba3* expression is reduced in Rpl5 morphants shown in this study.

In conclusion, the phenotypes arising upon Rpl5 knockdown during *Xenopus laevis* embryonic development resemble the symptoms that occur during ribosomal defects and ribosomopathies, respectively, in humans.

### 4.2.3 Molecular mechanisms underlying the Rpl5 MO-induced phenotype

Previous studies using the model organism *Xenopus laevis* suggested that early phenotypes (around stage 13) that occur upon depletion of ribosomal factors originate from a ribosomal independent mechanism since the embryos possess a large store of maternal ribosomes, mRNAs, and proteins (Bugner et al., 2011; Gessert et al., 2007; Griffin et al., 2015).

Early phenotypes have also been described for the knockdown using Rpl5 MO (Schreiner et al., 2022). Hence, during the investigation of the molecular mechanism underlying the Rpl5 MO-induced phenotype, ribosomal independent pathways were considered.

To analyze the underlying molecular mechanism of the Rpl5 MO-induced phenotype, different pathways were investigated.

GFP expression was found to be reduced at early stages of development, which presumably points toward an impaired translational machinery. A ribosomal independent pathway could include Tp53 or c-Myc which both have been shown to regulate translation through ribosomal independent ways. Tp53, which was found to be upregulated in this study, can inhibit the translational initiation complex (Kasteri et al., 2018) or can regulate translation through induction of eIF4E-binding protein 1, a repressor of translation (Tiu et al., 2021). c-Myc shown to be downregulated in this study affects translation by modulating mRNA cap methylation, which is a necessary step for successful translation (Cole and Cowling, 2008). However, by implementing experiments with low doses of Rpl5 MO and the translation blocking molecule CHX, which resulted in no synergistic effect, it may be concluded that impaired translation is not contributing to the Rpl5 MO-induced phenotype. A decrease in GFP expression may also be a result of fewer cells expressing GFP since apoptosis was found to be increased in Rpl5 morphants.

During *Xenopus laevis* development, Rpl5 depletion resulted in fewer pH3-positive, i.e., proliferative, cells. Therefore, the molecule c-Myc was further investigated since c-Myc - as described above - contributes to ribosomal processes and hence proliferation. Expression of *c-myc* was found to be decreased in the anterior neural tissue of *Xenopus laevis* embryos and by overexpressing *c-myc* a partial rescue of the reduced eye area phenotype was possible. The synergistic effect between Rpl5 and c-Myc led to the suggestion that Rpl5 and c-Myc act in a common signaling pathway.

These results are consistent with earlier publications showing that c-Myc knockdown leads to a similar phenotype of cranial cartilage structures in *Xenopus laevis* embryos (Bellmeyer et al., 2003). In contrast to the here shown results is that Liao and colleagues have shown that free Rpl5 and Rpl11 reduce *c-myc* levels in a cell line by transporting *c-myc* RNA to RISC which eventually degrades *c-myc* RNA.

Furthermore, they showed that Rpl5 overexpression results in a decrease of *c-myc* levels whereas Rpl5 depletion induces and hence increases *c-myc* expression (Liao et al., 2014). However, different mechanisms might be responsible for decreased *c-myc* expression levels. For example, by inducing ribosomal stress leading to free Rpl11, Rpl5 MO injection might lead to reduced *c-myc* expression (Challagundla et al., 2011). Reduced *c-myc* expression was detected at early stages in Rpl5 morphants pointing towards mechanisms that might be independent of ribosomal synthesis. Previous studies have shown that upon Ppan depletion, expression of *c-myc* is reduced in early *Xenopus laevis* development – interestingly this study proposed a function of Ppan which is independent of the ribosome (Bugner et al., 2011).
To summarize, Rpl5 knockdown reduced the expression of *c-myc*, the depletion of Rpl5 and overexpression of *c-myc* resulted in a synergistic effect and overexpressing *c-myc* partially rescued the Rpl5 MO-induced phenotype. These results suggest the hypothesis that Rpl5 and c-Myc functionally act in the same signaling pathway with Rpl5 being upstream of c-Myc.

In this study, Rpl5 knockdown led to an increase in the number of apoptotic cells as early as stage 13. Apoptotic pathways were further investigated by analyzing the molecule Tp53, which triggers apoptotic pathways through activating transcription of pro-apoptotic genes and by transcription-independent pathways, e.g., by inducing mitochondrial permeabilization resulting in cell death eventually (Kiraz et al., 2016). Here, it was demonstrated that Rpl5 knockdown resulted in increased *tp53* expression and a mutual signaling pathway of Rpl5 and Tp53 was suggested. Tp53-associated apoptotic pathways are connected to pathological ribosomal biogenesis as they are triggered by some free RPs (Dai and Lu, 2004). Additionally, the co-depletion of Tp53 rescues craniofacial abnormalities in different ribosomopathy model organisms (frogs, mice, and fish) (Calo et al., 2018; Griffin et al., 2015; Jones et al., 2008; Zhao et al., 2014). This contrasts with the result that Tp53 co-depletion did not rescue the Rpl5 MO-induced phenotype in *Xenopus laevis* embryos. Therefore, it is suggested that the Rpl5 MO-induced phenotype in *Xenopus laevis* is not uniquely caused by Tp53-dependent apoptosis initiated by disturbed ribosomal biogenesis, but is possibly the result of other ribosomal independent pathways.

Apoptotic pathways were further investigated utilizing antiapoptotic Bcl2. Besides antiapoptotic features, mutations in *BCL2* are linked to cancer development (Reed, 2008). By the co-injection of *hBCL2* RNA, a partial rescue of the Rpl5 MO-induced eye phenotype was achieved. This leads to the assumption that apoptosis, which is initiated by Rpl5 MO injection-dependent increased Tp53 levels, is blocked in rescue experiments by overexpressing Bcl2. This theory is in accordance with previous studies showing that Tp53 can block antiapoptotic BCL2 directly or indirectly further promoting apoptosis (Hemann and Lowe, 2006).
In conclusion, based on the here presented results that 1) Rpl5 knockdown led to increased *tp53* expression, 2) simultaneous injection of Rpl5 MO and *tp53* RNA resulted in a more than additive effect, and 3) by co-injecting antiapoptotic *hBCL2* RNA the Rpl5 MO-induced phenotype was rescued, it is suggested that apoptotic pathways majorly conduce to the phenotypes arising upon Rpl5 depletion and might also influence tissue-specificity of those phenotypes.

As described and proposed for the ribosomal factor Bop1, functions that are independent of ribosomal biogenesis rely on the well-accepted idea that *Xenopus laevis* early development is independent of *de novo* ribosomal biogenesis due to a maternal supply of ribosomes, mRNAs, and proteins. However, other pathways might be involved and might be conceivable for occurring morphogenesis phenotypes (tissue-specificity).
The morphogenesis phenotype of the Rpl5 MO-induced phenotype might result from a tissue-specific dependency of ribosomes, or a generally reduced translation with some tissues reacting more sensitive than others. In this context, the “specialized” ribosomes hypothesis and the ribosome concentration theory should be mentioned as both might lead to the acquirement of the specific morphogenesis phenotypes. The “specialized” ribosome hypothesis is based on the idea that ribosomes, which are *per se* heterogeneous in terms of their features and characteristics - acquire additional features in distinct tissues due to changes in ribosome assembly and structure (Farley-Barnes et al., 2019; Ferretti and Karbstein, 2019; Genuth and Barna, 2018; Mills and Green, 2017). Another hypothesis is the ribosome concentration theory; here, the ribosomal concentration, which differs in certain tissues, determines and favors the translation of specific mRNAs (Cheng et al., 2019; Farley-Barnes et al., 2019; Lodish, 1974; Mills and

Green, 2017). According to this theory, one might speculate that maternally supplied ribosomes might not be equally distributed throughout the embryos' cells which might result in tissues that require *de novo* ribosomal biogenesis earlier than others; hence, a morphogenesis phenotype might occur.

In conclusion, based on here presented data, it is suggested that Rpl5 plays a role during the early neural development of *Xenopus laevis*. Furthermore, several pathways - which might be independent of ribosomal biogenesis - have been identified that are affected upon Rpl5 depletion, e.g., proliferative, and apoptotic pathways. The investigation of these pathways sheds more light on some molecular mechanisms underlying the phenotype. Further studies investigating the underlying molecular mechanisms are proposed to thoroughly understand the basis of pathological ribosomal biogenesis.

## 4.3 Conclusion

During the first part of the present dissertation, the role of Bop1 during *Xenopus laevis* embryonic development was assessed. Bop1 was found to be specifically expressed in tissues that are also affected during pathological ribosomal biogenesis in humans. Furthermore, Bop1 was found to be required for anterior neural development of *Xenopus laevis*. Several tissue-specific marker genes were affected upon Bop1 MO-injection and since pathways typically affected during disturbed ribosomal biogenesis were not affected upon Bop1 depletion, a function independent of ribosomal biogenesis was considered and investigated for Bop1. A common signaling pathway between Bop1 and Pax6 and an extra-ribosomal function mediated through Pax6 is suggested.

The second part of this dissertation investigated Rpl5 during *Xenopus laevis* embryonic development. *rpl5* transcripts were detected in ribosomopathy-relevant tissues and upon Rpl5 MO-injection, phenotypes which recapitulate symptoms of ribosomopathies occurred. Analyzing the molecular underlying mechanism of the Rpl5 MO-induced phenotype revealed that proliferation, as well as apoptosis, are affected. By rescue experiments using the apoptosis blocker Bcl2, it is proposed that apoptotic mechanisms majorly contribute to the phenotypes.

# 5 Summary

Ribosomal synthesis is an essential step for each cell as ribosomes are required for cellular function, cell growth, and cell division. This process requires a tremendous amount of energy, three different RNA polymerases, ribosomal RNAs, small nucleolar RNAs, and more than 200 ribosomal proteins and factors for processing, assembling, and maturation.

At the occurrence of malfunctioned ribosomal biogenesis, the pathological condition of ribosomopathy arises in humans. This congenital disease manifests through different clinical observations, e.g., craniofacial malformations, eye malformations, cardiac defects, anemia, and bone marrow failure. Ribosomopathies are further associated with an increased incidence of tumor development. How this hypoproliferative state (e.g., anemia or bone marrow failure) switches to a hyperproliferative state (tumor development) remains unknown.

Several genes have been identified to be mutated and the cause of ribosomopathies.

The ribosomal factor block of proliferation 1 (Bop1) is required for the processing and maturation of the 5.8S and 28S rRNA during ribosomal biogenesis. Bop1 has not been associated with ribosomopathies yet, but it does play a role in several carcinomas.

In this study, Bop1 was investigated during the embryonic development of the model organism *Xenopus laevis*. By whole mount *in situ* hybridization (WMISH), *bop1* transcripts were detected in tissues that are affected during defective ribosomal biogenesis in humans. Thus, *bop1* expression was found to be enriched in the eye, the brain, and the neural crest cells (NCCs). *Antisense* morpholino oligonucleotide (MO)- based approaches, as well as the CRISPR/Cas9 method, were implemented and Bop1 was found to be crucial for *Xenopus laevis* embryonic development. Upon Bop1 depletion in anterior neural tissue, *Xenopus* embryos developed phenotypes of the eye (microphthalmia, coloboma), the brain, and the NCC-derived cranial cartilage (microcephaly) – symptoms similar to ribosomopathies. Additionally, the expression of tissue-specific marker genes was reduced upon Bop1 MO injection at very early developmental stages. Particularly noteworthy is the reduced expression of the master regulator of eye development *pax6*. A common signaling pathway of

Bop1 and Pax6 is suggested upon synergy experiments. During these early developmental stages (during which *pax6* expression was reduced), *Xenopus laevis* embryos are independent of *de novo* ribosome biogenesis due to a maternal supply of ribosomes, proteins, and mRNAs. Furthermore, pathways known to be affected during defective ribosomal synthesis - such as proliferation and apoptosis - are unaffected upon Bop1 depletion. Conclusively, based on these results, and in addition to its requirement during *Xenopus laevis* embryogenesis, a ribosomal independent function of Bop1 is proposed, which is at least in part mediated through Pax6.

During ribosomal biogenesis, the ribosomal protein Rpl5 forms a ribonucleoprotein complex together with Rpl11 and 5S rRNA; as a complex Rpl5 is incorporated into the large ribosomal subunit of the functional ribosome. Mutations in the human *RPL5* are linked to the pathological condition of ribosomopathy.
Here, Rpl5 was analyzed during *Xenopus laevis* embryogenesis. A comprehensive expression analysis of *rpl5* at different developmental stages using WMISH revealed *rpl5* expression in the eyes, the brain, the NCCs, and the ventral blood islands; tissues drastically affected in patients suffering from ribosomopathies. Additionally, Rpl5 knockdown via MO injection resulted in phenotypes that recapitulate clinical manifestations occurring during ribosomal defects. Thus, Rpl5 morphants developed malformed eyes and heads, and heart edema. By applying pH3 and TUNEL staining methods, it was shown that proliferative as well as apoptotic pathways are affected upon Rpl5 MO injection. Furthermore, the underlying molecular mechanism of the Rpl5 MO-induced phenotype was investigated. Low dose experiments using Rpl5 MO and c-Myc MO showed a common signaling mechanism between the two molecules. Also, low dose experiments with Rpl5 MO and *tp53* RNA revealed a common signaling pathway of Rpl5 and Tp53. Based on rescue experiments using the apoptosis blocker Bcl2 (*hBCL2* RNA), it is suggested that apoptosis is a major contributor to the Rpl5 MO-induced phenotype in *Xenopus laevis* embryos. In summary, the loss of Rpl5 function in *Xenopus laevis* embryos recapitulated clinical manifestations during the course of ribosomopathies, and analyzing the underlying molecular mechanism revealed apoptosis as a great driver of pathological outcomes during defective ribosomal biogenesis.

# 6 List of References

Ajore, R., Raiser, D., McConkey, M., Jöud, M., Boidol, B., Mar, B., Saksena, G., Weinstock, D. M., Armstrong, S., Ellis, S. R., Ebert, B. L., & Nilsson, B. (2017). Deletion of ribosomal protein genes is a common vulnerability in human cancer, especially in concert with TP53 mutations. *EMBO Molecular Medicine*, *9*(4), 498–507.

Allende, M. L., Amsterdam, A., Becker, T., Kawakami, K., Gaiano, N., & Hopkins, N. (1996). Insertional mutagenesis in zebrafish identifies two novel genes, pescadillo and dead eye, essential for embryonic development. *Genes & Development*, *10*(24), 3141–3155.

Arabi, A., Wu, S., Ridderstråle, K., Bierhoff, H., Shiue, C., Fatyol, K., Fahlén, S., Hydbring, P., Söderberg, O., Grummt, I., Larsson, L.-G., & Wright, A. P. H. (2005). C-Myc associates with ribosomal DNA and activates RNA polymerase I transcription. *Nature Cell Biology*, *7*(3), 303–310.

Aspesi, A., & Ellis, S. R. (2019). Rare ribosomopathies: Insights into mechanisms of cancer. *Nature Reviews Cancer*, *19*(4), 228–238.

Aubert, M., O'Donohue, M.-F., Lebaron, S., & Gleizes, P.-E. (2018). Pre-Ribosomal RNA Processing in Human Cells: From Mechanisms to Congenital Diseases. *Biomolecules*, *8*(4), E123.

Bailey, T. J., El-Hodiri, H., Zhang, L., Shah, R., Mathers, E. H., & Jamrich, M. (2004). Regulation of vertebrate eye development by Rx genes. *The International Journal of Developmental Biology*, *48*(8–9), 761–770.

Bange, G., Murat, G., Sinning, I., Hurt, E., & Kressler, D. (2013). New twist to nuclear import: When two travel together. *Communicative & Integrative Biology*, *6*(4), e24792.

Baßler, J., & Hurt, E. (2019). Eukaryotic Ribosome Assembly. *Annual Review of Biochemistry*, *88*, 281–306.

Bellmeyer, A., Krase, J., Lindgren, J., & LaBonne, C. (2003). The protooncogene c-myc is an essential regulator of neural crest formation in xenopus. *Developmental Cell*, *4*(6), 827–839.

Bento, C. (2018). Genetic basis of congenital erythrocytosis. *International Journal of Laboratory Hematology*, *40*, 62–67.

Bienert, S., Waterhouse, A., de Beer, T. A. P., Tauriello, G., Studer, G., Bordoli, L., & Schwede, T. (2017). The SWISS-MODEL Repository-new features and functionality. *Nucleic Acids Research*, *45*(D1), D313–D319.

Blum, M., & Ott, T. (2018). Xenopus: An Undervalued Model Organism to Study and Model Human Genetic Disease. *Cells, Tissues, Organs*, *205*(5–6), 303–313.

Bourque, D. K., Hartley, T., Nikkel, S. M., Pohl, D., Tétreault, M., Kernohan, K. D., Care4Rare Canada Consortium, & Dyment, D. A. (2018). A de novo mutation in RPL10 causes a rare X-linked ribosomopathy characterized by syndromic intellectual disability and epilepsy: A new case and review of the literature. *European Journal of Medical Genetics*, *61*(2), 89–93.

Briggs, J. A., Weinreb, C., Wagner, D. E., Megason, S., Peshkin, L., Kirschner, M. W., & Klein, A. M. (2018). The dynamics of gene expression in vertebrate embryogenesis at single-cell resolution. *Science (New York, N.Y.)*, *360*(6392), eaar5780.

Brinkman, E. K., Chen, T., Amendola, M., & van Steensel, B. (2014). Easy quantitative assessment of genome editing by sequence trace decomposition. *Nucleic Acids Research*, *42*(22), e168.

Brooks, S. S., Wall, A. L., Golzio, C., Reid, D. W., Kondyles, A., Willer, J. R., Botti, C., Nicchitta, C. V., Katsanis, N., & Davis, E. E. (2014). A novel ribosomopathy caused by dysfunction of RPL10 disrupts neurodevelopment and causes X-linked microcephaly in humans. *Genetics*, *198*(2), 723–733.

Brown, D. D. (1964). RNA SYNTHESIS DURING AMPHIBIAN DEVELOPMENT. *The Journal of Experimental Zoology*, *157*, 101–117.

Brown, D. D., & Gurdon, J. B. (1964). ABSENCE OF RIBOSOMAL RNA SYNTHESIS IN THE ANUCLEOLATE MUTANT OF XENOPUS LAEVIS. *Proceedings of the National Academy of Sciences*, *51*(1), 139–146.

Buglo, E., Sarmiento, E., Martuscelli, N. B., Sant, D. W., Danzi, M. C., Abrams, A. J., Dallman, J. E., & Züchner, S. (2020). Genetic compensation in a stable slc25a46 mutant zebrafish: A case for using F0 CRISPR mutagenesis to study phenotypes caused by inherited disease. *PloS One*, *15*(3), e0230566.

Bugner, V., Tecza, A., Gessert, S., & Kuhl, M. (2011). Peter Pan functions independently of its role in ribosome biogenesis during early eye and craniofacial cartilage development in Xenopus laevis. *Development*, *138*(11), 2369–2378.

Calo, E., Gu, B., Bowen, M. E., Aryan, F., Zalc, A., Liang, J., Flynn, R. A., Swigut, T., Chang, H. Y., Attardi, L. D., & Wysocka, J. (2018). Tissue-selective effects of nucleolar stress and rDNA damage in developmental disorders. *Nature*, *554*(7690), 112–117.

Chakraborty, A., Uechi, T., Higa, S., Torihara, H., & Kenmochi, N. (2009). Loss of ribosomal protein L11 affects zebrafish embryonic development through a p53-dependent apoptotic response. *PloS One*, *4*(1), e4152.

Challagundla, K. B., Sun, X.-X., Zhang, X., DeVine, T., Zhang, Q., Sears, R. C., & Dai, M.-S. (2011). Ribosomal protein L11 recruits miR-24/miRISC to repress c-Myc expression in response to ribosomal stress. *Molecular and Cellular Biology*, *31*(19), 4007–4021.

Cheng, Z., Mugler, C. F., Keskin, A., Hodapp, S., Chan, L. Y.-L., Weis, K., Mertins, P., Regev, A., Jovanovic, M., & Brar, G. A. (2019). Small and Large Ribosomal Subunit Deficiencies Lead to Distinct Gene Expression Signatures that Reflect Cellular Growth Rate. *Molecular Cell*, *73*(1), 36-47.e10.

Chow, R. L., Altmann, C. R., Lang, R. A., & Hemmati-Brivanlou, A. (1999). Pax6 induces ectopic eyes in a vertebrate. *Development (Cambridge, England)*, *126*(19), 4213–4222.

Chow, R. L., & Lang, R. A. (2001). Early eye development in vertebrates. *Annual Review of Cell and Developmental Biology*, *17*, 255–296.

Chung, K.-Y., Cheng, I. K.-C., Ching, A. K.-K., Chu, J.-H., Lai, P. B.-S., & Wong, N. (2011). Block of proliferation 1 (BOP1) plays an oncogenic role in hepatocellular carcinoma by promoting epithelial-to-mesenchymal transition. *Hepatology*, *54*(1), 307–318.

Cizelsky, W., Hempel, A., Metzig, M., Tao, S., Hollemann, T., Kühl, M., & Kühl, S. J. (2013). Sox4 And sox11 Function during Xenopus laevis Eye Development. *PLoS ONE*, *8*(7), e69372.

Cmejla, R., Cmejlova, J., Handrkova, H., Petrak, J., Petrtylova, K., Mihal, V., Stary, J., Cerna, Z., Jabali, Y., & Pospisilova, D. (2009). Identification of mutations in the ribosomal protein L5 (RPL5) and ribosomal protein L11 (RPL11) genes in Czech patients with Diamond-Blackfan anemia. *Human Mutation*, *30*(3), 321–327.

Cohen, J., Ghezzi, F., Gonçalves, L., Fuentes, J. D., Paulyson, K. J., & Sherer, D. M. (1995). Prenatal sonographic diagnosis of Treacher Collins syndrome: A case and review of the literature. *American Journal of Perinatology*, *12*(6), 416–419.

Cole, M. D., & Cowling, V. H. (2008). Transcription-independent functions of MYC: Regulation of translation and DNA replication. *Nature Reviews. Molecular Cell Biology*, *9*(10), 810–815.

Cordenonsi, M., Dupont, S., Maretto, S., Insinga, A., Imbriano, C., & Piccolo, S. (2003). Links between tumor suppressors: P53 is required for TGF-beta gene responses by cooperating with Smads. *Cell*, *113*(3), 301–314.

Cvekl, A., & Callaerts, P. (2017). PAX6: 25th anniversary and more to learn. *Experimental Eye Research*, *156*, 10–21.

Da Costa, L., Leblanc, T., & Mohandas, N. (2020). Diamond-Blackfan anemia. *Blood*, *136*(11), 1262–1273.

Dai, M.-S., & Lu, H. (2004). Inhibition of MDM2-mediated p53 ubiquitination and degradation by ribosomal protein L5. *The Journal of Biological Chemistry*, *279*(43), 44475–44482.

Dameshek, W. (1967). Riddle: What do aplastic anemia, paroxysmal nocturnal hemoglobinuria (PNH) and “hypoplastic” leukemia have in common? *Blood*, *30*(2), 251–254.

Danilova, N., Sakamoto, K. M., & Lin, S. (2008). Ribosomal protein S19 deficiency in zebrafish leads to developmental abnormalities and defective erythropoiesis through activation of p53 protein family. *Blood*, *112*(13), 5228–5237.

Daudin, F. M. (1802). *Histoire naturelle des rainettes, des grenouilles et des crapauds: Dédiée à B.G.E.L. Lacépède [1802]*.

Day, R. C., & Beck, C. W. (2011). Transdifferentiation from cornea to lens in Xenopus laevis depends on BMP signalling and involves upregulation of Wnt signalling. *BMC Developmental Biology*, *11*(1), 54.

De Keersmaecker, K., Sulima, S. O., & Dinman, J. D. (2015). Ribosomopathies and the paradox of cellular hypo- to hyperproliferation. *Blood*, *125*(9), 1377–1382.

Devlin, E. E., Dacosta, L., Mohandas, N., Elliott, G., & Bodine, D. M. (2010). A transgenic mouse model demonstrates a dominant negative effect of a point mutation in the RPS19 gene associated with Diamond-Blackfan anemia. *Blood*, *116*(15), 2826–2835.

Diofano, F., Weinmann, K., Schneider, I., Thiessen, K. D., Rottbauer, W., & Just, S. (2020). Genetic compensation prevents myopathy and heart failure in an in vivo model of Bag3 deficiency. *PLoS Genetics*, *16*(11), e1009088.

Duff, M. O., Olson, S., Wei, X., Garrett, S. C., Osman, A., Bolisetty, M., Plocik, A., Celniker, S. E., & Graveley, B. R. (2015). Genome-wide identification of zero nucleotide recursive splicing in Drosophila. *Nature*, *521*(7552), 376–379.

Dutt, S., Narla, A., Lin, K., Mullally, A., Abayasekara, N., Megerdichian, C., Wilson, F. H., Currie, T., Khanna-Gupta, A., Berliner, N., Kutok, J. L., & Ebert, B. L. (2011). Haploinsufficiency for ribosomal protein genes causes selective activation of p53 in human erythroid progenitor cells. *Blood*, *117*(9), 2567–2576.

Dyer, M. A., Livesey, F. J., Cepko, C. L., & Oliver, G. (2003). Prox1 function controls progenitor cell proliferation and horizontal cell genesis in the mammalian retina. *Nature Genetics*, *34*(1), 53–58.

Fagerberg, L., Hallström, B. M., Oksvold, P., Kampf, C., Djureinovic, D., Odeberg, J., Habuka, M., Tahmasebpoor, S., Danielsson, A., Edlund, K., Asplund, A., Sjöstedt, E., Lundberg, E., Szigyarto, C. A.-K., Skogs, M., Takanen, J. O., Berling, H., Tegel, H., Mulder J., Nilsson P., Schwenk J. M., Lindskog C., Danielsson F., Mardinoglu A., Sivertsson A., von Feilitzen K., Forsberg M., Zwahlen M., Olsson I., Navani S., Huss M., Nielsen J., Ponten F., & Uhlén M. (2014). Analysis of the Human Tissue-specific Expression by Genome-wide Integration of Transcriptomics and Antibody-based Proteomics. *Molecular & Cellular Proteomics*, *13*(2), 397–406.

Fairchild, C. L., Conway, J. P., Schiffmacher, A. T., Taneyhill, L. A., & Gammill, L. S. (2014). FoxD3 regulates cranial neural crest EMT via downregulation of tetraspanin18 independent of its functions during neural crest formation. *Mechanisms of Development*, *132*, 1–12.

Farley-Barnes, K. I., Ogawa, L. M., & Baserga, S. J. (2019). Ribosomopathies: Old Concepts, New Controversies. *Trends in Genetics*, *35*(10), 754–767.

Fazen, L. E., Elmore, J., & Nadler, H. L. (1967). Mandibulo-facial dysostosis. (Treacher-Collins syndrome). *American Journal of Diseases of Children (1960)*, *113*(4), 405–410.

Ferretti, M. B., & Karbstein, K. (2019). Does functional specialization of ribosomes really exist? *RNA (New York, N.Y.)*, *25*(5), 521–538.

Fumagalli, S., Ivanenkov, V. V., Teng, T., & Thomas, G. (2012). Suprainduction of p53 by disruption of 40S and 60S ribosome biogenesis leads to the activation of a novel G2/M checkpoint. *Genes & Development*, *26*(10), 1028–1040.

Furukawa, T., Kozak, C. A., & Cepko, C. L. (1997). Rax, a novel paired-type homeobox gene, shows expression in the anterior neural fold and developing retina. *Proceedings of the National Academy of Sciences of the United States of America*, *94*(7), 3088–3093.

Gärtner, C., Meßmer, A., Dietmann, P., Kühl, M., & Kühl, S. J. (2022). Functions of block of proliferation 1 during anterior development in Xenopus laevis. *PLoS ONE*, 17(8): e0273507.

Gazda, H. T., Sheen, M. R., Vlachos, A., Choesmel, V., O'Donohue, M.-F., Schneider, H., Darras, N., Hasman, C., Sieff, C. A., Newburger, P. E., Ball, S. E., Niewiadomska, E., Matysiak, M., Zaucha, J. M., Glader, B., Niemeyer, C., Meerpohl, J. J., Atsidaftos, E., Lipton, J. M., Gleizes, P.-E., & Beggs, A. H. (2008). Ribosomal protein L5 and L11 mutations are associated with cleft palate and abnormal thumbs in Diamond-Blackfan anemia patients. *American Journal of Human Genetics*, *83*(6), 769–780.

Genuth, N. R., & Barna, M. (2018). The Discovery of Ribosome Heterogeneity and Its Implications for Gene Regulation and Organismal Life. *Molecular Cell*, *71*(3), 364–374.

Georgala, P. A., Carr, C. B., & Price, D. J. (2011). The role of Pax6 in forebrain development. *Developmental Neurobiology*, *71*(8), 690–709.

Gessert, S., Maurus, D., Rössner, A., & Kühl, M. (2007). Pescadillo is required for Xenopus laevis eye development and neural crest migration. *Developmental Biology*, *310*(1), 99–112.

Gomez-Roman, N., Grandori, C., Eisenman, R. N., & White, R. J. (2003). Direct activation of RNA polymerase III transcription by c-Myc. *Nature*, *421*(6920), 290–294.

Green, L., Houck-Loomis, B., Yueh, A., & Goff, S. P. (2012). Large ribosomal protein 4 increases efficiency of viral recoding sequences. *Journal of Virology*, *86*(17), 8949–8958.

Griffin, J. N., Sondalle, S. B., del Viso, F., Baserga, S. J., & Khokha, M. K. (2015). The Ribosome Biogenesis Factor Nol11 Is Required for Optimal rDNA Transcription and Craniofacial Development in Xenopus. *PLoS Genetics*, *11*(3), e1005018.

Gupta, R., Bugide, S., Wang, B., Green, M. R., Johnson, D. B., & Wajapeyee, N. (2019). Loss of BOP1 confers resistance to BRAF kinase inhibitors in melanoma by activating MAP kinase pathway. *Proceedings of the National Academy of Sciences of the United States of America*, *116*(10), 4583–4591.

Hampp, S., Kiessling, T., Buechle, K., Mansilla, S. F., Thomale, J., Rall, M., Ahn, J., Pospiech, H., Gottifredi, V., & Wiesmüller, L. (2016). DNA damage tolerance pathway involving DNA polymerase ι and the tumor suppressor p53 regulates DNA replication fork progression. *Proceedings of the National Academy of Sciences of the United States of America*, *113*(30), E4311-4319.

Hardcastle, Z., & Papalopulu, N. (2000). Distinct effects of XBF-1 in regulating the cell cycle inhibitor p27(XIC1) and imparting a neural fate. *Development (Cambridge, England)*, *127*(6), 1303–1314.

He, J., Chen, Z., Xue, Q., & Shi, W. (2022). Block of Proliferation 1 Promotes Proliferation, Invasion and Epithelial Mesenchymal Transformation in Gastric Cancer. *Oxidative Medicine and Cellular Longevity*, *2022*, 2946989.

Hemann, M. T., & Lowe, S. W. (2006). The p53-Bcl-2 connection. *Cell Death and Differentiation*, *13*(8), 1256–1259.

Hemmati-Brivanlou, A., Frank, D., Bolce, M. E., Brown, B. D., Sive, H. L., & Harland, R. M. (1990). Localization of specific mRNAs in Xenopus embryos by whole-mount in situ hybridization. *Development (Cambridge, England)*, *110*(2), 325–330.

Henras, A. K., Plisson-Chastang, C., O'Donohue, M.-F., Chakraborty, A., & Gleizes, P.-E. (2015). An overview of pre-ribosomal RNA processing in eukaryotes: Pre-ribosomal RNA processing in eukaryotes. *Wiley Interdisciplinary Reviews: RNA*, *6*(2), 225–242.

Hill, R. E., Favor, J., Hogan, B. L. M., Ton, C. C. T., Saunders, G. F., Hanson, I. M., Prosser, J., Jordan, T., Hastie, N. D., & Heyningen, V. van. (1991). Mouse Small eye results from mutations in a paired-like homeobox-containing gene. *Nature*, *354*(6354), 522–525.

Hitchcock, P. F., Macdonald, R. E., VanDeRyt, J. T., & Wilson, S. W. (1996). Antibodies against Pax6 immunostain amacrine and ganglion cells and neuronal progenitors, but not rod precursors, in the normal and regenerating retina of the goldfish. *Journal of Neurobiology*, *29*(3), 399–413.

Hollemann, T., Bellefroid, E., & Pieler, T. (1998). The Xenopus homologue of the Drosophila gene tailless has a function in early eye development. *Development (Cambridge, England)*, *125*(13), 2425–2432.

Hölzel, M., Rohrmoser, M., Schlee, M., Grimm, T., Harasim, T., Malamoussi, A., Gruber-Eber, A., Kremmer, E., Hiddemann, W., Bornkamm, G. W., & Eick, D. (2005). Mammalian WDR12 is a novel member of the Pes1–Bop1 complex and is required for ribosome biogenesis and cell proliferation. *Journal of Cell Biology*, *170*(3), 367–378.

Hryhorowicz, M., Lipiński, D., Zeyland, J., & Słomski, R. (2017). CRISPR/Cas9 Immune System as a Tool for Genome Engineering. *Archivum Immunologiae Et Therapiae Experimentalis*, *65*(3), 233–240.

Iskander, D., Wang, G., Heuston, E. F., Christodoulidou, C., Psaila, B., Ponnusamy, K., Ren, H., Mokhtari, Z., Robinson, M., Chaidos, A., Trivedi, P., Trasanidis, N., Katsarou, A., Szydlo, R., Palii, C. G., Zaidi, M. H., Al-Oqaily, Q., Caputo, V. S., Roy, A., Harrington, Y., Karnik, L., Naresh, K., Mead, A. J., Thongjuea, S., Brand, M., de la Fuente, J., Bodine, D. M., Roberts, I., & Karadimitris, A. (2021). Single-cell profiling of human bone marrow progenitors reveals mechanisms of failing erythropoiesis in Diamond-Blackfan anemia. *Science Translational Medicine*, *13*(610), eabf0113.

Jacobson, M. (1991). Developmental Neurobiology. 3rd Edition. *Springer,* New York, pp.143-162

Jenkinson, E. M., Rodero, M. P., Kasher, P. R., Uggenti, C., Oojageer, A., Goosey, L. C., Rose, Y., Kershaw, C. J., Urquhart, J. E., Williams, S. G., Bhaskar, S. S., O'Sullivan, J., Baerlocher, G. M., Haubitz, M., Aubert, G., Barañano, K. W., Barnicoat, A. J., Battini, R., Berger, A., Blair, E. M., Brunstrom-Hernandez, J. E., Buckard, J. A., Cassiman, D. M., Caumes, R., Cordelli, D. M., De Waele, L. M., Fay, A. J., Ferreira, P., Fletcher, N. A., Fryer, A. E., Goel, H., Hemingway, C. A., Henneke, M., Hughes, I., Jefferson, R. J., Kumar, R., Lagae, L., Landrieu, P. G., Lourenço, C. M., Malpas, T. J., Mehta, S. G., Metz, I., Naidu, S., Õunap, K., Panzer, A., Prabhakar, P., Quaghebeur, G., Schiffmann, R., Sherr, E. H., Sinnathuray, K. R., Soh, C., Stewart, H. S., Stone, J., Van Esch, H., Van Mol, C. E., Vanderver, A., Wakeling, E. L., Whitney, A., Pavitt, G. D., Griffiths-Jones, S., Rice, G. I., Revy, P., van der Knaap, M. S., Livingston, J. H., O'Keefe, R. T., & Crow, Y. J.. (2016). Mutations in SNORD118 cause the cerebral microangiopathy leukoencephalopathy with calcifications and cysts. *Nature Genetics*, *48*(10), 1185–1192.

Jenner, L., Melnikov, S., de Loubresse, N. G., Ben-Shem, A., Iskakova, M., Urzhumtsev, A., Meskauskas, A., Dinman, J., Yusupova, G., & Yusupov, M. (2012). Crystal structure of the 80S yeast ribosome. *Current Opinion in Structural Biology*, *22*(6), 759–767.

Jones, N. C., Lynn, M. L., Gaudenz, K., Sakai, D., Aoto, K., Rey, J.-P., Glynn, E. F., Ellington, L., Du, C., Dixon, J., Dixon, M. J., & Trainor, P. A. (2008). Prevention of the neurocristopathy Treacher Collins syndrome through inhibition of p53 function. *Nature Medicine*, *14*(2), 125–133.

Kang, J., Brajanovski, N., Chan, K. T., Xuan, J., Pearson, R. B., & Sanij, E. (2021). Ribosomal proteins and human diseases: Molecular mechanisms and targeted therapy. *Signal Transduction and Targeted Therapy*, *6*(1), 323.

Kasteri, J., Das, D., Zhong, X., Persaud, L., Francis, A., Muharam, H., & Sauane, M. (2018). Translation Control by p53. *Cancers*, *10*(5), E133.

Kazerounian, S., Yuan, D., Alexander, M. S., Beggs, A. H., & Gazda, H. T. (2019). Rpl5-Inducible Mouse Model for Studying Diamond-Blackfan Anemia. *Discoveries (Craiova, Romania)*, *7*(3), e96.

Kellner, M., Rohrmoser, M., Forné, I., Voss, K., Burger, K., Mühl, B., Gruber-Eber, A., Kremmer, E., Imhof, A., & Eick, D. (2015). DEAD-box helicase DDX27 regulates 3' end formation of ribosomal 47S RNA and stably associates with the PeBoW-complex. *Experimental Cell Research*, *334*(1), 146–159.

Kietzmann, A., Wang, Y., Weber, D., & Steinbeisser, H. (2012). Xenopus paraxial protocadherin inhibits Wnt/β-catenin signalling via casein kinase 2β. *EMBO Reports*, *13*(2), 129–134.

Kikkawa, T., Casingal, C. R., Chun, S. H., Shinohara, H., Hiraoka, K., & Osumi, N. (2019). The role of Pax6 in brain development and its impact on pathogenesis of autism spectrum disorder. *Brain Research*, *1705*, 95–103.

Killian, A., Sarafan-Vasseur, N., Sesboüé, R., Le Pessot, F., Blanchard, F., Lamy, A., Laurent, M., Flaman, J.-M., & Frébourg, T. (2006). Contribution of theBOP1 gene, located on 8q24, to colorectal tumorigenesis. *Genes, Chromosomes and Cancer*, *45*(9), 874–881.

Kiraz, Y., Adan, A., Kartal Yandim, M., & Baran, Y. (2016). Major apoptotic mechanisms and genes involved in apoptosis. *Tumour Biology: The Journal of the International Society for Oncodevelopmental Biology and Medicine*, *37*(7), 8471–8486.

Klein, S. L., Strausberg, R. L., Wagner, L., Pontius, J., Clifton, S. W., & Richardson, P. (2002). Genetic and genomic tools for Xenopus research: The NIH Xenopus initiative. *Developmental Dynamics: An Official Publication of the American Association of Anatomists*, *225*(4), 384–391.

Köster, M., Dillinger, K., & Knöchel, W. (1998). Expression pattern of the winged helix factor XFD-11 during Xenopus embryogenesis. *Mechanisms of Development*, *76*(1–2), 169–173.

Kostjukovits, S., Klemetti, P., Valta, H., Martelius, T., Notarangelo, L. D., Seppänen, M., Taskinen, M., & Mäkitie, O. (2017). Analysis of clinical and immunologic phenotype in a large cohort of children and adults with cartilage-hair hypoplasia. *Journal of Allergy and Clinical Immunology*, *140*(2), 612-614.e5.

Kressler, D., Hurt, E., & Baßler, J. (2017). A Puzzle of Life: Crafting Ribosomal Subunits. *Trends in Biochemical Sciences*, *42*(8), 640–654.

Kuze, M., Matsubara, H., & Uji, Y. (2009). Ocular hypertelorism and exotropia as presenting signs in Diamond-Blackfan anemia. *Japanese Journal of Ophthalmology*, *53*(1), 67–68.

Lamb, T. M., Knecht, A. K., Smith, W. C., Stachel, S. E., Economides, A. N., Stahl, N., Yancopolous, G. D., & Harland, R. M. (1993). Neural induction by the secreted polypeptide noggin. *Science (New York, N.Y.)*, *262*(5134), 713–718.

Léger-Silvestre, I., Caffrey, J. M., Dawaliby, R., Alvarez-Arias, D. A., Gas, N., Bertolone, S. J., Gleizes, P.-E., & Ellis, S. R. (2005). Specific Role for Yeast Homologs of the Diamond Blackfan Anemia-associated Rps19 Protein in Ribosome Synthesis. *The Journal of Biological Chemistry*, *280*(46), 38177–38185.

Lequeux, L., Rio, M., Vigouroux, A., Titeux, M., Etchevers, H., Malecaze, F., Chassaing, N., & Calvas, P. (2008). Confirmation of RAX gene involvement in human anophthalmia. *Clinical Genetics*, *74*(4), 392–395.

Lerch-Gaggl, A., Haque, J., Li, J., Ning, G., Traktman, P., & Duncan, S. A. (2002). Pescadillo Is Essential for Nucleolar Assembly, Ribosome Biogenesis, and Mammalian Cell Proliferation. *Journal of Biological Chemistry*, *277*(47), 45347–45355.

Liao, J.-M., Zhou, X., Gatignol, A., & Lu, H. (2014). Ribosomal proteins L5 and L11 co-operatively inactivate c-Myc via RNA-induced silencing complex. *Oncogene*, *33*(41), 4916–4923.

Lipton, J. M., Atsidaftos, E., Zyskind, I., & Vlachos, A. (2006). Improving clinical care and elucidating the pathophysiology of Diamond Blackfan anemia: An update from the Diamond Blackfan Anemia Registry. *Pediatric Blood & Cancer*, *46*(5), 558–564.

Liu, R., Iadevaia, V., Averous, J., Taylor, P. M., Zhang, Z., & Proud, C. G. (2014). Impairing the production of ribosomal RNA activates mammalian target of rapamycin complex 1 signalling and downstream translation factors. *Nucleic Acids Research*, *42*(8), 5083–5096.

Lodish, H. F. (1974). Model for the regulation of mRNA translation applied to haemoglobin synthesis. *Nature*, *251*(5474), 385–388.

London, N. J. S., Kessler, P., Williams, B., Pauer, G. J., Hagstrom, S. A., & Traboulsi, E. I. (2009). Sequence alterations in RX in patients with microphthalmia, anophthalmia, and coloboma. *Molecular Vision*, *15*, 162–167.

Lufkin, T. (2007). In Situ Hybridization of Whole-Mount Mouse Embryos with RNA Probes: Hybridization, Washes, and Histochemistry. *Cold Spring Harbor Protocols*, *2007*(11), pdb.prot4823.

Macdonald, R., Barth, K. A., Xu, Q., Holder, N., Mikkola, I., & Wilson, S. W. (1995). Midline signalling is required for Pax gene regulation and patterning of the eyes. *Development (Cambridge, England)*, *121*(10), 3267–3278.

Maurus, D., Héligon, C., Bürger-Schwärzler, A., Brändli, A. W., & Kühl, M. (2005). Noncanonical Wnt-4 signaling and EAF2 are required for eye development in Xenopus laevis. *The EMBO Journal*, *24*(6), 1181–1191.

McGowan, K. A., Li, J. Z., Park, C. Y., Beaudry, V., Tabor, H. K., Sabnis, A. J., Zhang, W., Fuchs, H., de Angelis, M. H., Myers, R. M., Attardi, L. D., & Barsh, G. S. (2008). Ribosomal mutations cause p53-mediated dark skin and pleiotropic effects. *Nature Genetics*, *40*(8), 963–970.

Melnikov, S., Ben-Shem, A., Garreau de Loubresse, N., Jenner, L., Yusupova, G., & Yusupov, M. (2012). One core, two shells: Bacterial and eukaryotic ribosomes. *Nature Structural & Molecular Biology*, *19*(6), 560–567.

Mills, E. W., & Green, R. (2017). Ribosomopathies: There's strength in numbers. *Science (New York, N.Y.)*, *358*(6363), Article 6363.

Molavi, G., Samadi, N., & Hosseingholi, E. Z. (2019). The roles of moonlight ribosomal proteins in the development of human cancers. *Journal of Cellular Physiology*, *234*(6), 8327–8341.

Moody, S. A., & Kline, M. J. (1990). Segregation of fate during cleavage of frog (Xenopus laevis) blastomeres. *Anatomy and Embryology*, *182*(4), 347–362.

Moreno, R. L., Williams, K., Jones, K. L., & Ribera, A. B. (2018). Investigation of Islet2a function in zebrafish embryos: Mutants and morphants differ in morphologic phenotypes and gene expression. *PLoS ONE*, *13*(6), e0199233.

Moreno-Mateos, M. A., Vejnar, C. E., Beaudoin, J.-D., Fernandez, J. P., Mis, E. K., Khokha, M. K., & Giraldez, A. J. (2015). CRISPRscan: Designing highly efficient sgRNAs for CRISPR-Cas9 targeting in vivo. *Nature Methods*, *12*(10), 982–988.

Moss, T., & Stefanovsky, V. Y. (2002). At the center of eukaryotic life. *Cell*, *109*(5), 545–548.

Mughal, B. B., Leemans, M., Spirhanzlova, P., Demeneix, B., & Fini, J.-B. (2018). Reference gene identification and validation for quantitative real-time PCR studies in developing Xenopus laevis. *Scientific Reports*, *8*(1), 496.

Myers, K. C., Bolyard, A. A., Otto, B., Wong, T. E., Jones, A. T., Harris, R. E., Davies, S. M., Dale, D. C., & Shimamura, A. (2014). Variable Clinical Presentation of Shwachman–Diamond Syndrome: Update from the North American Shwachman–Diamond Syndrome Registry. *The Journal of Pediatrics*, *164*(4), 866–870.

Nakayama, T., Blitz, I. L., Fish, M. B., Odeleye, A. O., Manohar, S., Cho, K. W. Y., & Grainger, R. M. (2014). Cas9-based genome editing in Xenopus tropicalis. *Methods in Enzymology*, *546*, 355–375.

Nakayama, T., Fisher, M., Nakajima, K., Odeleye, A. O., Zimmerman, K. B., Fish, M. B., Yaoita, Y., Chojnowski, J. L., Lauderdale, J. D., Netland, P. A., & Grainger, R. M. (2015). Xenopus pax6 mutants affect eye development and other organ systems, and have phenotypic similarities to human aniridia patients. *Developmental Biology*, *408*(2), 328–344.

Narla, A., & Ebert, B. L. (2010). Ribosomopathies: Human disorders of ribosome dysfunction. *Blood*, *115*(16), 3196–3205.

Neilson, K. M., Pignoni, F., Yan, B., & Moody, S. A. (2010). Developmental expression patterns of candidate cofactors for vertebrate six family transcription factors. *Developmental Dynamics*, *239*(12), 3446–3466.

Nieuwkoop, P. D., & Faber, J. (Eds.). (1954). *Normal table of Xenopus laevis (Daudin): A systematical and chronological survey of the development from the fertilized egg till the end of metamorphosis*. North-Hollund Pub. Co.

Origa, R. (1993). Beta-Thalassemia. In M. P. Adam, G. M. Mirzaa, R. A. Pagon, S. E. Wallace, L. J. Bean, K. W. Gripp, & A. Amemiya (Eds.), *GeneReviews®*. University of Washington, Seattle.

Pecoraro, A., Pagano, M., Russo, G., & Russo, A. (2021). Ribosome Biogenesis and Cancer: Overview on Ribosomal Proteins. *International Journal of Molecular Sciences*, *22*(11), 5496.

Pestov, D. G., Strezoska, Ž., & Lau, L. F. (2001). Evidence of p53-Dependent Cross-Talk between Ribosome Biogenesis and the Cell Cycle: Effects of Nucleolar Protein Bop1 on G1/S Transition. *Molecular and Cellular Biology*, *21*(13), 4246–4255.

Pfaffl, M. W. (2001). A new mathematical model for relative quantification in real-time RT-PCR. *Nucleic Acids Research*, *29*(9), e45.

Phelps, P. D., Poswillo, D., & Lloyd, G. A. (1981). The ear deformities in mandibulofacial dysostosis (Treacher Collins syndrome). *Clinical Otolaryngology and Allied Sciences*, *6*(1), 15–28.

Pierandrei-Amaldi, P., & Amaldi, F. (1994). Aspects of regulation of ribosomal protein synthesis inXenopus laevis: Review. *Genetica*, *94*(2–3), 181–193.

Place, E. S., & Smith, J. C. (2017). Zebrafish atoh8 mutants do not recapitulate morpholino phenotypes. *PLoS ONE*, *12*(2), e0171143.

Pohl, B. S., & Knöchel, W. (2001). Overexpression of the transcriptional repressor FoxD3 prevents neural crest formation in Xenopus embryos. *Mechanisms of Development*, *103*(1–2), 93–106.

Qi, J., Yu, Y., Akilli Öztürk, Ö., Holland, J. D., Besser, D., Fritzmann, J., Wulf-Goldenberg, A., Eckert, K., Fichtner, I., & Birchmeier, W. (2016). New Wnt/β-catenin target genes promote experimental metastasis and migration of colorectal cancer cells through different signals. *Gut*, *65*(10), 1690–1701.

Quarello, P., Garelli, E., Carando, A., Brusco, A., Calabrese, R., Dufour, C., Longoni, D., Misuraca, A., Vinti, L., Aspesi, A., Biondini, L., Loreni, F., Dianzani, I., & Ramenghi, U. (2010). Diamond-Blackfan anemia: Genotype-phenotype correlations in Italian patients with RPL5 and RPL11 mutations. *Haematologica*, *95*(2), 206–213.

Reed, J. C. (2008). Bcl-2-family proteins and hematologic malignancies: History and future prospects. *Blood*, *111*(7), 3322–3330.

Riedel, G., Rüdrich, U., Fekete-Drimusz, N., Manns, M. P., Vondran, F. W. R., & Bock, M. (2014). An extended ΔCT-method facilitating normalisation with multiple reference genes suited for quantitative RT-PCR analyses of human hepatocyte-like cells. *PloS One*, *9*(3), e93031.

Robson, A., Owens, N. D. L., Baserga, S. J., Khokha, M. K., & Griffin, J. N. (2016). Expression of ribosomopathy genes during Xenopus tropicalis embryogenesis. *BMC Developmental Biology*, *16*(1), 38.

Rogers, C. D., Harafuji, N., Archer, T., Cunningham, D. D., & Casey, E. S. (2009). Xenopus Sox3 activates sox2 and geminin and indirectly represses Xvent2 expression to induce neural progenitor formation at the expense of non-neural ectodermal derivatives. *Mechanisms of Development*, *126*(1–2), 42–55.

Rohrmoser, M., Hölzel, M., Grimm, T., Malamoussi, A., Harasim, T., Orban, M., Pfisterer, I., Gruber-Eber, A., Kremmer, E., & Eick, D. (2007). Interdependence of Pes1, Bop1, and WDR12 Controls Nucleolar Localization and Assembly of the PeBoW Complex Required for Maturation of the 60S Ribosomal Subunit. *Molecular and Cellular Biology*, *27*(10), 3682–3694.

Ross, A. P., & Zarbalis, K. S. (2014). The emerging roles of ribosome biogenesis in craniofacial development. *Frontiers in Physiology*, *5*, 26

Rossi, A., Kontarakis, Z., Gerri, C., Nolte, H., Hölper, S., Krüger, M., & Stainier, D. Y. R. (2015). Genetic compensation induced by deleterious mutations but not gene knockdowns. *Nature*, *524*(7564), 230–233.

Rungger-Brändle, E., Ripperger, J. A., Steiner, K., Conti, A., Stieger, A., Soltanieh, S., & Rungger, D. (2010). Retinal patterning by Pax6-dependent cell adhesion molecules. *Developmental Neurobiology*, *70*(11), 764–780.

Rupp, R. A., Snider, L., & Weintraub, H. (1994). Xenopus embryos regulate the nuclear localization of XMyoD. *Genes & Development*, *8*(11), 1311–1323.

Salanga, C. M., & Salanga, M. C. (2021). Genotype to Phenotype: CRISPR Gene Editing Reveals Genetic Compensation as a Mechanism for Phenotypic Disjunction of Morphants and Mutants. *International Journal of Molecular Sciences*, *22*(7), 3472.

Salanga, M. C., Brun, N. R., Francolini, R. D., Stegeman, J. J., & Goldstone, J. V. (2020). CRISPR-Cas9-Mutated Pregnane X Receptor (pxr) Retains Pregnenolone-induced Expression of cyp3a65 in Zebrafish (Danio rerio) Larvae. *Toxicological Sciences*, *174*(1), 51–62.

Sapio, R. T., Nezdyur, A. N., Krevetski, M., Anikin, L., Manna, V. J., Minkovsky, N., & Pestov, D. G. (2017). Inhibition of post-transcriptional steps in ribosome biogenesis confers cytoprotection against chemotherapeutic agents in a p53-dependent manner. *Scientific Reports*, *7*(1), 9041.

Schedl, A., Ross, A., Lee, M., Engelkamp, D., Rashbass, P., van Heyningen, V., & Hastie, N. D. (1996). Influence of PAX6 Gene Dosage on Development: Overexpression Causes Severe Eye Abnormalities. *Cell*, *86*(1), 71–82.

Schneider-Poetsch, T., Ju, J., Eyler, D. E., Dang, Y., Bhat, S., Merrick, W. C., Green, R., Shen, B., & Liu, J. O. (2010). Inhibition of eukaryotic translation elongation by cycloheximide and lactimidomycin. *Nature Chemical Biology*, *6*(3), 209–217.

Scholnick, J., Sinor, C., Oakes, J., Outten, W., & Saha, M. (1997). Differential expression of Xenopus ribosomal protein gene XlrpS1c. *Biochimica Et Biophysica Acta*, *1354*(1), 72–82.

Schreiner, C., Kernl, B., Dietmann, P., Riegger, R. J., Kühl, M., & Kühl, S. J. (2022). The Ribosomal Protein L5 Functions During Xenopus Anterior Development Through Apoptotic Pathways. *Frontiers in Cell and Developmental Biology*, *10*, 777121.

Session, A. M., Uno, Y., Kwon, T., Chapman, J. A., Toyoda, A., Takahashi, S., Fukui, A., Hikosaka, A., Suzuki, A., Kondo, M., van Heeringen, S. J., Quigley, I., Heinz, S., Ogino, H., Ochi, H., Hellsten, U., Lyons, J. B., Simakov, O., Putnam, N., Stites, J., Kuroki, Y., Tanaka, T., Michiue, T., Watanabe, M., Bogdanovic, O., Lister, R., Georgiou, G., Paranjpe, S. S., van Kruijsbergen, I., Shu, S., Carlson, J., Kinoshita, T., Ohta, Y., Mawaribuchi, S., Jenkins, J., Grimwood, J., Schmutz, J., Mitros, T., Mozaffari, S. V., Suzuki, Y., Haramoto, Y., Yamamoto, T. S., Takagi, C., Heald, R., Miller, K., Haudenschild, C., Kitzman, J., Nakayama, T., Izutsu, Y., Robert, J., Fortriede, J., Burns, K., Lotay, V., Karimi, K., Yasuoka, Y., Dichmann, D. S., Flajnik, M. F., Houston, D. W., Shendure, J., DuPasquier, L., Vize, P. D., Zorn, A. M., Ito, M., Marcotte, E. M., Wallingford, J. B., Ito, Y., Asashima, M., Ueno, N., Matsuda, Y., Veenstra, G. J., Fujiyama, A., Harland, R. M., Taira, M., & Rokhsar, D. S. (2016). Genome evolution in the allotetraploid frog Xenopus laevis. *Nature*, *538*(7625), 336–343.

Sharma, R., Sharma, B., Babber, M., Singh, S., & Jain, G. (2016). Treacher Collins syndrome: A case report and review of ophthalmic features. *Taiwan Journal of Ophthalmology*, *6*(4), 206–209.

Shwachman, H., Diamond, L. K., Oski, F. A., & Khaw, K. T. (1964). THE SYNDROME OF PANCREATIC INSUFFICIENCY AND BONE MARROW DYSFUNCTION. *The Journal of Pediatrics*, *65*, 645–663.

Siddiqui, W. A., Ahad, A., & Ahsan, H. (2015). The mystery of BCL2 family: Bcl-2 proteins and apoptosis: an update. *Archives of Toxicology*, *89*(3), 289–317.

Sive, H. L., Grainger, R. M., & Harland, R. M. (2000). *Early development of Xenopus laevis: A laboratory manual*. Cold Spring Harbor, N.Y.: Cold Spring Harbor Laboratory Press.

Strezoska, Ž., Pestov, D. G., & Lau, L. F. (2000). Bop1 Is a Mouse WD40 Repeat Nucleolar Protein Involved in 28S and 5.8S rRNA Processing and 60S Ribosome Biogenesis. *Molecular and Cellular Biology*, *20*(15), 5516–5528.

Strezoska, Ž., Pestov, D. G., & Lau, L. F. (2002). Functional Inactivation of the Mouse Nucleolar Protein Bop1 Inhibits Multiple Steps in Pre-rRNA Processing and Blocks Cell Cycle Progression. *Journal of Biological Chemistry*, *277*(33), 29617–29625.

Sulima, S. O., Kampen, K. R., & De Keersmaecker, K. (2019). Cancer Biogenesis in Ribosomopathies. *Cells*, *8*(3), E229.

Summerton, J. (1999). Morpholino antisense oligomers: The case for an RNase H-independent structural type. *Biochimica et Biophysica Acta (BBA) - Gene Structure and Expression*, *1489*(1), 141–158.

Summerton, J., & Weller, D. (1997). Morpholino antisense oligomers: Design, preparation, and properties. *Antisense & Nucleic Acid Drug Development*, *7*(3), 187–195.

Taylor, A. M., Humphries, J. M., White, R. M., Murphey, R. D., Burns, C. E., & Zon, L. I. (2012). Hematopoietic defects in rps29 mutant zebrafish depend upon p53 activation. *Experimental Hematology*, *40*(3), 228-237.e5.

Tecza, A., Bugner, V., Kühl, M., & Kühl, S. J. (2011). Pescadillo homologue 1 and Peter Pan function during Xenopus laevis pronephros development. *Biology of the Cell*, *103*(10), 483–498.

*The Human Protein Atlas, BOP1 available from v21.0.proteinatlas.org.* (reviewed on 12.02.2022). https://www.proteinatlas.org/ENSG00000261236-BOP1/tissue

Tiu, G. C., Kerr, C. H., Forester, C. M., Krishnarao, P. S., Rosenblatt, H. D., Raj, N., Lantz, T. C., Zhulyn, O., Bowen, M. E., Shokat, L., Attardi, L. D., Ruggero, D., & Barna, M. (2021). A p53-dependent translational program directs tissue-selective phenotypes in a model of ribosomopathies. *Developmental Cell*, *56*(14), 2089-2102.e11.

Tsai, F. Y., Keller, G., Kuo, F. C., Weiss, M., Chen, J., Rosenblatt, M., Alt, F. W., & Orkin, S. H. (1994). An early haematopoietic defect in mice lacking the transcription factor GATA-2. *Nature*, *371*(6494), 221–226.

Ulirsch, J. C., Verboon, J. M., Kazerounian, S., Guo, M. H., Yuan, D., Ludwig, L. S., Handsaker, R. E., Abdulhay, N. J., Fiorini, C., Genovese, G., Lim, E. T., Cheng, A., Cummings, B. B., Chao, K. R., Beggs, A. H., Genetti, C. A., Sieff, C. A., Newburger, P. E., Niewiadomska, E., Matysiak, M., Vlachos, A., Lipton, J. M., Atsidaftos, E., Glader, B., Narla, A., Gleizes, P.-E., O'Donohue, M.F., Montel-Lehry, N., Amor, D. J., McCarroll, S. A., O'Donnell-Luria, A. H., Gupta, N., Gabriel, S. B., MacArthur, D. G., Lander, E. S., Lek, M., Da Costa, L., Nathan, D. G., Korostelev, A. A., Do, R., Sankaran, V. G., & Gazda, H. T. (2018). The Genetic Landscape of Diamond-Blackfan Anemia. *American Journal of Human Genetics*, *103*(6), 930–947.

Valdez, B. C., Henning, D., So, R. B., Dixon, J., & Dixon, M. J. (2004). The Treacher Collins syndrome (TCOF1) gene product is involved in ribosomal DNA gene transcription by interacting with upstream binding factor. *Proceedings of the National Academy of Sciences of the United States of America*, *101*(29), 10709–10714.

van Riggelen, J., Yetil, A., & Felsher, D. W. (2010). MYC as a regulator of ribosome biogenesis and protein synthesis. *Nature Reviews. Cancer*, *10*(4), 301–309.

Vellky, J. E., Ricke, E. A., Huang, W., & Ricke, W. A. (2020). Expression, Localization, and Function of the Nucleolar Protein BOP1 in Prostate Cancer Progression. *The American Journal of Pathology*, *191*, 168–179

Vlachos, A., Ball, S., Dahl, N., Alter, B. P., Sheth, S., Ramenghi, U., Meerpohl, J., Karlsson, S., Liu, J. M., Leblanc, T., Paley, C., Kang, E. M., Leder, E. J., Atsidaftos, E., Shimamura, A., Bessler, M., Glader, B., Lipton, J. M., & Participants of Sixth Annual Daniella Maria Arturi International Consensus Conference. (2008). Diagnosing and treating Diamond Blackfan anaemia: Results of an international clinical consensus conference. *British Journal of Haematology*, *142*(6), 859–876.

Vlachos, A., Osorio, D. S., Atsidaftos, E., Kang, J., Lababidi, M. L., Seiden, H. S., Gruber, D., Glader, B. E., Onel, K., Farrar, J. E., Bodine, D. M., Aspesi, A., Dianzani, I., Ramenghi, U., Ellis, S. R., & Lipton, J. M. (2018). Increased Prevalence of Congenital Heart Disease in Children With Diamond Blackfan Anemia Suggests Unrecognized Diamond Blackfan Anemia as a Cause of Congenital Heart Disease in the General Population: A Report of the Diamond Blackfan Anemia Registry. *Circulation: Genomic and Precision Medicine*, *11*(5), Article 5.

Wallace, H. (1960). The development of anucleolate embryos of Xenopus laevis. *Journal of Embryology and Experimental Morphology*, *8*, 405–413.

Wan, F., Anderson, D. E., Barnitz, R. A., Snow, A., Bidere, N., Zheng, L., Hegde, V., Lam, L. T., Staudt, L. M., Levens, D., Deutsch, W. A., & Lenardo, M. J. (2007). Ribosomal protein S3: A KH domain subunit in NF-kappaB complexes that mediates selective gene regulation. *Cell*, *131*(5), 927–939.

Warren, A. J. (2018). Molecular basis of the human ribosomopathy Shwachman-Diamond syndrome. *Advances in Biological Regulation*, *67*, 109–127.

Waterhouse, A., Bertoni, M., Bienert, S., Studer, G., Tauriello, G., Gumienny, R., Heer, F. T., de Beer, T. A. P., Rempfer, C., Bordoli, L., Lepore, R., & Schwede, T. (2018). SWISS-MODEL: Homology modelling of protein structures and complexes. *Nucleic Acids Research*, *46*(W1), W296–W303.

Watkins-Chow, D. E., Cooke, J., Pidsley, R., Edwards, A., Slotkin, R., Leeds, K. E., Mullen, R., Baxter, L. L., Campbell, T. G., Salzer, M. C., Biondini, L., Gibney, G., Phan Dinh Tuy, F., Chelly, J., Morris, H. D., Riegler, J., Lythgoe, M. F., Arkell, R. M., Loreni, F., Flint, J., Pavan, W. J., & Keays, D. A. (2013). Mutation of the diamond-blackfan anemia gene Rps7 in mouse results in morphological and neuroanatomical phenotypes. *PLoS Genetics*, *9*(1), e1003094.

Weaver, K. N., Watt, K. E. N., Hufnagel, R. B., Navajas Acedo, J., Linscott, L. L., Sund, K. L., Bender, P. L., König, R., Lourenco, C. M., Hehr, U., Hopkin, R. J., Lohmann, D. R., Trainor, P. A., Wieczorek, D., & Saal, H. M. (2015). Acrofacial Dysostosis, Cincinnati Type, a Mandibulofacial Dysostosis Syndrome with Limb Anomalies, Is Caused by POLR1A Dysfunction. *The American Journal of Human Genetics*, *96*(5), 765–774.

Wischnewski, J., Sölter, M., Chen, Y., Hollemann, T., & Pieler, T. (2000). Structure and expression of Xenopus karyopherin-beta3: Definition of a novel synexpression group related to ribosome biogenesis. *Mechanisms of Development*, *95*(1–2), 245–248.

Wormington, W. M. (1989). Developmental expression and 5S rRNA-binding activity of Xenopus laevis ribosomal protein L5. *Molecular and Cellular Biology*, *9*(12), 5281–5288.

Wu, Q., Hong, J., Wang, Z., Hu, J., Chen, R., Hu, Z., Li, B., Hu, X., Zhang, Z., & Ruan, Y. (2019). Abnormal Ribosome Biogenesis Partly Induced p53-Dependent Aortic Medial Smooth Muscle Cell Apoptosis and Oxidative Stress. *Oxidative Medicine and Cellular Longevity*, *2019*, 1–19.

Young, T. L., Schaffer, D. B., & Cohen, A. R. (1992). Infantile glaucoma associated with the Diamond-Blackfan syndrome. *Journal of Pediatric Ophthalmology and Strabismus*, *29*(1), 55–58.

Yue, F., Cheng, Y., Breschi, A., Vierstra, J., Wu, W., Tyrone Ryba, Sandstrom, R., Ma, Z., Davis, C., Pope, B. D., Shen, Y., Pervouchine, D. D., Djebali, S., Thurman, R. E., Kaul, R., Rynes, E., Kirilusha, A., Marinov, G. K., Williams, B. A., Trout, D., Amrhein, H., Fisher-Aylor, K., Antoshechkin, I., DeSalvo, G., See, L. H., Fastuca, M., Drenkow, J., Zaleski, C., Dobin, A., Prieto, P., Lagarde, J., Bussotti, G., Tanzer, A., Denas, O., Li, K., Bender, M. A., Zhang, M., Byron, R., Groudine, M. T., McCleary, D., Pham, L., Ye, Z., Kuan, S., Edsall, L., Wu, Y. C., Rasmussen, M. D., Bansal, M. S., Kellis, M., Keller, C. A., Morrissey, C. S., Mishra, T., Jain, D., Dogan, N., Harris, R. S., Cayting, P., Kawli, T., Boyle, A. P., Euskirchen, G., Kundaje, A., Lin, S., Lin, Y., Jansen, C., Malladi, V. S., Cline, M. S., Erickson, D. T., Kirkup, V. M., Learned, K., Sloan, C. A., Rosenbloom, K. R., Lacerda de Sousa, B., Beal, K., Pignatelli, M., Flicek, P., Lian, J., Kahveci, T., Lee, D., Kent, W. J., Ramalho Santos M., Herrero, J., Notredame, C., Johnson, A., Vong, S., Lee, K., Bates, D., Neri, F., Diegel, M., Canfield, T., Sabo, P. J., Wilken, M. S., Reh, T. A., Giste, E., Shafer, A., Kutyavin, T., Haugen, E., Dunn, D., Reynolds, A. P., Neph, S., Humbert, R., Hansen, R. S., De Bruijn, M., Selleri, L., Rudensky, A., Josefowicz, S., Samstein, R., Eichler, E. E., Orkin, S. H., Levasseur, D., Papayannopoulou, T., Chang, K. H., Skoultchi, A., Gosh, S., Disteche, C., Treuting, P., Wang, Y., Weiss, M. J., Blobel, G. A., Cao, X., Zhong, S., Wang, T., Good, P. J., Lowdon, R. F., Adams, L. B., Zhou, X. Q., Pazin, M. J., Feingold, E. A., Wold, B., Taylor, J., Mortazavi, A., Weissman, S. M., Stamatoyannopoulos, J. A., Snyder, M. P., Guigo, R., Gingeras, T. R., Gilbert, D. M., Hardison, R. C., Beer, M. A., Ren, B., & Mouse ENCODE Consortium. (2014). A comparative encyclopedia of DNA elements in the mouse genome. *Nature*, *515*(7527), 355–364.

Zhang, J., Harnpicharnchai, P., Jakovljevic, J., Tang, L., Guo, Y., Oeffinger, M., Rout, M. P., Hiley, S. L., Hughes, T., & Woolford, J. L. (2007). Assembly factors Rpf2 and Rrs1 recruit 5S rRNA and ribosomal proteins rpL5 and rpL11 into nascent ribosomes. *Genes & Development*, *21*(20), 2580–2592.

Zhang, Y., & Lu, H. (2009). Signaling to p53: Ribosomal proteins find their way. *Cancer Cell*, *16*(5), 369–377.

Zhao, C., Andreeva, V., Gibert, Y., LaBonty, M., Lattanzi, V., Prabhudesai, S., Zhou, Y., Zon, L., McCann, K. L., Baserga, S., & Yelick, P. C. (2014). Tissue Specific Roles for the Ribosome Biogenesis Factor Wdr43 in Zebrafish Development. *PLoS Genetics*, *10*(1), e1004074.

Zhou, X., Liao, W.-J., Liao, J.-M., Liao, P., & Lu, H. (2015). Ribosomal proteins: Functions beyond the ribosome. *Journal of Molecular Cell Biology*, *7*(2), 92–104.

# 7 Appendix

## *bop1.S* and *bop1.L* alignment via Emboss

```
########################################
# Program: needle
# Rundate: Tue 25 Feb 2020 10:27:52
# Commandline: needle
########################################

#=======================================
#
# Aligned_sequences: 2
# 1: EMBOSS_001 bop1 L
# 2: EMBOSS_002 bop1 S
# Matrix: EBLOSUM62
# Gap_penalty: 10.0
# Extend_penalty: 0.5
#
#=======================================
```

**Primer 6L**

**Primer 6S**

**gRNAs #1-#3**

```
EMBOSS_001      3338 CCAGGACATGAGCAGTCCTACAACCCCCCTCCAGAGTATCTAATGAGTGA   3387
                     ||||||.||.||||||||||||||||||||||||||||||||||||||||
EMBOSS_002       532 CCAGGGCACGAGCAGTCCTACAACCCCCCTCCAGAGTATCTAATGAGTGA    581

EMBOSS_001      3388 GGAAGAGGTAAATGTTTTTGAAATGTTCATACATATTATAATAATGAATG   3437
                     ||||||||||||||||||||.||||||||.|.|..|||..||||||||||||
EMBOSS_002       582 GGAAGAGGTAAATGTTTTTGGAATGTTCCTTCCCATTCAAATAATGAATG    631

EMBOSS_001      3438 TCCTGTGGGTTCCTCACTGCCC---AACTTTCTCCTGGATCAGACTA-AT   3483
                     |||||||.||||||||||...   ...|||.||    ||||||||| ||
EMBOSS_002       632 TCCTGTGAGTTCCTCACTGTAAGTTGTATTTGTC----ATCAGACTATAT    677

EMBOSS_001      3484 GT-ATGTTCC--ATCTCACTTCCTGCTCAGGGGAGCCCTGTGTCCCTCCC   3530
                     .| ||.||.|  ||.|..||||||||||||.||||||||.||||||||||||
EMBOSS_002       678 ATAATATTACATATATATCTTCCTGCTCAGAGGAGCCCGGTGTCCCTCCC    727

EMBOSS_001      3531 AGGATCTTCCCTTCCTGT----TTCTGTGGTTGGATCATAACTGAGTAAT   3576
                     ||..||||||   |||||    |.||||||||||||.||||||||||||||
EMBOSS_002       728 AGTCTCTTCC---CCTGTTGGCTCCTGTGTTTGGATCAGAACTGAGTAAT    774

EMBOSS_001      3577 TGTCCCCATGTTCTCTCTGACCCACAGCGTTTGGCCTGGGAGCAGCAAGA   3626
                     ||||||||||||||||||||||||||||||||||.||||||||||||||||
EMBOSS_002       775 TGTCCCCATGTTCTCTCTGACCCACAGCGTTTGTCCTGGGAGCAGCAAGA    824

EMBOSS_001      3627 TCCAGAGGATCGAAAACTGCCGTTTCTTCCCCAGAGATTTAACTGCCTGC   3676
                     .||||||||||.||||||||.||||||||||||||||||||||||||||||
EMBOSS_002       825 CCCAGAGGATCGGAAACTGCCCTTTCTTCCCCAGAGATTTAACTGCCTGC    874

EMBOSS_001      3677 GGGCTGTGCCTGGATACGCCCGATTCATCCACGAGAGGTTTGAGCGATGC   3726
                     ||||||||||||||||||.||||||||||||||||||||||||||||||||
EMBOSS_002       875 GGGCTGTGCCTGGATACGCTCGATTCATCCACGAGAGGTTTGAGCGATGC    924

EMBOSS_001      3727 CTGGACCTGTACCTGTGCCCGCGCCAGAGGAAGATGAGGGTGAGTGGCTT   3776
                     ||||||||||||||||||||||||||||||||||||||||||||||||.|||
EMBOSS_002       925 CTGGACCTGTACCTGTGCCCGCGCCAGAGGAAGATGAGGGTGAGTGACTT    974

EMBOSS_001      3777 GGTGTTTGAGG-GGGGATACATTAGAACTGGGGTTATTATATTAAAGGAA   3825
                     ||||||||.|| ||.||||||.|||||
EMBOSS_002       975 GGTGTTTGGGGAGGAGATACTTTAGA------------------------    1000
```

Forward primer *gRNA #1 – L homeologue*

Forward primer *gRNA #1 – S homeologue*

Target site *bop1 gRNA #1* + PAM sequence

```
EMBOSS_001      3826 CGAACACCATAAGATGAAAGTGTTTTACAGTGATTAAACTATAATGTATT   3875

EMBOSS_002      1001 --------------------------------------------------   1000

EMBOSS_001      3876 GTTTCCCTGCACTGGTACAGCTATAAACACACTGCTGTGTAGCCATGGGG   3925

EMBOSS_002      1001 --------------------------------------------------   1000

EMBOSS_001      3926 GCGGCCATTCATAGCACAGGTTGCACAGCAGATACCAGATGCATCTACTG   3975

EMBOSS_002      1001 --------------------------------------------------   1000

EMBOSS_001      3976 AATCCCATTGTATTCTATTGCTCAGCTGATCAGTTGTCTGCTAAATAGCC   4025
                                                     ||||.||||
EMBOSS_002      1001 ------------------------------------------TAAAAAGCC   1009

EMBOSS_001      4026 TGTGCCCTTTCTCCTTTTTTAGCTTGGGCTACACAATAGGCAATTTACAT   4075

EMBOSS_002      1010 --------------------------------------------------   1009

EMBOSS_001      4076 ATACTATTCTTGTCTTTCTACAGCAAGTGCATAACCTTTACCAGTTCATA   4125

EMBOSS_002      1010 --------------------------------------------------   1009

EMBOSS_001      4126 GCAACAGTACATTACTTTAAAGTACTTTTATTTTTTTGGTGTTTCTGTTC   4175

EMBOSS_002      1010 --------------------------------------------------   1009

EMBOSS_001      4176 CTTTAATGATAAATCCAATAGAAATTGTGACTTTGCTGATATTTAGCTGG   4225
                                                       ..||||||||
EMBOSS_002      1010 ------------------------------------------AATAGCTGG   1018

EMBOSS_001      4226 AAGGAGACGTTGTAACAAAATCAGAAGTT---TCATTTGGTTCGGAATGT   4272
                     |.|||||.||||||      |.||.|||   ||||||||.||.|.||||
EMBOSS_002      1019 AGGGAGACATTGTAA------CCGATGTTTGATCATTTGGATCAGCATGT   1062

EMBOSS_001      4273 TCTGTTCCTACACAGCAGGA-TTCAGTTCC-----TCCCAGTCCTTAGCC   4316
                     |||||||||||||.|.||| |||||||||     ||||||||||...|
EMBOSS_002      1063 TCTGTTCCTACACAACTGGATTTCAGTTCCCCCCATCCCAGTCCTTGTTC   1112

EMBOSS_001      4317 AGGTTATACTGTAACTACATGTCTTACTTGTGTCTGATCCAGGTCAATGT   4366
                     |||||||.||||...||||||||||||||||||||||||||||||||||
EMBOSS_002      1113 AGGTTACACTGCCGCTACATGTCTTACTTGTGTCTGATCCAGGTCAATGT   1162

EMBOSS_001      4367 GGATCCTGAGGACCTGATACCCAAATTACCCAAGCCTAGAGATTTGCAAC   4416
                     |||||||||||||||||||||||||||.|||||.||.||||||||||.|
EMBOSS_002      1163 GGATCCTGAGGACCTGATACCCAAATTGCCCAAACCCAGAGATTTGCAGC   1212

EMBOSS_001      4417 CCTTCCCCACAATACAGTCCATGGTGAGGGCAATTTCTTTACTCTTTCAC   4466
                     |||||||||||||||||||||.||||||||.||||||||||.|||||.|..
EMBOSS_002      1213 CCTTCCCCACAATACAGTCCCTGGTGAGTGCAATTTCTTTGCTCTATTT-   1261

EMBOSS_001      4467 CTCCTCCTTTTTAGCTTCTTTTGCAGCTTCCTGTTCCTTCTGCCTCCTAA   4516
                      ||.||..|||.|.||.||..|.||||||    ||.||.||||
EMBOSS_002      1262 -TCTTCTGTTTCACCTCCTCATTCAGCTT----TTTCTGCTGC-------   1299

EMBOSS_001      4517 TTGGCTCCTTACTTTCTCCTTCTTC-AATCTGAACATTCACTCTTTGCCT   4565
                     |||||||        ||||||..|.. ..||||..| |.|.|.||.|
EMBOSS_002      1300 TTGGCTC--------CTCCTATTGAGCCTCTGTTC-TACCCACTGT----   1336

EMBOSS_001      4566 TCCTTTATTCACAGCCTCCTC------CCTCCTTTATTTGGAGCCTTCTC   4609
                       ||.|.|...|.||||||||      ||||||.||||  |||.||.||.
EMBOSS_002      1337 --CTGTTTGAGCTGCCTCCTCACTTCTCCTCCTCTATT--GAGACTCCTG   1382

EMBOSS_001      4610 ACTTTCTCCTCCCTCATTTCCTCCTCCTTTATTTGGAGCCTCTTCATTTC   4659
                     .|||...||||||||.||||..|.|||          |.||        ||
EMBOSS_002      1383 GCTTCTGCCTCCCTCCTTTTATTCTC----------AACC--------TC   1414

EMBOSS_001      4660 CTCATTTCTTTCTCCTCCCCCCTCCTTTATTCTGAGCTTCCTCACGCCCC   4709
                     |.|.||||   |||||.||.|||  |||||..|||||||.||||   |.||
EMBOSS_002      1415 CACTTTTC---CTCCTACCTCCT--TTTATGATGAGCTGCCTC---CTCC   1456

EMBOSS_001      4710 CTTCCTCCATTATTTGGAGCTTCCTCATTTCCTCCTCATTTCCTCCTTTA   4759
                     |||..|   ||||.|.||||..||||||..|||||||||    |||||||||
```

Reverse primer *gRNA #1 – L homeologue*

Reverse primer *gRNA #1 – S homeologue*

```
EMBOSS_002      1457 CTTGTT---TTATGTTGAGTCTCCTCTCTTCCTCCTC----CCTCCTTTA   1499

EMBOSS_001      4760 TTCAAAGCCACCTCGCTTCCTCCTT-CTTCTTTTATTTCGAGCCTCCCTC   4808
                     |||..||.|.||...|||.|||||. ||.|||||||...||| ||.||||
EMBOSS_002      1500 TTCTGAGACTCCCTACTTTCTCCTACCTCCTTTTATGATGAG-CTGCCTC   1548

EMBOSS_001      4809 TTTTCCTTCCTCTATTGT------GAGCCTCCTCATTTCCTCCTCCCTCC   4852
                     |.|||| ||||||..||||      ..|.|||||||..|||||||||||||
EMBOSS_002      1549 TCTTCC-TCCTCCCTTGTTTTATGTTGTCTCCTCTCTTCCTCCTCCCTCC   1597

EMBOSS_001      4853 TTTATTCTGAGCTTCCTCACTTCTTCCTCCCTCCTTTATTTG--GAGCCT   4900
                     ||||||||||||.||||..||||..|||||.|||.|.||.|.||  |||||..
EMBOSS_002      1598 TTTATTCTGAGCCTCCCTACTTTCTCCTACCTTCCTTTTATGATGAGCTG   1647

EMBOSS_001      4901 CCTCATTTCCTCCTCCCTCCTTT-ATTTGGAGCCTTGACGCTTCTTCCTT   4949
                     |||||.|..|||||||||||.||| ||...||||||   |.||.||||||
EMBOSS_002      1648 CCTCTTGCCCTCCTCCCTCTTTTGATAATGAGCCT---CCCTGCTTCC--   1692

EMBOSS_001      4950 CATCCGTTACTCTTAGCTTTCTCCTCCTTTTTATTCTGTGCCTCCTCGCT   4999
                       ||||               ||.|||  |||||||||.||||||...||
EMBOSS_002      1693 --TCCG---------------TCTTCC--TTTATTCTGAGCCTCCCTACT   1723

EMBOSS_001      5000 TTATCCTTCCTCTATTCTTAGTCCCTTCTCTTTTTCCTCCCTCTATTCTG   5049
                     ||.||||.||||                 ||||          |||..||
EMBOSS_002      1724 TTCTCCTCCCTC-----------------CTTT----------TATGATG   1746

EMBOSS_001      5050 AGCCTCCTCAATTTCTCCTCCTCTATTATTTGGACCCTCCCTCTATTACT   5099
                     ||.|||||..||.||||||..|.||.|.||                |
EMBOSS_002      1747 AGTCTCCTCTCTTCCTCCTCCCTTGTTTTATG-----------------T   1779

EMBOSS_001      5100 CGGAGCTCCTCCCTTATTCCTCCCTCCATTACTCGGAGCTCCTCCCTTAT   5149
                     .|...|||||.|||..|||||.|||.|||.||.|||  |||||    |
EMBOSS_002      1780 TGAGTCTCCTCTCTTCCTCCTCCTTCCTTTATTCTGAG--CCTCC----T   1823

EMBOSS_001      5150 TCCTCCCTCCATTACTCGGAGCTCCTCCCTTATTCCTCCCTCCATCACTC   5199
                     |.|||.||||.           .|||||.||..|..|
EMBOSS_002      1824 TACTCTCTCCT-----------ACCTCCTTTTATGAT-------------   1849

EMBOSS_001      5200 GGAGCTCCTCCCTTATTCCTCCCTCCATCACTCGGAGCTCCTCCCTTATT   5249
                      ||||          |.||||.||.|          ||||||
EMBOSS_002      1850 -GAGC----------TGCCTCTCTTC-----------CTCCTC-------   1870

EMBOSS_001      5250 CCTCCCTCCATTACT-CGGAG-CTCCTCCCTTATTCCTCCCTCCATTACT   5297
                     ||||||||||||..| ..||| ||||||.|||..|||||||...|.|||.|
EMBOSS_002      1871 CCTCCCTCCATTGATGATGAGCCTCCTCTCTTCCTCCTCCTGACTTTATT   1920

EMBOSS_001      5298 CGGAGCTCCTCCCTTGCACATATCTGTAGAACTTCATCAGTTTCATGTTG   5347
                     ||||||||||||||||||||||||||||||||||||||||||||||||||.
EMBOSS_002      1921 CGGAGCTCCTCCCTTGCACATATCTGTAGAACTTCATCAGTTTCATGTTC   1970

EMBOSS_001      5348 TCCTTCCTCAGATTTACAAGGGACACAAGGATCTTGTTCGCTGTATCAGT   5397
                     ||||||||||||||||||||||||||||||||||||||||||||||||||||
EMBOSS_002      1971 TCCTTCCTCAGATTTACAAGGGACACAAGGATCTTGTTCGCTGTATCAGT   2020

EMBOSS_001      5398 GTTTCACCCTCGGGGCAGTGGTTGGTCTCTGGTAAGTGATTGTTCCTTAT   5447
                     ||||||||||||||||||||||||||||||||||||||||||||||||||||
EMBOSS_002      2021 GTTTCACCCTCGGGGCAGTGGTTGGTCTCTGGTAAGTGATTGTTCCTTAT   2070

EMBOSS_001      5448 CTGCCCCGTCTCCCCCCATTCCCTTCCTGCCCCTCATTAATTCTCTTTAC   5497
                     |||||||||||||||  ||||||||||||||||||||||||||.||.|
EMBOSS_002      2071 CTGCCCCGTCTCCCCC--TTCCCTTCCTGCCCCTCATTAATTCTCCTTCC   2118

EMBOSS_001      5498 TGCCCCCCAACAGGCTCTGACGACTGCTCCGTGCGGTTCTGGGAGGTCAG   5547
                     ||||||||||||||||||||||||||||||||||||||||||||||||||||
EMBOSS_002      2119 TGCCCCCCAACAGGCTCTGACGACTGCTCCGTGCGGTTCTGGGAGGTCAG   2168

EMBOSS_001      5548 CACCGGGCGCTGTATGAAGTCTGTAGTCCTGGAAGGCGCAGTTAAAAGTA   5597
                     ||||||||||||||||||||.||||||||||||||||||||||||||||||
EMBOSS_002      2169 CACCGGGCGCTGTATGAAGTCCGTAGTCCTGGAAGGCGCAGTTAAAAGTA   2218

EMBOSS_001      5598 TCAGCTGGAACCCAAATCCAGTGCTGGTTCTGGTGGCGGCATGTGTGTGA   5647
                     ||||||||||||||||||||||.||||||||||||||||||||||||||||
EMBOSS_002      2219 TCAGCTGGAACCCAAATCCAGGGCTGGTTCTGGTGGCGGCATGTGTGTGA   2268

EMBOSS_001      5648 GTTGCCACTTTGTGTTACACAATAGCCACTTCTCTATTCTGACGCACTTA   5697
```

Forward primer *gRNA #2+#3 – L homeologue*

Forward primer *gRNA #2+#3 – S homeologue*

Target site *bop1 gRNA #2* + PAM sequence




**Suppl. Figure 1: *bop1.S* and *bop1.L* alignment via Emboss.**
Partial alignment of *bop1* homeologue S and *bop1* homeologue L. *bop1 gRNAs #1*, *#2*, and *#3* are highlighted in yellow. Primers on homeologue L are written in red letters. Primers of homeologue S are written in blue letters.

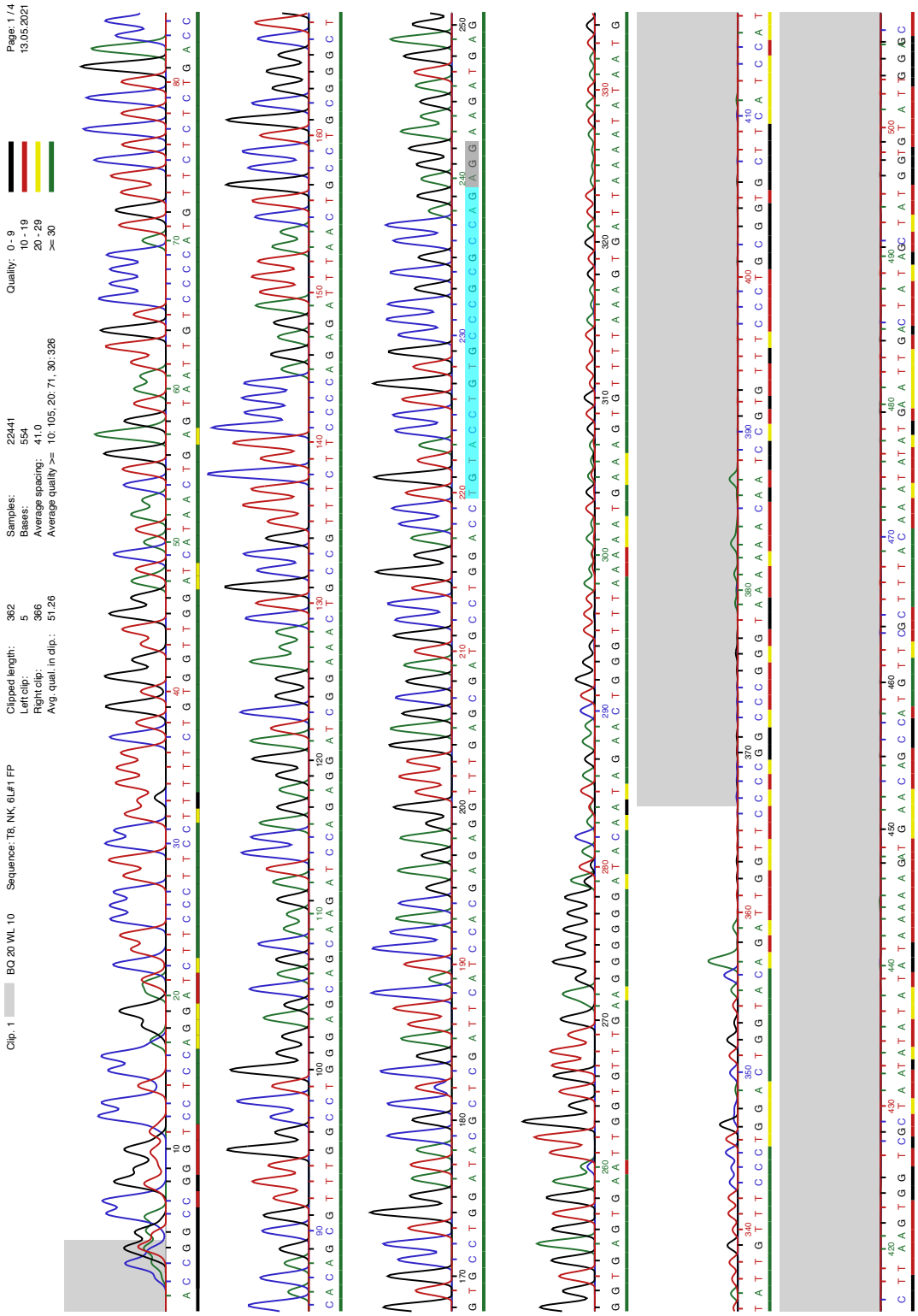

**Suppl. Figure 2: Sequence of wild-type DNA pool using the forward primer on chromosome 6L for *bop1 gRNA #1*.**

Target site of *bop1 gRNA #1* on chromosome 6L indicated in teal. PAM sequence is indicated in grey.

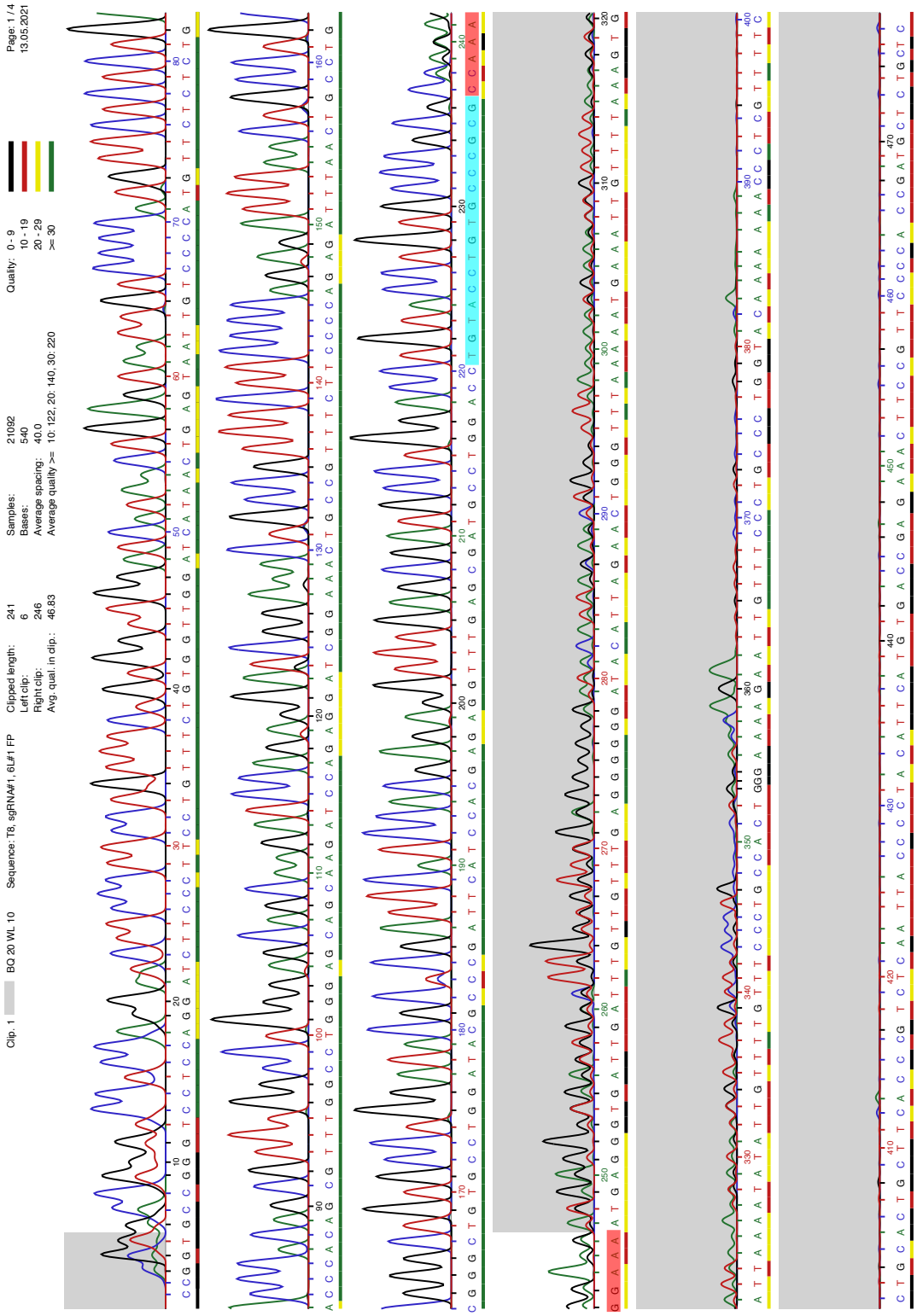


**Suppl. Figure 3: Sequence of *bop1* CRISPant DNA pool using the forward primer on chromosome 6L for *bop1 gRNA #1.***

Target site of *bop1 gRNA #1* on chromosome 6L indicated in teal. Heterogenous sequence due to mutations is indicated in red.

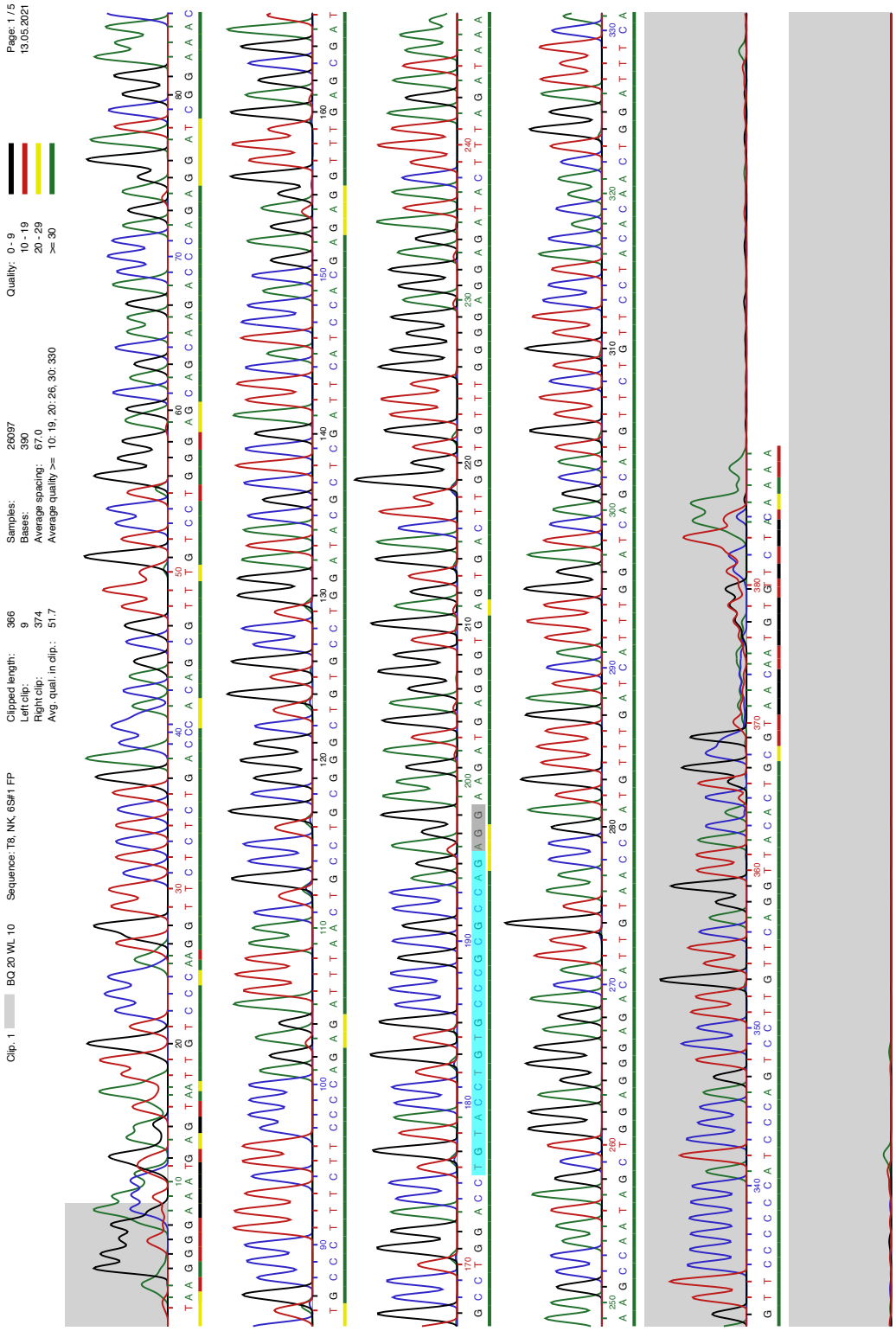


**Suppl. Figure 4: Sequence of wild-type DNA pool using the forward primer on chromosome 6S for *bop1 gRNA #1*.**

Target site of *bop1 gRNA #1* on chromosome 6S indicated in teal. PAM sequence is indicated in grey.

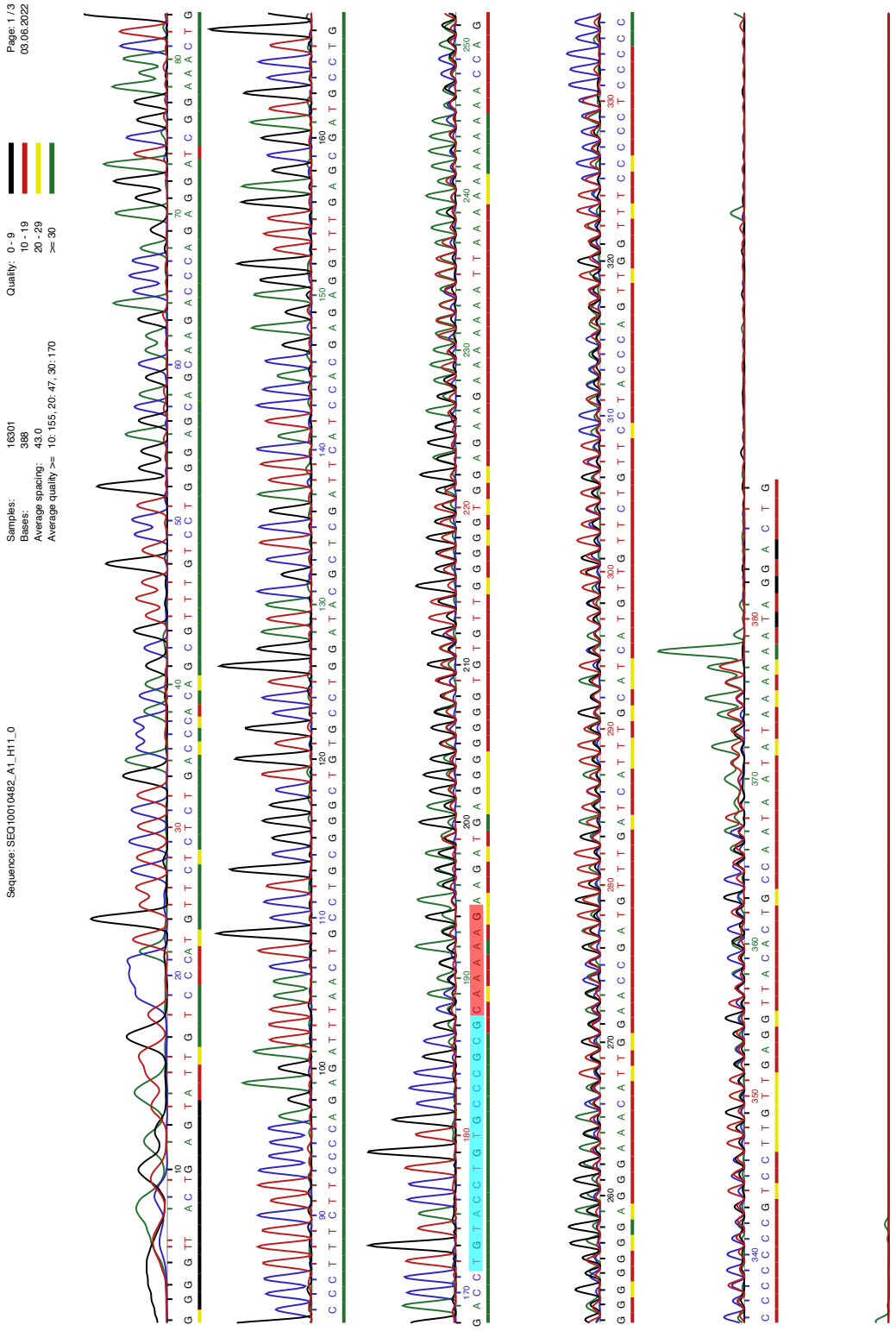


**Suppl. Figure 5: Sequence of *bop1* CRISPant DNA pool using the forward primer on chromosome 6S for *bop1 gRNA #1.***

Target site of *bop1 gRNA #1* on chromosome 6S indicated in teal. Heterogenous sequence due to mutations is indicated in red.

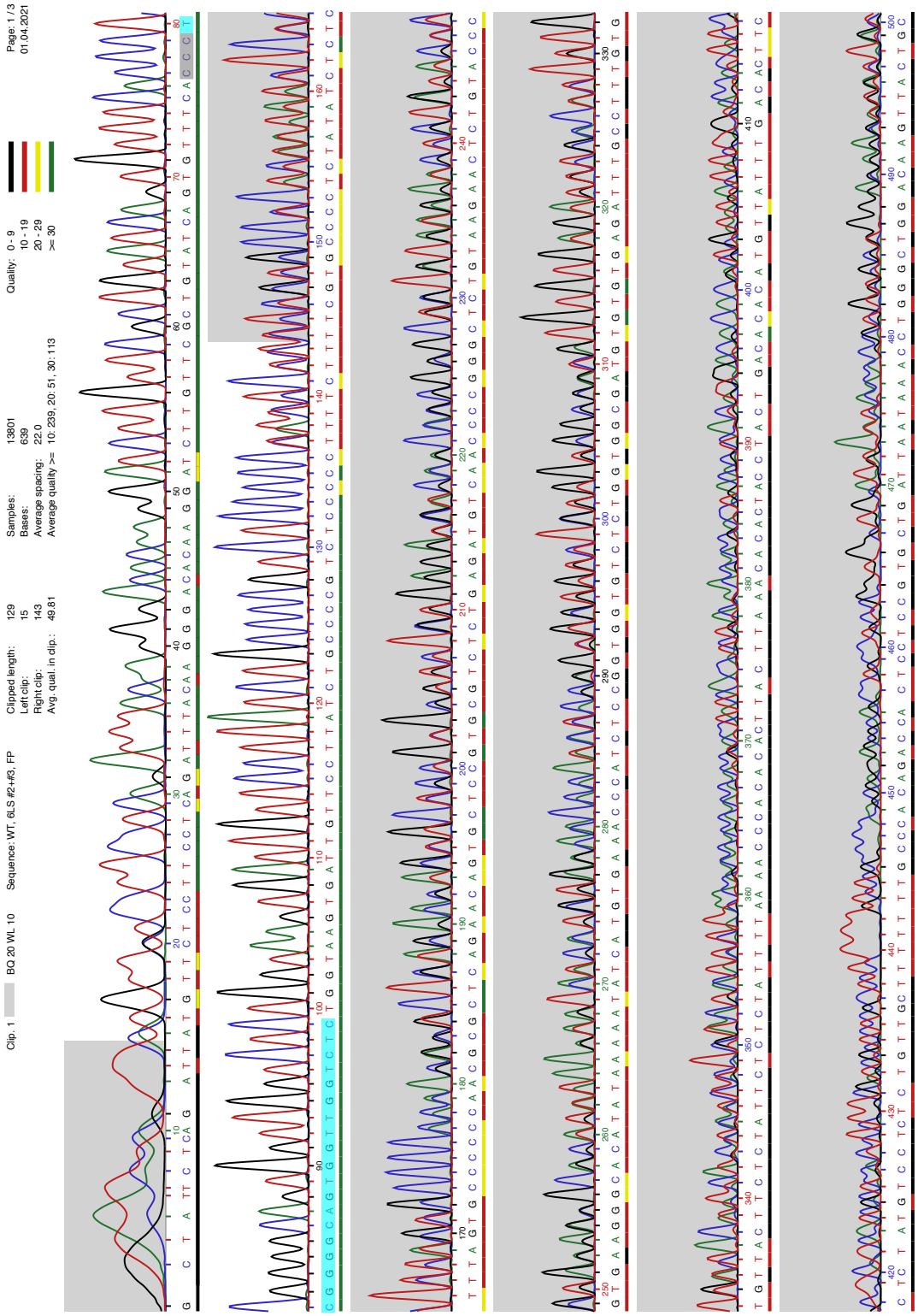


**Suppl. Figure 6: Sequence of wild-type DNA pool using the forward primer on chromosome 6S+L for *bop1 gRNA #2*.**

Target site of *bop1 gRNA #2* on chromosome 6S+L indicated in teal. PAM sequence is indicated in grey.

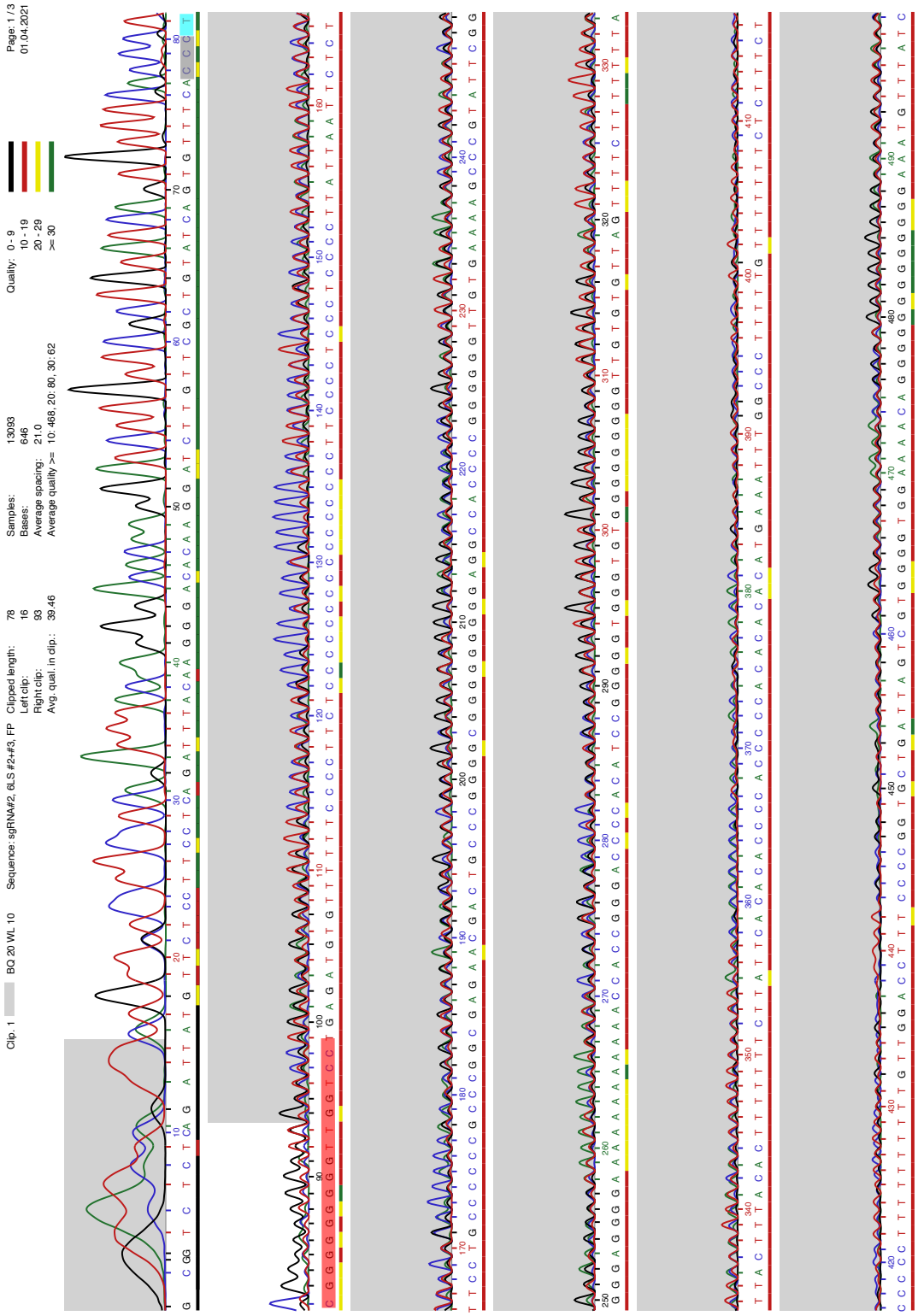

**Suppl. Figure 7: Sequence of *bop1* CRISPant DNA pool using the forward primer on chromosome 6S+L for *bop1 gRNA #2.***

Target site of *bop1 gRNA #2* on chromosome 6S+L indicated in teal. PAM sequence is indicated in grey. Heterogenous sequence due to mutations is indicated in red.

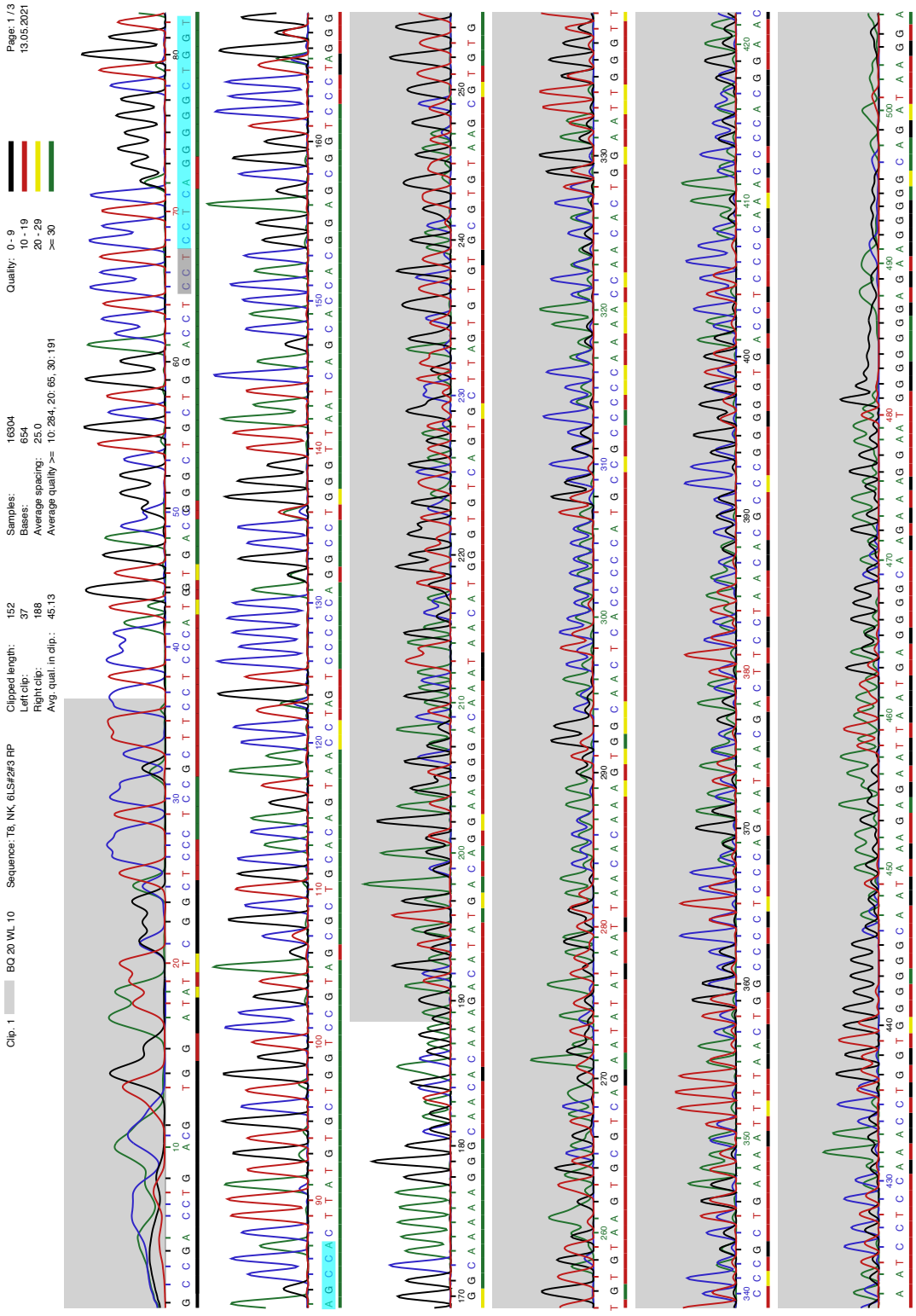

**Suppl. Figure 8: Sequence of wild-type DNA pool using the reverse primer on chromosome 6S+L for *bop1 gRNA #3*.**

Target site of *bop1 gRNA #3* on chromosome 6S+L indicated in teal. PAM sequence is indicated in grey.

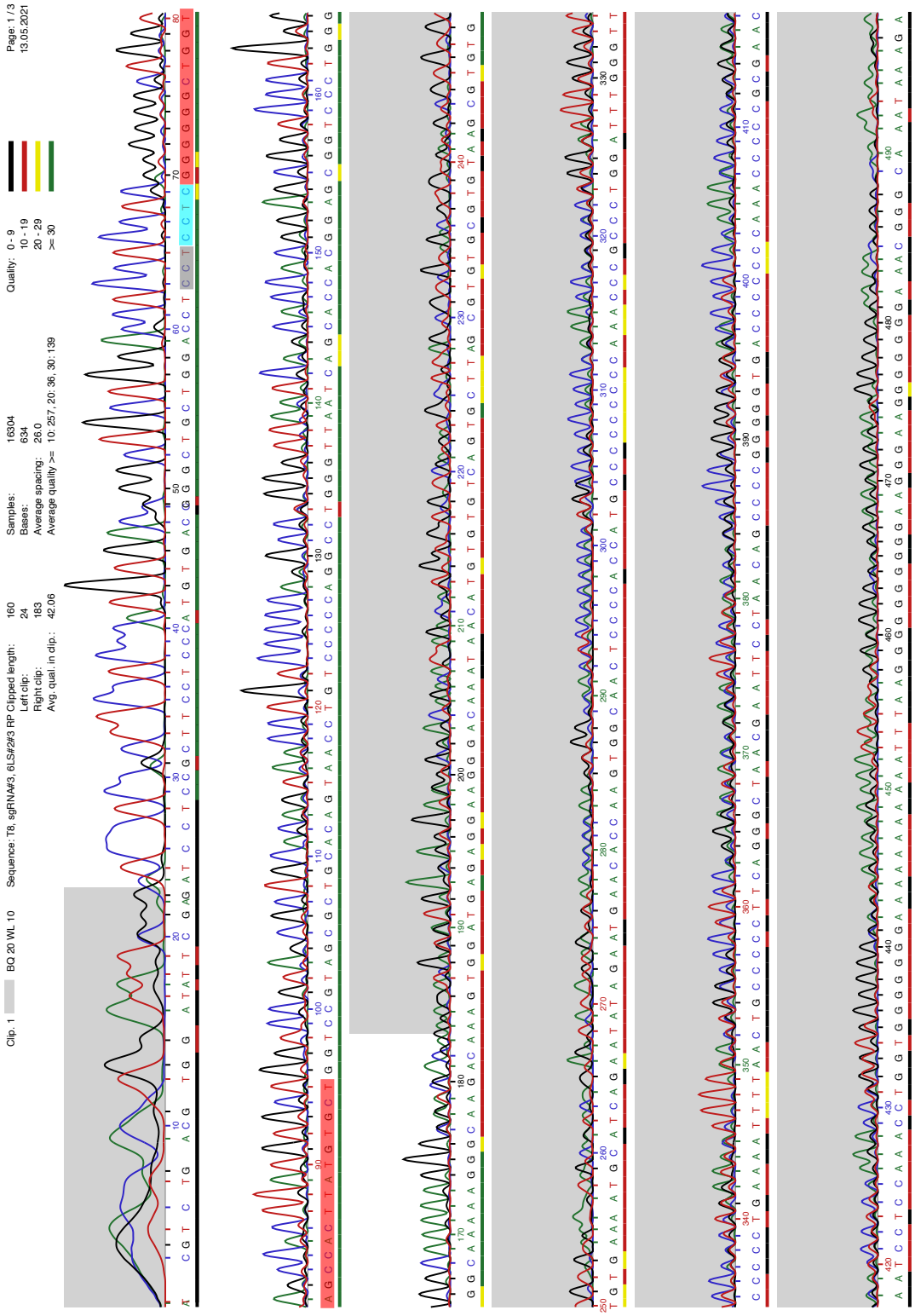

**Suppl. Figure 9: Sequence of *bop1* CRISPant DNA pool using the reverse primer on chromosome 6S+L for *bop1 gRNA #3.***

Target site of *bop1 gRNA #3* on chromosome 6S+L indicated in teal. PAM sequence is indicated in grey. Heterogenous sequence due to mutations is indicated in red.

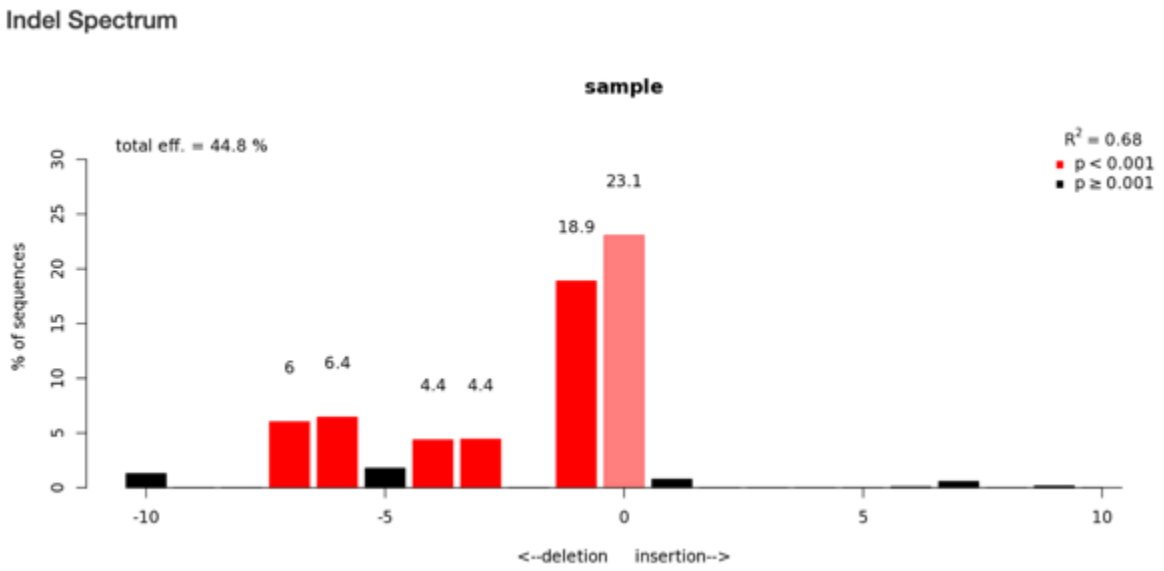


**Suppl. Figure 10: Raw data from TIDE software. Predicted gRNA efficacy for *bop1 gRNA #1* on chromosome 6L.**

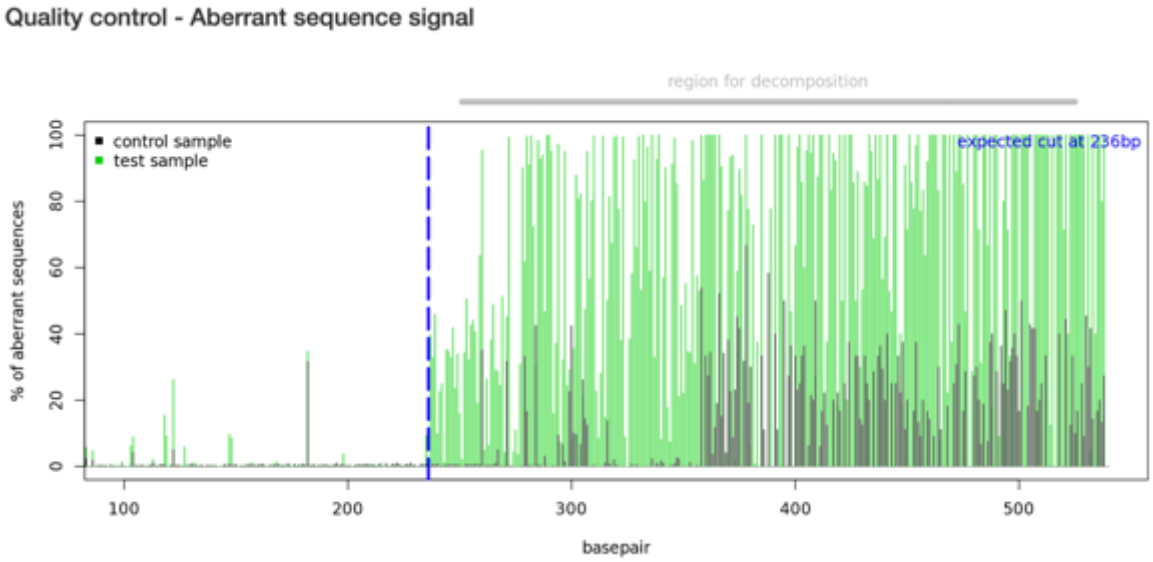


**Suppl. Figure 11: Raw data from TIDE software. Quality control for input data of above shown predicted gRNA efficacy for *bop1 gRNA #1* on chromosome 6L.**

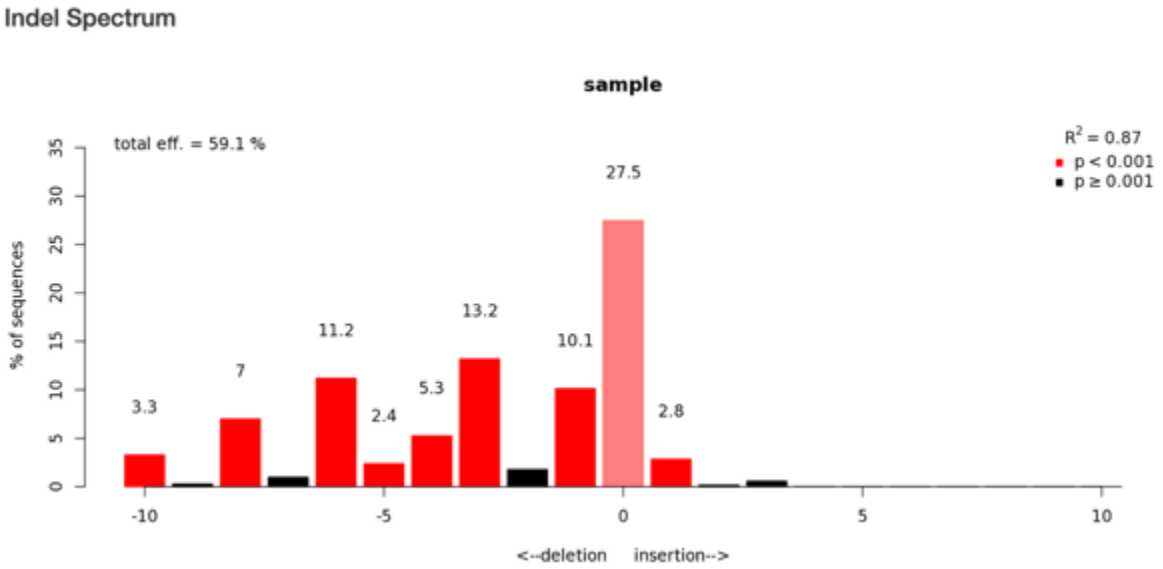


**Suppl. Figure 12: Raw data from TIDE software. Predicted gRNA efficacy for *bop1 gRNA #1* on chromosome 6S.**

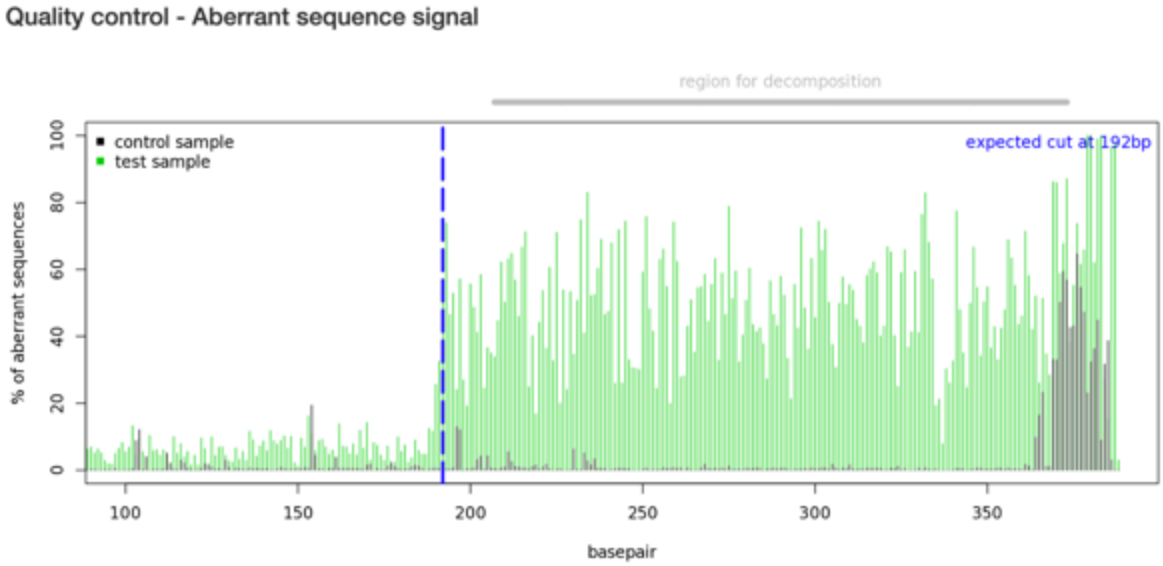


**Suppl. Figure 13: Raw data from TIDE software. Quality control for input data of above shown predicted gRNA efficacy for *bop1 gRNA #1* on chromosome 6S.**

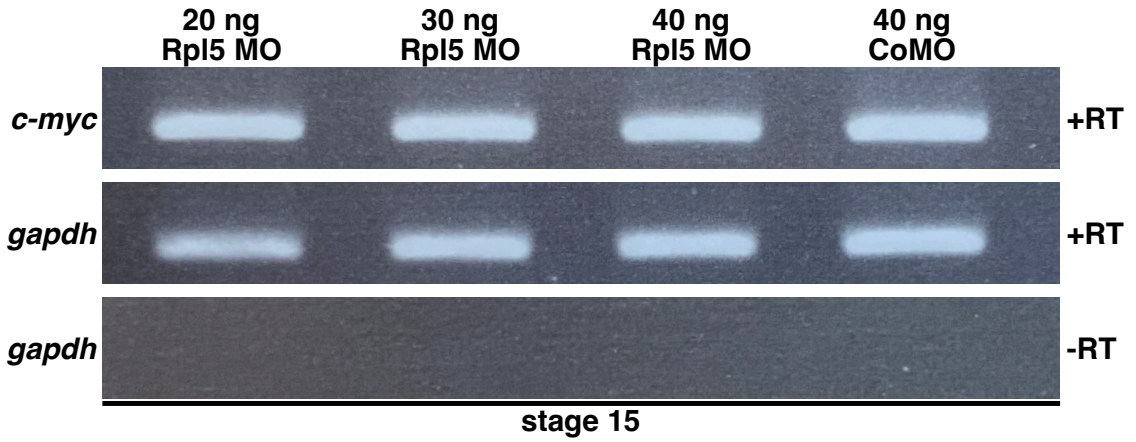


**Suppl. Figure 14: *c-myc* expression was not affected upon Rpl5 depletion when analyzed using RT PCR.** Embryos were bilaterally injected at two-cell stage using 20, 30, or 40 ng Rpl5 MO or 40 ng Control MO. At stage 15, RNA was isolated and RT PCR was performed. *c-myc* expression did not alter between the different conditions. *gapdh* served as loading control. *gapdh* minus reverse transcriptase (-RT) served as negative control. Abbreviations: *c-myc*, *MYC protooncogene*; CoMO, control morpholino oligonucleotide; *gapdh*, *glyceraldehyde 3-phosphate dehydrogenase*; Rpl5 MO, ribosomal protein L5 morpholino oligonucleotide; RT, reverse transcriptase.

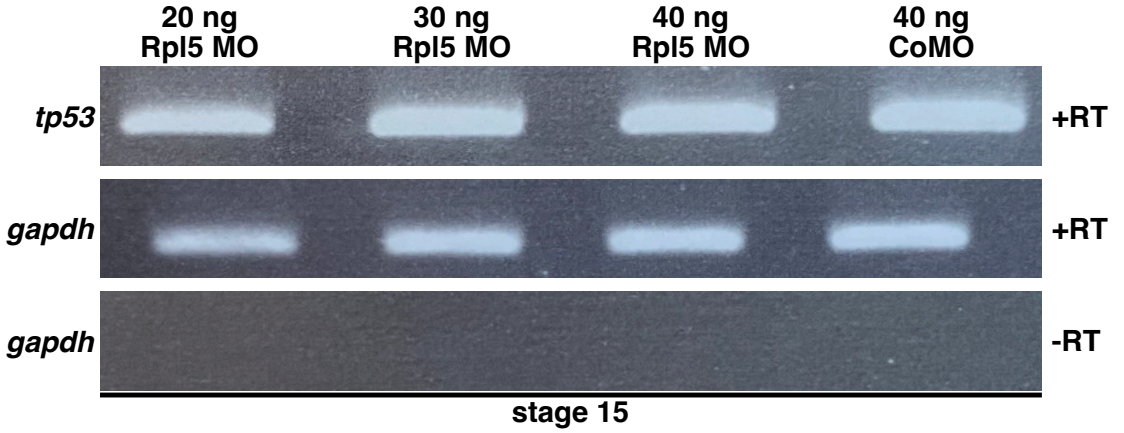


**Suppl. Figure 15: *tp53* expression was not affected in RT PCR analysis.**
Embryos were bilaterally injected at two-cell stage using 20, 30, or 40 ng Rpl5 MO or 40 ng Control MO. At stage 15, RNA was isolated and RT PCR was performed. *tp53* expression did not alter between the different conditions. *gapdh* served as loading control. *gapdh* minus reverse transcriptase (-RT) served as negative control. Abbreviations: CoMO, control morpholino oligonucleotide; *gapdh*, *glyceraldehyde 3-phosphate dehydrogenase*; Rpl5 MO, ribosomal protein L5 morpholino oligonucleotide; RT, reverse transcriptase; *tp53*, *tumor protein p53*.

## Publications during the time as a PhD student

**Gärtner, C.***, Meßmer, A.*, Dietmann, P., Kühl, M., & Kühl, S. J. (2022). Functions of block of proliferation 1 during anterior development in Xenopus laevis. *PLoS One*, 17(8): e0273507. * contributed equally

**Schreiner, C.***, Kernl, B.*, Dietmann, P., Riegger, R. J., Kühl, M., & Kühl, S. J. (2022). The Ribosomal Protein L5 Functions During Xenopus Anterior Development Through Apoptotic Pathways. *Front. Cell Dev. Biol.*, 10, 777121. * contributed equally

Flach, H., Basten, T., **Schreiner, C.**, Dietmann, P., Greco, S., Nies, L., Roßmanith, N., Walter, S., Kühl, M., & Kühl, S. J. (2021). Retinol binding protein 1 affects Xenopus anterior neural development via all-trans retinoic acid signaling. *Dev. Dyn. Off. Publ. Am. Assoc. Anat.*, 250, 1096–1112.

Henrich, T.J.*, **Schreiner, C.***, Cameron, C.*, Hogan, L.E., Richardson, B., Rutishauser, R.L., Deitchman, A.N., Chu, S., Rogers, R., Thanh, C., Gibson, E.A., Zarinsefat, A., Bakkour, S., Aweeka, F., Busch, M.P., Liegler, T., Baker, C., Milush, J., Deeks, S.G., & Stock, P.G. (2021). Everolimus, an mTORC1/2 inhibitor, in ART-suppressed individuals who received solid organ transplantation: A prospective study. *Am. J. Transplant. Off. J. Am. Soc. Transplant. Am. Soc. Transpl. Surg.*, 21, 1765–1779. * contributed equally

Bischof, J., Gärtner, F., Zeiser, K., Kunz, R., **Schreiner, C.**, Hoffer, E., Burster, T., Knippschild, U., & Zimecki, M., (2019). Immune Cells and Immunosenescence. *Folia Biol. (Praha)*, 65, 53–63.

## Statutory Declaration

I hereby declare that I wrote the present dissertation with the topic:

“Functions of the ribosomal factors block of proliferation 1 and ribosomal protein L5 during embryogenesis of *Xenopus laevis*”

independently and used no other aids that those cited. In each individual case, I have clearly identified the source of the passages that are taken word for word or paraphrased from other works.

I also hereby declare that I have carried out my scientific work according to the principles of good scientific practice in accordance with the current „Satzung der Universität Ulm zur Sicherung guter wissenschaftlicher Praxis“ [Rules of the University of Ulm for Assuring Good Scientific Practice].

_____ _____

Corinna Nicoline Gärtner

## Acknowledgements

First of all, I want to express my gratitude to Prof. Dr. Michael Kühl and PD Dr. Susanne Kühl for giving me the great opportunity to perform my PhD thesis at the Institute of Biochemistry and Molecular Biology and for giving me the chance and possibility to improve personally as well as professionally. Thank you for your support, your guidance, and your scientific input.

I would like to thank the members of my Thesis Advisory Committee, Prof. Dr. Michael Kühl, Prof. Dr. Karin Danzer, and PD Dr. Kerstin Feistel for their time and evaluation of this dissertation. I also want to thank all further reviewers of this dissertation. A special thank you to PD Dr. Kerstin Feistel - together with Dr. Tim Ott - who helped me understand and implement the CRISPR/Cas9 system in the frogs. Additionally, I want to thank the International Graduate School of Molecular Medicine for their support.

I am grateful for all the people I have met in the institute - working “directly” in the lab or “indirectly”, keeping the system running!! It wouldn’t have worked without you and your help and it was my pleasure working with all of you. Especially I want to thank Petra for her endless time and patience and unconditional support in all situations in life. Furthermore, Ernestine (always keep in mind: “everything is awesome”) and Hannah for many discussions - work and non-work related -, traveling together, and sticking together in difficult times. I want to thank Anja for her help and for being who she is. Seriously girls, you are great, and it was always fun and a pleasure working with you - in the good and in the bad times (which sometimes exist in science!). This is really a great team to work with and I will miss you.

Furthermore, I want to say thank you to my family and friends who encouraged and endorsed me through all this time. Especially I want to thank my Mum, my Dad, and Caro – for always supporting me and having the necessary foresight and distance to certain things.

In the end, I thank Fabi for being my tower of strength, my safe haven, for his unconditional support and love. To the moon - not yet discovered, somewhere in the Andromeda galaxy - and back.

Thank you all for helping me accomplish this goal!